PETROGRAPHY, MINERAL CHEMISTRY AND GEOCHEMISTRY OF THE HARDWICK TONALITE AND ASSOCIATED IGNEOUS ROCKS, CENTRAL MASSACHUSETTS

BY CHARLES KENNETH SHEARER

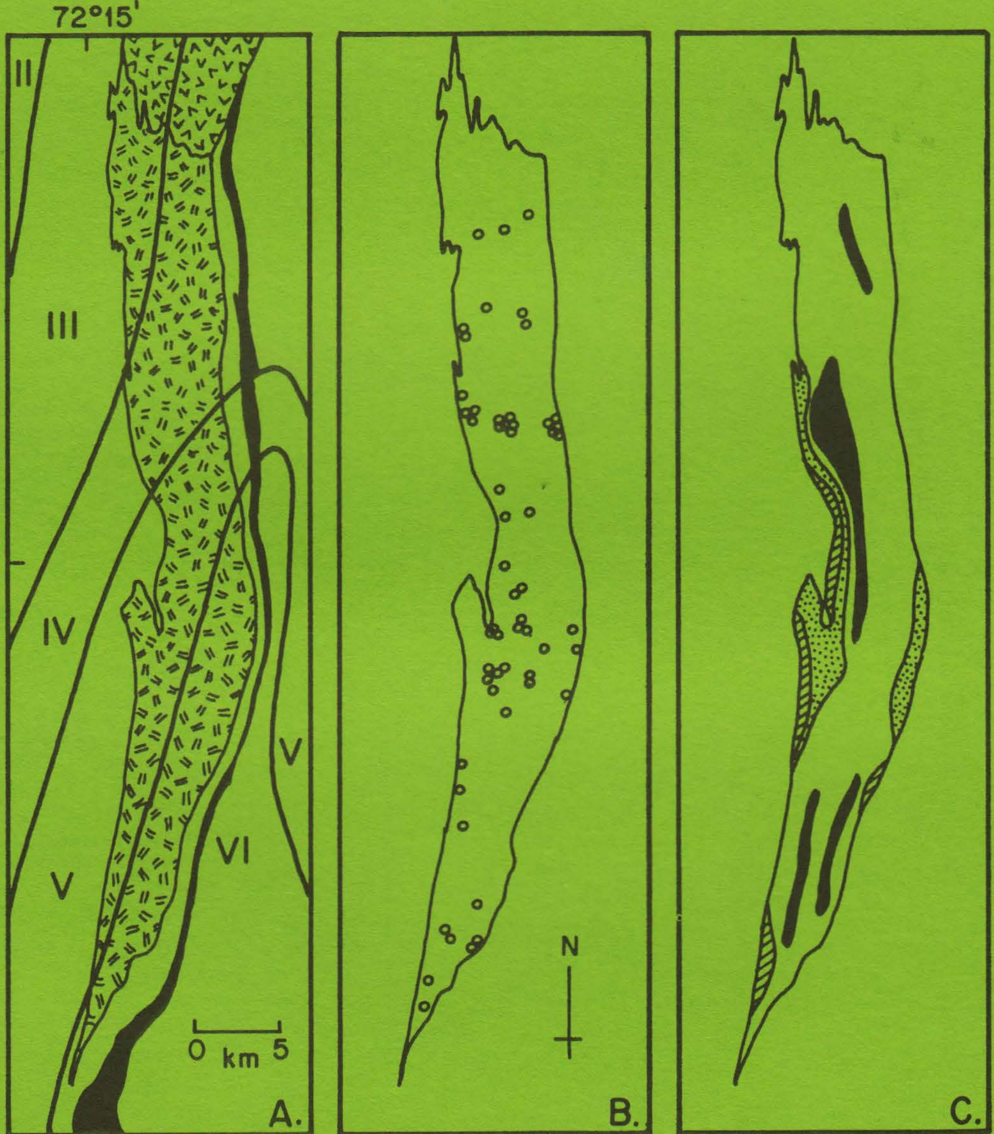

CONTRIBUTION NO. 51
DEPARTMENT OF GEOLOGY & GEOGRAPHY
UNIVERSITY OF MASSACHUSETTS
AMHERST, MASSACHUSETTS

PETROGRAPHY, MINERAL CHEMISTRY, AND GEOCHEMISTRY

OF THE HARDWICK TONALITE AND ASSOCIATED IGNEOUS ROCKS

CENTRAL MASSACHUSETTS

(Ph.D. Thesis)

by

Charles Kenneth Shearer

Contribution No. 51

Department of Geology and Geography

University of Massachusetts

Amherst, Massachusetts

September, 1983

TABLE OF CONTENTS

FOREWORD ix

PART I. PETROGRAPHY AND MINERAL CHEMISTRY OF THE HARDWICK TONALITE AND ASSOCIATED IGNEOUS ROCKS. 1

ABSTRACT 2

INTRODUCTION 4

Location 4
Regional Setting 4
Previous Work. 7
Purpose of Study 7
Acknowledgments. 10

DISTRIBUTION AND CORRELATION OF THE HARDWICK PLUTON AND ASSOCIATED IGNEOUS ROCKS 11

Introduction 11
Hardwick Tonalite. 11
Augite-Hornblende Quartz Diorite and Tonalite. 13
Bear Den Sill of Hornblende Diorite. 13
Diorite at Goat Hill 13
Porphyritic Microcline Granite 16
Equigranular Biotite-Muscovite Granite 16

PETROGRAPHY. 17

Petrographic Methods 17
HARDWICK TONALITE. 17
Hornblende-Biotite Tonalite. 17
Biotite Tonalite 19
Biotite-Muscovite Tonalite 25
Biotite-Garnet Tonalite. 33
Mylonite 33
Summary of Petrography of the Hardwick Tonalite and Petrographic Evidence for Magma Origin 34
AUGITE-HORNBLENDE QUARTZ DIORITE AND TONALITE. 36
Nichewaug Sill of Quartz Diorite 36
Augite-bearing Tonalite within Tonalite Pluton 40
BEAR DEN SILL OF HORNBLENDE DIORITE. 40
GOAT HILL DIORITE DIORITE. 43
SUMMARY OF PETROGRAPHY OF MAFIC IGNEOUS ROCKS ASSOCIATED WITH THE HARDWICK TONALITE. 43
PORPHYRITIC MICROCLINE GRANITE 46
EQUIGRANULAR BIOTITE-MUSCOVITE GRANITES. 51
Granites at Sheep Rock and Tom Swamp 51
Fitzwilliam Granite and Sills Intruding the Hardwick Tonalite. 51

MINERAL CHEMISTRY. 55

Analytical Methods 55
Pyroxene 55
Hornblende 60
Biotite. 73
Muscovite. 83
Garnet 95
Plagioclase. 100
Potassium Feldspar 110
Oxides 114
Sphene 121

DISCUSSION OF IGNEOUS AND METAMORPHIC PHASE RELATIONSHIPS 124

ACF Relationships 124
Igneous Crystallization. 126
Metamorphic Reequilibration. 128

ESTIMATES OF T-f_{O_2} RELATIONS 134

Feldspar Geothermometry 134
Estimates of f_{O_2} from Biotite-Oxide Phase Relations. 137

PART II. GEOCHEMISTRY OF THE HARDWICK TONALITE 143

ABSTRACT 144
INTRODUCTION 145
GEOLOGIC SETTING 145
GEOLOGICAL RELATIONS AND PETROGRAPHY OF THE HARDWICK TONALITE. 148
SAMPLING AND ANALYTICAL PROCEDURES 154
ANALYTICAL RESULTS 154
Major Element Characteristics. 162
Trace Element Characteristics. 169
DISCUSSION 176
Fractional Crystallization 176
Contamination with a Peraluminous, Reduced Component 179
In situ Contamination Versus Mixing within Source Region . . . 183
Oxidized Metaluminous Source 183
Reduced Peraluminous Source 185
Implications Concerning Tectonic Setting 186

REFERENCES CITED 187

APPENDIX: SUMMARY OF THE GEOCHEMISTRY OF THE PLUTONIC ROCKS ASSOCIATED WITH THE HARDWICK TONALITE. 194

INTRODUCTION 194
BEAR DEN SILL OF HORNBLENDE DIORITE. 194
Major Element Geochemistry 194
Trace Element Geochemistry 194

NICHEWAUG SILL OF QUARTZ DIORITE 198
Major Element Geochemistry 198
Trace Element Geochemistry 198
GOAT HILL DIORITE. 199
Major Element Geochemistry 199
Trace Element Geochemistry 199
PORPHYRITIC MICROCLINE GRANITE 199
Major Element Geochemistry 199
Trace Element Geochemistry 199
EQUIGRANULAR BIOTITE-MUSCOVITE GRANITE 200
Major Element Geochemistry 200
Trace Element Geochemistry 200
DISCUSSION OF THE GEOCHEMISTRY OF THE PLUTONIC ROCKS ASSOCIATED WITH THE HARDWICK TONALITE. 201
Major Element Geochemistry 201
Trace Element Geochemistry 207

LIST OF TABLES

1. Point-counted modes of hornblende-biotite tonalite. 20
2. Characteristics of mineral phases in the Hardwick Tonalite. . 22
3. Point-counted modes of biotite tonalite 26
4. Point-counted modes of biotite-muscovite tonalite 30
5. Point-counted modes of biotite-garnet tonalite, mylonitized tonalite and tonalite matrix. 32
6. Point-counted modes of augite-hornblende quartz diorite . . . 38
7. Characteristics of mineral phases from the mafic plutonic units associated with the Hardwick Tonalite 41
8. Point-counted modes of the Bear Den sill of diorite 44
9. Point-counted modes of the diorite at Goat Hill 45
10. Point-counted modes of porphyritic microcline granite 48
11. Characteristics of mineral phases from the granites associated with the Hardwick Tonalite 50
12. Point-counted modes of the granite at Tom Swamp and Sheep Rock. 52
13. Point-counted modes of the Fitzwilliam Granite. 54
14. Electron microprobe analyses of augite. 56
15. Electron microprobe analyses of orthopyroxene 58
16. Electron microprobe-wet chemical analyses of amphibole. . . . 61
17. Electron microprobe analyses of amphibole 62
18. Analyses of biotite 74
19. Electron microprobe analyses of muscovite 87
20. Electron microprobe analyses of muscovite from sample SA251 89
21. Electron microprobe analyses of garnet. 98
22. Electron microprobe analyses of plagioclase 102
23. Electron microprobe analyses of potassium feldspar. 111
24. Electron microprobe analyses of ilmenite and hematite 115
25. Electron microprobe analyses of magnetite 118
26. Electron microprobe analyses of sphene. 122
27. Whole rock analyses and CIPW norms for the Hardwick Tonalite. 155
28. Whole rock analyses and CIPW norms for the Gray Schist Member, Littleton Formation and the Augen Gneiss Member Partridge Formation 161

LIST OF TABLES
(continued)

29. Correlation coefficient matrix for the major elements in the Hardwick Tonalite 164
30. Whole rock analyses and CIPW norms for plutonic rocks associated with the Hardwick Tonalit 195

LIST OF FIGURES

1. Generalized bedrock geologic map of central Massachusetts . . 5
2. Relationship between Hardwick pluton and metamorphic zones . . 8
3. Schematic outline of relationship between deformation history, regional metamorphism and plutonism 9
4. Distribution of rock types within the Hardwick pluton and surrounding plutons. 12
5. Bedrock geologic map of the Nichewaug sill and surrounding intrusions 14
6. Bedrock geologic map of the Bear Den sill and surrounding intrusions 15
7. Distribution of rock types within the Hardwick Tonalite. . . . 18
8. Plot of modes of Hardwick Tonalite 23
9. Textural features of hornblende-biotite tonalite 24
10. Textural features of the Nichewaug sill. 37
11. Plot of modes of mafic intrusions associated with the Hardwick Tonalite. 39
12. Textural features of the hornblende diorite from the Bear Den sill 42
13. Plot of modes of the porphyritic microcline granite. 47
14. Plot of modes of granites at Sheep Rock, and Tom Swamp and Fitzwilliam Granite. 53
15. Augites and orthopyroxenes plotted on pyroxene quadrilateral . 59
16. Amphibole nomenclature diagram.. 67
17. Plot of (Mg/(Mg+Fe) versus Si for amphiboles 68
18. Plot of A-site versus Al(IV) for amphiboles. 69
19. Plot of Al(VI)-2Ti-Fe^{3+} for amphiboles 70
20. Plot of Ti versus Al(IV) for amphiboles. 72
21. Plot of Al(IV) versus Fe^{2+}/(Fe^{2+}+Mg) for biotites from the Hardwick Tonalite. 78
22. Plot of Al(IV) versus Fe^{2+}/(Fe^{2+}+Mg) for biotites from igneous rocks associated with Hardwick Tonalite. 78
23. Plot of Mg, Fe^{2+}+Mn, Al(VI)+Fe^{3+}+Ti for biotite from the Hardwick Tonalite 79
24. Plot of Mg,Fe^{2+}+Mn, Al(VI)+Fe^{3+}+Ti for biotites from igneous rocks associated with Hardwick Tonalite. 79
25. Plot of biotites in terms of trioctahedral and dioctahedral components 80
26. Plot of Fe^{2+}, Fe^{3+}, Ti^{4+} for biotites. 82
27. Plot of Fe^{2+}, Fe^{3+}, Ti^{4+} versus color for biotites 82
28. Relationship between Al(IV), Fe^{2+}/(Fe^{2+}+Mg) and metamorphic grade for biotites 84

LIST OF FIGURES
(continued)

29. Textural types of muscovites 86
30. Ti zoning in type 4 muscovites 90
31. Interlayer site composition and occupancy in muscovites. . . . 92
32. Plot of Fe^{3+} versus Al(VI) for muscovites. 93
33. Plot of Ti versus Al(VI) and Ti versus Al(IV) for muscovites . 94
34. Plot of muscovites in terms of trioctahedral and dioctahedral components. 96
35. Garnets plotted in terms of spessartine-almandine-pyrope . . . 99
36. Plagioclase plotted in ternary system An-Ab-Or 108
37. Analysis traverse across two plagioclase grains. 109
38. Potassium feldspar plotted in ternary system Ab-Or-Cn. 113
39. Ilmenites plotted in FeO-Fe_2O_3-TiO_2. 117
40. Ilmenites plotted in $FeTiO_3$-Fe_2O_3-$MnTiO_3$ 120
41 Plot of Ti versus Al for sphene. 123
42. ACF plot of hornblende, biotite, and muscovite from the Hardwick Tonalite. 125
43. ACF plot of hornblende, biotite, and muscovite from igneous rocks associated with the Hardwick Tonalite. 125
44. AFM plot of mineral compositions from the Hardwick Tonalite. . 127
45. AFM plot of mineral compositions from igneous rocks associated with the Hardwick Tonalite. 127
46. Schematic phase relationships in AFM plot. 129
47. Variations in mineral assemblage and chemistry for magnetite-ilmenite and biotite in terms of TiO_2-FeO-Fe_2O_3. . . 131
48. Subsolidus reactions in the system Na_2O-CaO-FeO-TiO_2(+SiO_2, +K_2O,+H_2O) 132
49. Sulfide-oxide-biotite assemblages represented in TiO_2-Fe-S-Fe_2O_3. 133
50. AFM plot of muscovites and biotites from metamorphic zone VI and Quabbin Reservoir area 135
51. Feldspar geothermometer superimposed upon plot of Ab in plagioclase versus Ab in alkali feldspar 136
52. Biotite compositions plotted in ternary system Fe^{2+}-Fe^{3+}-Mg with projected oxygen buffers. 138
53. T°C--$\log_{10} f_{O_2}$ stability curves for biotite from the Hardwick Tonalite 140
54. T°C--$\log_{10} f_{O_2}$ stability curves for biotite from igneous rocks associated with the Hardwick Tonalite. 141
55. Generalized bedrock geologic map of central Massachusetts . . 146
56. Schematic outline of relationship between deformation history, regional metamorphism and plutonism. 149
57. Distribution of rock types within the Hardwick pluton and surrounding plutons. 150
58. Plot of modes of Hardwick Tonalite 152
59. Distribution of rock types within the Hardwick Tonalite. . . . 153
60. Frequency diagram of SiO_2 content in Hardwick Tonalite 163
61. Na_2O plotted against K_2O for Hardwick Tonalite 165
62. Frequency diagrams of Al/[K+Na+(Ca/2)] and normative 166
diopside and corundum

LIST OF FIGURES
(continued)

63. Hardwick Tonalite contoured with % normative diopside-corundum 167
64. ACF plot of Hardwick Tonalite 168
65. AFM plot of Hardwick Tonalite. 170
66. Plot of Rb versus Sr for the Hardwick Tonalite 171
67. Plot of Rb versus Sr for the Hardwick Tonalite 172
68. Plot of Rb versus Ba for the Hardwick Tonalite 173
69. Plot of Sr versus Ba for the Hardwick Tonalite 174
70. Plot of normalized Rb, K, Sr, P, Nb, Zr and Ti for the Hardwick Tonalite. 175
71. Plot of normative diopside-corundum versus SiO_2 for the Hardwick Tonalite. 177
72. Model for tonalite variability in normative mineralogy and SiO_2 178
73. Plot of modal hornblende and biotite for the hornblende-biotite tonalite 180
74. Plot of normative diopside-corundum versus an oxidation index for the Hardwick Tonalite. 181
75. Comparison of normative diopside-corundum and oxidation index between tonalite and schist. 182
76. Model of trace element variability in Hardwick Tonalite. . . . 184
77. AFM plot of igenous rocks associated with Hardwick Tonalite. . 202
78. AFM plot of Hardwick Tonalite, Fitchburg plutonic complex and Belchertown complex. 203
79. Plot of normative diopside-corundum versus SiO_2 for igneous rocks associated with Hardwick Tonalite. 204
80. Plot of normative diopside-corundum versus oxidation index for igneous rocks associated with the Hardwick Tonalite. . . . 205
81. Plot of K_2O versus Na_2O for igneous rocks associated with Hardwick Tonalite 206
82. Plot of Rb versus Sr for igneous rocks associated with Hardwick Tonalite. 208
83. Plot of Rb versus K for igneous rocks associated with Hardwick Tonalite. 209

FOREWORD

This manuscript is divided into several sections. Petrography and Mineral Chemistry of the Hardwick Tonalite and Associated Igneous Rocks is to be modified for later publication. Geochemistry of the Hardwick Tonalite is in a format designed for publication. Brief summaries of the geochemistry of the mafic plutons and granites (Appendix) will be combined with the petrography and mineral chemistry of those rocks for future publication. References are here amalgamated into a single section. Since the publication of the original thesis in September 1983, additional geochemical data has been gathered. This data is included in the publication.

PART I

PETROGRAPHY AND MINERAL CHEMISTRY OF THE HARDWICK TONALITE AND ASSOCIATED IGNEOUS ROCKS

ABSTRACT

The Hardwick Tonalite and associated plutonic rocks are intruded into a sequence of metmorphosed Middle Ordovician to Lower Devonian clastic sedimentary and subsidiary volcanic rocks of the Merrimack synclinorium. The plutonic rocks are considered to be members of the Acadian (Devonian) New Hampshire Plutonic Series. During the Acadian most of them were involved in several phases of deformation and metamorphism, reaching sillimanite-cordierite-garnet grade in the southeast to sillimanite-muscovite grade in the northwest.

The Hardwick Tonalite forms an irregular west-dipping syntectonic sheet earlier thought to occupy an isoclinal stratigraphic syncline in the Devonian Littleton Formation. Locally, however, the tonalite is in direct contact with or contains inclusions of the Augen Gneiss Member of the Ordovician Partridge Formation and the Silurian Fitch Formation. Estimated minimum volume of the tonalite is 1200 km^3. The tonalite has been subdivided into four petrographic types: hornblende-biotite tonalite, biotite tonalite, biotite-muscovite tonalite and biotite-garnet tonalite. The distribution of these rock types defines a mineralogical zoning in the sheet from hornblende-biotite tonalite and biotite tonalite in the interior to biotite-muscovite tonalite and biotite-garnet tonalite at the perimeter. Accompanying this outward metaluminous to peraluminous zoning, is a change in the accessory mineralogy from a sphene-magnetite-ilmenite assemblage to ilmenite only.

The tonalite exhibits a textural range from a very weakly foliated relict igneous texture to a fine-grained, strongly foliated metamorphic texture. With increasing metamorphic recrystallization, primary plagioclase zoning is eradicated, biotite commonly changes from a red-brown to a brown to green color, and clinozoisite and sphene form rims around allanite and ilmenite, respectively.

Plutonic rocks associated with the tonalite include augite-hornblende quartz diorite and tonalite in the Nichewaug sill and within the Hardwick Tonalite, hornblende diorite in the Bear Den sill, two-pyroxene diorite at Goat Hill, porphyritic microcline granite, Fitzwilliam Granite, and granites at Tom Swamp and Sheep Rock.

The metaluminous-oxidized to peraluminous-reduced trend observed in the petrography of the tonalite is further indicated by the chemistry of the individual minerals. In biotite, $Fe^{3+}/(Fe^{3+}+Fe^{2+})$ decreases and Al (IV) increases from hornblende-bearing tonalites to garnet-bearing tonalites. There is a decrease in the hematite component in the coexisting ilmenite. Estimates of f_{O2} for the associated plutonic rocks suggests the mafic rocks crystallized at higher f_{O2} than the granites.

Mineral assemblages within the Hardwick Tonalite and associated plutonic rocks are considered to be made up of magmatic phases which have reequilibrated to varying degrees under subsolidus conditions. The reequilibration mineral assemblages are typified by high Wo component (42 to 50) in clinopyroxene; Wo component of less than 0.5 in orthopyroxene; Ti loss in hornblende, biotite, muscovite, and magnetite, and a decrease in the anorthite and orthoclase component in plagioclase.

Reequilibration reactions during metamorphic recrystallization may be summarized as (1) ilmenite + Ti-biotite + andesine = sphene + Ti-poor biotite + oligoclase, and (2) ilmenite + Ca plagioclase + K-feldspar + quartz + H_2O = biotite + Na plagioclase + sphene.

INTRODUCTION

Location

The Hardwick Tonalite and associated plutonic rocks are exposed over an area of approximately 295 square kilometers in the Merrimack synclinorium in central Massachusetts. They are situated in the Petersham, Ware, Athol, Templeton, Royalston, Winchendon and Barre 7½-minute quadrangles. The tonalite extends into the Mt. Monadnock 15-minute quadrangle in New Hampshire.

Regional Setting

The Hardwick Tonalite and associated plutonic rocks are intruded into a sequence of metamorphosed clastic sedimentary rocks and subsidiary volcanics of the Merrimack synclinorium. The stratigraphic sequence in the Merrimack synclinorium occurs in two major divisions: (1) metamorphosed Middle Ordovician sedimentary rocks and volcanics and (2) metamorphosed Silurian and Lower Devonian sedimentary rocks and volcanics.

The Middle Ordovician of the Merrimack synclinorium is represented by the Partridge Formation, typically a pyrrhotite-graphite-mica schist which weathers "rusty" yellow-brown. Lenticular calc-silicate pods one half to two meters long and several centimeters thick occur throughout the sequence. An Augen Gneiss Member of the Partridge Formation is commonly in contact with the western edge of the Hardwick Tonalite, but its stratigraphic location within the formation is not known in this area. In the Mt. Grace quadrangle the Augen Gneiss Member is above the basal unit of sulfidic schist and amphibolite (Robinson, 1977).

The Silurian and Lower Devonian rocks unconformably overlie the Middle Ordovician. The Silurian in the Merrimack synclinorium is represented by the Fitch Formation in the extreme western portion and the Paxton Schist which is the major Silurian unit in the central and eastern portions of the synclinorium. It has been argued that the Paxton Schist is the eastern equivalent of the Fitch Formation (Field, 1975). In the immediate vicinity of the Hardwick Tonalite, the Fitch Formation is typically a pyrrhotite-graphite calc-silicate rock. The Paxton Schist, which does not occur near the pluton, consists of gray granular schist with calc-silicate beds, sulfidic biotite schist and sulfidic white schist (Field, 1975).

To the west, the Merrimack synclinorium is bounded by the Bronson Hill anticlinorium and to the east by the Milford anticlinorium (Zen, 1968; Skehan _et al_., 1978). The geology of the Bronson Hill anticlinorium and the Merrimack synclinorium in central Massachusett is illustrated in Figure 1. The Bronson Hill anticlinorium consists of a series of en echelon gneiss domes mantled by amphibolites, mica schists, quartzites and calc-silicate rocks. The stratigraphic sequence in the Bronson Hill anticlinorium has been described by Billings (1937, 1956), Robinson (1967a,b, 1979) and Thompson _et al_. (1968). The Milford anticlinorium contains metamorphic rocks of Late Precambrian and younger ages. Gneisses

Figure 1. Generalized bedrock geologic map of central Massachusetts showing major stratigraphic and plutonic units.

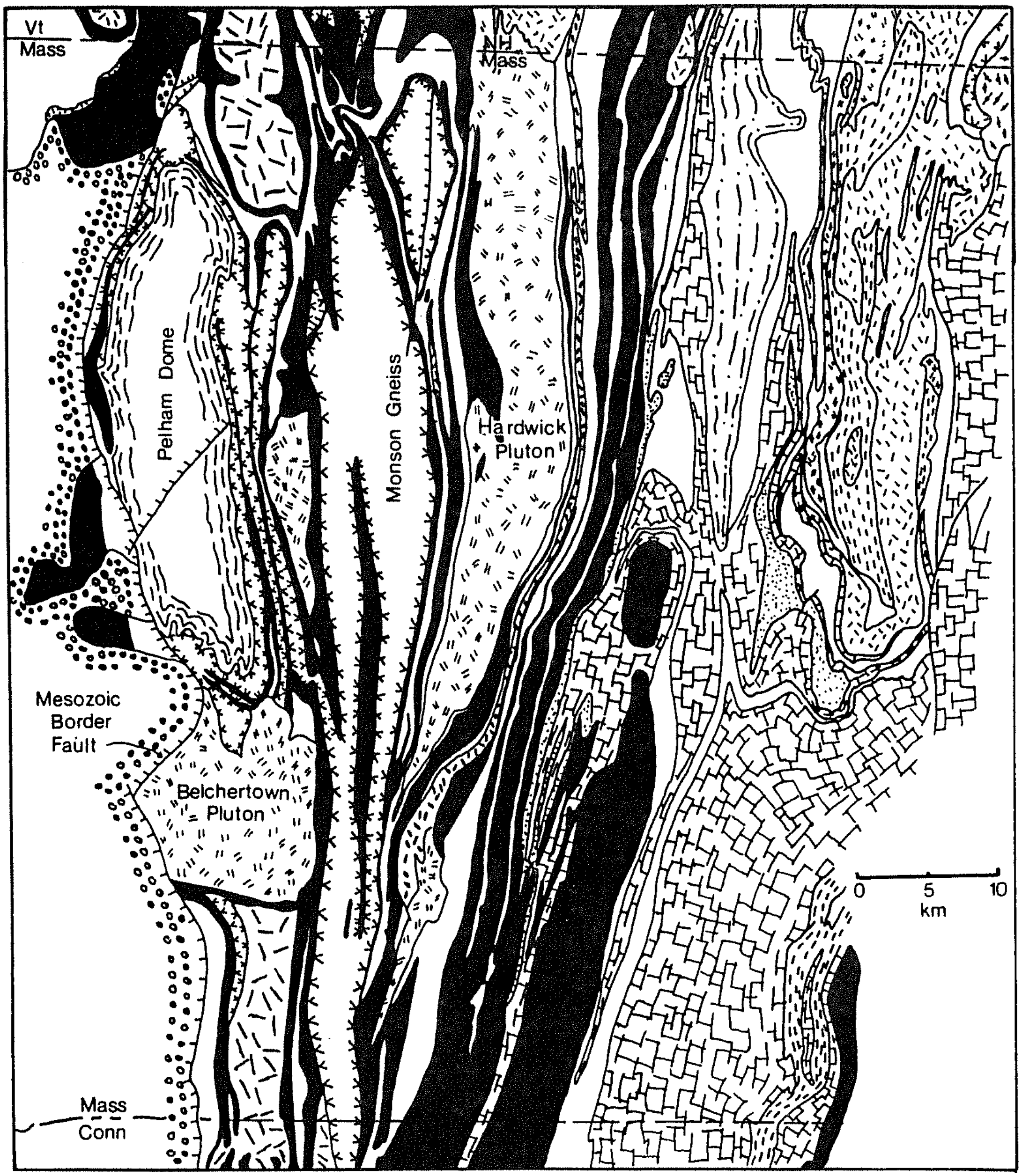

Lower Jurassic-Upper Triassic	Conglomerate, sandstone, shale, and basalt.
Upper Pennsylvanian	Weakly foliated biotite granite.
Devonian	Weakly foliated muscovite granite.
	Foliated muscovite granite gneiss.
	Coys Hill Granite.
	Granodiorite, quartz diorite, tonalite, gabbro.
Lower Devonian	Littleton, Erving, and Waits River Formations.
Silurian	Paxton Formation-sulfidic schist where separately mapped.
	Paxton Formation Granulite member.
	Clough Quartzite in western portion of map, Paxton Formation schist and quartzite members in central and eastern portion of map.
Middle Ordovician	Ammonoosuc Volcanics and Partridge Formation. Tatnic Hill Formation in southeastern portion of map.
Ordovician	Massive gneiss of plutonic origin in cores of domes.
Ordovician Late Precambrian?	Monson and related layered gneisses.
Late Precambrian	Dry Hill and related gneisses, schists and quartzites.
	Major normal faults with hatches on downthrown side.

in the core of the Milford anticlinorium have been correlated to those in the Pelham dome of the Bronson Hill anticlinorium (Hall and Robinson, 1982). An uncertain relationship exists between the metamorphosed rocks of the Milford anticlinorium and the unmetamorphosed Precambrian rocks and associated fossiliferous Cambrian sandstones and shales of the "Avalon Platform" further to the east (Rodgers, 1973). Correlation of the rock types within the Merrimack synclinorium of Massachusetts (Peper and Pease, 1975; Field, 1975; Tucker, 1977) has been extended into the Bronson Hill anticlinorium (Robinson, 1967a; Field, 1975; Robinson et al., 1982) as well as south and central Maine (Osberg, 1979), southeastern New Hampshire (Billings, 1956) and eastern Connecticut (Dixon, 1968).

Most of the plutonic rocks of the Merrimack synclinorium are southern extensions of the Acadian New Hampshire Plutonic Series (Billings, 1956). They form either syntectonic concordant to quasiconcordant sheets, or late- to post-tectonic discordant plutons. Syntectonic sheets are dominant and the contrasting styles are probably a function of relative temperature and rheologic differences between the intruding magma and the country rock, and the deformational stage in which the intrusion occurred (Nielson et al., 1976).

Mapped plutonic rocks account for 21% by area of the rocks exposed in the Bronson Hill anticlinorium and Merrimack synclinorium in Massachusetts. Of this 21%, 5% are gabbro and diorite; 53% are tonalite, granodiorite, and monzodiorite; and 42% are granite. These plutonic rocks are compositionally strongly bimodal, having high frequencies of plutonic rocks with SiO_2 59% and 71%. The Hardwick Tonalite is a major contributor to the first peak.

The distribution of the plutonic rocks is shown in Figure 1. The Belchertown Quartz Monzodiorite pluton has been described by Guthrie (1972), Guthrie and Robinson (1967), Hall (1973), Ashwal (1974) and Ashwal et al. (1979). The Fitchburg plutonic complex has been mapped by Grew (1970), Hepburn (1975), Peper and Wilson (1978), Tucker (1978) and Tucker and Robinson (1977, 1978, unpublished data). Maczuga (1981) described the modal and geochemical variations within the complex.

In many of the plutonic rocks of the Bronson Hill anticlinorium and the Merrimack synclinorium, the igneous texture has been replaced with a metamorphic texture and a mineralogy developed during the Acadian deformation and metamorphism. Metamorphic effects on the texture and mineralogy of some of the plutonic rocks have been described by Ashwal et al. (1979) and Maczuga (1981). The sequence of Acadian deformations in central Massachusetts as interpreted by Robinson (1967 a,b), Field (1975), Tucker (1977) and Hall and Robinson (1982) consists of four phases: 1) Recumbent, isoclinal, west-directed nappes of a large amplitude (tens of kilometers). Several plutonic sheets including the Hardwick Tonalite were intruded prior to or during this structural stage. The Spaulding Quartz Diorite in New Hampshire is thought to have been intruded into the Littleton Formation early in the deformational history, but after the intrusion of the Kinsman Quartz Monzonite (Nielson et al., 1976). A low pressure "contact" metamorphism, possibly resulting from the intrusion of the plutonic sheets, is suggested by aggregates of sillimanite that appear to be pseudomorphs after andalusite (Tracy and Robinson, 1980). 2) Recumbent back-folding of isoclinal folds developed in stage 1. During this stage in the deformation, metamorphic grade in the immediate area of the Hardwick pluton reached sillimanite-K-feldspar-cordierite-garnet grade at the southeast margin of the tonalite and sillimanite-muscovite grade at the northwest margin of the tonalite (Figure 2). Rocks previously exposed to low pressure metamorphism attained peak metamorphic conditions of up to 700°C and 6.3kb (Tracy *et al.*, 1976, Robinson *et al.*, 1982). Mylonites found at the margins and southern end of the tonalite were formed late in this stage. 3) Formation of a series of broad open folds about north-trending axes. The relationship between the deformational history, the metamorphism and the plutonism in the Merrimack synclinorium and the Bronson Hill anticlinorium in central Massachusetts is schematically outined in Figure 3.

Previous Work

The "Hardwick granite", with its type locality in Hardwick, Massachusetts, was interpreted by Emerson (1898, 1917) to be a series of intrusive sheets composed predominantly of "black granite" gneiss. It was assigned a late- or post-Carboniferous age (Emerson, 1917). Emerson also differentiated between the dominantly biotite-bearing "black granite", a hornblende-bearing variety and a garnet-fibrolite-bearing variety. In addition, he also noted a porphyritic rock type occurring as sheets intruding the "black granite" and mafic border rocks typified by biotite-hypersthene diorite at Gilbertville, Massachusetts and garnet-hypersthene diorite/norite near Brimfield, Massachusetts. Field (1975) has shown that rocks near Brimfield and possibly the diorite at Gilbertville are not intimately related to the Hardwick pluton.

Fahlquist (1935) studied the geology of the Quabbin Aqueduct Tunnel which passes through the southern part of the Hardwick pluton. Fowler-Billings (1949) studied the geology of the Mt. Monadnock 15-minute quadrangle and established the type locality for the Spaulding Quartz Diorite Member of the New Hampshire Plutonic Series at the northern extension of the Hardwick pluton. Subsequent mapping by Fitzgerald in the Royalston quadrangle (1960), Mook in the Athol quadrangle (1967), D'Onfro in the Templeton quadrangle (unpublished data, 1974), Field in the Ware quadrangle (1975) and Tucker in the Barre quadrangle (1977) further defined the relationship between the Hardwick pluton and associated plutonic rocks and the region's deformational history and stratigraphy.

Purpose of Study

Previous investigations in the western part of the Merrimack synclinorium have been primarily concerned with the stratigraphy and the structural and metamorphic history of the area rather than the numerous plutonic rocks. Aspects of this investigation of the Hardwick pluton and spatially related plutonic rocks include detailed mapping of the plutonic and country rocks in the Petersham and Athol 7.5-minute quadrangles, reconnaissance mapping in the Ware, Templeton, Barre, Royalston

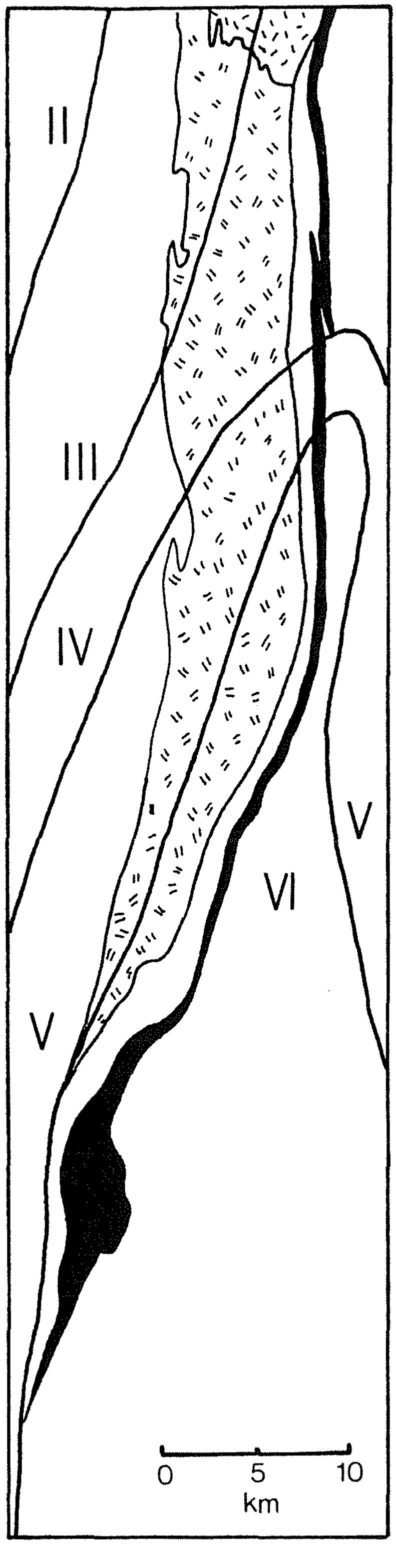

Figure 2. Relationship between the Hardwick Pluton and the metamorphic zones. II sillimanite-muscovite-staurolite, III sillimanite-muscovite, IV sillimanite-muscovite-K-feldspar, V sillimanite-K-feldspar, VI sillimanite-cordierite-garnet.

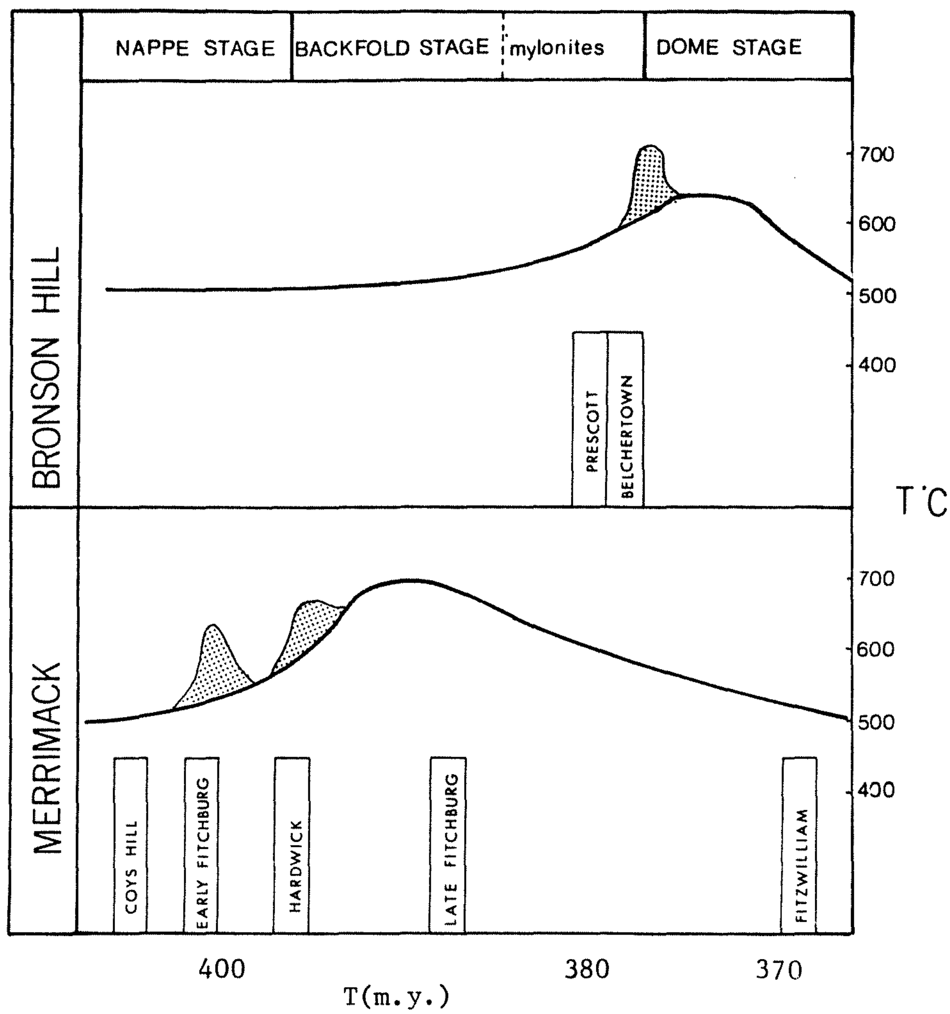

Figure 3. Schematic outline of the relationship between the deformational history, regional metamorphism and plutonism in the Merrimack synclinorium and the Bronson Hill anticlinorium in central Massachusetts. Dotted peaks represent thermal pulses during intrusion of plutons. Estimates of metamorphic temperatures are from Tracy et al. (1976) and Shearer and Robinson(1980).

and Winchendon 7.5-minute quadrangles in Massachusetts and the Mt. Monadnock 15-minute quadrangle in New Hampshire, thin section petrography, major and trace element analysis of the plutonic rocks and local metamorphosed sedimentary rocks, and electron microprobe analysis of silicates and oxides. One hundred and one modal analyses were done on thin sections of plutonic rocks and in addition 38 thin sections were examined for texture and mineralogy. One hundred and seven samples of plutonic and metamorphosed sedimentary rocks were analyzed for major elements and many were analyzed for trace elements.

Aspects of this investigation are aimed at addressing the following problems: (1) Evaluation of the expanded compositional spectrum of the plutonic rocks in the study area from diorite to granite (52% to 74% SiO_2) with regard to whether or not they define a coherent calc-alkaline association or whether their relationship is strictly spatial. Are the generated magmas a result of a similar melting episode in several chemically and tectonically distinct source regions, or a result of melting, mixing and fractionation processes in a single source? (2) Determination of possible source areas, materials, and processes capable of generating plutonic rocks with the observed mineralogical and geochemical characteristics. Conclusions reached concerning magma source and melting processes will contribute to understanding of Acadian plutonism in the Merrimack synclinorium and to regional tectonic interpretations. (3) Evaluation of the effects of reequilibration during regional metamorphism on the primary igneous mineral compositions and assemblages.

Acknowledgments

This report was submitted in partial fulfillment of the requirements for the degree of Doctor of Philosophy in Geology at the University of Massachusetts, Amherst. Peter Robinson provided unyielding enthusiasm, patience and many hours of advice and discussion concerning the contents of this manuscript. The other members of my committee, J.M. Rhodes, S.A. Morse and T.R. Stengle provided valuable insight, technical advice, guidance and critique of this manuscript. John Schumacher and David Maczuga were helpful in discussions concerning granitoid genesis and analytical methods. Joel Sparks and John Allison have provided advice on analytical methods and computer programming. Patricia W. Shearer typed this manuscript and contributed encouragement throughout the duration of my graduate studies. To these individuals I am deeply indebted. I would also like to acknowledge the cooperation of the Metropolitan District Commission (Boston) for providing access to samples taken for the Quabbin Aqueduct Tunnel during its construction. Partial academic year assistantships and summer subsistance and funds for field and laboratory work were provided in part by a Grant from the U.S. Geological Survey (to Robinson), National Science Foundation Grants EAR-79-15246 and EAR-81-16197 (to Robinson) and Geological Society of America Grant 2527-79 (to Shearer).

DISTRIBUTION AND CORRELATION OF THE HARDWICK PLUTON AND ASSOCIATED PLUTONIC ROCKS

Introduction

The distribution of the rock types within the Hardwick pluton and surroundings is shown in Figure 4. The plutonic rocks included in this figure range in composition from diorite to granite with tonalite dominant. The variability of intrusive style and of preservation of textures and mineral assemblages suggest that these plutonic rocks were intruded during various periods of Acadian deformation and metamorphism. Correlation between units is based upon the observations of this study and previous investigations.

Hardwick Tonalite

The Hardwick Tonalite forms an irregular west-dipping sheet which appears to represent a single intrusive episode. A number of smaller tonalite sills occur within the country rock surrounding the main tonalite sheet. The Hardwick Tonalite crudely occupies an isoclinal stratigraphic syncline in the Devonian Littleton Formation (Field, 1975), although on the northwest side the tonalite is in direct contact with the Augen Gneiss Member of the Ordovician Partridge Formation. Large country rock inclusions of the Ordovician Partridge Formation, the Silurian Fitch Formation and the Lower Devonian Littleton Formation are distributed throughout the tonalite.

To the north, the tonalite is intruded by the post-Acadian Fitzwilliam Granite which cuts off the tonalite from the type locality of the "Spaulding Quartz Diorite" in the Mt. Monadnock quadrangle, in New Hampshire (Fowler-Billings, 1949). The type locality for the Spaulding Quartz Diorite has been correlated to other tonalite and quartz diorite intrusions in the New Hampshire Plutonic Series (Nielson et al., 1976).

The Hardwick Tonalite is here subdivided into hornblende-biotite tonalite, biotite tonalite, biotite-muscovite tonalite and biotite-garnet tonalite. Details of the distribution and characteristics of these subdivisions are discussed in detail in the petrography section of this manuscript.

The quasi-concordant style of intrusion for the Spaulding Quartz Diorite led Nielson et al. (1976) to suggest intrusion early in the deformational history. The well developed foliation and the development of mylonite in the tonalite, in addition to the character of the regional metamorphic isograds, suggests a similar early intrusive age for the Hardwick Tonalite.

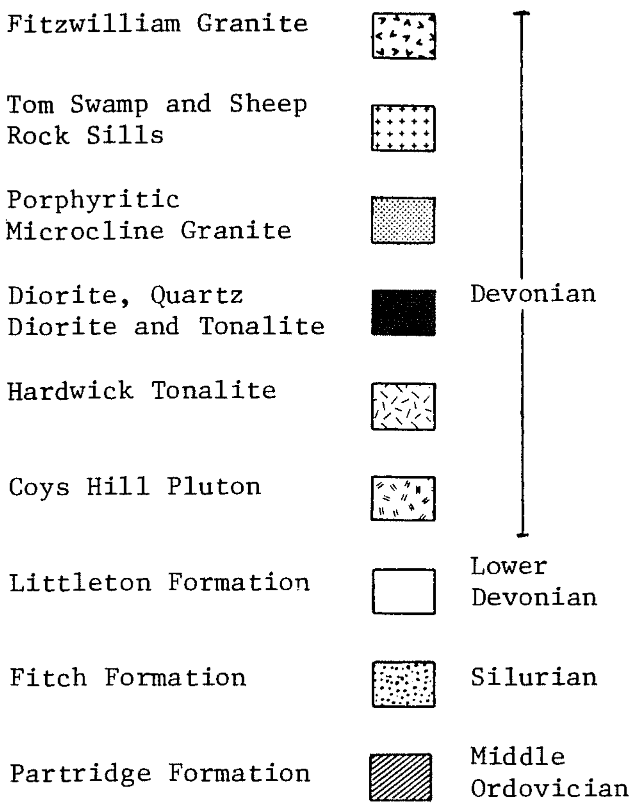

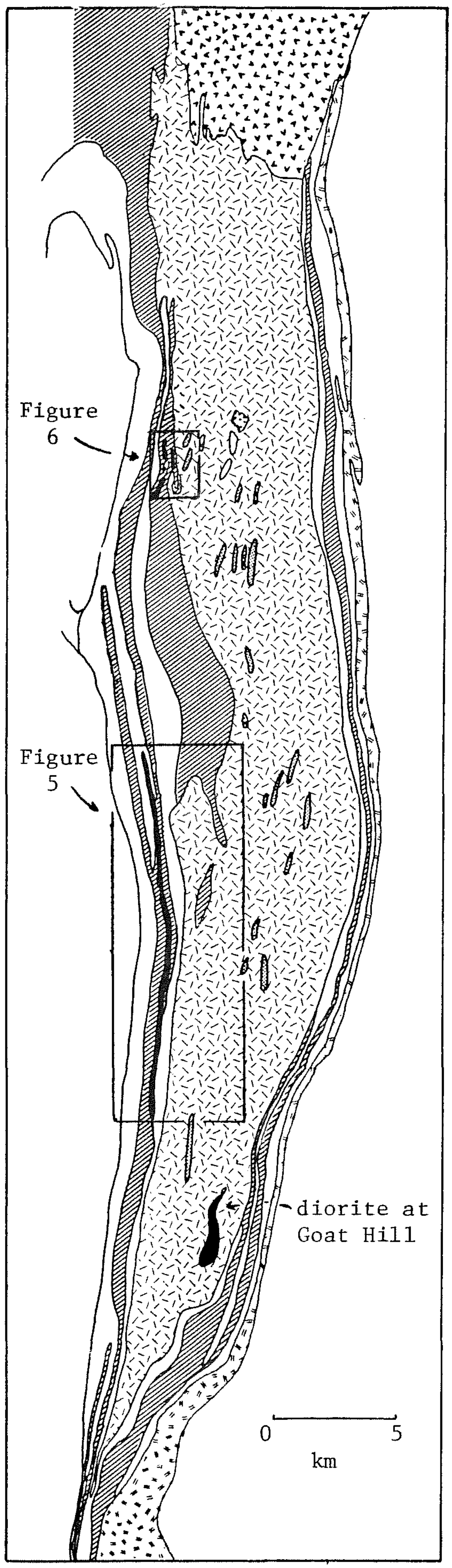

Figure 4. Distribution of rock types within the Hardwick Tonalite and surrounding plutons. Diorite, quartz diorite, and tonalite units include the diorite at Goat Hill and Bear Den, quartz diorite of the Nichewaug sill and small tonalite sills intruding the country rock surrounding the Hardwick Tonalite.

Augite-Hornblende Quartz Diorite and Tonalite

The augite-hornblende quartz diorite and tonalite forms a north-south trending sill, the Nichewaug sill, to the west of the Hardwick pluton and a body of unknown geometry within the Hardwick pluton. The later body is noted only in samples taken from the Quabbin Aqueduct Tunnel (Figure 5). The Nichewaug sill extends along strike a total distance of approximately 14 km from its occurrence in the Quabbin Aqueduct Tunnel to Brooks Pond. It may, however, extend further to the north and south. The sill reaches an estimated maximum thickness of 50 meters in the Quabbin Aqueduct Tunnel location and is nearly pinched out by boudinage at the Breen Road location, suggesting a possibly discontinuous nature. Although the sill extends along the strike of the country rock, it is not truly concordant (Figure 5) because it intrudes the Littleton Schist in the Brooks Pond area, the Partridge Formation in the Trot Hill area and lies along the contact between these two units in the Quabbin Aqueduct Tunnel area (Field, 1975).

In the Brooks Pond area a chilled-contaminated porphyry margin and a relict contact metamorphic aureole (Shearer and Robinson, 1980) have been preserved. The relict contact aureole with a regional metamorphic overprint suggests the sill was intruded prior to the peak of regional metamorphism and probably late in the first stage of Acadian deformation in central Massachusetts. In the Ware area the quartz diorite of the sill was correlated to the Goat Hill Diorite and the Belchertown pluton (Field, 1975). The northern extension was located and mapped in the present study.

Bear Den Sill of Hornblende Diorite

Hornblende diorite forms a small sill in the northwest corner of the Athol quadrangle in the Bear Den area of the Athol town forest (Figures 4 and 6). The sill, approximately 18 to 25 meters in thickness and at least 920 meters in length, intrudes the Augen Gneiss Member of the Partridge Formation (Ordovician) to the west of the major Hardwick Tonalite intrusive sheet and closely associated with smaller sills of tonalite and intrusions of granite. Mook (1967) suggested a post-Acadian age for the diorite, but the development of a foliated, metamorphic texture at the margins of the sill suggests syntectonic emplacement. The sill has not been correlated to any major rock type elsewhere in the Merrimack synclinorium.

Diorite at Goat Hill

The diorite at Goat Hill (Figure 4) forms an elongate north-south trending intrusion within the Hardwick Tonalite, north of Gilbertville in the Ware quadrangle. The pristine igneous texture of the diorite is suggestive of an emplacement after Acadian regional metamorphism and deformation (Field, 1975). It is possible, however, that the relict igneous texture may have been protected and preserved by the surrounding Hardwick Tonalite. The contact relationship between the tonalite and

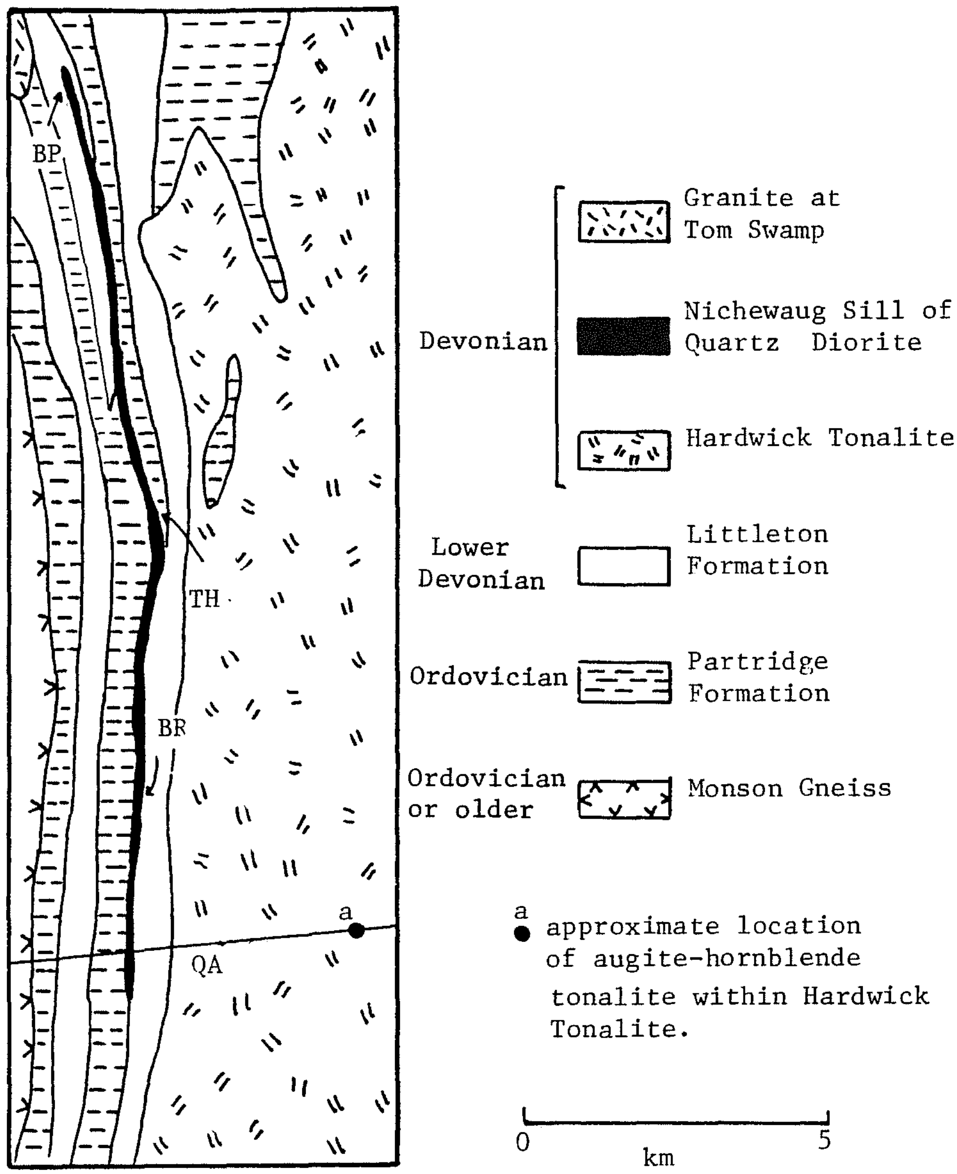

Figure 5. Bedrock geologic map of the Nichewaug sill of augite-hornblende quartz diorite, granite at Tom Swamp and surrounding plutonic and metamorphic rocks. Sill locations mentioned in text are represented: BP-Brooks Pond area, TH-Trot Hill, BR-Breen Road, QA-Quabbin Aqueduct Tunnel.

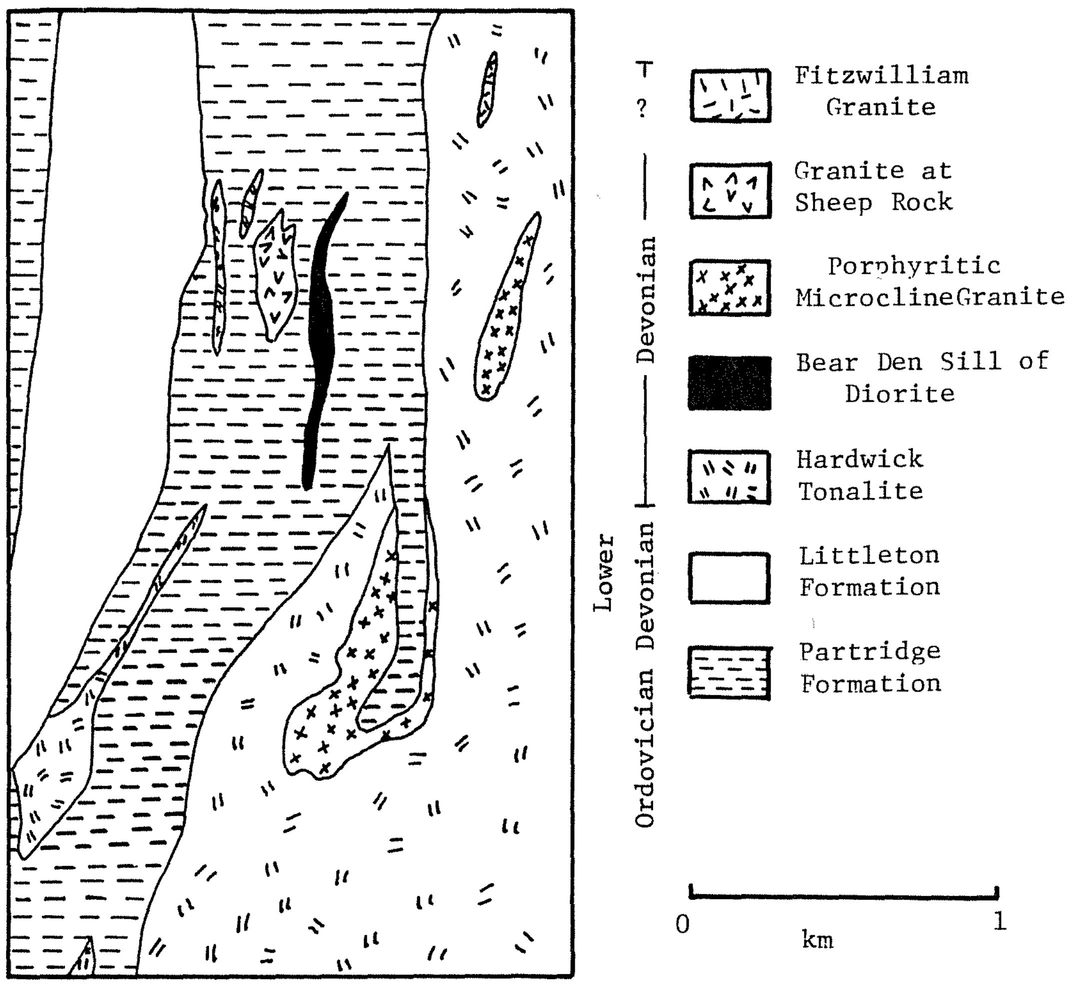

Figure 6. Bedrock geologic map of the Bear Den sill of diorite, Sheep Rock intrusion of granite and surrounding plutonic and metamorphic rocks.

the diorite, although obscure in many instances, has been observed to be gradational. The contact is commonly associated with schist and lacks recognizable inclusions of either tonalite or diorite. The diorite was correlated by Field (1975) with the Nichewaug sill and with the Belchertown pluton.

Microcline Porphyritic Granite

The microcline porphyritic granite intrudes the Hardwick Tonalite along the planes of foliation that commonly trend north-south. The distribution of the sills is shown in Figure 4. These granites occur only within the Hardwick Tonalite. The sills are up to 100 meters wide and may extend more than 2 km along strike. The intrusion of the granite along planes of foliation in the tonalite and the development of a tectonic foliation in the perimeters of the granite and throughout the granite intruding the southern portion of the tonalite suggests a syntectonic emplacement after intrusion of the tonalite. Field (1975), considered the granite a compositional variation of the Hardwick Tonalite although it has a casual similarity to the Coys Hill Granite.

Equigranular Biotite-Muscovite Granites

The equigranular biotite-muscovite granites are subordinate in amount to the tonalites in the immediate area of the Hardwick pluton. This contrasts with the tonalite to granite ratio in the Fitchburg Plutonic Complex in central Massachusetts where the tonalites are subordinate in amount to the granites and granite gneisses (Maczuga, 1981). The equigranular granites cut across the Hardwick Tonalite or intrude the country rock surrounding it, and appear to be younger.

The Sheep Rock intrusion of granite (Figures 4 and 6) intrudes the Augen Gneiss Member of the Partridge Formation and the Tom Swamp intrusion of granite (Figures 4 and 5) intrudes the Sulfidic Schist Member of the Partridge Formation. Contacts between these granites and the host rocks are always sharp. A tectonic foliation is faint at the perimeter, and rare in the interior of the granite intrusions. Although similar in appearance to the Concord Granite Member of the New Hampshire Plutonic Series, each intrusion has its own characteristic field appearance which is described in the next section.

The Fitzwilliam Granite intrudes the Hardwick Tonalite near the New Hampshire-Massachusetts border and contains inclusions of the Hardwick Tonalite and Kinsman Quartz Monzonite. Small sills similar in field appearance intrude the tonalite and commonly strike north-south. Correlated with the Concord Granite Member of the New Hamshire Plutonic Series, the Fitzwilliam Granite is considered post-Acadian because of its general lack of foliation, intrusive relationships and intrusive style (Nielson *et al.*,1976).

PETROGRAPHY

Petrographic Methods

In an attempt to evaluate compositional variability within the Hardwick Tonalite, the body was extensively sampled in the Athol and Petersham quadrangles and sampled to a lesser extent in the Ware, Barre, Royalston, Templeton and Winchendon quadrangles in Massachusetts and the Monadnock quadrangle in New Hampshire. Other rock types spatially associated with the tonalite were sampled to evaluate this association.

Standard petrographic thin-sections were used for microscopic examination of mineralogical and textural characteristics, and modal analysis of rock specimens. In order to differentiate rapidly and precisely among potassic feldspar, plagioclase, and quartz during modal analysis, most thin-sections were etched with hydrofluoric acid vapor under a vented hood and then stained with a saturated sodium cobaltinitrite solution. The potassium feldspars were stained yellow, plagioclase was etched to a grainy character and quartz was not etched or stained. To insure a precision of ± 2% at the 95% confidence level in the modal mineralogy, over 2000 points were counted per specimen during modal analysis (Van Der Plas, 1965). Modes of extremely coarse-grained rocks (porphyritic microcline granite) were determined by combining outcrop/slab determinations of the phenocryst/groundmass ratio with thin-section determinations of groundmass mode. A 7.5 by 11 inch transparent grid was used to measure the phenocryst/groundmass ratio. The etching and staining of the thin sections and groundmass-phenocryst integration technique insured precise application of the IUGS nomenclature (Streckeisen, 1973) and assisted in identifying modal variations within and between rock types.

HARDWICK TONALITE

Approximately 90% to 95% of the Hardwick pluton and associated plutonic rocks are composed of tonalite. The tonalite has been subdivided into hornblende-biotite tonalite, biotite tonalite, biotite-muscovite tonalite, and biotite-garnet tonalite. Hornblende-biotite tonalite predominantly occurs in north-south trending belts to the west and to the east of the center of the pluton (Figure 7). Biotite-muscovite tonalite and biotite-garnet tonalite are commonly situated within 1.0 km of the contact with the country rock. Biotite tonalite regularly occupies the center of the pluton and is located transitionally between the hornblende- and muscovite-bearing tonalites. Volumetrically, biotite tonalite is the dominant tonalite type. Contacts between tonalite types are gradational, suggesting that the units collectively represent a single intrusive sheet.

Hornblende-Biotite Tonalite

The field appearance of hornblende-biotite tonalite is extremely variable from light-gray, coarse-grained and massive to weakly foliated to dark gray, fine-grained and slabby. Color index ranges from 30 to 45.

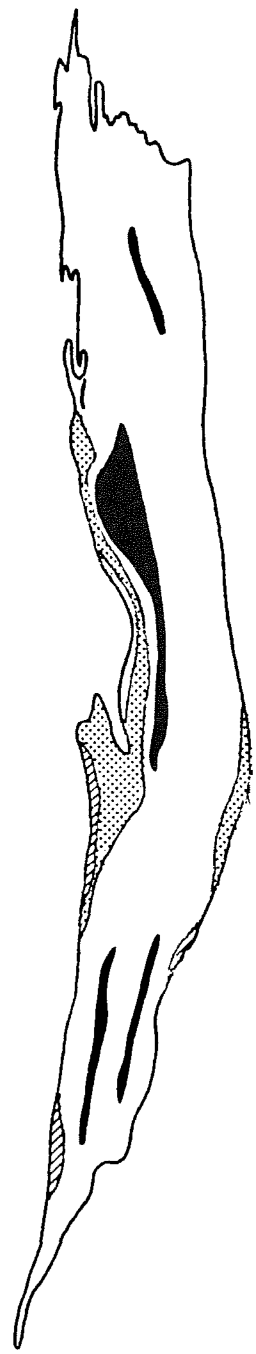

Figure 7. Distribution of rock types within the Hardwick Tonalite. Hornblende-biotite tonalite (black), biotite tonalite (white), biotite-muscovite tonalite (dotted), and biotite-garnet tonalite (lined).

Hornblende-biotite tonalite modes (Table 1) vary from 27 to 49% plagioclase, 5 to 22% quartz, 20 to 42% biotite, 0.3 to 20% hornblende and 0.0 to 3.8% potassic feldspar. The ratio 100 Pl/(Pl+Ksp) ranges from 91 to 100 and the ratio 100 Qz/(Qz+Fsp) ranges from 13 to 42. Primary accessory minerals include sphene, allanite, zircon, apatite, magnetite, ilmenite, pyrite, and pyrrhotite. Muscovite and clinozoisite occur locally as secondary accessory minerals. Goethite and chalcopyrite occur locally as alteration products of pyrite. Characteristics of mineral phases in the hornblende-biotite tonalite are outlined in Table 2. Modes from Table 1, plotted in Figure 8 in terms of quartz, plagioclase and potassic feldspar, show that these rocks are tonalites and quartz diorites as defined by the IUGS classification scheme (Streckeisen, 1973).

The tonalites have a variety of textures. The coarser-grained, weakly foliated types exhibit a holocrystalline, hypidiomorphic-granular texture with aggregates of mafic minerals (Figure 9a). A relict igneous texture is suggested. Within this type, plagioclase forms elongate grains which exhibit broad, normal zoning with uncommon oscillatory zoning, rare myrmekitic rims and well developed twinning. FeTi oxide rods are commonly in plagioclase cores. Hornblende commonly occurs in glomeroporphyritic clusters with biotite, sphene, and FeTi oxides. Biotite with Y=Z=red brown to brown is in tonalites possessing a relict igneous texture or is at contacts with pelitic country rock inclusions. In the former association, biotite either lacks pronounced orientation or defines a weak foliation.

At the other textural extreme (Figure 9b), the fine-grained, strongly foliated types exhibit a holocrystalline, allotriomorphic-granular texture. With increasing metamorphic recrystallization, plagioclase grains become increasingly smaller and equigranular, and optical zoning, twinning and FeTi oxide rods in plagioclase cores become increasingly scarce. Plagioclase grains which remain elongate are oriented parallel to foliation. The anorthite content in the plagioclase of the partially recrystallized tonalite is commonly less than the anorthite content of the igneous-textured tonalite. This is perhaps a result of clinozoisite- and sphene-forming metamorphic reactions.

With increasing metamorphic recrystallization, quartz forms a mosaic of interlocking grains with plagioclase and minor potassic feldspar or forms elongate mosaic aggregates. Hornblende is equally scattered throughout and there are no textural characteristics to suggest that hornblende is a replacement or alteration product of pyroxene. Biotite with Y=Z=green to brown is common and defines the prominent foliation. The thickness of clinozoisite rims around allanite and the abundance and thickness of the sphene rims around ilmenite increase with developing metamorphic texture. The modal abundance of oxides decreases with increasing metamorphic crystallization.

Biotite Tonalite

In outcrop the biotite tonalite of the Harwick Tonalite is typically moderately to strongly foliated with a massive to slabby appearance.

Table 1. Point-counted modes of hornblende-biotite tonalite.

	SW16	SB6	SW21	SA160-3	SA100-1	SA100-2	SP65-1
Quartz	12.1	21.0	13.2	17.0	19.2	20.3	11.2
Plagioclase	45.2	27.8	44.7	37.1	39.9	40.0	45.1
(mol.% An)	(38-32)*	(36-30)	(38-26)*	(34-26)*	(38)*	(36-24)*	(43)
Potassic Feldspar	0.9	0.5	2.4	3.8	1.2	0.9	0.6
Biotite	31.9	39.7	39.8	29.0	30.1	29.2	32.0
Hornblende	3.5	2.8	3.9	2.8	1.7	3.0	2.8
Sphene	0.8	3.5	1.4	2.8	1.9	1.8	2.6
Allanite	0.5	0.1	tr	0.2	tr	tr	0.4
Apatite	2.6	1.0	2.6	1.5	2.5	2.3	2.6
Zircon	tr	tr	tr	tr	tr	tr	tr
Opaque Minerals	2.5	1.8	2.1	0.3	1.9	2.4	1.0
magnetite	x	x	x	x	x	x	x
ilmenite	x	x	x	x	x	x	x
pyrite	x	x	x	x	x	x	x
pyrrhotite							
Muscovite		1.7			1.0		
Clinozoisite		0.2		5.5	0.2	0.1	1.7
Calcite					0.3		
100Pl/(Pl+Ksp)	98	98	95	91	97	98	99
100Qz/(Qz+Fsp)	21	43	22	30	32	33	20

	SW12	SA61-1	SA61-2	Athol	SP205	SA4	1056	1072
Quartz	13.9	5.0	12.3	22.2	9.5	13.1	11.8	20.3
Plagioclase	34.0	33.4	49.0	41.6	46.0	36.8	39.3	34.3
(mol.% An)	(36-28)*	(40)	(32)*	(42)	(51-35)	(39-27)	(46)	(42)
Potassic Feldspar	2.6	tr	0.6	0.4	2.1	tr	0.5	1.0
Biotite	38.9	31.8	30.9	20.8	33.5	31.2	42.2	36.5
Hornblende	5.9	20.1	0.4	9.9	0.3	11.9	1.7	2.7
Sphene	1.0	5.2	2.8	1.3	1.5	3.5	2.2	2.1
Allanite	0.3	tr	0.4	0.1	0.5	0.3	0.2	0.3
Apatite	2.0	2.8	2.2	1.2	3.5	2.1	1.0	2.1
Zircon	tr	tr	tr	0.1	tr	tr	tr	tr
Opaque Minerals	1.5	0.7	0.7	2.4	2.3	0.9	1.0	0.8
magnetite	x	x	x	x	x		x	x
ilmenite	x	x	x	x	x	x	x	x
pyrite	x	x	x	x	x	x	x	x
pyrrhotite						x		
Muscovite								
Cinozoisite	tr	0.9	0.9	0.1	0.6	tr		
Calcite						0.1	0.3	
100Pl/(Pl+Ksp)	93	100	99	99	96	100	99	97
100Qz/(Qz+Fsp)	28	13	20	35	17	26	23	36

Plagioclase composition determined by Michel-Levy extinction angle method and electron microprobe(*).

x opaque mineral observed in polished section.

Table 1, continued. Hand specimen descriptions and sample locations of hornblende-biotite tonalite.

SW16 Medium-grained, moderately foliated, gray tonalite. Ware 7.5-minute quadrangle. Southeast side of Poverty Hill at 1070 feet, 1.3 km north of Hardwick village.

SR6 Medium- to coarse-grained, weakly foliated, light gray tonalite. Aggregates of megacrysts are present. Royalston 7.5-minute quadrangle. South side of Winchendon Road, 10 meters east of intersection with New Boston Road.

SW21 Medium-grained, weakly foliated, gray tonalite. Ware 7.5-minute quadrangle. West side of Church Street, 0.35 km north of intersection with Goddard Road.

SA1060-3 Medium-grained, weakly foliated, gray to rusty tonalite. Athol 7.5-minute quadrangle. Along north side of Route 2, 150 meters west of Highland Road overpass.

SA100-1 Medium- to coarse-grained tonalite with weak to absent foliation. Along north side of Route 2, 50 meters east of Templeton Road underpass, west of Phillipston Reservoir.

SA100-2 Medium-grained, weakly foliated tonalite with rare biotite patches. Location same as SA100-1.

SP65-1 Massive, medium-grained, weakly foliated, dark gray tonalite. Ware 7.5-minute quadrangle. 0.55 km west of intersection of Old Gildertville Road and Route 32 on east side of hill at 850 feet.

SA61-1 Fine-grained, strongly foliated, dark gray tonalite. Athol 7.5-minute quadrangle. North side of railroad cut on Boston and Maine railroad line, 0.8 km east of Duck Pond, west end of outcrop.

SA61-2 Medium-grained, moderately foliated, dark gray tonalite. Same location as SA61-1, but at east end of outcrop.

Athol Medium- to coarse-grained, weakly foliated, dark gray tonalite. East side of Templeton Road, 75 meters north of Route 2 underpass, near Phillipston Reservoir.

SP205 Fine-grained, strongly foliated, dark gray tonalite. Petersham 7.5-minute quadrangle. Southside of intersection of Woodward Road and Carter Pond Road.

SA4 Medium- to coarse-grained, moderately foliated, dark gray tonalite. In contact with Partridge Formation rusty schist. Athol 7.5 minute quadrangle. Along north side of Route 2, 140 meters west of Highland Road underpass.

1056+00 Medium- to coarse-grained, weakly foliated, dark gray tonalite. Petersham 7.5-minute quadrangle. Quabbin Aqueduct Tunnel sample. 0.5 km east of Quabbin Aqueduct Tunnel-Jackson Road intersection.

1072+00 Coarse-grained, weakly foliated, dark gray tonalite. Petersham 7.5-minute quadrangle. Quabbin Aqueduct Tunnel sample. At Quabbin Aqueduct Tunnel-Jackson Road intersection.

Table 2. Characteristics of mineral phases in the Hardwick Tonalite.

	HORNBLENDE-BIOTITE TONALITE	BIOTITE TONALITE	BIOTITE-MUSCOVITE TONALITE	BIOTITE-GARNET TONALITE
PLAGIOCLASE	Anhedral to subhedral, to 3.7mm long, An_{51-22}, average composition An_{33}, normal and uncommon oscillatory zoning, rare myrmekitic rims, sericite and calcite alteration.	Anhedral to subhedral, to 4.5mm long, An_{52-24}, normal and oscillatory zoning, myrmekitic rims common, sericite alteration.	Anhedral to subhedral, to 3.6mm long, An_{45-21}, normal and oscillatory zoning, myrmekitic rims common, calcite and sericite alteration.	Equant and elongate subhedral, to 2.3mm, An_{38-28}, normal zoning.
POTASSIUM FELDSPAR	Microperthitic orthoclase, anhedral, to 2.0mm, Exsolution in groundmass grains rare.	Mildly perthitic to homogeneous orthoclase or microcline($2V_x$=80-85°), subhedral to anhedral grains from 1.5 to 4.5mm and interstitial grains from 0.1 to 1.2mm.	Microperthitic orthoclase or microcline, anhedral grains to 3.5mm and interstitial to 1.1mm.	Orthoclase without microscopic exsolution, anhedral and interstitial to 0.4mm.
QUARTZ	Anhedral grains to 1.8mm and interstitial, undulatory extinction common.	Anhedral grains to 2.6mm and interstitial, elongate, irregular aggregates, undulatory extinction common.	Anhedral and interstitial, elongate aggregates of polygonal grains to 3.5mm, undulatory extinction common.	Anhedral grains to 0.7mm and interstitial, multigrain clusters, undulatory extinction common.
HORNBLENDE	Subhedral to anhedral, to 1.5mm, moderate pleochroism X=yellow green to yellow brown, Y=green to brownish green, Z=green to blue green.			
BIOTITE	Subhedral to anhedral, to 3.6mm, X=tan, yellow green, Y=Z=red brown, brown, green.	Subhedral, to 4.6mm, X=pale brown, yellow brown, Y=Z=brown, red brown, partially altered to iron-rich chlorite.	Subhedral, to 1.8mm, X=yellow to yellow brown, Y=Z=red brown.	Subhedral, to 1.8mm, X=pale brown, Y=Z=red brown, partially altered to iron-rich chlorite.
MUSCOVITE			Subhedral to anhedral, to 0.7mm, independent grains and intergrown with biotite parallel to cross-cutting biotite cleavage.	Subhedral to anhedral, to 0.6mm, retrograde alteration of garnet and independent grains and intergrown with biotite parallel to cross-cutting biotite cleavage.
GARNET				Equant, euhedral to subhedral, 1.5 to 2.0mm, retrograde rim of muscovite and chlorite intergrowth.
SPHENE	Euhedral to subhedral, (221) polysynthetic twinning, also form anhedral rims around ilmenite, weak pleochroism, X=pale brown, Z=brown.	Euhedral to subhedral, (221) polysynthetic twinning, also forms anhedral rims around ilmenite, weak pleochroism, X=pale brown, Z=brown, hornblende inclusion in SP139.	Anhedral rims around ilmenite, weak pleochroism, X=pale yellow brown, Z=pale brown.	Anhedral rims around ilmenite uncommon.
ALLANITE	Anhedral to subhedral cores with euhedral to subhedral rims of clinozoisite, strong concentric zoning, partially to totally metamict, moderate pleochroism X=light orange, Z=brown orange.	Anhedral to subhedral cores with euhedral to subhedral rims(0.1mm) or clinozoisite, strong concentric zoning, partially to totally metamict, moderate pleochroism X=light orange, Z=orange.	Anhedral to subhedral cores with euhedral to subhedral rims of clinozoisite, strong concentric zoning, partially to totally metamict, moderate to weak pleochroism, X=light orange, Z=orange.	
OXIDES	ilmenite + magnetite ilmenite: subhedral to anhedral, homogeneous or with lamellae of titanohematite, bireflectant tan to pink. magnetite: equant, subhedral homogeneous grains.	ilmenite $\pm$ magnetite ilmenite: subhedral to anhedral grains, to 0.6mm, homogeneous or with lamellae of titanohematite, bireflectant tan to pink. magnetite: equant, subhedral, homogeneous grains.	ilmenite: subhedral to anhedral, to 0.5mm, minor titanohematite exsolution, bireflectant tan to pink.	ilmenite: subhedral to anhedral, titanohematite exsolution rare, bireflectant tan.
APATITE	Euhedral, elongate prisms, and subhedral hollow prisms.	Euhedral prisms.	Euhedral prisms.	Rare, equant grains with biotite.
ZIRCON	Minute inclusions in biotite and hornblende.	Minute inclusions in biotite.	Minute inclusions in biotite.	Minute inclusions in biotite.
SULFIDES	Euhedral pyrite intergrown with chalcopyrite, pyrrhotite near contact with Partridge Formation inclusions (SA4).	Euhedral pyrite intergrown with chalcopyrite, anhedral pyrrhotite coexists with pyrite and ilmenite in several samples.	Euhedral pyrite intergrown with chalcopyrite, anhedral pyrrhotite coexists with pyrite and ilmenite in several samples.	Minor euhedral to subhedral pyrite $\pm$ anhedral pyrrhotite.

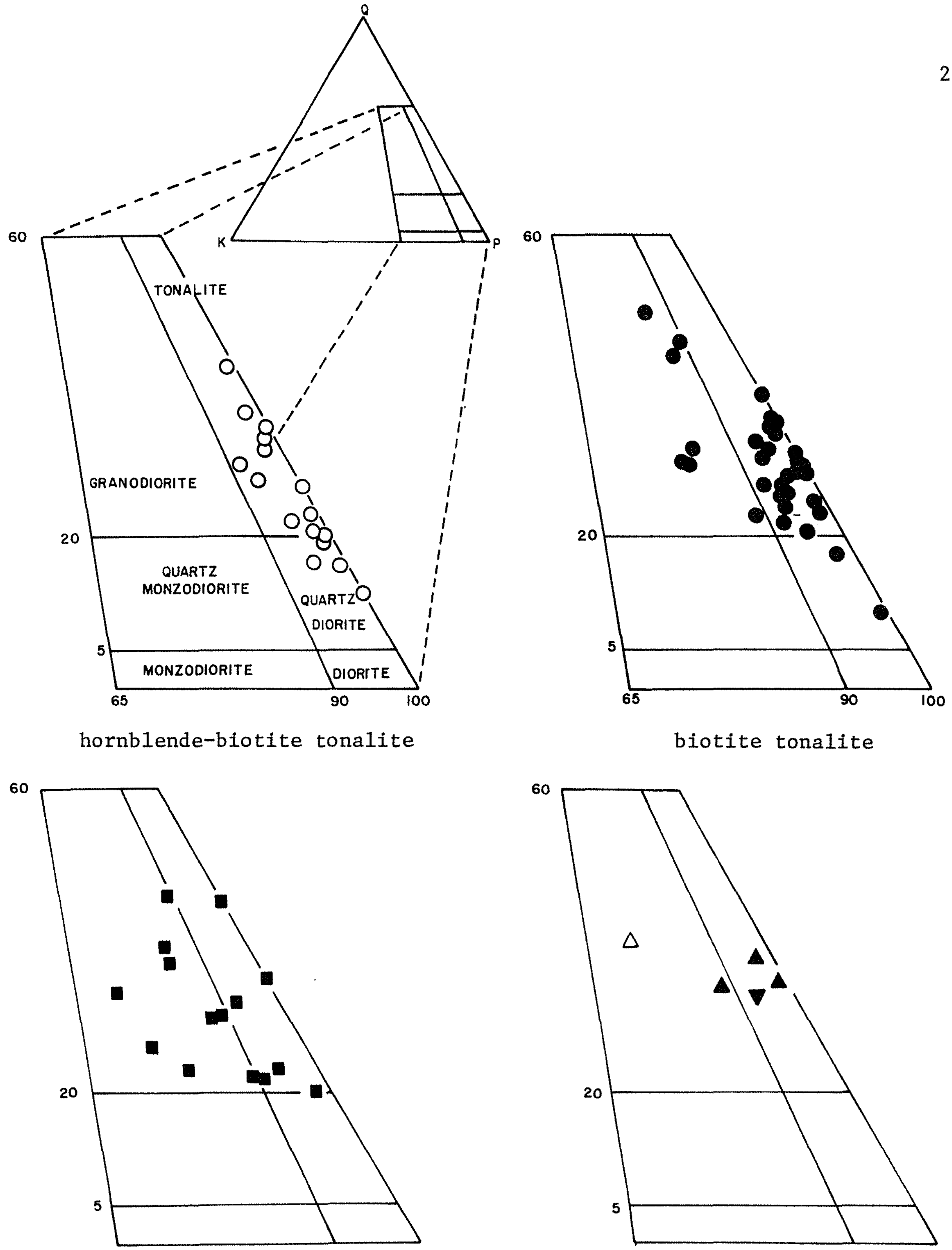

hornblende-biotite tonalite

biotite tonalite

biotite-muscovite tonalite

biotite-garnet tonalite (▲), mylonite (△), tonalite matrix (▼).

Figure 8. Quartz-Plagioclase-K-Feldspar plot of modes of the various rock types of the Hardwick Tonalite.

(a)

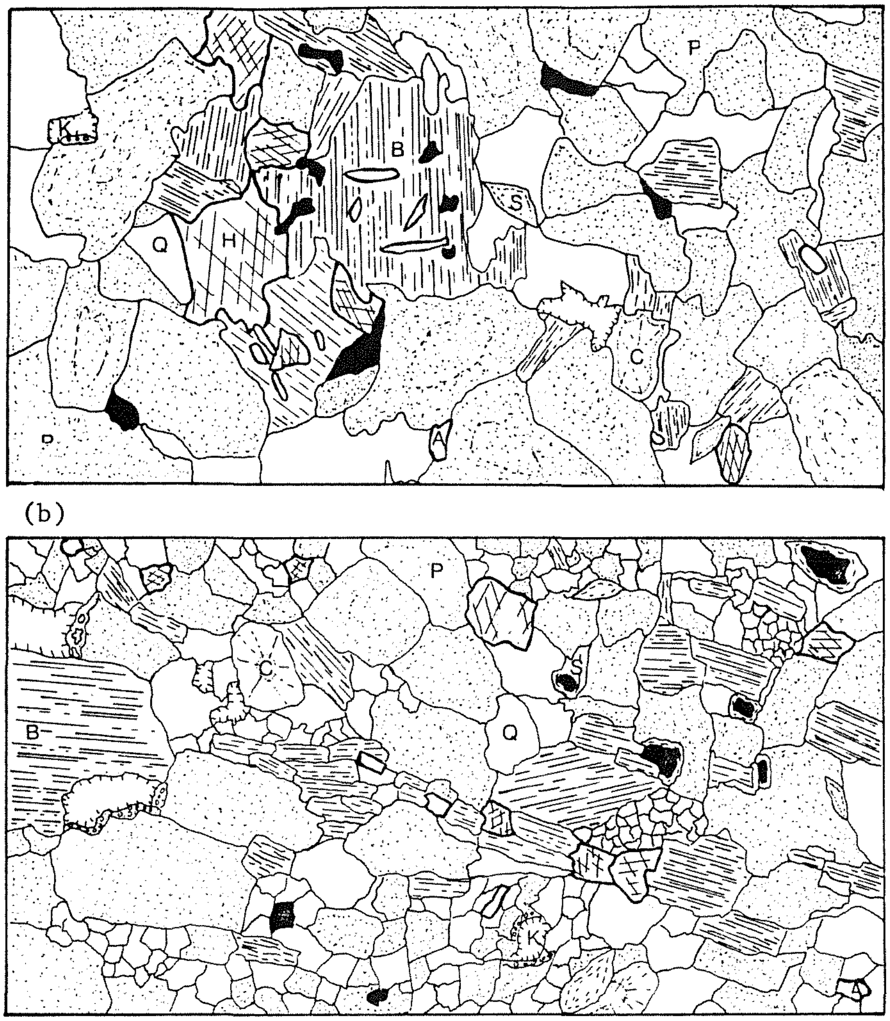

Figure 9. Textural features of hornblende-biotite tonalite. (a) Relict igneous texture. C:allanite with clinozoisite rim, B:biotite, Q: quartz, S:sphene, P:plagioclase, A:apatite, H: hornblende, K:potassium feldspar, and dark minerals:ilmenite and magnetite. (b) Partially recrystallized metamorphic texture.

Medium to dark gray in color (color index 19 to 47), the biotite tonalite characteristically contains "phenocrysts" 2 to 4 mm across of plagioclase, potassic feldspar or aggregates of quartz and/or feldspar immersed in a dark "biotite-rich" matrix. The plagioclase "phenocrysts" are modally the most abundant.

Biotite tonalite modes (Table 3) vary from 29 to 53% plagioclase, 4 to 36% quartz, 0.0 to 9% potassic feldspar (microcline or orthoclase), and 19 to 46% biotite. The ratio 100 Pl/(Pl+Ksp) ranges from 80 to 100. The ratio 100 Qz/(Qz+Fsp) ranges from 10 to 46. Sphene, allanite, magnetite, ilmenite, pyrite, pyrrhotite, apatite and zircon occur as primary accessory minerals. Muscovite, chlorite, clinozoisite, sphene, and calcite are secondary. Characteristics of mineral phases in the biotite tonalite are outlined in Table 2. Modes from Table 3 plotted in Figure 8, in terms of quartz, plagioclase, and potassic feldspar, show that these rocks are primarily tonalites but also granodiorites and quartz diorites as defined by the IUGS classification scheme (Streckeisen, 1973).

The biotite tonalite exhibits holocrystalline, hypidiomorphic to allotriomorphic texture. The latter texture is associated with the fine, strongly foliated varieties. The well developed glomeroporphyritic texture commonly exhibited by the hornblende-biotite tonalite is poorly developed to absent and has been replaced in abundance by a lepidoblastic texture defined by biotite and elongate plagioclase grains.

The larger plagioclase phenocrysts are commonly surrounded by a mosaic-textured irregular rim less than 0.8 mm wide composed predominantly of plagioclase and quartz with minor potassic feldspar and biotite. This rim is wider and better developed in those rocks which are strongly foliated. In allotriomorphic textured biotite tonalite, the quartz forms a mosaic of irregular interlocking grains. In the highly recrystallized rocks, secondary sphene forms anhedral rims around ilmenite, and clinozoisite forms rims around allanite. Clinozoisite is also associated with the larger sericitized plagioclase. Ilmenite is the prevailing FeTi oxide in the biotite tonalite, although in a few samples it coexists with magnetite. The modal abundance of ilmenite decreases with increasing recrystallization.

Biotite-Muscovite Tonalite

The field appearance of biotite-muscovite tonalite is nearly identical to that of the biotite tonalite. Outcrops are massive to slabby and contain feldspar phenocrysts immersed in a dark matrix giving the rock a mottled look. Whereas in the biotite tonalite, plagioclase composes a majority of the phenocrysts, the phenocrysts of the biotite-muscovite tonalite are composed of plagioclase and potassic feldspar in nearly equal proportions. The biotite-muscovite tonalite is slightly lighter in color (color index 15 to 30) than the biotite tonalite and muscovite is commonly visible in hand-specimen. Biotite-muscovite tonalite is distinguished from biotite tonalite with secondary muscovite by the textural character of the muscovite. Independent, coarse, subhedral, cleanly terminated grains or coarse, subhedral, cleanly terminated grains closely associated with biotite are considered primary. Ragged,

Table 3. Point-counted modes of biotite tonalite.

	SR5	SM7	SW22	SW11-2	SA13	SP87	SW1-1	SW1-2	SR4	SA40	SW19	SA3-2	SP3	SW18	SR7
Quartz	16.3	23.1	20.6	19.8	20.2	13.0	34.6	35.8	14.8	19.2	15.3	16.6	23.6	14.5	14.1
Plagioclase	41.2	43.6	37.5	41.3	35.5	41.7	38.1	36.9	53.2	30.2	45.2	38.1	41.5	37.1	31.5
(mol.% An)	(51-35)	(33-27)*	(35-26)	(36-25)	(37-31)	(35)	(42-27)	(43-31)	(35-28)	(41)	(39-29)*	(35)*	(29-23)*	(52-43)*	(32-27)
Potassic Feldspar	4.0	11.2	0.5	2.2	0.9	3.4	5.1	4.6	3.2	0.2	0.7	0.1	tr	0.6	tr
Biotite	33.1	19.5	33.3	31.9	36.0	34.1	19.6	20.7	24.9	43.2	38.0	38.1	30.2	41.8	46.6
Sphene	2.5	0.7	tr	1.3	2.8	3.5			1.6	3.9	tr	2.2	0.4	tr	3.1
Allanite	tr	0.1		0.2	0.2	tr			tr	0.1		0.2	0.4	tr	0.3
Apatite	1.1	0.5	1.3	2.6	2.1	1.8	1.0	0.7	1.1	2.2	tr	2.9	1.0	1.9	1.9
Zircon	0.1	tr	tr	0.3	0.2	tr	0.1	tr	tr	0.3	tr	tr	0.2	0.5	1.1
Opaque Minerals	1.5	0.6	2.9	0.4	0.8	0.3	0.4	0.6	0.3	0.7	0.8	1.7	0.2	3.6	1.3
magnetite															
ilmenite	x	x	x	x	x	x	x	x	x	x	x	x	x	x	x
pyrite	x		x	x	x	x		x	x	x	x	x	x	x	
pyrrhotite				x		x								x	
Muscovite	0.2	0.3	1.7	tr	1.1	2.1	1.2	0.8	0.6			0.2			
Chlorite	tr	tr	0.2								tr				
Clinozoisite	tr	0.4		tr	0.1				0.4			0.1			
Calcite															
100Pl/(Pl+Ksp)	91	80	99	95	99	92	88	89	94	99	99	100	100	98	100
100Qz/(Qz+Fsp)	27	30	35	31	36	22	44	46	21	39	25	30	36	28	31

Plagioclase composition determined by Michel-Levy extinction angle method and electron microprobe(*).

x opaque mineral observed in polished section.

Table 3, continued.

	SP322	SP139-21	SP139-22	SP139-23	SR2	SR3	SP146	ST2	SB2	SP186	SA402	SM1-1	SP2	SA45	1087-50	1037-00	972-50
Quartz	19.5	16.9	18.0	17.2	21.1	18.0	4.8	13.7	10.1	21.9	15.2	19.1	20.2	12.1	20.7	19.9	23.5
Plagioclase	36.4	46.0	45.5	47.1	40.9	45.0	44.9	41.1	44.0	42.1	45.7	38.3	37.5	40.0	40.1	48.5	41.6
(mol.% An)	(34-30)	(35-28)*	(36-30)*	(32)	(34)	(37-29)	(32-28)	(45-36)	(45-25)	(30-26)*	(32-23)	(29)	(38-32)*	(40-32)	(34)	(31)	(34-15)*
Potassic Feldspar	0.7	3.2	2.4	2.6	0.6	0.4	0.7	5.5	1.1	2.3	3.4	1.5	0.8	0.8	9.3	1.6	8.5
Biotite	39.4	29.6	29.5	29.1	32.4	30.1	41.1	32.6	41.0	28.5	31.6	36.8	35.3	41.7	23.9	24.3	23.7
Sphene	0.7	2.1	2.0	1.7	1.3	3.5	0.7	3.7	0.8	0.1	2.6	1.3	2.6	3.2	0.1	2.0	tr
Allanite	0.4	0.2	0.3	0.3		0.5	0.6	0.2	tr	0.1		tr	tr	tr	tr	0.3	
Apatite	2.4	1.4	1.3	1.1	2.5	1.9	1.9	2.2	1.3	2.5	0.8	2.0	2.9	1.5	2.3	1.8	1.2
Zircon	tr	tr	0.3	0.1	tr	tr	0.2	0.2	tr	0.1	tr	0.1	tr	0.4	tr	0.1	0.1
Opaque Minerals	0.7	0.7	0.8	0.9	0.1	tr	2.7	0.6	1.7	2.4	0.8	0.8	0.8	0.3	3.4	1.0	1.2
magnetite		x	x	x									x				
ilmenite	x	x	x	x	x	x	x	x	x	x	x	x	x	x	x	x	x
pyrite	x	x	x	x	x		x	x	x	x	x	x		x	x	x	x
pyrrhotite																	
Muscovite						0.5	0.1		tr			0.1			0.4	0.7	0.3
Chlorite		tr	tr	tr			tr										
Clinozoisite		tr	tr	tr	1.1	0.1	1.1	0.2					tr		tr		
Calcite							1.3										
100Pl/(Pl+Ksp)	98	94	95	95	99	99	98	88	98	95	93	96	98	98	81	97	83
100Qz/(Qz+Fsp)	35	26	27	26	34	29	10	23	18	33	24	32	35	23	30	28	32

Table 3, continued. Hand specimen descriptions and sample locations for biotite tonalite.

SR5 Medium-grained, weakly foliated, drak gray tonalite. Royalston 7.5-minute quadrangle. North side of Winchendon Road, west of intersection with Stone Road at 910 contour.

SM7 Medium- to coarse-grained, weakly foliated, light gray granodiorite. Mt. Monadnock 15-minute quadrangle. Quarry south of Boston-Maine railroad line west out of the Fitzwilliam depot.

SW22 Fine-grained, strongly foliated, dark gray to rusty tonalite. Ware 7.5-minute quadrangle. 400 meters southwest of intersection of Cezesky Road and Patrill Hollow Road at 950 contour on north side of hill.

SWi-1-2 Fine-grained, moderately foliated, dark gray tonalite with aggregates of quartz and potassic feldspar. Winchendon 7.5-minute quadrangle. 500 meters south of Birch Hill Dam, south side of Boston and Maine railroad cut.

SA13 Coarse-grained, weakly foliated, gray tonalite. Athol 7.5-minute quadrangle. On north side of Route 2, 300 meters east of Route 2 - Highland Road overpass.

SP87 Medium-grained, weakly to moderately foliated, light gray tonalite. Petersham 7.5-minute quadrangle. 850 meters northeast of Route 32 and Butterworth Road intersection east side of hill at 1100 contour.

SW1-1 Coarse-grained, strongly foliated, gray tonalite. Cliff just west of Mara Road at 730 contour. Ware 7.5-minute quandrangle.

SW1-2 Description and location is the same at SW1-1.

SR4 Medium-grained, weakly foliated, gray tonalite. Royalston 7.5-minue quadrangle. Large flat outcrop on south side of Route 68, 1.2 km west of South Royalston.

SA40 Medium-grained, strongly foliated, dark gray tonalite. Intruded with many pegmatites. Athol 7.5-minute quadrangle. 1 ms south on Whitney Road, on east side at 1180 contour.

SW19 Fine-grained, moderately foliated, dark gray tonalite. Ware 7.5-minute quadrangle. West side of Old Gilbertville Road, 1.5 km norht of Reservoir at 800 contour.

SA3-2 Coarse-grained, weakly foliated, dark gray tonalite. Athol 7.5-minute quadrangle. South side of Route 2, 240 meters east of Route 2 - Highland Road overpass.

SP3 Massive, medium grained, moderately foliated, dark gray tonalite. Aggregates of quartz and potassic feldspar and thin felsic streaks Petersham 7.5-minute quadrangle. East of Ridge Hill Road at 1150 contour on southern most portion of Ridge Hill.

SW18 Medium-grained, weakly foliated tonalite. Associated with thin (2 cm) pegmatites. Ware 7.5-minute quadrangle. West side of Gilbertville Road, 0.6 km north of Reservoir.

SR7 Massive, fine-grained tonalite with coarse-grained biotite giving the rock a speckled appearence. soyalston 7.5-minute quadrangle. North side of Winchendon Road, 0.6 km west of Turnpike Road.

SP322 Fine-grained, strongly foliated tonalite. Petersham 7.5-minute quadrangle. On east side of Spooner Road, 0.7 km north of the Taylor cemetery.

SP139-21 Medium-grained, strongly foliated, dark gray tonalite. Petersham 7.5-minute quadrangle. NNW side of Sherman Hill at 1110 contour.

SP139-22 Description and location same as SP139-21

SP139-23 Description and location same as SP139-21

SR3 Massive to lightly foliated, coarse grained, light gray tonalite. Royalston 7.5-minute quadrangle. On Route 68, 0.9 km west of South Royalston center.

SP146 Medium-grained, strongly foliated, dark gray tonalite. Petersham 7.5-minute quadrangle. On south side of Dana Road, 0.4 km east of Cleveland Road.

ST2 Coarse- to medium-grained, lightly foliated, dark gray tonalite. Templeton 7.5-minute quadrangle. Between east-west lanes of route 2, 101 km NW of Brooks Village.

SB2 Medium-grained, strongly foliated, dark gray to black tonalite. Barre 7.5-minute quadrangle. North side of Baldwin Road, 0.4 km east of intersection with Hawes Hill Road

SP186 Fine-grained, strongly foliated, dark gray tonalite. Petersham 7.5 minute quadrangle. Along utility poles, 0.35 km west of Cleveland Road at 1080 contour.

SA402 Coarse- to medium-grained, strongly foliated tonalite. Athol 7.5 minute quadrangle. East side of Searle Hill at 1230 contour.

SM1-1 Coarse-grained, lightly foliated, light gray granodiorite. Monadnock 15-minute quadrangle. North side of Route 124, south of Marlborough.

SP2 Medium-grained, massive, dark gray tonalite with minor associated pegmatite. Petersham 7.5 minute quadrangle. On Thresher Road, 0.4 km east of intersection with Petersham Road.

SA45 Fine-grained, strongly foliated, dark gray tonalite. Athol 7.5-minute quadrangle. SE side of hill at 1110 contour, located 1.1 km NNW of Popple Camp Road crossing of the East Branch of the Swift River.

1087-50 Coarse-grained, lightly foliated, drak gray tonalite. Petersham 7.5-minute quadrangle. Quabbin Aqueduct specimen, 0.4 km west of Jackson Road.

1037-00 Coarse-grained, moderately foliated, dark gray tonalite. Petersham 7.5-minute quadrangle. Quabbin Aqueduct specimen, 0.25 km west of North Road.

972-50 Medium- to fine-grained, strongly foliated, dark gray to black tonalite. Petersham 7.5-minute quadrangle. Quabbin Aqueduct specimen, 0.4 km west of Jewett Road.

subhedral to anhedral grains associated with plagioclase or potassic feldspar are clearly a product of hydrous alteration of feldspar.

Modes of the biotite-muscovite tonalite (Table 4) plotted in Figure 8 are equally distributed in the tonalite and granodiorite regions of the IUGS classification scheme (Streckeisen, 1973). The major mineral content of the biotite-muscovite tonalite ranges from 12 to 30% quartz, 23 to 46% plagioclase, trace to 14% potassic feldspar, 17 to 32% biotite and trace to 7% muscovite. The ratio 100 Pl/(Pl+Ksp) ranges from 72 to 100 and the ratio 100 Qz/(Qz+Fsp) ranges from 20 to 46. Primary accessory phases include allanite, ilmenite, apatite, zircon, pyrite and pyrrhotite. Secondary accessory minerals include chlorite, sphene, clinozoisite and calcite. Characteristics of mineral phases in the biotite-muscovite are outlined in Table 2.

The texture of the biotite-muscovite tonalite varies from hypidiomorphic granular to allotriomorphic granular. The former texture may contain distinct clusters of biotite and has been interpreted as a relict igneous glomeroporphyritic texture. The latter textural type approaches a lepidoblastic to granoblastic texture of metamorphic origin.

In those rock with an interpreted relict igneous texture, the biotite defines the glomeroporphyritic texture occurring as clusters with sphene, apatite, and ilmenite. The muscovite is commonly intergrown with the biotite approximately parallel to or cross-cutting biotite cleavage. Quartz is interstitial to anhedral.

In those rocks with a more metmorphic, recrystallized texture, the biotite along with muscovite defines the foliation. Quartz commonly forms elongate aggregates of polygonal grains.

Ilmenite is the only FeTi oxide in the biotite-muscovite tonalite. Sphene most commonly occurs as rims around ilmenite and biotite and is considered metamorphic in origin.

To the east of the eastern edge of the Hardwick pluton, in rock cuts on Route 2 in Templeton, there is a 5-7 m layer which contains 4 to 50 cm blocks of fine-grained gray granite and coarse-grained pegmatite immersed in a fine- to medium-grained matrix of tonalitic appearance. The fine-grained granite blocks are dominant in abundance. The shapes of the blocks are ovoidal, although a few have a more irregular shape. Contacts between the felsic blocks and the matrix is sharp. This layer, the only one of its type yet described within central Massachusetts, has been interpreted as a conglomerate, as a fault breccia in which the felsic blocks are relict dikes of granite and pegmatite, and as an intrusive breccia within a small tonalite sill associated with the Hardwick pluton. A point-counted mode (ST3) for the matrix is presented in Table 5 and plotted in Figure 8. The matrix is defined as a tonalite based on the IUGS classification scheme (Streckeisen, 1973) and is similar to many of the tonalite members of the Hardwick Tonalite. The tonalite matrix is equigranular with a grain size between 0.1 and 1.0 mm for major phases. Plagioclase forms subhedral, equant, well twinned grains with a composition of An_{33}. Orthoclase is interstitial to anhedral and is perthitic

Table 4. Point-counted modes of biotite-muscovite tonalite.

	SA250-1	SA251	SB1	SP233-1	SP233-2	SP233-3	SA19	SM5	SB3	SP265	SP55	SA119	SP10-1	SP10-2	SM6
Quartz	19.6	11.8	22.6	14.0	15.0	15.1	29.8	21.0	29.9	16.4	30.0	21.1	21.2	21.7	24.4
Plagioclase	42.8	46.8	32.1	45.6	46.6	46.3	38.6	43.0	31.6	43.8	36.8	40.9	43.9	42.9	36.4
(mol.% An)	(32-23)*	(30-22)	(34-22)*	(33-24)	(36-24)	(33-26)	(31)	(45-26)	(38)	(41-28)	(35-28)*	(33-24)	(35-30)*	(32-26)	(38-27)
Potassic Feldspar	13.8	1.2	6.6	4.9	3.4	5.0	7.9	5.0	4.2	10.7	tr	0.5	5.7	3.5	14.3
Biotite	17.0	32.1	32.8	29.9	27.53	28.5	18.4	26.6	31.5	21.2	27.9	32.4	24.7	25.8	21.9
Muscovite	6.7	4.6	3.6	1.3	2.3	1.7	3.0	0.9	1.3	3.6	0.5	0.6	1.1	0.7	0.1
Sphene	tr		0.2	2.1	2.2	2.0	0.6	1.2	tr	0.5	0.7	1.6	0.2	0.2	1.0
Allanite				0.4	0.6	0.2	0.7		0.8	0.7	0.5	0.5	0.4	1.5	0.7
Apatite	0.1	1.6	1.1	1.0	1.1	0.7	0.8	1.8	0.5	1.1	2.2	1.4	1.0	1.0	0.7
Zircon	tr	0.4	0.1	0.2	0.1	tr	tr	tr	tr	tr	tr	tr	tr	tr	0.1
Opaque Minerals	0.1	0.4	1.0	0.5	1.0	0.5	0.3	0.5	0.3	2.1	1.3	1.0	1.4	1.5	0.3
magnetite															
ilmenite	x	x	x	x	x	x	x	x	x	x	x	x	x	x	x
pyrite	x	x	x	x	x	x	x	x	x	x	x	x	x	x	x
pyrrhotite	x	x													
Chlorite				tr	tr	tr									
Clinozoisite				0.1	0.3	0.1	tr			0.1	0.1	0.1	0.3	1.0	
Calcite		1.2													
100Pl/(Pl+Ksp)	76	98	83	90	93	90	83	90	88	80	100	99	89	93	72
100Qz/(Qz+Fsp)	26	20	37	22	23	23	39	30	46	23	45	35	30	32	33

Plagioclase composition determined by Michel-Levy extinction angle method and electron microprobe(*).

x opaque mineral observed in polished section.

Table 4, continued. Hand specimen descriptions and sample locations for biotite-muscovite tonalite.

SA250-1 Coarse-grained, strongly foliated, light gray colored tonalite-granodiorite. Athol 7.5-minute quadrangle. South side of Route 2, 0.7 km east of Petersham Road exit.

SA251 Coarse-grained, moderately to strongly foliated, light gray colored granodiorite. Athol 7.5-minute quadrangle. 115 meters south of Reservoir No. 1, on south side of Route 2.

SB1 Medium-grained, strongly foliated, dark gray colored tonalite. Barre 7.5-minute quadrangle. 0.6 km east of Hardwick Road on north side of Route 32.

SP233-1 Medium-grained, strongly foliated, gray colored tonalite with 0.5 cm allanite. Petersham 7.5-minute quadrangle. 0.75 km north of Betterworth Road-Dana Road intersection.

SP233-2 Sample description and location same as SP233-1

SP233-3 Sample description and location same as SP233-1

SA19 Medium-grained, moderately foliated, dark gray tonalite. Athol 7.5-minute quadrangle. Cliff SW side of Pratt Hill at 1150 contour.

SM5 Medium-grained, lightly foliated, gray tonalite. Monadnock 15-minute quadrangle. Quarry 0.2 km south of Boston-Maine RR line, 1.6 km west of Fitzwilliam center.

SB3 Medium-grained, strongly foliated, gray colored tonalite. Barre 7.5-minute quadrangle. West side of SW corner of Old Reservoir at 1050 contour.

SP265 Medium-grained, moderately foliated tonalite interlayered with pegmatite. Petersham 7.5-minute quadrangle. 0.65 km south of Russell Road-Route 32 intersection at 1000 contour.

SP55 Massive, equigranular, gray colored tonalite. Petersham 7.5-minute quadrangle. North side of East Street, 125 meters west of Ledgeville Cemetary.

SA119 Coarse-grained, moderately foliated, gray tonalite. Athol 7.5-minute quadrangle. 0.2 km west of Round Top at 1100 contour

SP10-1 Medium-grained, moderately foliated, dark gray tonalite. Petersham 7.5-minute quadrangle. Cliff of ridge west side of Route 32, west of Conner Pond.

SP10-2 Sample description and location same as SP10-1

SM6 Sample description and location same as SM5.

Table 5. Point-counted modes of biotite-garnet tonalite (SA54-1, SA54-2, and SP43), mylonitized tonalite (FW992-B) and tonalite matrix of the "intrusive breccia" on the east side of the Hardwick Pluton (ST3).

	SA54-1	SA54-2	SP43	Mylonite FW992-B	Breccia Matrix ST3
Quartz	23.9	24.3	25.2	18.0	21.1
Plagioclase	42.4	38.7	44.3	19.9	40.0
(mol.% An)	(38)	(40-28)*	(32)	(26)	(33)
Potassic Feldspar	0.6	1.6	3.2	17.3	3.0
Biotite	25.9	27.1	13.4	36.0	31.8
Garnet	2.0	2.6	7.8		
Muscovite	2.1	2.4	3.7		2.5
Sphene	0.2	tr	0.4	1.5	0.3
Allanite			0.3	5.9	
Apatite	0.3	0.1	0.4	0.7	0.8
Opaque Minerals	1.8	2.2	0.9	0.7	0.3
magnetite				x	
ilmenite	x	x	x		x
pyrite	x		x		x
pyrrhotite	x				
Chlorite	0.5	1.2	0.4		
Clinozoisite				1.0	
Calcite					0.2
100Pl/(Pl+Ksp)	99	96	93	54	93
100Qz/(Qz+Fsp)	35	38	34	40	33

Plagioclase composition determined by Michel-Levy extinction angle method and electron microprobe(*).

x opaque mineral observed in polished section.

Table 5, continued. Hand specimen descriptions and sample locations for biotite-garnet tonalite, mylonitized tonalite and tonalite matrix of the "intrusive breccia".

SA54-1 Medium-grained, moderately foliated, dark gray tonalite with 0.5 to 1.0 cm garnets. Athol 7.5-minute quadrangle. Top of hill, north side of Popple Camp Road, 1.7 km east of Petersham Road.

SA54-2 Sample description and location same as SA54-1

SP43 Fine-grained, strongly foliated, dark gray tonalite with 0.2 to 0.5 cm garnets. Petersham 7.5-minute quadrangle. 0.1 km NW of Carter Road-Woodward Road intersection at 800 contour.

FW992-B Fine-grained, strongly developed mylonite texture in this gray tonalite. Monson 7.5-minute quadrangle. Specimen collected by M.T. Field (1975)

ST3 Medium- to fine-grained, moderately foliated, dark gray to black tonalite. Templeton 7.5-minute quadrangle. South side of Route 2, 0.8 km NW of Brooks Village.

(0.2 mm, An_7). Quartz occurs in polycrystalline clusters to 1.8 mm in length or as anhedral grains. Biotite defines the foliation in the rock and has a pleochroic scheme X=yellow brown and Y=Z=red brown. Muscovite is closely associated with the biotite and occurs as discrete grains. Apatite occurs as equant crystals and is evenly dispersed throughout the rock. Ilmenite forms subhedral to anhedral, homogeneous grains.

In conclusion, based on the mineralogical and textural similarity between the matrix and the biotite-muscovite tonalite, and the absence of a texture that is suggestive of severe tectonic deformation, it is proposed that this outcrop represents an intrusive breccia.

Biotite-Garnet Tonalite

Outcrops of the biotite-garnet tonalite typically appear to be dark gray and fine-grained or light gray and medium-grained and are massive to slabby. In the Ware and Petersham quadrangles, the slabby nature is typical and tonalites may be interlayered with gray schist of the Littleton Formation. Feldspar "phenocrysts" characteristic of the other members of the Harwick Tonalite are rare, but garnets up to 4 mm in diameter are visible in outcrop. Color index ranges from 10 to 30.

The texture of these tonalites is generally hypidiomorphic-granular with biotite, muscovite, and elongate plagioclase defining a moderate to strong foliation. Quartz ranges from 23 to 25%, plagioclase ranges from 38 to 44%, potassic feldspar ranges from 0.6 to 3.2%, biotite ranges from 13 to 27%, muscovite ranges from 2 to 4%, and garnet ranges from 2 to 8%. The ratio 100 Pl/(Pl+Ksp) varies from 93 to 99 and the ratio Qz/(Qz+Fsp) varies from 34 to 38. Based on the ratio of plagioclase: potassic feldspar: quartz (Figure 8) these rocks are tonalites and granodiorites as defined by the IUGS classification scheme (Streckeisen, 1973). Ilmenite is the only FeTi oxide in the biotite-garnet tonalite. Apatite forms rare equant grains and unlike the other members of the Hardwick Tonalite, allanite and clinozoisite are absent. Other primary accessory minerals include pyrite, pyrrhotite, and zircon. Secondary accessory phases include sphene and chlorite. Muscovite is primary, secondary, or absent form the assemblage. Characteristics of the mineral phases are presented in Table 2.

Mylonite

In the Ware quadrangle, the Hardwick Tonalite becomes increasingly narrow, finally terminating into a 20-meter-wide mylonite zone. Mylonitic streaking is common in the tonalite, particularly along the west contact in the Ware quadrangle and the southern portion of the Petersham quadrangle. The mylonites are fine-grained, dark gray to black and commonly have a laminated fabric, and usually contain porphyroclasts of microcline, plagioclase, and quartz. In hand specimens, microcline porphyroclasts are the most obvious.

The mylonite texture is defined by ovoid to partially granulated relict crystals of plagioclase, microcline, quartz, and allanite in a fine-grained schistose matrix of biotite, quartz, plagioclase, and microcline. An estimated mode of a mylonite from the 20 meter wide mylonite zone (FW992B) is presented in Table 5. As shown in Figure 8, this mode plots in the granodiorite field of the IUGS classification scheme (Streckeisen, 1973).

Plagioclase porphyroclasts are anhedral, range in size between 0.6 and 1.6 mm and have a composition of An_{25}. Ovoidal porphyroclasts of microcline range in size from 1.3 to 4.0 mm and do not exhibit microscopic exsolution texture. Elongate quartz porphyroclasts ranging in size up to 5.0 mm in length consist commonly of polycrystalline aggregates. Undulatory extinction is displayed by the quartz; commonly as bands parallel to the c axis. Plagioclase, microcline and quartz are also abundant in the fine-grained matrix (less than .01 mm).

Biotite is restricted to the matrix of the mylonite (to 0.26 mm) forming ragged anhedral to subhedral grains. The pleochroic scheme of the biotite is X=pale brown, and Y=Z=brown.

Pleochroic allanite (X=yellow orange to brown orange and Z=brown) forms anhedral grains to 1.8 mm which are rimmed by euhedral to subhedral clinozoisite (X=colorless, and Z=pale yellow green). The formation of the epidote rims clearly follows the mylonitization.

Anhedral to subhedral sphene ranges in size from 0.2 to 1.8 mm. Opaque minerals include magnetite and rutile. The magnetite is homogeneous and forms grains up to 1.4 mm. Rutile, a product of secondary alteration of ilmenite, occurs as anhedral grains to 0.3 mm in size.

Summary of Petrography of the Hardwick Tonalite and Petrographic Evidence for Magma Origin

The Hardwick Tonalite exhibits a continuous variation in mineralogical indicators of alumina saturation, from the metaluminous hornblende-bearing tonalite to the intermediate biotite tonalite to the peraluminous muscovite- and garnet-bearing tonalites.

As shown in Figure 8, the hornblende-biotite tonalite is compositionally more restricted with regard to the modal abundance of potassic feldspar than the muscovite-biotite tonalite. The hornblende-biotite tonalite plots within the quartz diorite and tonalite fields, near the plagioclase-quartz join. The biotite-muscovite tonalite extends to the potassic-feldspar-rich end of the granodiorite field and the biotite tonalite is intermediate in composition with regard to modal potassic feldspar. The biotite-muscovite tonalite also does not extend to the low modal quartz content of the hornblende-biotite tonalite and the biotite tonalite. On the basis of limited data, the biotite-garnet tonalite does not exhibit the potassic feldspar enrichment of some biotite-muscovite tonalites. The mylonite has a higher potassic feldspar component than most of the tonalites and this suggests the possibility of alterations in the original plutonic chemistry, either by potassium-migration or by physical admixture of tonalite and granite during mylonitization.

With change from the metaluminous assemblage to a peraluminous assemblage, the accessory mineralogy changes from magnetite-ilmenite-sphene to ilmenite. Czamanske, and Mihalik (1973), Tsusue and Ishihara (1974), Ivonova and Butuzova (1968), Ishihara (1977, 1978, 1979), Wones (1980, 1982) and Czamanske et al. (1981) have suggested that these differences in accessory mineral assemblages reflect different oxygen fugacities. Oxygen fugacity is estimated to differ by 2 to 3 orders of magnitude between the magnetite series granites (oxidized) and ilmenite series granites (reduced) of the Cretaceous-Paleocene batholith in southwestern Japan (Czamanske et al., 1981). Wones (1982) demonstrated, using the reaction HEDENBERGITE + ILMENITE = SPHENE + MAGNETITE + QUARTZ, that the sphene-magnetite assemblage indicates a higher oxygen fugacity than an ilmenite assemblage and occurs above the FMQ buffer. At subsolidus temperatures, however, sphene may be produced below the FMQ buffer by the same reaction. Sphene rims around ilmenite in the Hardwick Tonalite verify this subsolidus process and make the problem of identifying primary sphene formidable. Based on the mineralogical evidence, the Hardwick Tonalite exhibits a trend from an oxidized metaluminous composition to a reduced peraluminous composition with increasing modal quartz and possibly with increasing modal potassic feldspar.

A relict primary glomeroporphyritic texture exhibited by weakly foliated tonalites is erased by deformation and metamorphic recrystallization. The mafic clusters which define the glomeroporphyritic texture consist of hornblende and/or biotite grains with closely associated apatite and FeTi oxides. These mafic clusters may be analogous to the restites in the "I-type" granitoids of Chappell and White (1974, 1977). In addition to the textural suggestion that these clusters represent restitic or refractory products of melting, granitoid melting experiments of Wyllie et al. (1976), Stern and Wyllie (1973), Stern et al. (1975) and Huang and Wyllie (1973, 1974, 1981), and fluorapatite solubility experiments by Watson (1979, 1980) and Watson and Capobianco (1981), indicate that tonalites are not primary magmas, but a mixture of granitic liquid with plagioclase and refractory clusters from the source. The tonalite melting experiments with excess water (Wyllie et al., 1976) indicate that the tonalite liquidus ranges from 1100°C at 1 atmosphere to 950°C at 15 kbar. Between 10 and 15 kbar hornblende is a stable phase near or on the liquidus and biotite is stable 150° below the liquidus. Within the same pressure interval, plagioclase, orthoclase and quartz stability curves are between the solidus and liquidus at 625°C and 750°C. Tonalitic magma produced at crustal pressures and temperatures must therefore be a mixture of melt (felsic minerals and mafic restite. The preferred interstitial to anhedral habit of the quartz and potassic feldspar and the mafic clusters of the Hardwick Tonalite, particularly in the metaluminous members, may be analogous.

The fluorapatite solubility experiments of Watson indicate a solubility limit of 0.14 wt% dissolved P_2O_5 or approximately 0.33 wt% apatite for felsic to intermediate magmas (60 wt% to 69 wt% SiO_2) at 750° to

900°C. The solubility limit is only slightly higher for magmas with a SiO_2 between 55% and 60% at the same temperature. The modal apatite content for the hornblende-biotite tonalite ranges from 0.95 to 3.49%, for the biotite tonalite between 0.49 and 2.88%, for the biotite-muscovite tonalite between 0.13 and 2.23%, and for the biotite-muscovite-garnet tonalite between 0.00 and 0.26%. The conflict between the experimental data and the modal data suggests much of the apatite in the Hardwick Tonalite is a refractory component entrained in a rising tonalitic magma. Pointcounted determinations of the ratio of apatite in mafic clusters against apatite associated with felsic minerals range from 5/1 to 3/1.

In conclusion, the petrography of the Hardwick hornblende-biotite tonalite suggests that a metaluminous crystal/liquid mixture evolved by the separation of a refractory component. Further magmatic evolution requires the mixing of the oxidized, metaluminous component with a reduced, peraluminous component during or after initial melting of the source material. Deformation and metamorphic recrystallization eradicated some or all of the igneous texture, imprinting a foliated-equigranular to mylonitic texture on the tonalites. Reequilibration at metamorphic temperature produced sphene rims around ilmenite, clinozoisite rims around allanite and eradicated igneous characteristics of the feldspars.

AUGITE-HORNBLENDE QUARTZ DIORITE AND TONALITE

Augite-hornblende quartz diorite and tonalite forms the north-south trending Nichewaug sill to the west of the Hardwick pluton (Figure 5) and also a body of unknown geometry within the Hardwick pluton. Samples of the sill were taken from the Brooks Pond area, Trot Hill, a hill north of Breen Road and where the sill crosses the Quabbin Aqueduct Tunnel (sample 1153+50). Samples of the augite-hornblende tonalite from within the Hardwick pluton were taken from the Quabbin Aqueduct Tunnel collection (samples 1080+00 to 1084+00).

Nichewaug Sill of Quartz Diorite

The predominant rock type of the sill is dark gray, coarse-grained non-foliated augite-hornblende quartz diorite with relict igneous texture. Near some contacts and in areas of tectonic thinning the sill becomes moderately foliated and fine-grained. In the Brooks Pond area a chilled-contaminated porphyry margin and a relict contact metamorphic aureole (Shearer and Robinson, 1980) have been preserved. Diagrams illustrating textural differences between the chilled margin and the interior of the sill are given in Figure 10.

The mode (Table 6, Figure 11) ranges from 7 to 12% quartz, 34 to 46% plagioclase, 0.7 to 13% microperthitic orthoclase, 21 to 31% biotite, 0.3 to 15.7% hornblende and trace to 6% augite. The ratio of plagioclase to total feldspar (100 Pl/(Pl+Ksp)) ranges from 98 to 75. Accessory minerals include apatite, clinozoisite, allanite, ilmenite, magnetite,

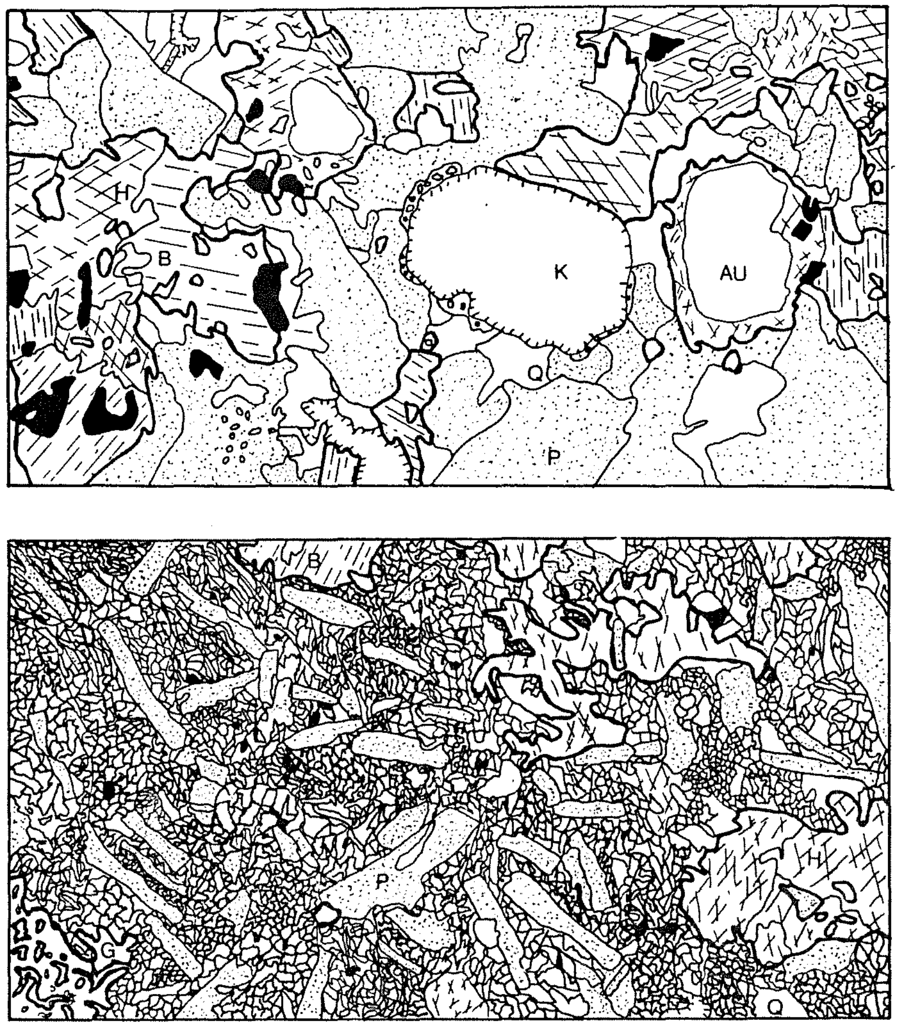

Figure 10. Sketches from thin sections to illustrate textural differences in the Nichewaug sill between a) interior and b) chilled margin. AU: augite with hornblende alteration, Q: quartz, K: potassium feldspar, H: hornblende, B: biotite, P: plagioclase, G: garnet, A: apatite, black: opaque minerals. In the chilled margin sketch the matrix is composed of fine-grained quartz, feldspar and mafic minerals.

Table 6. Point-counted modes of augite-hornblende quartz diorite from the Nichewaug Sill and within the Hardwick Tonalite.

	Nichewaug Sill									Within Hardwick Pluton	
	SP236-3	SP236-4	SP236-2	SP209	SP28	1153-50	SP239-3	1083-50	SP179	1084	1080
Quartz	8.3	10.0	7.1	8.3	8.9	9.8	12.0	9.3	11.0	10.7	9.1
Plagioclase	43.5	44.0	41.3	42.5	45.8	34.3	36.9	30.5	46.9	36.1	25.6
(mol% An)	(46-30)*	(43-26)	(52-27)	(42-15)	(45-21)	(35)	(46-40)*	(45-13)*	(50-28)*	(40)	(42-21)
Potassic Feldspar	3.4	2.8	13.2	0.7	5.2		1.7		2.5	tr	0.2
Biotite	21.4	22.9	21.2	31.2	21.7	28.8	29.4	32.1	28.2	33.8	34.2
Hornblende	15.7	14.3	9.5	9.5	8.3	17.3	15.00	17.3	0.3	11.0	19.4
Augite	1.6	0.9	2.7	tr	4.7	3.2	tr	3.7	6.2	2.8	7.2
Garnet							0.5				
Sphene	0.2	tr	0.1	3.3	0.6	0.2				0.7	
Allanite	tr	tr	tr	0.1	tr	0.2					
Apatite	3.3	2.8	3.5	3.1	3.0	3.9	1.7	3.3	2.0	2.8	4.2
Opaque Minerals	2.7	2.5	1.5	1.2	1.8	2.1	2.9	3.8	2.8	2.2	0.2
magnetite	x	x	x	x	x	x		x	x	x	x
ilmenite	x	x	x	x	x	x	x	x	x	x	x
pyrite	x	x			x	x		x	x		x
Zircon	tr	tr	tr	tr	tr	0.2		tr	tr	tr	tr
Clinozoisite				tr	tr						
100Pl/(Pl+Ksp)	93	94	76	98	90	100	96	100	95	100	99
100Qz/(Qz+Ksp)	15	18	12	16	15	22	24	23	18	23	26

Plagioclase composition determined by Michel-Levy extinction angle method and electron microprobe (*).
x opaque mineral observed in polished section.

Table 6, continued. Hand specimen descriptions and sample locations for the augite-hornblende quartz diorite.

SP236-3 Coarse-grained, unfoliated, augite-hornblende quartz diorite. Petersham 7.5-minute quadrangle. Located on ridge, 0.2 km south of Brooks Pond in center of sill.

SP236-4 Sample description and location the same as SP236-3

SP236-2 Sample description and location the same as SP236-3

SP209 Sample description and location the same as SP236-3

SP28 Coarse-grained, lightly foliated, augite-hornblende quartz diorite. Petersham 7.5-minute quadrangle. 720 contour on Trot Hill.

1153-50 Coarse-grained, unfoliated, augite-hornblende quartz diorite. Petersham 7.5-minute quadrangle. Quabbin Aqueduct sample, near Muddy Pond.

PS239-3 Fine-grained, moderately foliated chilled margin, augite-hornblende quartz diorite. Petersham 7.5-minute quadrangle. Same location as SP236-3, but at contact of sill with Littleton Formation.

1083-50 Coarse-grained, lightly foliated, augite-hornblende quartz diorite. Petersham 7.5-minute quadrangle. Quabbin Aqueduct sample, 0.15 km west of Jackson Road.

SP179 Coarse-grained, moderately foliated, augite-hornblende quartz diorite. Petersham 7.5-minute quadrangle. Ridge north of Breen Road at 870 contour.

1084 Coarse-grained, unfoliated, augite-hornblende quartz diorite. Petersham 7.7-minute quadrangle. Quabbin Aqueduct sample, 0.2 km west of Jackson Road.

1080 Coarse-grained, lightly foliated, augite-hornblende quartz diorite. Petersham 7.5-minue quadrangle. Quabbin Aqueduct sample, 75 meters west of Jackson Road.

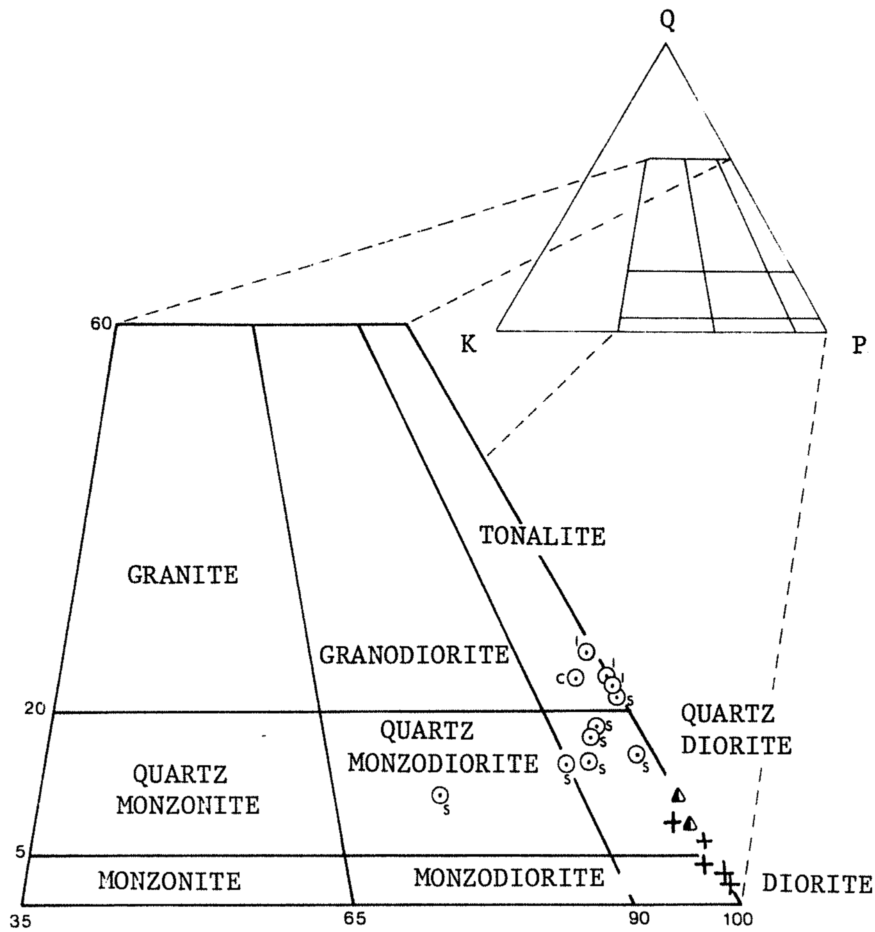

Figure 11. Quartz-Plagioclase-K-Feldspar plot of modes of the augite-hornblende quartz diorite (⊙ , S=Nichewaug Sill, C=chilled margin of Nichewaug Sill, and I= tonalite within the Hardwick Tonalite), Bear Den Sill of diorite (+), and the diorite at Goat Hill (▲).

sphene, and zircon. Garnet occurs at the margin of the sill where it is in contact with pelitic schist. A description of the mineral phases is given in Table 7. These rocks are defined as tonalites, quartz diorites and quartz monzodiorites by the IUGS classification scheme (Streckeisen, 1973).

Augite-bearing Tonalite within Tonalite Pluton

The augite-hornblende tonalite samples collected from the Quabbin Aqueduct Tunnel at locations 1080+00 to 1084+00 are within the tonalite sheet of the Hardwick pluton. The relationship between the augite-bearing tonalite-quartz diorite and the normal tonalite is unknown but the augite-bearing tonalite may represent inclusions within the normal tonalite, a sill intruding it or a more mafic-primitive member of the tonalite sheet. The first is perhaps the least likely because the tunnel (distance from sample 1080+00 to 1084+00 is approximately 400 feet) across strike.

Modes of this rock type (Table 6) at this location range from 6 to 10% quartz, 25 to 36% plagioclase, tr. to 0.2% microperthite, 34 to 32% biotite, 11 to 19% hornblende and 2.8 to 7.2% augite. The ratio of plagioclase to total feldspar (100 Pl/(Pl + Ksp)) is approximately 100. All specimens plot in the quartz-poor region of the tonalite field in the Streckeisen (1973) classification (Figure 11). Accessory minerals include apatite, allanite, clinozoisite, ilmenite, magnetite and zircon.

Mineralogy, grain size and textural relations are nearly identical to the tonalite-quartz diorite in the sill. The differences between the two are: (1) the sill has a higher modal percent of potassic feldspar and a lower quartz/(quartz + feldspar) ratio (2) the sill has sphene and intergrowths of vermicular quartz in the hornblende, (3) slightly more sodic rims on the plagioclase in samples 1080+00 to 1084+00 (An_{13}) than samples from the sill (An_{25}) as determined by the Michel-Levy extinction angle method.

BEAR DEN SILL OF HORNBLENDE DIORITE

The hornblende diorite is black to greenish black on both fresh and weathered surfaces (color index 40 to 66). The rock is coarse-grained (to 6 mm) and biotite and hornblende are clearly identifiable in hand-specimen. Pyrite is also quite evident and abundant. The coarse-grained igneous texture partially preserved in the interior of the sill, is changed along the sill's exterior to a fine-grained, granular rock.

In general, the hornblende diorite exhibits a holocrystalline, hypidiomorphic-granular to a holocrystalline, poikilitic, hypidiomorphic-granular texture. The poikilitic nature of the texture is best developed in the center of the sill. The plagioclase defines the poikilitic texture (Figure 12). The modes range from 24 to 29% plagioclase, 0.9 to 2.6% quartz, 17 to 35% biotite, and 15 to 45.7% hornblende. The ratio of plagioclase to total feldspar 100 Pl/(Pl + Ksp) ranges from 98 to 100

Table 7. Characteristics of mineral phases from the mafic plutonic units associated with the Hardwick Tonalite.

	AUGITE-HORNBLENDE QUARTZ DIORITE	BEAR DEN SILL OF HORNBLENDE DIORITE	DIORITE AT GOAT HILL
PLAGIOCLASE	Euhedral to subhedral, equant to elongate, to 4.5mm (ave.=1.8mm), An_{48-25}, normal zoning. In chilled margin of Nichewaug sill: laths to 1.3mm, An_{55-44}, matrix: 0.1mm, An_{42}.	Anhedral, 10-15mm in interior of sill, 0.8 to 5.6mm at perimeter of sill, An_{45-9}, normal zoning.	Subhedral laths to 4.6mm in length, FeTi oxides common in core, An_{51-32}, sharp normal zoning.
POTASSIUM FELDSPAR	Microperthitic orthoclase, anhedral from 1.0 to 3.6mm (ave=1.8mm) lamellae to 0.25mm, and An_4.	Microperthitic orthoclase, anahedral, from .05 to 2.0mm.	Microperthitic orthoclase, minute interstitial grains to 0.8 mm.
QUARTZ	Four textural varieties: thin interstitial quartz, poikilitic with hornblende, myrmekitic with plagioclase, and anhedral grains to 0.9mm.	Myrmekitic with plagioclase, granular anhedral grains from 0.5 to 1.8mm, polycrystalline aggregates and interstitial grains to 0.3mm.	Interstitial grains to 1.3mm with limited undulatory extinction.
PYROXENE	Augite:euhedral to subhedral, to 1.8mm, rimmed and intergrown with hornblende, light green, weak pleochroism.	Augite: intergrown with hornblende, FeTi oxide concentrated in intergrowth, rimmed by hornblende.	Augite:euhedral to subhedral, to 1.1mm, light green with very weak pleochroism, subordinate in amount to orthopyroxene to being the only pyroxene. Orthopyroxene:subhedral, from 0.3 to 1.1mm, X=pink, Y=green, Z=gray green, r v, 2v=55 to 62, (-), En_{67-63}.
HORNBLENDE	Occurs as discrete grains(ave. 1.4 mm), intergrowths with vermicular quartz, rimming or intergrown with augite. Pleochroism in discrete grains X=yellow, Y=yellow green, Z =dark green to brownish green, other textural types Z=green to blue green.	Occurs as discrete, subhedral to anhedral grains with intergrowths of vermicular quartz, intergrowths of hornblende and biotite, polycrystalline aggregates and subhedral to anhedral grains with fibrous cores of augite, X=yellow to yellow green, Y=green, Z=green to blue green.	Anhedral grains to 1.3mm and rims around both augite and orthopyroxene, latter textural type is prevalent, X-yellow green, Y=green, Z=dark green.
BIOTITE	Anhedral, to 3.5mm, X=yellow brown, Y=Z=red brown.	Intergrowths with hornblende individual grains from .25 to 3.6mm, X=yellow brown, Y=Z=red brown.	Subhedral grains from 0.3 to 5.2mm, X-light brown, Y=Z= dark red brown.
GARNET	Subhedral to anhedral poikilitic garnet in chilled margin of the Nichewaug sill.		
SPHENE	Thin anhedral rims around ilmenite and is absent in chilled margin.	Fine, anhedral grains as inclusions and thin rims around ilmenite.	Anhedral to subhedral grains to 0.2mm, weakly pleochroic with X=light brown and Z=brown.
ALLANITE	Subhedral, rimmed by clinozoisite, partially metamict, X=light orange brown, Z=orange to orange brown.	Subhedral, with rare rims of clinozoisite, weakly pleochroic with X=light orange, Z=orange to orange brown.	
OXIDES	Ilmenite and magnetite ilmenite:euhedral, lath-shaped with titanohematite lamellae, in the chilled margin the ilmenite is homogeneous. magnetite:homogeneous equant grains.	Ilmenite $\pm$ magnetite ilmenite:optically homogeneous, subhedral to anhedral grains from 0.05 to 1.3mm. magnetite:very minor, homogeneous, equant grains.	Ilmenite and magnetite ilmenite:subhedral, rectangular grains with an average size of 0.4mm, titanohematite lamellae very common. magnetite:homogeneous, equant grains.
APATITE	Euhedral.	Euhedral.	Euhedral.
ZIRCON	Minute inclusions in biotite and discrete grains.	Minute inclusions in biotite and discrete grains.	Minute inclusions in biotite and discrete grains.
SULFIDES	Euhedral pyrite intergrown with chalcopyrite.	Euhedral pyrite intergrown with chalcopyrite.	

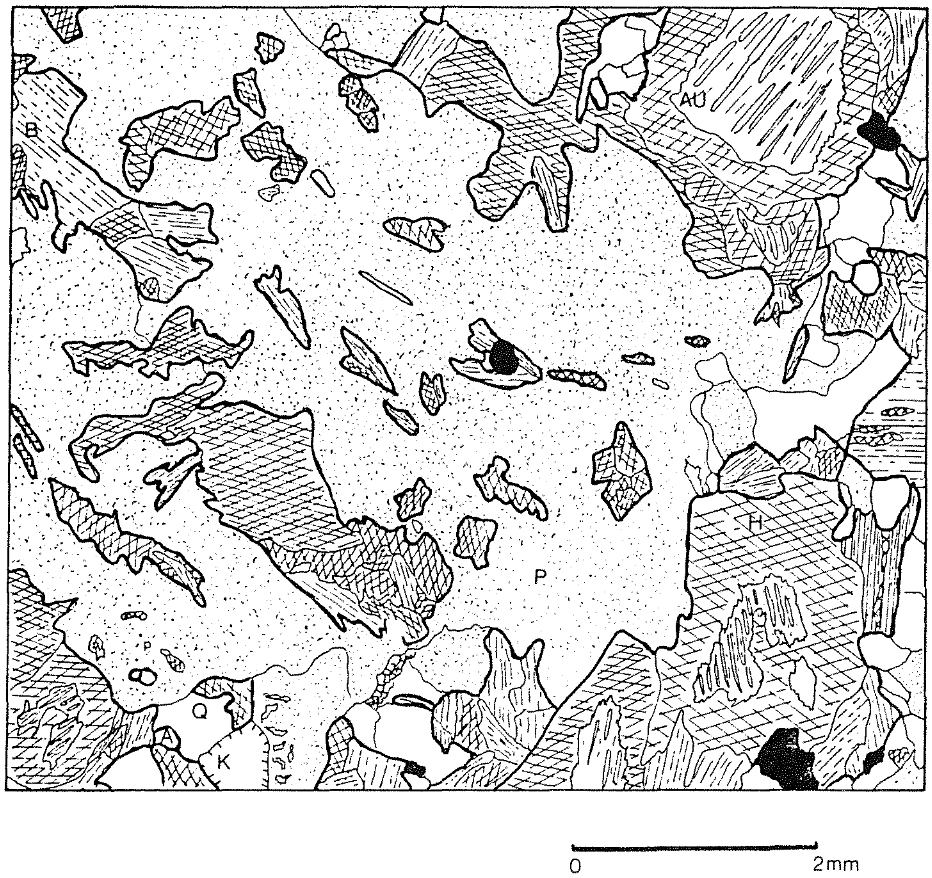

Figure 12. Sketch from a thin section of the hornblende diorite from the Bear Den Sill. P:plagioclase, H:hornblende, B:biotite, AU:augite with hornblende alteration, Q:quartz, K:potassium feldspar, A:apatite, black:opaque minerals.

to 100 and the ratio of quartz to total feldspar 100 Qz/(Qz + Fsp) ranges from 2.8 to 8.7. Accessory minerals include augite, sphene, allanite, epidote, apatite, pyrite and ilmenite. A description of the mineral phases is given in Table 7.

Modes from Table 8 plotted in Figure 11 in terms of quartz, plagioclase, and potassic feldspar, show that these rocks are quartz diorites (quartz and potassic feldspar deficient region of the field) and diorites as defined by the IUGS classification scheme (Streckeisen, 1973).

GOAT HILL DIORITE

The Goat Hill Diorite forms an elongate north-south trending intrusion within the Hardwick Tonalite, north of Gilbertville in the Ware quadrangle. The diorite is dark-gray to brown in color with a coarse-grained igneous texture. This pristine igneous texture suggested to Field (1975) that emplacement took place after Acadian regional metamorphism and deformation. It is possible, however, that the relict igneous texture may have been protected and preserved by the surrounding Hardwick Tonalite during the regional metamorphism and deformation. The contact relationship between the tonalite and the diorite is gradational in nature. Schist is common at the contact and there is an absence of recognizable inclusions of tonalite or diorite.

The modes of the thin sections studied vary from 52 to 54% plagioclase, 5 to 7% quartz, 26% biotite, 1 to 6% hornblende, 1 to 7% augite and traces to 5% orthopyroxene. Accessory minerals include microperthitic orthoclase, apatite, ilmenite, magnetite, zircon, and sphene. Description of the mineral phases is given in Table 7. These rocks exhibit a holocrystalline, hypidiomorphic-granular texture.

Figure 11 shows that the rocks from the Goat Hill Diorite are defined as quartz diorites by the IUGS classification scheme (Streckeisen, 1973). Estimated modes of the Goat Hill Diorite from Field (1975) plot within both the quartz diorite and diorite fields of the IUGS classification.

SUMMARY OF PETROGRAPHY OF MAFIC IGNEOUS ROCKS ASSOCIATED WITH THE HARDWICK TONALITE

Mafic intrusive igneous rocks associated with the Hardwick Tonalite plot within diorite, quartz diorite, and tonalite compositional fields (Figure 11). All rocks contain pyroxene or hornblende pseudomorphs after pyroxene. A magnetite-ilmenite oxide assemblage is common and suggests an oxygen fugacity above the FMQ buffer. Of the mafic rocks, the augite-hornblende quartz diorite appears to be the most similiar to the Hardwick Tonalite based upon textural and accessory mineral (allanite, high modal apatite) features.

Table 8. Point-counted modes of the Bear Den Sill of Diorite.

	SA176-1	SA176-2A	SA176-2B	SA176-3	SA176-4
Quartz	2.6	1.7	2.1	1.0	2.4
Plagioclase	35.6	49.3	45.9	32.7	24.8
(mol.% An)	(43-15)	(45-9)*	(40-15)*	(38-11)*	(36-10)
Potassic Feldspar		tr	0.7		0.4
Biotite	35.4	26.0	25.6	17.4	34.7
Hornblende	20.1	16.0	16.0	45.7	31.5
Augite		tr	0.3	0.4	0.8
Sphene	3.9	4.2	4.2	0.7	0.6
Allanite	tr	tr	0.4		
Apatite	2.2	2.2	2.6	0.6	2.2
Zircon	tr	tr	tr	0.2	0.2
Opaque Minerals	0.1	0.8	2.2	1.6	2.5
magnetite	x				
ilmenite	x	x	x	x	x
pyrite	x	x	x	x	x
Clinozoisite			0.1		
100Pl/(Pl+Ksp)	100	100	99	100	98
100Qz/(Qz+Fsp)	7	3	4	3	9

Plagioclase composition determined by Michel-Levy extinction angle method and electron microprobe(*).

x opaque mineral observed in polished section.

Hand specimen descriptions and sample locations for the Bear Den sill of diorite.

SA176-1 Coarse-grained, nonfoliated, black to greenish black diorite. Athol 7.5-minute quadrangle. In Bears Den Road, east of Sheep Rock.

SA176-2A Sample description and location the same as SA176-1.

SA176-2B Sample description and sample location same as SA176-1.

SA176-3 Coarse-grained, lightly foliated, black colored diorite. Location the same as SA176-1.

SA176-4 Sample description and location the same as SA176-3.

Table 9. Point-counted modes of the diorite at Goat Hill.

	SW522	SW4-2
Quartz	5.2	7.0
Plagioclase	52.1	54.4
(mol.% An)	(51-35)*	(43-32)
Potassic Feldspar		0.7
Biotite	26.0	26.4
Hornblende	6.1	0.8
Augite	1.3	6.9
Orthopyroxene	5.3	tr
Sphene	tr	tr
Apatite	2.3	2.0
Zircon	tr	tr
Opaque Minerals	1.7	2.0
magnetite	x	x
ilmenite	x	x
pyrite		
pyrrhotite		
100Pl/(Pl+Ksp)	100	99
100Qz/(Qz+Fsp)	9	11

Plagioclase composition determined by Michel-Levy extinction angle method and electron microprobe(*).

x opaque mineral observed in polished section.

Sample description and location.

SW522 Coarse-grained, nonfoliated, hornblende-biotite-pyroxene diorite. Ware 7.5 minute quadrangle. Steep slope east of high point of Goat Hill, 0.37 km west of Church Street

SW4-2 Medium-grained, lightly to moderately foliated diorite. Ware 7.5 minute quadrangle. Southern knob of Goat Hill.

PORPHYRITIC MICROCLINE GRANITE

This granite is characterized by rectangular to augen-shaped white microcline phenocrysts which have an average length of 3 cm and an average width of 1 cm. The long axes of the microclines are commonly oriented parallel to the strikes of the sills, which are commonly north-south. The rectangular microcline crystals may exhibit a zoning visible in the field. The phenocrysts are immersed in a medium- to dark-gray groundmass which consists primarily of biotite, quartz, plagioclase, and microcline. A thin envelope (to 0.4 mm wide) of fine-grained quartz and myrmekitic plagioclase (to .04 mm) partially to completely surrounds the microcline phenocrysts. The modal amount of phenocrysts ranges between 1 and 20% as determined using a 11 to 7.5 inch transparent grid to measure pheno-cryst area on outcrops, and cut and stained slabs.

Elongate, foliated fragments of the tonalite, up to 8 meters long occur as inclusions. Single grain inclusions up to 3 cm long of sillimanite pseudomorphs after andalusite occur in most sills, although only 2 to 4 grains were observed per sill on the average. The sillimanite may be partially replaced by muscovite. Corundum occurs as inclusions within the outermost portions of the sillimanite.

Matrix modes of the microcline granite vary from 9 to 31% quartz, 34 to 54% plagioclase, trace to 30% microcline, 8 to 27% biotite, and trace to 4% muscovite. The total modes for the porphyritic microcline granite vary from 7 to 28% quartz, 29 to 48% plagioclase, 11 to 44% microcline, 7 to 23% biotite and trace to 3% muscovite. The ratio 100 Qz/(Qz + Fsp) ranges from 8 to 29 and the ratio 100 Pl/(Pl + Ksp) ranges from 47 to 82. The porphyritic microcline granite (Table 10, Figure 13) is classified as granite and quartz monzonite by the IUGS nomenclature (Streckeisen, 1973). The matrix alone is classified as a granodiorite, tonalite, or quartz monzodiorite by the IUGS nomenclature (Streckeisen, 1973). Primary accessory minerals include apatite, ilmenite, magnetite, pyrite, and zircon. Secondary accessory minerals include chlorite, calcite, and sphene. Description of the mineral phases in the porphyritic microcline granite is presented in Table 11.

Corundum within the outer portion of the sillimanite inclusions suggests the porphyritic microcline granite was not saturated with quartz at the time the inclusion was incorporated in the melt. The reaction between the inclusion and the melt added SiO_2 to the melt: Al_2SiO_5 (inclusion) = Al_2O_3 + SiO_2 (melt). The fact that quartz was not an initial liquidus phase indicates the granite was not a minimum melt compostion and not directly derived from the partial melting of quartz-rich sediments. The large rectangular shape of the potassium feldspar, and zoning and plagioclase inclusions within them suggests both plagioclase and potassium feldspar were liquidus phases. The matrix of the granite is almost identical to the composition of the biotite muscovite tonalite suggesting a genetic affinity between the two units.

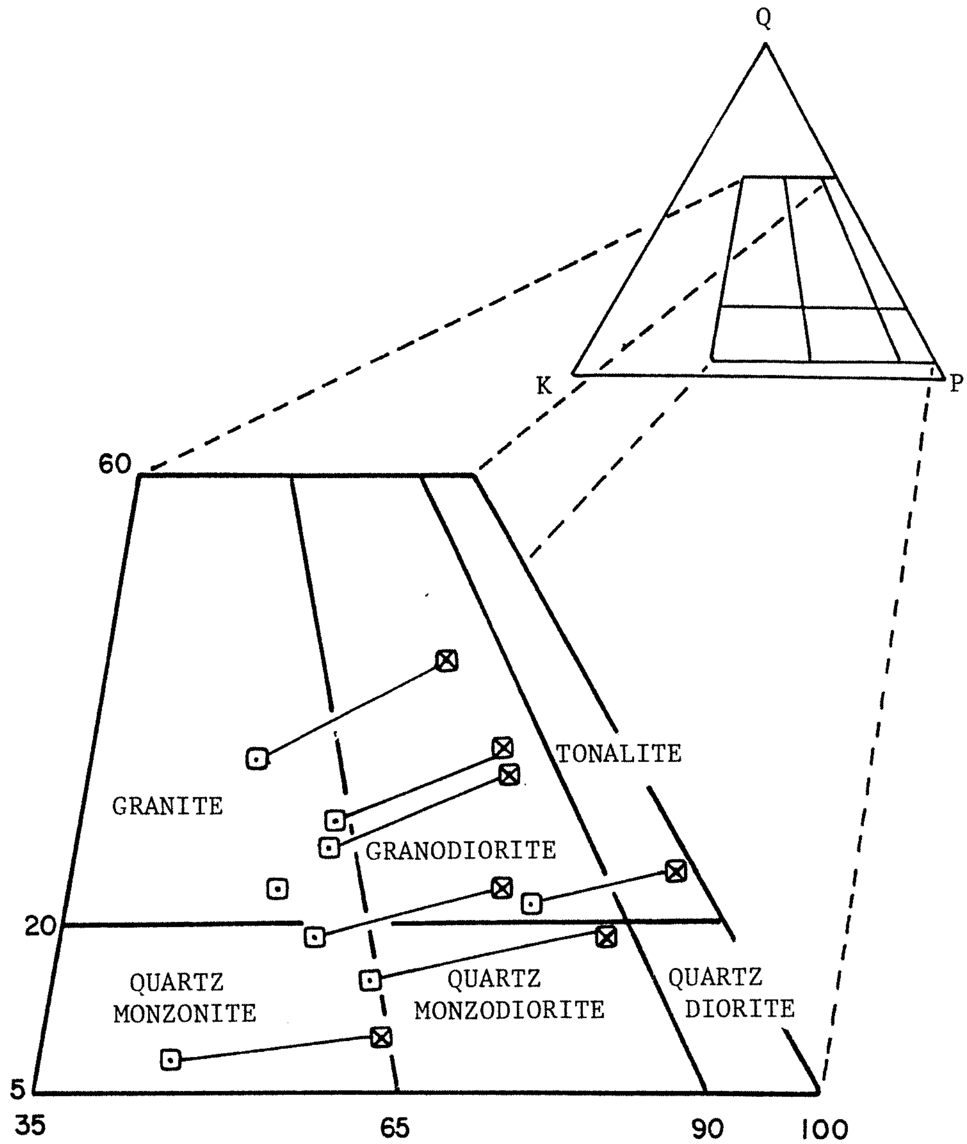

Figure 13. Quartz-Plagioclase-K-Feldspar plot of modes of the porphyritic microcline granite and matrix of the porphyritic microcline granite (⊠).

Table 10. Point-counted modes of porphyritic microcline granite.

	SA1m	SA1	SP56m	SP56	SA3-4m	SA3-4	SA160-1m	SA160-1	SA78m	SA78	SA3-6m	SA3-6	SP9-2m	SP9-2	SA3-5
Quartz	31.8	27.6	17.6	14.9	27.7	23.6	12.9	10.8	27.1	22.7	18.3	16.4	8.9	6.9	20.1
Plagioclase	34.0	29.5	45.3	38.1	43.0	36.7	47.5	39.7	45.8	38.3	53.7	48.2	49.7	38.7	39.2
(mol% An)	(26-10)*	(26-10)*	(27-14)	(27-14)	(23-17)	(23-17)	(32-22)	(32-22)	(27-24)	(27-24)	(26)	(26)	(27-19)	(27-19)	(24)
Potassic Feldspar	7.5	19.6	11.8	25.7	7.7	21.2	6.5	21.9	8.0	23.0	0.5	10.6	28.0	43.9	29.5
Biotite	22.2	19.3	22.7	19.1	13.8	11.8	27.2	22.7	14.1	11.8	22.6	20.3	9.5	7.4	8.3
Muscovite	1.3	1.1	0.3	0.2	2.2	1.9	1.2	1.0	3.5	2.9	3.0	2.7	3.0	2.3	2.0
Sphene	0.4	0.3	0.1	0.1			1.8	1.5			0.1	0.1			tr
Allanite	tr	tr	0.7	0.6											
Apatite	1.6	1.4	0.8	0.7	0.8	0.6	0.4	0.4	0.6	0.5	0.6	0.5	0.5	0.4	0.4
Zircon	0.1	0.1	tr	tr	0.1	0.1	tr	tr	0.2	0.1	0.3	0.2	tr	tr	tr
Opaque Minerals	1.1	0.9	0.7	0.6	2.0	1.7	2.5	2.1	0.8	0.7	1.1	1.0	0.5	0.4	0.4
magnetite	x	x													
ilmenite	x	x	x	x	x	x	x	x	x	x	x	x	x	x	x
pyrite	x	x	x	x	x	x	x	x	x	x	x	x	x	x	x
pyrrhotite															
Chlorite	tr	tr	0.2	0.1	1.9	1.6									
Calcite					0.8	0.6									
100Pl/(Pl+Ksp)	82	60	79	60	85	63	88	64	85	63	99	82	64	47	57
100Qz/(Qz+Fsp)	43	36	24	19	35	29	19	15	34	27	25	22	10	8	23
% Phenocryst	13%		16%		15%		17%		16%		10%		22%		0%

m point-counted mode of the groundmass. Second mode is an intergrated groundmass-phenocryst mode.

Plagioclase composition determined by Michel-Levy extinction angle method and electron microprobe(*)

Table 10, continued. Hand specimen description and sample location for the porphyritic microcline granite.

SA1 Rectangular to augen-shaped microcline phenocrysts in medium-to coarse-grained, moderately foliated matrix of quartz, microcline, Olagioclase, biotite and muscovite. Light colored granite. Athol 7.5-minute quadrangle. 0.7 km north of Ward Hill (BM 1338) at the Templeton Road entrance onto Route 2.

SP56 Coarse-grained, moderately foliated, light gray colored granite with augen-shaped microcline phenocrysts. Petersham 7.5-minute quadrangle. 50 meters west of intersection of East Street and Glashene.

SA3-4 Coarse-grained, lightly foliated, light gray granite with rectangular-shaped microcline phenocrysts. Athol 7.5-minute quadrangle. 0.2 km east of Route 2 - Highland Road overpass, on south side of Route 2.

SA160-1 Doarse-grained, moderately to strongly foliated, light colored to rusty granite with augen-shaped microcline phenocrysts. Athol 7.5-minute quadrangle. 60 meters west of Route 2 - Highland Road overpass, on north side of Route 2.

SA78 Coarse-grained, lightly foliated, light grav colored granite with rectangular- and augen-shaped microcline phenocrysts. Petersham 7.5-minute quadrangle. East side of hill between Quaker Road and Rutland stream at 930 contour.

SA3-6 Specimen description and location same as SA3-4, collected 20 meters to the west.

SP9-2 Coarse-grained, strongly foliated, light gray colored granite with augen-shaped microcline phenocrysts. Petersham 7.5-minute quadrangle. North side of Dana Road, 0.2 km east of intersection with Cleveland Road.

SA3-5 Medium- to fine-grained, non-foliated, light gray colored granite associated with perimeter of porphyritic microcline sill. Same location as SA3-4.

Table 11. Characteristics of mineral phases from the granites associated with the Hardwick Tonalite.

	PORPHYRITIC MICROCLINE GRANITE	GRANITES AT SHEEP ROCK AND TOM SWAMP	FITZWILLIAM GRANITE
PLAGIOCLASE	Euhedral to anhedral, to 6.5mm, broad and normal zoning, An_{28-12}, intergrown with quartz when it is adjacent to microcline. Plagioclase partially enclosed by microcline commonly have exsolved plagioclase rims (An_{12-6}).	Subhedral, to 4.2mm, zoning usually normal, although oscillatory zoning does occur, An_{31-15}, plagioclase enclosed by or adjacent to microcline rimmed by sodic plagioclase An_{10-4}.	Euhedral to subhedral, to 3.8mm, normal zoning, An_{32-24}, sericitic alteration most pronounced in SA61-3.
POTASSIUM FELDSPAR	Prominent subhedral to anhedral phenocrysts and as interstitial groundmass, perthitic microcline exhibiting mild to moderate exsolution, small blebs (0.13mm) of plagioclase exsolution may collectively form chains 4.0mm in length.	Microcline, subhedral to interstitial, to 5.5mm, exhibits strongly to (Z91) to weakly(SA68)exsolved plagioclase, An_8, exsolution blebs less than 0.40mm.	Microcline, anhedral and interstitial, to 3.6mm, exsolution poorly developed, less than 0.08mm in size.
QUARTZ	Anhedral and interstitial, from 0.2 to 2.8mm and forms elongate polycrystalline aggregates.	Anhedral and interstitial, from 0.1 to 3.8mm (ave. 1.2mm), also forms polycrystalline aggregates.	Anhedral, from 0.1 to 3.2mm, polycrystalline aggregates (3.8mm in length), and interstitial quartz.
BIOTITE	Subhedral, 0.1 to 1.8mm (ave. 1.0mm), X=pale yellow brown, Y=Z=brown to red brown.	Subhedral, 0.1 to 1.8mm, X=pale yellow brown to pale red brown, Y=Z=red brown, partially altered green Fe-rich chlorite along fringes.	Subhedral, 0.05 to 1.5mm, X=yellow brown, Y=Z=red brown to brown, partially altered to green Fe-rich chlorite along fringes.
MUSCOVITE	Subhedral, intergrown with biotite cross-cutting or parallel to biotite cleavage, average grain size 0.9mm.	Subhedral, 0.2 to 1.3mm, Tom Swamp muscovite forms independent grains, Sheep Rock muscovite intimately intergrown with biotite.	Subhedral, to 1.1mm, intergrown with biotite and forms independent grains.
SPHENE	Subhedral to anhedral rims around ilmenite and partial rims around biotite, pleochroism weak, X=pale brown, Z=light brown.		
ALLANITE	Euhedral to subhedral, to .055mm, poorly defined zoning, weakly pleochroic with X=pale yellow orange, Z=yellow orange.		
OXIDES	Ilmenite $\pm$ magnetite (SA1), ilmenite:commonly homogeneous, minor titanohematite lamellae. magnetite:small equint grains, homogeneous.	Ilmenite:elongate, subhedral to anhedral, from 0.13 to 0.40mm, homo geneous.	Ilmenite:anhedral to subhedral to 0.25mm, homogeneous.
APATITE	Euhedral, 0.13 to 0.35mm.	Euhedral, to 0.3mm, associated with biotite and randomly distributed.	Euhedral, 0.02 to 0.25mm, inclusions in biotite.
ZIRCON	Minute inclusions in biotite and muscovite, to 0.13mm.	Minute inclusions in biotite and randomly distributed.	Minute inclusions in biotite, and randomly distributed.
SULFIDES	Euhedral pyrite to 0.8mm.	Subhedral pyrite to 0.6mm.	Rare, subhedral to anhedral pyrite to 0.03mm.

EQUIGRANULAR BIOTITE-MUSCOVITE GRANITES

Granites at Sheep Rock and Tom Swamp

The granites at Sheep Rock and Tom Swamp are light gray, medium-grained binary granites. In the field these granites are differentiated from the Fitzwilliam Granite by their light yellow gray color on weathered outcrop surfaces and a slightly higher percentage of microcline phenocrysts. Foliation is faint to absent and is defined by poorly aligned muscovite and biotite.

The modes (Table 12, Figure 14) range from 31 to 39% plagioclase, 20 to 30% quartz, 22 to 31% microcline, 7 to 9% biotite, and trace to 7% muscovite. The ratio 100 Pl/(Pl + Ksp) varies form 51 to 63 and the ratio 100 Qz/(Qz + Ksp) varies from 25 to 33. Modes of the granites at Sheep Rock and Tom Swamp plot within the granites region of the IUGS plutonic rock classification scheme (Streckeisen, 1973). Primary accessory minerals in these granites include ilmenite, apatite, zircon and pyrite; chlorite and calcite are secondary minerals. A description of the mineral phases is given in Table 12. In general the specimens exhibit a hypidiomorphic granular texture.

Fitzwilliam Granite and Sills Intruding the Hardwick Tonalite

The Fitzwilliam Granite is a light gray, fine- to medium-grained binary granite. Locally, the granite is moderately porphyritic and lightly foliated at its perimeter (Fowler-Billings, 1949). Poorly aligned muscovite and biotite define the foliation. The granite contains inclusions of the Hardwick Tonalite and Kinsman Quartz Monzonite (Coys Hill Granite).

Within the equigranular biotite-muscovite granite of the Fitzwilliam pluton and associated sills (Sm3, Sm4, Sm9, Sm11, and SA61-3) the mode ranges from 15 to 39% plagioclase, 17 to 35% quartz, 30 to 38% potassium feldspar, 5 to 7% biotite, and 2 to 5% muscovite. The ratio Pl/(Pl + Ksp) ranges from 30 to 52 and the ratio 100 Qz/(Qz + Fsp) ranges from 19 to 40 (Table 13). Primary accessory minerals include apatite, zircon, ilmenite, and pyrite. Sphene, chlorite and calcite occur as secondary accessory minerals. A description of the mineral phases is given in Table 11.

Although giving the appearance of being homogeneous in hand specimen, modes show the Fitzwilliam Granite is heterogeneous. Based on the IUGS nomenclature (Streckeisen, 1973), the modes of the Fitzwilliam Granite plot within the composition fields of granite, quartz syenite, and quartz monzonite (Figure 14).

Table 12. Point-counted modes of the granite at Tom Swamp(Z93) and the granite at Sheep Rock(SA68)

	Z93-1	Z93-2	SP68-1	SP68-2
Quartz	20.6	23.0	30.2	28.0
Plagioclase	32.0	32.9	38.3	38.6
(mol.% An)	(26-20)*	(28-20)	(28-23)*	(30-23)
Potassic Feldspar	31.0	29.6	22.8	24.2
Biotite	8.7	8.0	7.5	7.7
Muscovite	6.9	6.0	0.6	1.0
Apatite	tr	tr	tr	tr
Zircon	0.2	tr	tr	tr
Opaque Minerals	0.7	0.5	0.5	0.6
magnetite				
ilmenite	x	x	x	x
pyrite	x		x	x
pyrrhotite				
Chlorite	tr			
100Pl/(Pl+Ksp)	51	53	63	61
100Qz/(Qz+Fsp)	25	27	33	31

Plagioclase composition determined by Michel-Levy extinction angle method and electron microprobe(*).

x opaque mineral observed in polished section.

Hand specimen description and sample location for the granites at Tom Swamp and Sheep Rock.

Z93-1 Medium-grained, equigranular, lightly foliated, gray yellow colored granite. Athol 7.5 minute quadrangle. 40 meters north of Tom Swamp Road, 0.9 km south of Burrage Corner.

Z93-2 Hand specimen description and sample location are the same as Z93-1.

SP68-1 Medium-grained, euqigranular, nonfoliated, gray to yellow gray colored granite. Top of Sheep Rock at 970 contour.

SP68-2 Hand specimen description and sample location are the same as SP68-1

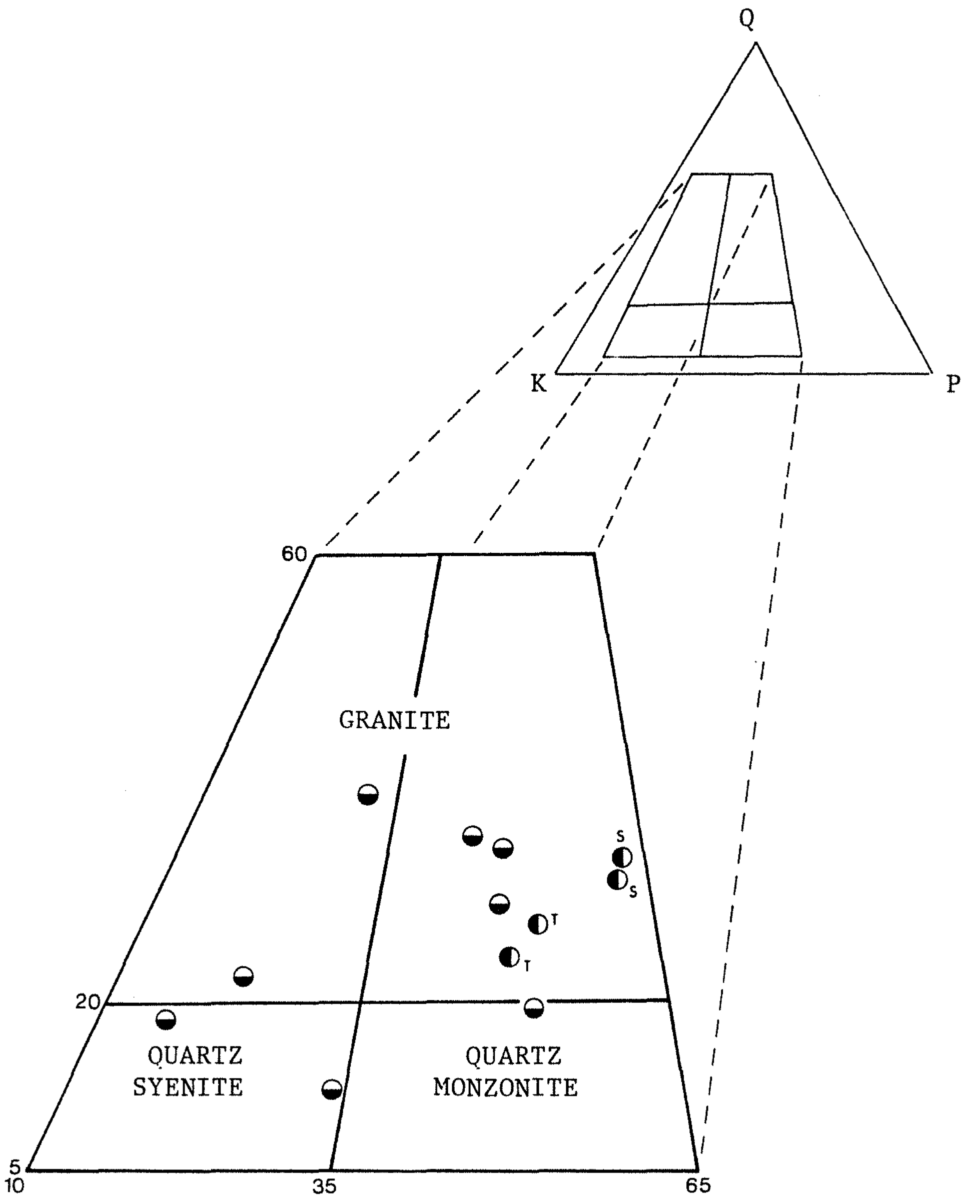

Figure 14. Quartz-Plagioclase-K-Feldspar plot of modes of the granite at Sheep Rock (◐ S), the granite at Tom Swamp (◐ T), and the Fitzwilliam Granite (⊖).

Table 13. Point-counted modes of the Fitzwilliam Granite and associated granitic sill(SA61-3)

	SM3	SM4	SM9	SM11	SA61-3
Quartz	30.6	26.3	31.6	17.6	35.1
Plagioclase	28.5	30.5	26.2	38.7	16.0
(mol.% An)	(28)	(26-19)*	(32)	(30-22)	(26)
Potassic Feldspar	30.8	32.7	32.6	35.8	38.4
Biotite	4.8	5.3	7.1	6.6	6.0
Muscovite	5.3	4.8	2.2	2.2	3.0
Apatite	0.2	0.3	tr	tr	0.4
Zircon	tr	tr	0.1	tr	0.1
Opaque Minerals	tr	0.1	0.3	0.1	0.3
magnetite					
ilmenite	x	x	x	x	x
pyrite	x	x	x	x	x
pyrrhotite					
Chlorite			tr		0.5
Calcite					0.3
100Pl/(Pl+Ksp)	48	48	44	52	30
100Qz/(Qz+Fsp)	34	29	35	19	39

Plagioclase composition determined by Michel-Levy extinction angle method and electron microprobe(*).

x opaque mineral observed in polished section.

Hand specimen description and sample location of the Fitzwilliam Granite.

SM3 Coarse-grained, nonfoliated, light gray colored granite. Mt. Monadnock 15-minute quadrangle. Quarry on east side of Route 12, across from Fitzwilliam solid waste dump, between Fitzwilliam and Troy.

SM4 Medium-grained, lightly foliated, light gray colored granite. Mt. Monadnock 15-minute quadrangle. Quarry on north side of Route 119, 1.7 km west of Fitzwilliam.

SM9 Coarse-grained, nonfoliated, light gray colored granite. Mt. Monadnock 15-minute quadrangle. On Boston-Maine RR line, 2.2 km west of Fitzwilliam.

SM11 Coarse-grained, nonfoliated, light gray colored granite. Mt. Monadnock 15-minute quadrangle. South side of Route 119, across from SM4.

SA61-3 Medium-to fine-grained, moderately foliated, light gray colored granite. Athol 7.5-minute quadrangle. South side of Boston-Maine RR line, 0.9 km east of Duck Pond.

MINERAL CHEMISTRY

Analytical Methods

To determine precise mineral compositions, samples representative of all the plutonic units were analyzed using a three-spectrometer, wavelength-dispersive ETEC electron microprobe at the Department of Geology and Geography, University of Massachusetts, Amherst. Analyses were done on carbon-coated standard petrographic thin sections. Standards used were all well characterized natural minerals. The probe operating conditions were: accelerating potential of 15,000 volts, beam current of 0.02 amperes, chamber vacuum of 1.5×10^{-5} to 8.0×10^{-6} torr, electron beam diameter of 2 to 10 μm and peak and background counting time of 15 seconds. Corrections were made for machine dead time and background count rate, followed by empirical alpha factor corrections of Bence and Albee (1968) and Albee and Ray (1970).

Electron microprobe analysis cannot distinguish between the oxidation states of iron. Calculations for ferric iron were done on minerals known to exhibit near perfect cation stoichiometry. In minerals exhibiting deviations from ideal stoichiometry a range of ferric-ferrous ratios was calculated or FeO was determined directly. In muscovite, only maximum and minimum ferric corrections are given. Biotite and amphibole were separated from selected samples for wet analytical determination of FeO using the cold acid digestion analytical technique described by Maxwell (1968). The correlation between the biotite and the whole rock FeO-Fe_2O_3 ratio was used to approximate that ratio in biotite analyses with only total iron determinations. Interpretations and approximations of amphibole ferric-ferrous ratios were made for electron microprobe analyses using the complete analyses from amphibole separates.

Pyroxene

In plutonic rocks associated with the Hardwick Tonalite, pyroxene occurs only in those with normative diopside and less than 56 weight percent SiO_2. Augite is the only pyroxene in augite-hornblende quartz diorite and diorite of the Bear Den sill, and occurs with orthopyroxene in the diorite from Goat Hill.

Most pyroxenes are rimmed by hornblende and some are completely pseudomorphed by it. The augite and orthopyroxene in plutonic rocks lying within metamorphic zones VI and V are rimmed by hornblende. At lower grades of metamorphism, hornblende forms wide rims around cores with intricate intergrowths of augite and hornblende.

Representative pyroxene analyses are shown in Tables 14 and 15. Structural formulae are based on four cations and six oxygens and assigned sites as suggested by Robinson (1980). Assuming a perfectly stoichiometric pyroxene, total iron from microprobe analyses was corrected to Fe^{3+} and Fe^{2+}. Pyroxene quadrilateral components are plotted in Figure 15.

Table 14. Electron microprobe analyses of augite from plutonic rocks associated with the Hardwick Tonalite. Structural formulae based on 4 cations and 6 oxygens.

	Nichewaug Sill								augite-hornblende quartz diorite within the Hardwick Pluton	
	SP179	SP179	SP179	SP179	SP236-3	SP236-3	SP236-2	SP236-2	1080-00	1080-00
SiO_2	50.94	51.17	52.24	50.96	52.02	52.08	52.53	52.34	52.46	53.14
TiO_2	0.13	0.10	0.14	0.18	0.13	0.10	0.04	0.09	0.16	0.14
Al_2O_3	1.56	1.34	1.46	1.74	1.05	0.76	0.73	0.82	1.13	1.12
FeO*	8.05	7.90	7.82	8.09	10.36	10.82	10.18	10.17	8.55	8.38
MgO	14.50	14.50	14.23	14.41	12.20	12.13	12.33	12.16	13.73	13.41
MnO	1.32	1.34	1.35	1.35	1.13	1.06	1.11	1.05	0.86	0.81
CaO	22.36	22.70	22.69	21.52	22.35	22.58	22.59	22.60	22.35	22.51
Na_2O	0.56	0.51	0.50	0.57	0.42	0.30	0.11	0.30	0.60	0.52
Total	99.42	99.56	100.43	98.82	99.77	99.29	99.62	99.53	99.84	100.03
n**	16	6	6	5	5	8	4	3	10	8
Structural Formulae										
Si	1.897	1.901	1.930	1.910	1.963	1.976	1.987	1.980	1.954	1.980
Al	.068	.061	.063	.077	.037	.024	.013	.020	.046	.020
Fe^{3+}	.035	.038	.007	.013						
	2.000	2.000	2.000	2.000	2.000	2.000	2.000	2.000	2.000	2.000
Al					.010	.010	.020	.017	.004	.029
Fe^{3+}	.137	.132	.098	.121	.054	.030		.019	.075	.022
Ti	.004	.002	.004	.005	.002	.003	.001	.003	.005	.004
Fe^{2+}	.054	.061	.114	.068	.248	.271	.283	.275	.153	.200
Mg	.805	.805	.784	.806	.686	.686	.696	.686	.763	.745
Mn										
	1.000	1.000	1.000	1.000	1.000	1.000	1.000	1.000	1.000	1.000
Fe^{2+}	.026	.015	.023	.053	.025	.025	.039	.028	.039	.039
Mn	.041	.042	.043	.043	.036	.034	.035	.034	.027	.026
Ca	.893	.906	.899	.864	.908	.919	.917	.916	.892	.898
Na	.040	.037	.036	.041	.031	.022	.008	.022	.043	.038
	1.000	1.000	1.001	1.001	1.000	1.000	0.999	1.000	1.001	1.001
Ca+Na/2	.467	.472	.468	.453	.470	.471	..463	.469	.468	.468
Wo	50	50	49	48	49	48	47	47	48	48
En	45	45	43	45	37	36	36	37	41	40
Fs	5	5	8	7	14	16	17	16	11	12
$Mn/(Mn+Fe^{2+})$	.339	.356	.239	.262	.117	.103	.098	.102	.123	.098
$Mg/(Mg+Fe^{2+})$	.76	.77	.76	.76	.68	.68	.68	.68	.74	.74

Table 14, continued.

	augite-hornblende quartz diorite within the Hardwick Pluton		diorite sill at Bear Den			diorite at Goat Hill					
	1080-00	1083-50	SA176-3	SA176-3	SA176-3	SW522a	SW522a	SW522b	SW522b	SW522b	SW522b
SiO_2	52.52	52.99	53.00	53.33	552.88	52.78	53.28	51.13	52.08	53.01	53.18
TiO_2	0.18	0.14	0.17	0.18	0.18	0.40	0.13	0.44	0.10	0.13	0.21
Al_2O_3	1.14	1.16	2.20	2.35	2.30	2.26	1.35	3.21	1.34	1.64	2.02
FeO*	8.52	8.54	6.99	7.18	7.17	8.75	10.17	8.99	7.75	8.19	8.46
MgO	13.59	13.58	15.57	15.14	15.29	13.97	15.01	14.60	15.03	14.39	14.31
MnO	0.87	0.85	0.26	0.31	0.32	x	x	0.40	0.50	0.46	0.48
CaO	22.34	22.31	21.96	22.00	21.89	21.71	20.26	20.36	22.51	21.66	21.39
Na_2O	0.56	0.58	0.42	0.46	0.42	0.53	0.41	0.66	0.50	0.57	0.59
Total	99.72	100.15	100.57	100.97	100.44	100.40	100.61	99.97	99.81	100.05	100.28
n**	13	3	4	3	3	5	5	3	3	6	8
Structural Formulae											
Si	1.960	1.969	1.938	1.945	1.939	1.951	1.966	1.894	1.926	1.962	1.958
Al	.040	.031	.062	.055	.061	.049	.034	.106	.058	.038	.042
Fe^{3+}											
	2.000	2.000	2.000	2.000	2.000	2.000	2.000	2.000	2.000	2.000	2.000
Al	.010	.020	.033	.047	.039	.050	.025	.034		.034	.046
Fe^{3+}	.061	.046	.050	.031	.042	.015	.033	.094	.103	.037	.025
Ti	.005	.004	.005	.005	.006	.011	.003	.012	.003	.004	.006
Fe^{2+}	.167	.178	.063	.093	.078	.154	.113	.054	.065	.130	.137
Mg	.757	.752	.849	.824	.835	.770	.826	.806	.829	.795	.786
Mn											
	1.000	1.000	1.000	1.000	1.000	1.000	1.000	1.000	1.000	1.000	1.000
Fe^{2+}	.038	.044	.101	.098	.100	.102	.168	.131	.056	.086	.099
Mn	.028	.027	.008	.010	.011	x	x	.013	.016	.014	.015
Ca	.894	.888	.861	.860	.859	.860	.802	.809	.892	.859	.844
Na	.041	.042	.030	.033	.031	.038	.030	.047	.036	.041	.042
	1.000	1.000	1.000	1.000	1.000	1.000	1.000	1.000	1.000	1.000	1.000
Ca+Na/2	.468	.465	.446	.447	.445	.449	.416	.428	.464	.450	.444
Wo	48	48	46	46	46	46	42	45	48	46	45
En	41	40	45	44	45	41	43	45	45	43	42
Fs	11	12	9	10	9	13	15	10	7	11	13
$Mn/(Mn+Fe^{2+})$	.120	.108	.047	.050	.058	x	x	.066	.117	.061	.060
$Mg/(Mg+Fe^{2+})$	.74	.74	.80	.79	.79	.74	.73	.74	.78	.76	.75

Total iron as (*), Number of analyses (**), element not analyzed (x).

Table 15. Electron microprobe analyses of orthopyroxene from the diorite at Goat Hill. Structural formulae based on 4 cations and 6 oxygen.

	SW522a	SW522a	SW522b	SW522b	SW522b
SiO_2	51.40	51.60	52.49	51.34	52.68
TiO_2	0.10	0.11	0.11	0.10	0.11
Al_2O_3	0.77	0.75	0.83	0.70	0.62
FeO*	23.34	23.38	23.10	23.16	23.35
MgO	22.63	21.98	22.47	22.84	22.48
MnO	1.20	1.25	1.24	1.24	1.30
CaO	0.08	0.13	0.15	0.36	0.15
Na_2O					
Total	99.52	99.20	100.39	99.74	100.69
n**	12	7	8	10	9
Structural Formulae					
Si	1.931	1.942	1.956	1.928	1.955
Al	.035	.043	.037	.033	.035
Fe^{3+}	.034	.015	.007	.039	.010
	2.000	2.000	2.000	2.000	2.000
Al					
Fe^{3+}	.063	.052	.047	.066	.039
Ti	.003	.003	.003	.003	.003
Mg	.934	.945	.950	.931	.958
	1.000	1.000	1.000	1.000	1.000
Mg	.327	.293	.293	.343	.280
Fe^{2+}	.633	.666	.665	.615	.676
Mn	.037	.038	.039	.039	.041
Ca	.003	.003	.003	.003	.003
	1.000	1.000	1.000	1.000	1.000
Wo					
En	67	65	65	67	65
Fs	33	35	35	33	35
$Mn/(Mn+Fe^{2+})$	.055	.054	.055	.060	.057

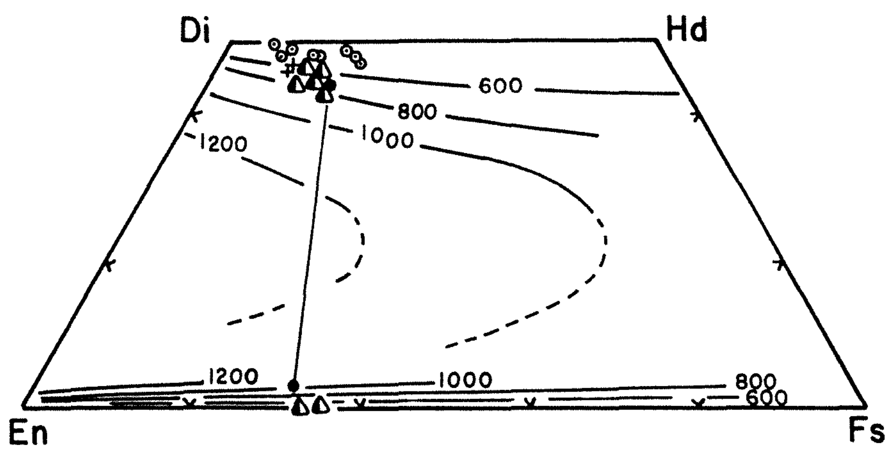

Figure 15. Composition of augites and orthopyroxenes from the augite-hornblende quartz diorite (⊙), diorite at Bear Den (+), diorite at Goat Hill (▲), and the Belchertown Pluton (●) plotted on a pyroxene quadrilateral. Augite-pigeonite solvus and augite-orthopyroxene solvus of Lindsley (1983) are superimposed.

The clinopyroxenes are variable in CaO content with those from the augite-hornblende quartz diorite having a Wo content of between 48 and 50, and the clinopyroxene from the diorites from Bear Den and Goat Hill having a Wo content of between 42 and 48. The Wo component in the orthopyroxene from Goat Hill is less than 0.2.

Clinopyroxenes are uniformly low in Al(IV + VI) and Ti and high in Mn. The sum of Al(IV) + Al(VI) ranges from .033 to .140 cations per unit formula and is highest in the diorite at Bear Den. Ti is extremely low in all the pyroxenes ranging from .001 to .012 cations per unit formula. Mn in the Nichewaug pyroxenes ranges from .034 to .043 cations per formula unit and has a Mn/(Mn + Fe^{2+}) ratio of between .098 and .356. Mn from the pyroxene from Goat Hill and Bear Den ranges from .008 to .016 cations per unit formula and have a Mn/(Mn + Fe^{2+}) ratio of between .047 and .117.

Superimposed upon the pyroxene quadrilateral in Figure 15 is the augite-pigeonite solvus and augite-orthopyroxene solvus of Lindsley (1983). Also plotted in Figure 15 are coexisting igneous pyroxenes from the Belchertown pluton. Temperature estimates derived from the comparison with the augite-orthopyroxene solvus range from metamorphic temperatures (less than 600°C) to plutonic temperatures (900°C). $CaSiO_3$ content of the pyroxenes and estimated temperature variations appear not to be correlated to metamorphic grade. Although the Goat Hill clinopyroxene is suggestive of a magmatic composition, the low $CaSiO_3$ content of the pyroxenes and estimated temperature variations appear not to be correlated to metamorphic grade. Although the Goat Hill clinopyroxene is suggestive of a magmatic composition, the low $CaSiO_3$ (Wo) component of the coexisting orthopyroxene and its hornblende overgrowth indicates a metamorphic reequilibration.

In summary, the pyroxenes of plutonic rocks associated with the Hardwick Tonalite are probably igneous in origin and not a result of prograde regional metamorphism. Many of the plutonic pyroxenes have reequilibrated under metamorphic conditions as shown by large hornblende rims and intimate intergrowths with hornblende.

Hornblende

Hornblende occurs in augite-hornblende quartz diorite, Bear Den sill of diorite, diorite at Goat Hill and the hornblende-biotite tonalite member of the Hardwick Tonalite. Table 16 presents amphibole analyses determined by a combination of electron microprobe and wet chemical analyses. With both ferric and ferrous iron determined in these amphibole analyses, Ca in the M1-M3 sites is negligible and Na in the M4 site ranges form .141 to .226. Structural formulae for electron microprobe analyses (Table 17) were corrected for ferrous iron using the criteria suggested by microprobe-wet chemical analysis and Robinson *et al.* (1982). Each amphibole structural formula was recalculated based upon

Table 16. Analyses of amphibole from the hornblende-biotite tonalite determined by a combination of electron microprobe and wet chemical determination of FeO.

	SP65-1a	SP65-1b	SP65-1c	SP65-1d	SP65-1e	SP65-1f	SP65-1g	SP65-1h	SP65-1i	SA100-1	SA100-2
SiO_2	43.37	42.99	42.97	43.56	43.50	43.46	43.48	43.09	42.97	43.47	43.49
TiO_2	1.00	1.19	0.95	0.96	0.99	0.95	0.98	0.99	0.90	1.26	1.23
Al_2O_3	11.45	11.18	11.27	11.54	11.36	11.44	11.28	11.54	11.36	10.75	10.80
Fe_2O_3	6.06	5.62	6.02	6.34	5.28	5.71	5.92	5.82	6.02	4.80	4.62
FeO	11.82	11.82	11.82	11.82	11.82	11.82	11.82	11.82	11.82	13.55	13.55
MgO	10.41	10.68	10.51	10.41	10.79	10.62	10.54	10.38	10.37	9.45	9.61
MnO	0.53	0.60	0.53	0.51	0.61	0.51	0.52	0.53	0.53	1.07	1.05
CaO	11.66	11.53	11.35	11.45	11.44	11.36	11.59	11.51	11.46	11.31	11.13
Na_2O	1.67	1.60	1.52	1.48	1.50	1.51	1.67	1.46	1.56	1.60	1.53
K_2O	0.88	0.98	0.88	0.93	0.90	0.83	0.82	0.92	0.86	1.30	1.31
Total	98.87	98.19	97.82	99.00	98.19	98.21	98.62	98.06	97.85	98.56	98.82
n*	3	2	5	3	3	8	6	1	2	8	5
Structural Formulae											
Si	6.400	6.391	6.406	6.412	6.442	6.435	6.425	6.403	6.405	6.489	6.499
Al	1.600	1.609	1.594	1.588	1.588	1.565	1.575	1.597	1.595	1.511	1.501
tet. total	8.000	8.000	8.000	8.000	8.000	8.000	8.000	8.000	8.000	8.000	8.000
Al	.392	.349	.386	.414	.424	.431	.389	.424	.400	.380	.401
Fe^{3+}	.672	.629	.675	.702	.589	.637	.659	.650	.675	.540	.519
Ti	.111	.133	.107	.106	.110	.106	.109	.111	.101	.142	.138
Fe^{2+}	1.459	1.469	1.473	1.455	1.464	1.463	1.461	1.469	1.473	1.691	1.693
Mg	2.290	2.367	2.336	2.284	2.382	2.344	2.322	2.299	2.304	2.103	2.140
Mn	.069	.053	.023	.039	.031	.019	.060	.047	.047	.135	.109
Ca	.007									.009	
M1-M3 total	5.000	5.000	5.000	5.000	5.000	5.000	5.000	5.000	5.000	5.000	5.000
Mn		.023	.044	.025	.046	.045	.005	.020	.020		.024
Ca	1.836	1.836	1.813	1.806	1.815	1.602	1.835	1.832	1.830	1.800	1.782
Na	.164	.141	.143	.169	.139	.153	.160	.148	.150	.200	.194
M4 total	2.000	2.000	2.000	2.000	2.000	2.000	2.000	2.000	2.000	2.000	2.000
Na	.313	.320	.296	.254	.292	.281	.318	.273	.301	.263	.250
K	.165	.186	.167	.175	.171	.157	.154	.175	.163	.248	.250
A total	.478	.506	.463	.429	.463	.438	.472	.448	.464	.511	.500

	SA100-3	SA100-4	SA100-5	SA100-6	SA100AVE
SiO_2	43.46	43.20	43.52	43.67	43.47
TiO_2	1.14	1.42	1.01	1.23	1.22
Al_2O_3	11.04	11.03	11.04	10.47	10.86
Fe_2O_3	4.32	4.37	4.75	4.89	4.62
FeO	13.55	13.55	13.55	13.55	13.55
MgO	9.56	9.21	9.06	9.42	9.42
MnO	1.00	1.04	1.04	1.05	1.04
CaO	11.11	11.19	11.07	11.14	11.16
Na_2O	1.54	1.51	1.54	1.49	1.54
K_2O	1.28	1.28	1.21	1.26	1.27
Total	98.00	97.80	97.79	98.17	98.15
n*	7	10	11	9	50
Structural Formulae					
Si	6.504	6.486	6.531	6.536	6.505
Al	1.496	1.514	1.469	1.464	1.495
tet. total	8.000	8.000	8.000	8.000	8.000
Al	.452	.438	.484	.383	.420
Fe^{3+}	.487	.494	.536	.550	.520
Ti	.129	.161	.114	.139	.138
Fe^{2+}	1.696	1.701	1.700	1.696	1.696
MgO	2.133	2.061	2.027	2.102	2.101
MnO	.103	.133	.133	.130	.125
CaO		.012	.006		
M1-M3 total	5.000	5.000	5.000	5.000	5.000
Mn	.024			.003	.007
Ca	1.781	1.788	1.774	1.786	1.789
Na	.195	.212	.226	.211	.204
M4 total	2.000	2.000	2.000	2.000	2.000
Na	.251	.228	.221	.221	.242
K	.245	.245	.231	.241	.243
A total	.496	.473	.452	.462	.485

Number of analyses(*)

Table 17. Electron microprobe analyses of amphibole from hornblende-biotite tonalite, augite-hornblende quartz diorite, diorite sill at Bear Den and the Goat Hill diorite.

	hornblende-biotite tonalite									
	SA160-3a	SA160-3b	SA160-3c	SA160-3d	SA160-3e	SA160-3f	SA160-3g	SA160-3h	SA160-3i	SA160-3j
SiO_2	42.75	42.19	42.63	42.07	42.99	41.85	42.23	42.27	42.10	43.29
TiO_2	1.08	0.88	1.02	1.03	1.12	0.95	1.02	1.03	0.86	1.37
Al_2O_3	10.69	10.87	10.76	10.72	10.74	10.96	10.65	10.60	10.93	11.19
FeO^{+3}	18.91	18.83	18.87	18.54	18.61	18.91	18.95	19.06	19.14	17.48
MgO	9.78	9.70	9.85	9.78	9.80	9.46	9.87	9.90	9.62	10.05
MnO	0.67	0.71	0.64	0.68	0.62	0.59	0.62	0.59	0.59	0.61
CaO	11.51	11.53	11.28	11.51	11.61	11.58	11.68	11.63	11.61	11.56
Na_2O	1.63	1.51	1.64	1.72	1.74	1.83	1.78	1.79	1.61	1.76
K_2O	1.26	1.19	1.23	1.26	1.20	1.29	1.25	1.28	1.17	1.24
Total	98.28	97.41	97.92	97.31	98.43	97.42	98.05	98.15	97.63	98.55
n*	1	1	1	1	3	1	1	2	1	1
Struct. Form.	a	a	d	a	a	b	b	b	b	d
Si	6.379	6.336	6.380	6.340	6.404	6.317	6.320	6.324	6.316	6.424
Al	1.621	1.664	1.620	1.660	1.596	1.683	1.680	1.676	1.684	1.576
tet. total	8.000	8.000	8.000	8.000	8.000	8.000	8.000	8.000	8.000	8.000
Al	.259	.259	.279	.244	.289	.267	.199	.193	.249	.381
Fe^{3+}	.727	.879	.722	.775	.666	.767	.840	.830	.892	.471
Ti	.121	.099	.115	.117	.125	.108	.115	.116	.097	.152
Fe^{2+}	1.633	1.501	1.639	1.580	1.666	1.641	1.552	1.574	1.529	1.698
Mg	2.176	2.172	2.197	2.197	2.176	2.129	2.202	2.208	2.152	2.334
Mn	.084	.090	.049	.087	.078	.076	.079	.075	.075	.075
Ca						.012	.013	.004	.006	
M1-M3 total	5.000	5.000	5.000	5.000	5.000	5.000	5.000	5.000	5.000	5.000
Mn	.001		.032							.001
Ca	1.840	1.855	1.808	1.859	1.853	1.859	1.860	1.860	1.860	1.838
Na	.159	.145	.160	.141	.147	.141	.140	.140	.140	.161
M4 total	2.000	2.000	2.000	2.000	2.000	2.000	2.000	2.000	2.000	2.000
Na	.312	.295	.315	.363	.356	.394	.377	.379	.328	.346
K	.240	.228	.235	.242	.228	.248	.239	.245	.224	.235
A total	.552	.523	.550	.605	.584	.642	.616	.624	.552	.581

	hornblende-biotite tonalite										
	SW12	SA61-1a	SA61-1b	SA61-1c	SA61-1d	SA61-1e	SA61-1f	SA61-1g	SA61-1h	SA61-1i	SA61-1j
SiO_2	42.27	42.76	42.53	42.60	42.17	42.92	43.05	42.90	42.39	42.70	42.36
TiO_2	1.49	0.60	0.38	0.52	0.57	0.54	0.57	0.48	0.48	0.56	0.53
Al_2O_3	11.45	11.37	11.67	10.86	11.94	11.22	10.59	10.99	11.37	11.65	11.35
FeO^{+3}	17.06	17.00	17.31	16.85	17.45	17.03	16.49	17.05	17.03	16.82	17.06
MgO	10.64	11.26	10.71	11.16	10.56	11.11	11.59	11.04	11.10	11.00	10.87
MnO	0.83	0.59	0.61	0.56	0.61	0.59	0.56	0.51	0.56	0.50	0.50
CaO	11.00	11.63	11.89	11.76	11.73	11.75	11.83	11.84	11.72	11.53	11.79
Na_2O	1.59	1.51	1.63	1.69	1.44	1.62	1.45	1.53	1.48	1.66	1.67
K_2O	1.50	0.85	0.85	0.71	0.88	0.75	0.75	0.84	0.78	0.77	0.82
Total	97.83	97.56	97.58	96.71	97.39	97.53	96.88	97.18	96.91	97.19	96.95
n*	24	1	1	1	1	1	1	1	2	1	1
Struct. Form.	d	c	b	b	b	b	b	b	b	d	b
Si	6.304	6.310	6.295	6.347	6.252	6.341	6.377	6.364	6.293	6.331	6.307
Al	1.696	1.690	1.705	1.653	1.748	1.659	1.623	1.636	1.707	1.669	1.693
tet. total	8.000	8.000	8.000	8.000	8.000	8.000	8.000	8.000	8.000	8.000	8.000
Al	.317	.286	.331	.255	.339	.295	.226	.285	.282	.366	.299
Fe^{3+}	.618	.998	1.007	1.004	1.044	.984	1.056	.985	1.086	.875	.979
Ti	.167	.067	.042	.059	.064	.060	.064	.054	.054	.063	.060
Fe^{2+}	1.510	1.100	1.155	1.115	1.140	1.140	1.007	1.150	1.048	1.211	1.166
Mg	2.366	2.477	2.363	2.479	2.334	2.447	2.559	2.442	2.457	2.431	2.413
Mn	.022	.072	.076	.070	.076	.073	.070	.064	.070	.054	.063
Ca			.026	.018	.003	.001	.018	.020	.003		.020
M1-M3 total	5.000	5.000	5.000	5.000	5.000	5.000	5.000	5.000	5.000	5.000	5.000
Mn	.083	.001								.009	
Ca	1.758	1.839	1.860	1.859	1.861	1.860	1.860	1.822	1.861	1.831	1.860
Na	.159	.150	.140	.141	.139	.140	.140	.138	.139	.160	.140
M4 total	2.000	2.000	2.000	2.000	2.000	2.000	2.000	2.000	2.000	2.000	2.000
Na	.301	.272	.328	.347	.245	.324	.276	.302	.287	.317	.343
K	.285	.160	.160	.135	.166	.141	.142	.159	.148	.145	.156
A total	.586	.432	.488	.482	.441	.465	.418	.461	.435	.462	.499

Explanation for Table 17.

Each amphibole structural formula was recalculated based upon one of the following assumptions. Letter coding for each type of recalculation is given in the tables of analyses.

a: Total cations to 13 exclusive of K, Na, and Ca. This assumption excludes Ca from M1-3 sites and Mn, Fe^{2+}, and Mg from the M4 site.

b: Na in M4 set to .140

c: Na in M4 set to .150

d: Na in M4 set to .160

e. Na in M4 set to .200

Number of analyses (*)

Symbols for the Goat Hill diorite, Bear Den sill of diorite, and the augite-hornblende quartz diorite: (s) single grain, (b) inclusion in augite-hornblende intergrowth, (c) outer rim around augite-hornblende intergrowth, (o) rim around orthopyroxene, (r) rim of blue green amphibole around olive green amphibole, (i) inclusion in augite, and (ib) inclusion in biotite.

Table 17, continued.

	hornblende-biotite tonalite											
	SA61-1k	SA61-1l	SA61-1m	SA61-1n	SA61-1o	SA61-1p	SA61-1q	SA61-1r	SA4	SA4	SA4	SA4
SiO_2	43.63	43.48	43.50	43.89	43.97	43.90	43.90	43.64	44.27	43.59	43.85	44.53
TiO_2	0.54	0.94	0.68	0.73	0.72	0.76	0.75	0.57	0.78	0.64	0.84	0.83
Al_2O_3	10.60	9.99	10.02	10.29	10.45	10.30	10.32	10.05	10.92	11.80	11.13	10.76
FeO^{+}	16.26	16.67	16.55	16.47	16.33	16.08	16.38	16.21	16.94	17.26	17.03	16.80
MgO	11.59	11.64	11.70	11.67	11.91	11.86	11.62	11.83	10.03	10.03	10.40	10.48
MnO	0.59	0.50	0.52	0.59	0.57	0.50	0.53	0.55	0.77	0.73	0.73	0.72
CaO	11.74	11.67	11.77	11.64	11.73	11.71	11.76	11.86	11.74	11.67	11.64	11.85
Na_2O	1.41	1.41	1.55	1.46	1.42	1.47	1.43	1.49	1.23	1.32	1.28	1.18
K_2O	0.70	0.88	0.78	0.80	0.75	0.76	0.81	0.69	1.03	1.04	1.07	0.98
Total	97.06	97.18	97.07	97.54	97.85	97.34	97.30	96.89	97.98	98.08	97.97	98.13
n*	2	1	1	1	1	1	2	3	14	7	5	8
Struct. Form.	a	a	b	a	a	a	a	b	b	a	a	b
Si	6.444	6.440	6.445	6.468	6.442	6.469	6.453	6.459	6.564	6.438	6.479	6.555
Al	1.556	1.560	1.555	1.532	1.558	1.531	1.547	1.541	1.436	1.562	1.521	1.445
tet. total	8.000	8.000	8.000	8.000	8.000	8.000	8.000	8.000	8.000	8.000	8.000	8.000
Al	.289	.184	.195	.255	.247	.258	.249	.211	.472	.492	.417	.422
Fe^{3+}	.956	.931	.964	.868	.930	.872	.915	.987	.586	.680	.667	.661
Ti	.060	.105	.075	.080	.079	.084	.083	.064	.087	.071	.094	.092
Fe^{2+}	1.072	1.146	1.106	1.162	1.072	1.118	1.128	1.039	1.535	1.457	1.439	1.427
Mg	2.552	2.571	2.584	2.564	2.601	2.605	2.558	2.610	2.218	2.208	2.291	2.800
Mn	.073	.063	.067	.071	.071	.063	.067	.069	.097	.092	.092	.090
Ca			.009					.020	.005			.003
M1-M3 total	5.000	5.000	5.000	5.000	5.000	5.000	5.000	5.000	5.000	5.000	5.000	5.000
Mn												
Ca	1.858	1.852	1.859	1.838	1.841	1.849	1.860	1.861	1.860	1.847	1.843	1.861
Na	.142	.148	.141	.159	.159	.151	.140	.139	.140	.153	.157	.139
M4 total	2.000	2.000	2.000	2.000	2.000	2.000	2.000	2.000	2.000	2.000	2.000	2.000
Na	.262	.257	.305	.258	.245	.269	.269	.289	.214	.225	.210	.198
K	.132	.167	.147	.150	.140	.143	.153	.130	.195	.196	.202	.184
A total	.394	.424	.452	.408	.385	.412	.422	.419	.409	.421	.412	.382

	hornblende-biotite tonalite		augite-hornblende quartz diorite							
	SA4	SA4	SP179-1s	SP179-2s	SP179-3s	SP179-4s	SP179-5s	SP179-6s	SP236-3s	SP236-3s
SiO_2	44.55	44.24	44.44	44.41	42.90	44.38	44.01	44.63	43.17	43.78
TiO_2	0.85	0.88	1.23	1.24	1.14	1.20	1.19	1.28	1.29	1.33
Al_2O_3	10.38	10.59	10.71	10.53	10.91	10.97	10.84	10.84	9.57	9.49
FeO^{+}	16.98	16.86	18.08	18.08	18.70	17.63	18.04	16.47	18.41	18.08
MgO	10.61	10.55	10.18	10.13	10.05	9.90	9.97	10.81	9.86	9.98
MnO	0.63	0.71	0.66	0.67	0.63	0.66	0.62	0.50	0.61	0.62
CaO	11.71	11.74	10.42	10.33	10.84	10.38	10.73	11.50	11.48	11.29
Na_2O	1.32	1.26	1.61	1.50	1.56	1.47	1.53	1.35	1.65	1.63
K_2O	1.03	1.04	1.13	1.14	1.17	1.19	1.16	0.77	1.17	1.16
Total	98.06	97.87	98.46	98.03	97.90	97.68	98.09	98.15	97.21	97.36
n*	2	10	5	6	9	9	9	9	5	3
Struct. Form.	a	a	e	e	e	e	e	d	a	a
Si	6.572	6.539	6.576	6.599	6.388	6.660	6.537	6.557	6.515	6.590
Al	1.428	1.461	1.401	1.424	1.612	1.440	1.463	1.443	1.485	1.410
tet. total	8.000	8.000	8.000	8.000	8.000	8.000	8.000	8.000	8.000	8.000
Al	.377	.384	.443	.444	.303	.527	.434	.434	.217	.274
Fe^{3+}	.623	.667	.430	.431	.781	.352	.503	.520	.615	.458
Ti	.095	.098	.139	.137	.128	.135	.133	.141	.146	.150
Fe^{2+}	1.482	1.438	1.744	1.742	1.548	1.786	1.722	1.504	1.726	1.818
Mg	2.344	2.325	2.244	2.246	2.231	2.200	2.208	2.368	2.218	2.240
Mn	.079	.089			.009			.033	.078	.060
Ca										
M1-M3 total	5.000	5.000	5.000	5.000	5.000	5.000	5.000	5.000	5.000	5.000
Fe			.073	.065		.060	.015			
Mn			.084	.083	.071	.083	.078	.029		.019
Ca	1.851	1.860	1.644	1.652	1.729	1.657	1.707	1.810	1.856	1.821
Na	.149	.140	.199	.200	.200	.200	.200	.161	.144	.160
M4 total	2.000	2.000	2.000	2.000	2.000	2.000	2.000	2.000	2.000	2.000
Na	.229	.221	.233	.262	.250	.225	.240	.224	.339	.315
K	.193	.196	.216	.213	.222	.226	.220	.144	.225	.223
A total	.422	.417	.449	.475	.472	.451	.460	.368	.564	.538

Table 17, continued.

	augite-hornblende quartz diorite					Bear Den sill of diorite				
	SP236-3a	SP236-3a	SP236-3b	SP236-3b	SP236-3c	SA176-3	SA176-3	SA176-3	SA176-3	SA176-3
SiO_2	45.41	45.06	44.97	44.89	42.60	51.39	49.92	49.41	49.60	50.00
TiO_2	1.05	1.03	0.90	1.01	1.27	0.21	0.29	0.47	0.43	0.95
Al_2O_3	8.82	8.61	8.01	8,98	11.00	5.73	7.08	7.56	9.14	7.19
FeO^+	17.98	17.88	17.34	17.56	18.84	11.42	11.45	12.51	13.28	9.92
MgO	10.51	10.32	10.98	10.79	9.12	16.26	15.17	14.53	13.32	16.31
MnO	0.69	0.79	0.65	0.73	0.53	0.53	0.39	0.50	0.40	0.27
CaO	11.51	11.54	11.97	11.56	11.39	11.69	11.96	11.53	11.95	12.19
Na_2O	1.49	1.52	1.47	1.55	1.44	0.99	1.22	1.35	1.51	1.16
K_2O	0.90	0.86	0.78	0.94	1.17	0.09	0.13	0.16	0.18	0.38
Total	98.36	97.61	97.07	98.01	97.36	98.31	97.61	98.02	97.81	98.37
n*	2	2	2	3	3	6	4	4	5	4
Struct. Form.	d	a	b	d	d	d	d	d	a	a
Si	6.725	6.731	6.718	6.662	6.416	7.258	7.137	7.080	6.872	7.060
Al	1.275	1.269	1.282	1.338	1.584	.742	.863	.920	1.128	.940
tet. total	8.000	8.000	8.000	8.000	8.000	8.000	8.000	8.000	8.000	8.000
Al	.264	.247	.128	.232	.369	.212	.330	.357	.427	.257
Fe^{3+}	.498	.516	.725	.574	.604	.517	.427	.374	.488	.422
Ti	.117	.116	.101	.113	.144	.023	.031	.051	.047	.101
Fe^{2+}	1.729	1.723	1.462	1.605	1.769	.824	.941	1.115	1.125	.753
Mg	2.321	2.298	2.445	2.387	2.048	3.424	3.232	3.103	2.866	3.434
Mn	.071	..100	.083	.089	.066		.039		.048	.033
Ca			.055							
M1-M3 total	5.000	5.000	5.000	5.000	5.000	5.000	5.000	5.000	5.000	5.000
Fe						.008		.010		
Mn	.015			.003	.002	.063	.009	.061		
Ca	1.826	1.846	1.860	1.838	1.837	1.769	1.832	1.770	1.848	1.844
Na	.160	.154	.140	.159	.161	.160	.159	.159	.152	.156
M4 total	2.000	2.000	2.000	2.000	2.000	2.000	2.000	2.000	2.000	2.000
Na	.268	.286	.264	.287	.259	.111	.179	.217	.270	.161
K	.170	.164	.149	.178	.225	.016	.024	.029	.033	.068
A total	.438	.450	.413	.465	.484	.127	.203	.246	.304	.229

	Bear Den sill of diorite			Goat Hill diorite								
	SA176-3	SA176-3	SA176-3a	SW522s	SW522s	SW522a	SW522i	SW522o	SW522o	SW522s	SW522ib	SW522r
SiO_2	52.19	50.93	49.63	44.02	44.87	43.32	43.82	43.97	43.57	44.27	43.75	45.49
TiO_2	0.20	0.62	0.40	1.80	1.84	2.04	1.70	1.96	1.98	2.10	1.90	1.48
Al_2O_3	4.74	5.88	7.06	10.64	10.58	10.78	10.20	9.79	10.12	9.65	9.68	14.07
FeO^+	10.64	11.47	11.43	13.55	13.68	13.30	13.76	12.93	12.98	13.64	13.60	12.62
MgO	16.27	15.89	15.23	13.51	13.46	13.99	13.54	13.59	13.23	13.27	13.36	14.07
MnO	0.36	0.38	0.21	0.22	0.25	0.29	0.27	0.28	0.27	0.31	0.29	0.31
CaO	12.57	11.52	13.56	11.46	11.55	11.47	11.59	11.87	11.92	11.88	11.81	11.59
Na_2O	0.68	1.00	0.82	1.27	1.20	1.55	1.25	1.37	1.47	1.48	1.36	1.32
K_2O	0.01	0.15	0.23	1.13	1.18	1.12	1.13	1.04	1.13	1.09	1.07	0.99
Total	97.66	97.84	98.57	97.60	98.61	97.86	97.26	96.80	96.67	97.69	96.84	98.01
n*	6	2	1	2	2	1	2	5	4	5	5	3
Struct. Form.	b	d	b	d	d	d	d	b	b	b	b	d
Si	7.386	7.249	6.999	6.414	6.477	6.298	6.409	6.460	6.429	6.479	6.442	6.286
Al	.614	.751	1.001	1.586	1.523	1.702	1.591	1.540	1.571	1.521	1.558	1.714
tet. total	8.000	8.000	8.000	8.000	8.000	8.000	8.000	8.000	8.000	8.000	8.000	8.000
Al	.177	.235	.172	.241	.277	.145	.168	.155	.189	.144	.121	.578
Fe^{3+}	.549	.401	.827	.701	.614	.789	.803	.708	.651	.634	.770	.618
Ti	.022	.066	.042	.197	.199	.223	.187	.217	.220	.231	.211	.154
Fe^{2+}	.730	.927	.541	.926	1.014	.811	.880	.901	.970	1.056	.924	.664
Mg	3.433	3.371	3.202	2.935	2.896	3.032	2.952	2.977	2.911	2.895	2.933	2.898
Mn	.043		.026				.010	.034	.034	.038	.038	
Ca	.046		.189					.009	.025	.003	.003	
M1-M3 total	5.000	5.000	5.000	5.000	5.000	5.000	5.000	5.000	5.000	5.000	5.000	5.000
Fe		.037		.024	.024	.017						.176
Mn		.046		.028	.031	.035	.023					.037
Ca	1.840	1.757	1.839	1.789	1.786	1.787	1.817	1.860	1.860	1.860	1.840	1.628
Na	.140	.160	.140	.159	.159	.161	.160	.140	.140	.140	.140	.159
M4 total	2.000	2.000	2.000	2.000	2.000	2.000	2.000	2.000	2.000	2.000	2.000	2.000
Na	.047	.116	.084	.199	.176	.276	.195	.231	.280	.280	.229	.194
K	.002	.027	.041	.210	.217	.207	.211	.195	.213	.203	.201	.175
A total	.049	.143	.125	.409	.393	.483	.406	.426	.493	.483	.430	.369

one of the following assumptions: (1) total cations were set to 13 exclusive of K, Na, and Ca, (2) Na in M4 was set to .140, (3) Na in M4 was set to .150, (4) Na in M4 was set to .160, or (5) Na in M4 was set to .200. The assumption used in each formula recalculation is noted and indexed in Table 17.

In the nomenclature of Leake (1978), these amphiboles are members of the calcic amphibole group ((Ca + Na) $_{M4}$ 1.34; Na_{M4} 0.65) with $(Ca + Na)_{M4}$ ranging from 1.843 to 2.000 and Na_{M4} ranging from .139 to .226. Further classification of the amphiboles based on the nomenclature of Leake (1978) is illustrated in Figure 16.

The $Mg/(Mg + Fe^{2+})$ ratio in the amphiboles ranges form .53 to .72 for the hornblende-biotite tonalite, .54 to .63 for augite-hornblende quartz diorite, .73 to .79 for the diorite at Goat Hill and .72 to .85 for the diorite from the Bear Den Sill. A comparison of the amphiboles of the Hardwick Tonalite and associated plutonic rocks with variations in tetrahedral Si and $Mg/(Mg+Fe^{2+})$ ratio of amphiboles in other plutonic complexes is shown in Figure 17. The amphiboles from the Bear Den sill are similar to the amphiboles from the Finnmarka complex (Czamanske and Wones, 1973) with the tetrahedral Si greater than 6.8/formulae unit, whereas the amphiboles from the other plutonic units are similar to the amphiboles from the southern California batholith (Dodge et al., 1968) with tetrahedral Si less than 6.8/formula unit.

Substitution of Na^+ and K^+ in the A site and Al^{3+}, Fe^{3+} or Ti^{4+} in the octahedral sites is compensated by the substitution of Al for Si in the tetrahedral sites. A plot of Al(IV) against A-site occupancy (Figure 18) shows that the amphibole from the diorite from the Bear Den sill plots at lower values of Al(IV) and A-site occupancy.

The variation of Al(VI), Fe^{3+} and Ti^{4+} in the octahedral sites of the amphiboles is illustrated in Figure 19. The amphiboles from each individual plutonic unit exhibit a range of Al(VI)/Fe^{3+} ratios with limited Ti variation. Although it is expected that some of the Al(VI)/ Fe^{3+} variability is the result of Fe^{3+} corrections, much of the compositional variability in Figure 19 is considered real. In the hornblende-biotite tonalite, samples SA61-1 and SA160-3 plot at lower Al(VI)/Fe^{3+} ratios than other samples of the unit and this appears to reflect the lower Al/Fe^{3+} of the bulk composition. Wet chemical analyses of amphiboles from the hornblende-biotite tonalite plot at higher Al(VI)/Fe^{3+} ratios (with the exception of SP179-3s) than the amphiboles at the northern part of the sill. The amphiboles in the northern part of the sill are commonly intimately related to augite as intergrowths, rims and complete pseudomorphs. The amphiboles of the diorite from Goat Hill show limited variation in Fe^{3+}, Al(VI) and Ti^{4+} but higher Ti^{4+} than in any other unit. A blue-green amphibole rim surrounding an olive green amphibole in this unit has a higher Al(VI)/Fe^{3+} ratio and is lower in Ti^{4+}. Ti^{4+} is generally highest in the diorite from Goat Hill, lowest in the Bear Den sill of diorite and intermediate in the hornblende-biotite tonalite and the augite-hornblende quartz diorite.

The $Fe^{2+}/(Fe^{2+}+Fe^{3+})$ ratio in the amphiboles ranges from .50 to .78 in the hornblende-biotite tonalite, .68 to .80 in the augite-hornblende

A. $(Na+K)_A < 0.50$; $Ti < 0.50$

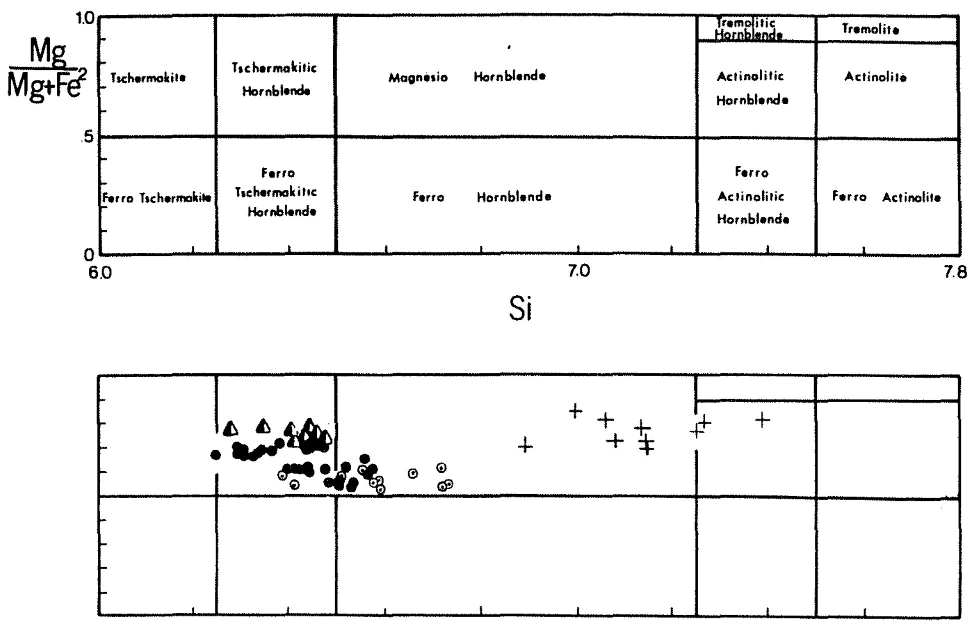

B. $(Na+K)_A > 0.50$; $Ti < 0.50$; $Fe^{3+} > Al(VI)$

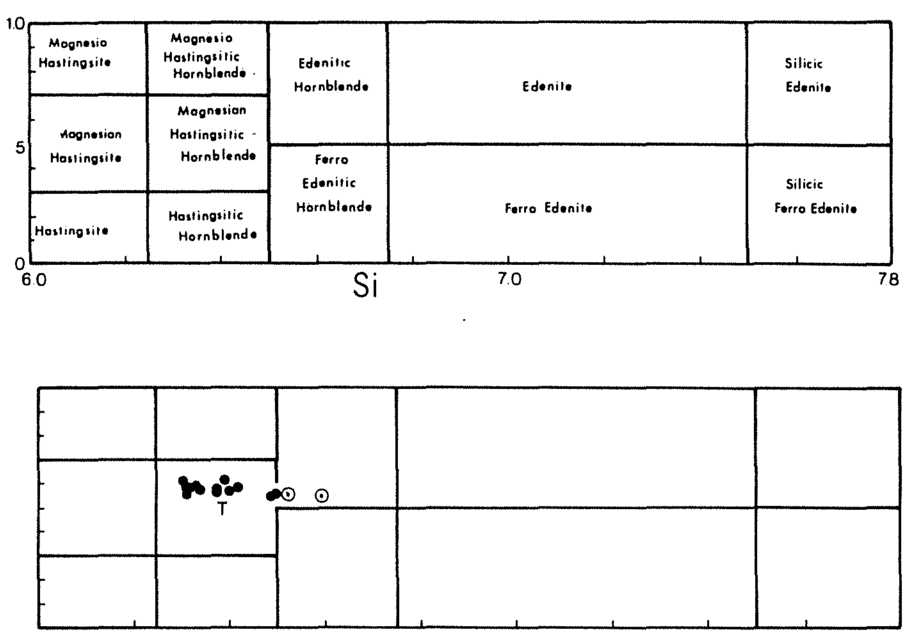

Figure 16. Amphibole compositions from the hornblende-biotite tonalite (●), augite-hornblende quartz diorite (⊙), diorite at Goat Hill (▲), and the diorite of the Bear Den Sill (+) plotted in a modified nomenclature diagram after Leake (1978).

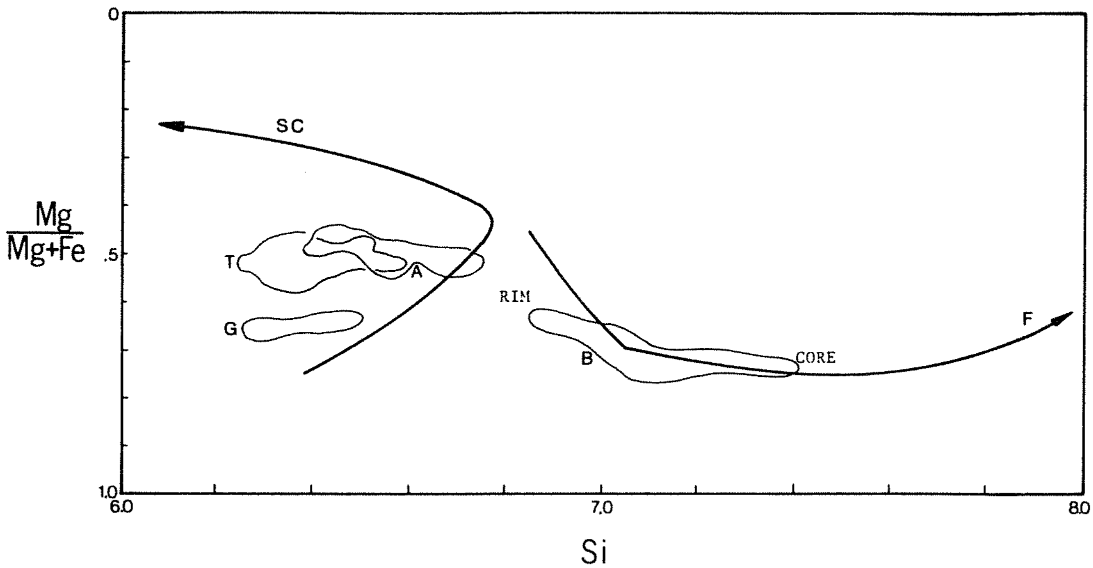

Figure 17. Comparison of the amphibole compositions from the hornblende-biotite tonalite (T), augite-hornblende quartz diorite (A), diorite at Bear Den (B) and diorite at Goat Hill (G) with amphibole compositional variations in the Southern California Batholith (SC) and the Finnmarka Complex, Norway (F).

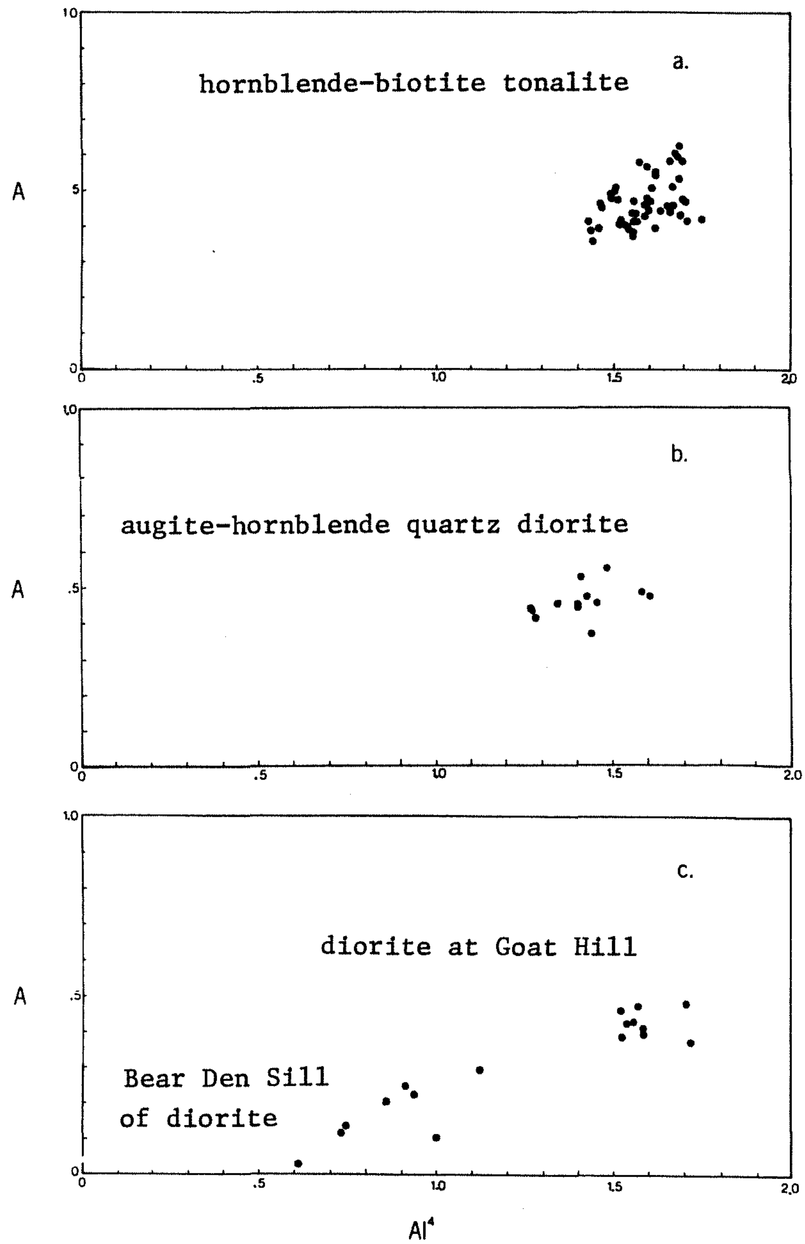

Figure 18. Plot of A site versus Al(IV) for the amphiboles of the Hardwick Tonalite and associated plutonic rocks.

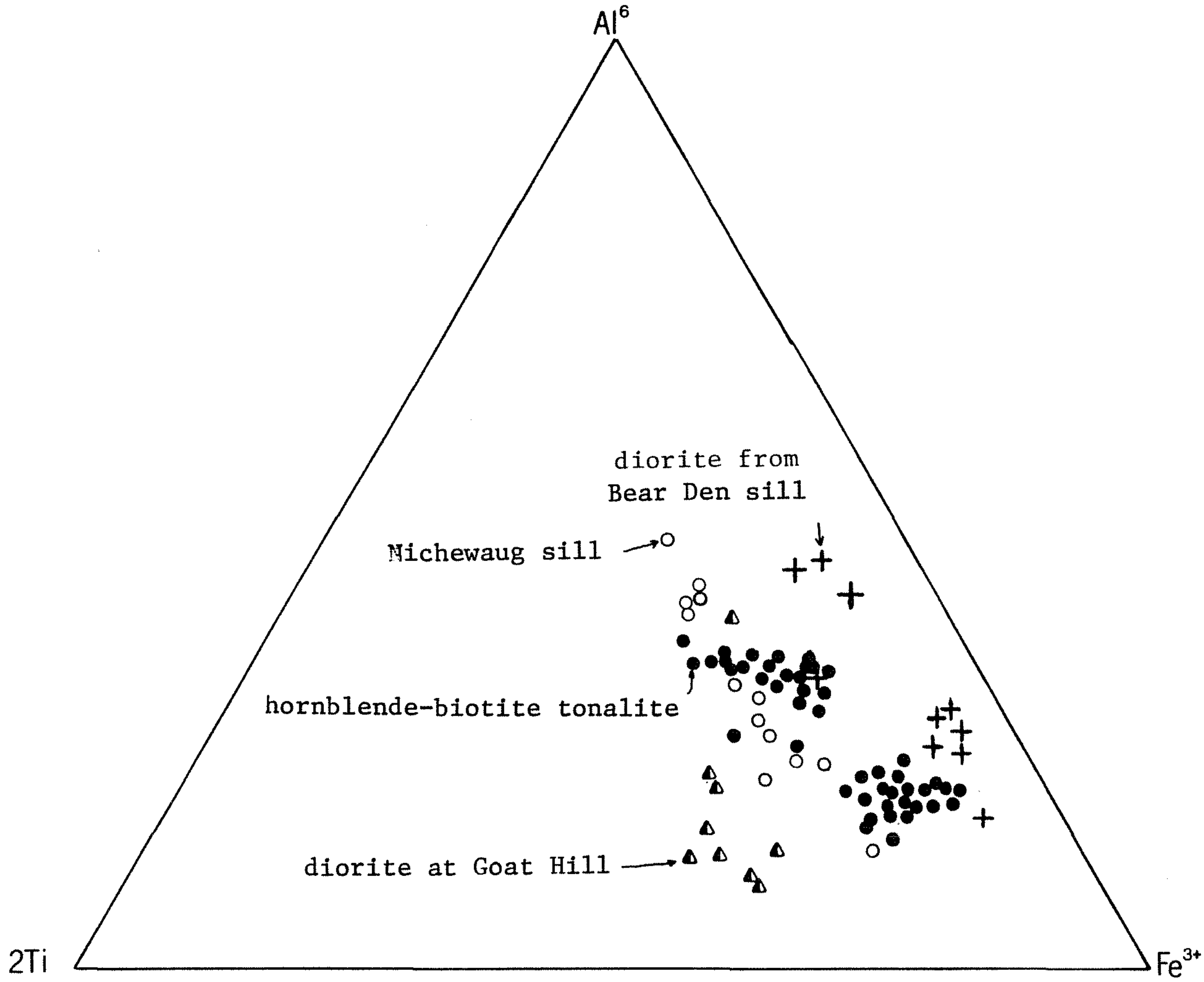

Figure 19. Plot of Al(VI)-2Ti-Fe^{3+} for the amphiboles of the Hardwick Tonalite and associated plutonic rocks.

quartz diorite, .39 to .70 in the diorite of the Bear Den sill and .50 to .62 in the diorite from Goat Hill. The high proportion of ferric iron in these amphiboles is similar to the hornblende of the Belchertown pluton [$Fe^{2+}/(Fe^{2+}+Fe^{3+})$ = .48] and is consistent with high oxygen fugacity (Ashwal et al., 1979).

The amphiboles in the plutonic rocks under investigation exhibit a wide variety of textural types: single euhedral to subhedral grains, rims around pyroxene, intergrowths with/or replacement of pyroxene and intergrowths with quartz. The latter two textural types are less ambiguous, but problems still arise relating textural type and chemistry to magmatic crystallization, subsolidus reequilibration or metamorphic recrystallization and hydration.

In the diorite of the Bear Den sill, the amphiboles show a decrease in Si from core amphibole intergrown with and replacing pyroxene to amphibole rims (Figure 17). In addition, the amphibole also exhibits an increase in Al(IV), A-site occupancy and Al(VI)/Fe^{3+} ratio from core to rim (Figures 18 and 19). The amphiboles of augite-hornblende quartz diorite exhibit a slight increase in Al(IV) and A-site occupancy from those intergrown with or rimming augite to the single euhedral-subhedral grains (Figure 18). In the Belchertown pluton, amphiboles resulting from recrystallization and hydration of pyroxene have a lower degree of Al(IV) and A-site substitution than the magmatic amphiboles (Ashwal et al., 1979). Secondary amphibole from the Cretaceous-Paleocene plutonic complex in southwestern Japan also has a lower Al(IV) and A-site component than the magmatic amphibole (Czamanske et al., 1981). Smaller variations in Al(IV) and A-site occupancy are recognized in the amphibole of the hornblende-biotite tonalite and the diorite from Goat Hill, but are not correlated to textural variability (Figure 18).

It has been demonstrated that Ti content decreases with the development of secondary amphibole (Czamanske et al., 1979; Anderson, 1980; Ashwal, et al., 1979; Raase, 1974). The amphiboles of the hornblende-biotite tonalite exhibit a limited variation in Al(IV) with relatively large, scattered variation in Ti (Figure 20). Those amphiboles with low Ti usually coexist with green to green-brown biotite and are associated with anhedral, secondary sphene. The release of Ti from the amphibole during reequilibration goes to making secondary sphene. All amphibole coexists with ilmenite indicating that the Ti-saturation limit in the amphibole decreases with decreasing temperature. Plots of Ti against Al(IV) for the augite-hornblende quartz diorite, the diorite at Goat Hill and the Bear Den sill of diorite (Figure 20), show varying degrees of importance of Al(IV) and Ti substitution. The degree of Al(IV) and Ti(VI) substitution is low in the diorite from the Bear Den sill, high in the diorite at Goat Hill and intermediate in the amphibole from the augite-hornblende quartz diorite. In conclusion, amphiboles of the hornblende-biotite tonalite are primary magmatic phases that have reequilibrated at subsolidus and/or at slightly above solidus temperatures. This reequilibration is shown mainly in Ti loss. The high Ti content of the amphiboles from the diorite at Goat Hill probably also reflects a magmatic relationship between the hornblende and augite (intergrowths and rimming). Based on Ti content, some of the amphibole of the augite-hornblende quartz diorite and perhaps all the amphibole of the diorite of the Bear Den sill are products of partial to total hydration of pyroxene.

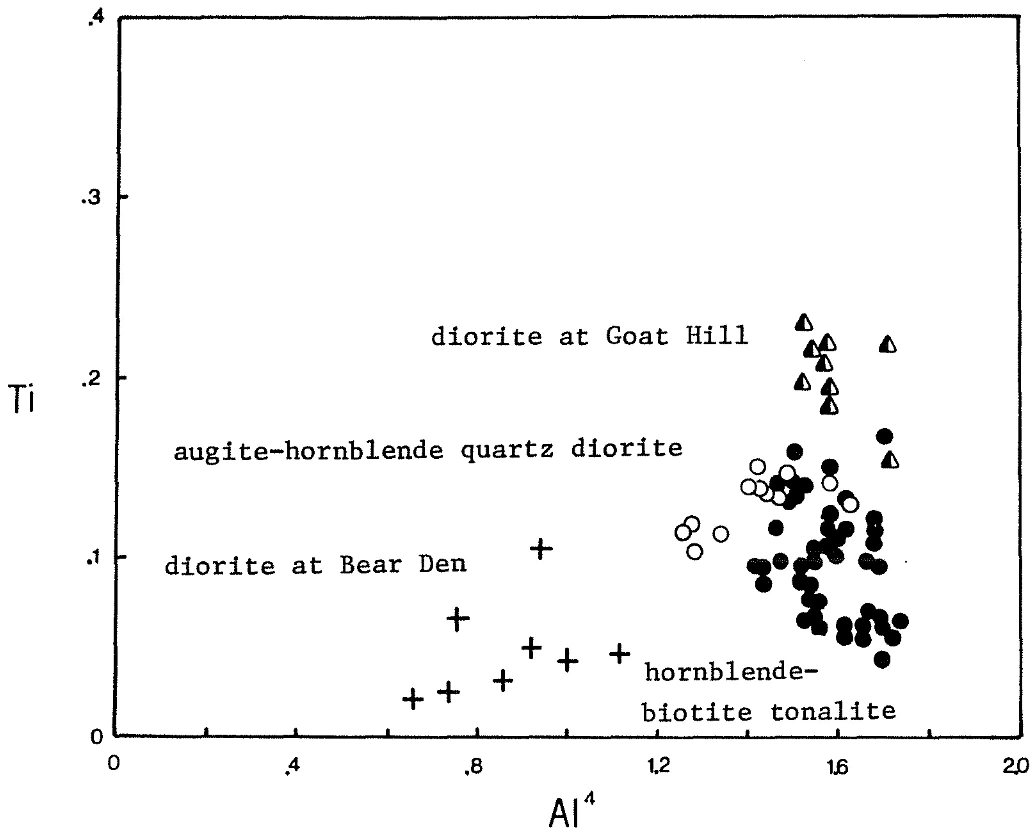

Figure 20. Plot of Ti versus Al(IV) for the amphiboles from the Hardwick Tonalite and associated plutonic rocks.

Biotite

Biotite is common in granitoids and as such has been used as a petrologic indicator of a variety of parameters describing plutonic conditions. Initial research on biotite stability by Wones and Eugster (1965) and subsequent improvement and expansion allowed the approximation of fugacitites of oxygen and water. Although its presence is not a specific indicator of aluminum oversaturation, excess Al in biotite does contribute to the peraluminous character of granitoids. Because it is usually the dominant, if not the only mafic mineral phase in granitoids, it also usually controls the distribution of the transition elements. One goal of this study is to place constraints on the physical characteristics of granitoid genesis. To this end, it is necessary to evaluate biotite chemistry in relation to coexisting minerals and to reequilibration reactions at subsolidus temperatures.

Biotite is ubiquitous in the Hardwick Tonalite and all the associated plutonic rocks. The tonalites contain up to approximately 40% biotite. In addition to being the dominant mafic phase in all the plutonic rocks, it is also the dominant potassium-bearing phase in all except the porphyritic microcline granite and the equigranular granites.

Table 18 presents biotite analyses determined by (1) combination of electron microprobe and wet chemical analyses and (2) ferric-iron-corrected microprobe analyses. The combined analyses are designated (*). The microprobe-only analyses were corrected for ferric iron by correlation of the ferric-ferrous iron ratio between biotite and the whole rock chemistry. Structural formulae were calculated based on 11 oxygens. Criteria for cation site assignment in the structural formulae were as follows: (1) First Si, then Al was assigned to the tetrahedral site. If tetrahedral sites were not full, Fe^{3+} was assigned to the tetrahedral sites (i.e. in biotite from the diorite at Goat Hill). (2) the remaining Al, Ti, Fe^{3+}, Fe^{2+}, Mn and Mg were assigned to the octahedral sites. (3) Na and K were assigned to the A site.

Biotite compositions can be simply approximated by the end members:

phlogopite	$KMg_3AlSi_3O_{10}(OH)_2$
annite	$KFe_3AlSi_3O_{10}(OH)_2$
eastonite	$KMg_{2.5}Al(VI)_{0.5}Si_{2.5}Al_{1.5}O_{10}(OH)_2$
siderophyllite	$KFe_{2.5}Al(VI)_{0.5}Si_{2.5}Al_{1.5}O_{10}(OH)_2$

These end members account for the simple substitution Mg = Fe^{2+} and the coupled substitution Al(VI) + Al(IV) = (Fe^{2+},Mg) + Si.

Deviations from the four end-members phlogopite, annite, eastonite, and siderophyllite are common in natural biotites. These deviations occur in the interlayer sites, octrahedral sites and the (OH) sites. In the structural formulae (Table 18), the interlayer site occupancy ranges from .859 to .982 and the octahedral site occupancy ranges from 2.654 to

Table 18. Electron microprobe analyses and combined electron microprobe and wet chemical analyses of biotite from the Hardwick Tonalite and associated plutonic rocks. Combined analyses noted by (*).

	hornblende-biotite tonalite											
	SA100*	SA100*	SA100*	SA100*	SA61-1*	SA61-1*	SW12*	SA4*	SA4*	SA160-3*	SA160-3*	SA160-3*
SiO_2	37.88	37.30	37.58	37.60	36.96	36.49	36.45	37.03	37.07	36.66	36.71	36.42
TiO_2	3.43	3.52	3.37	3.48	1.76	1.68	4.30	1.79	1.83	1.69	1.73	1.58
Al_2O_3	15.18	15.19	15.54	15.55	16.18	16.31	15.21	15.84	15.78	15.85	16.06	15.68
Fe_2O_3	5.63	5.36	5.36	5.33	6.00	6.14	6.17	3.53	3.41	4.46	4.30	4.91
FeO	14.46	14.46	14.46	14.46	10.91	10.91	11.59	15.72	15.72	15.13	15.13	15.13
MnO	0.67	0.63	0.64	0.60	0.28	0.32	0.39	0.45	0.46	0.41	0.49	0.46
MgO	10.48	10.92	10.79	11.16	14.05	14.00	12.94	11.51	11.46	12.33	12.65	12.08
Na_2O	0.09	0.03	0.06	0.07	0.03	0.04	0.07	0.08	0.08	0.04	0.04	0.02
K_2O	9.55	9.40	9.43	9.43	9.36	9.37	9.72	9.46	9.41	9.72	9.59	9.75
Total	97.37	96.81	96.80	97.78	95.53	95.26	96.81	95.41	95.22	96.29	96.70	96.23
n	13	10	30	17	12	6	22	30	6	8	12	4
Structural Formulae												
Si	2.806	2.778	2.774	2.772	2.742	2.720	2.693	2.801	2.805	2.752	2.740	2.743
Al	1.194	1.222	1.226	1.228	1.258	1.280	1.307	1.199	1.195	1.248	1.260	1.257
	4.000	4.000	4.000	4.000	4.000	4.000	4.000	4.000	4.000	4.000	4.000	4.000
Al	.132	.111	.123	.125	.157	.153	.019	.213	.212	.156	.154	.152
Ti	.191	.197	.186	.193	.098	.094	.240	.102	.106	.095	.096	.091
Fe^{3+}	.313	.304	.298	.297	.336	.344	.343	.200	.194	.253	.242	.278
Fe^{2+}	.898	.899	.886	.892	.678	.680	.715	.998	.996	.952	.946	.952
Mn	.036	.031	.040	.031	.018	.022	.027	.023	.032	.023	.027	.023
Mg	1.157	1.213	1.194	1.228	1.556	1.554	1.425	1.300	1.291	1.380	1.408	1.358
	2.727	2.755	2.730	2.764	2.843	2.847	2.769	2.833	2.831	2.859	2.873	2.853
Na	.013	.005	.009	.009	.002	.003	.005	.009	.009	.005	.005	.003
K	.889	.895	.888	.886	.883	.896	.915	.909	.909	.929	.915	.941
	.912	.900	.897	.895	.885	.899	.920	.918	.918	.934	.920	.944
$X^{oct}_{Fe^{2+}}$	.330	.326	.326	.322	.239	.239	.258	.351	.352	.333	.329	.333

	hornblende-biotite tonalite							biotite tonalite				
	SA160-3*	SA160-3*	SP65-1*	SP65-1*	SP65-1*	SW16	SW21	SW1*	SW1*	SP139*	SP139*	SP139*
SiO_2	36.60	37.02	37.43	37.28	36.85	34.91	36.36	34.78	34.83	36.15	36.38	36.23
TiO_2	1.67	1.62	2.18	2.15	2.12	4.07	4.48	4.28	4.09	2.68	2.54	2.54
Al_2O_3	15.86	17.04	16.54	16.53	16.99	15.84	15.24	17.37	17.42	15.76	15.52	15.71
Fe_2O_3	4.69	4.21	6.11	6.16	6.22	6.04	5.98	3.28	3.28	5.88	5.73	5.77
FeO	15.13	15.13	12.94	12.94	12.94	14.34	11.97	17.84	17.84	16.17	16.17	16.17
MnO	0.43	0.42	0.28	0.25	0.27	0.39	0.41	0.20	0.27	0.51	0.51	0.53
MgO	12.16	12.61	12.55	12.51	12.62	11.53	12.53	8.22	8.36	10.31	10.31	10.26
Na_2O	0.02	0.10	0.02	0.12	0.08			0.20	0.01	0.03	0.03	0.01
K_2O	9.71	9.81	9.12	9.05	8.80	9.85	9.77	10.08	9.94	9.57	9.57	9.74
Total	96.37	96.96	97.17	97.00	96.89	96.97	96.78	96.02	96.32	97.07	96.76	96.96
n	10	12	4	6	10	9	15	11	14	21	20	32
Structural Formulae												
Si	2.749	2.762	2.749	2.740	2.710	2.708	2.692	2.656	2.651	2.719	2.742	2.732
Al	1.251	1.238	1.251	1.260	1.290	1.292	1.308	1.344	1.349	1.281	1.258	1.268
	4.000	4.000	4.000	4.000	4.000	4.000	4.000	4.000	4.000	4.000	4.000	4.000
Al	.154	.173	.181	.174	.183	.156	.024	.219	.216	.117	.122	.127
Ti	.095	.092	.121	.119	.117	.238	.249	.245	.233	.151	.145	.145
Fe^{3+}	.265	.236	.338	.342	.345	.351	.332	.187	.189	.330	.325	.326
Fe^{2+}	.949	.942	.787	.795	.800	.932	.743	1.138	1.153	1.021	1.021	1.016
Mn	.023	.022	.018	.018	.018	.028	.027	.009	.014	.027	.027	.027
Mg	1.372	1.403	1.372	1.373	1.383	.960	1.389	.936	.947	1.157	1.159	1.155
	2.857	2.868	2.815	2.821	2.846	2.755	2.764	2.734	2.752	2.803	2.799	2.796
Na	.003	.018	.003	.018	.009			.002	.001	.005	.004	.002
K	.930	.899	.856	.848	.822	.979	.926	.982	.970	.922	.924	.933
	.933	.917	.859	.866	.831	.979	.926	.982	.971	.927	.928	.935
$X^{oct}_{Fe^{2+}}$	.332	.340	.280	.282	.281	.338	.269	.416	.419	.366	.366	.365

n=number of analyses $\qquad X^{oct}_{Fe^{2+}} = Fe^{2+}/(Fe^{2+}+Fe^{3+}+Al(VI)+Ti+Mn+Mg)$

Table 18, continued.

	augite-hornblende quartz diorite					Goat Hill diorite				Bear Den sill of diorite		
	SP236	SP236	SP239	SP239	SP239	SW522	SW522	SW522	SW522	SA176-1	SA176-1	SA176-3
SiO_2	36.11	36.39	36.63	36.49	36.61	36.93	36.24	37.28	36.70	37.71	38.07	38.22
TiO_2	3.36	3.54	4.31	4.47	4.42	5.68	5.58	5.89	5.33	1.85	1.87	1.82
Al_2O_3	14.50	14.68	15.74	15.78	15.76	14.54	14.54	14.66	14.86	16.80	16.76	16.65
Fe_2O_3	5.62	5.79	3.50	3.01	2.99	4.94	4.86	4.91	4.92	3.32	3.31	3.36
FeO	15.13	15.13	15.36	15.35	15.36	11.01	10.83	10.93	10.97	10.51	10.47	10.66
MnO	0.33	0.32	0.13	0.13	0.10	0.14	0.13	0.15	0.15	0.18	0.17	0.16
MgO	11.64	11.32	11.67	11.74	12.12	14.23	14.52	14.34	14.44	15.21	15.04	15.22
Na_2O			0.01			0.04	0.04	0.04	0.04	0.12	0.08	0.06
K_2O	9.43	9.32	9.37	9.22	9.21	9.76	9.88	9.64	9.64	9.67	9.46	9.52
Total	96.12	96.49	96.72	96.20	96.57	97.27	96.59	97.84	97.05	95.37	95.23	95.67
n	3	6	10	4	4	14	10	8	11	9	8	3
Structural Formulae												
Si	2.729	2.735	2.724	2.723	2.720	2.689	2.671	2.694	2.678	2.765	2.787	2.789
Al	1.271	1.265	1.276	1.277	1.280	1.248	1.264	1.248	1.277	1.235	1.213	1.211
Fe^{3+}						.063	.065	.058	.045			
	4.000	4.000	4.000	4.000	4.000	4.000	4.000	4.000	4.000	4.000	4.000	4.000
Al	.021	.036	.103	.113	.100					.217	.233	.225
Ti	.191	.201	.241	.251	.248	.311	.315	.319	.292	.101	.103	.096
Fe^{3+}	.321	.328	.197	.170	.170	.232	.230	.234	.250	.206	.205	.208
Fe^{2+}	.953	.949	.956	.959	.955	.674	.673	.665	.675	.643	.642	.649
Mn	.022	.023	.009	.009	.005	.003	.003	.003	.003	.013	.013	.013
Mg	1.312	1.265	1.295	1.304	1.343	1.545	1.595	1.546	1.568	1.661	1.641	1.654
	2.820	2.802	2.801	2.806	2.821	2.765	2.816	2.766	2.789	2.841	2.837	2.845
Na						.005	.005	.005	.005	.018	.009	.009
K	.908	.895	.893	.879	.875	.910	.930	.886	.894	.908	.880	.886
	.908	.895	.893	.879	.875	.915	.935	.891	.899	.926	.889	.895
$X^{oct}_{Fe^{2+}}$	.338	.339	.341	.342	.339	.244	.239	.240	.242	.226	.226	.228

	porphyritic microcline granite					granite at Sheep Rock		Fitzwilliam granite		granite at Tom Swamp
	SA1-1	SA1-6	SA1-7	SA1-10	SP86	SA68-1	SA68-2	SM4-1	SM4-2	Z93
SiO_2	36.17	36.19	36.32	36.30	35.67	35.13	34.96	35.85	35.42	34.15
TiO_2	2.82	2.86	2.86	2.72	3.13	3.83	3.17	3.00	3.18	3.11
Al_2O_3	15.55	15.70	16.10	15.63	16.46	17.16	17.64	17.29	18.30	19.32
Fe_2O_3	2.38	2.42	2.38	2.44	2.25	2.12	2.12	4.73	4.70	1.46
FeO	19.28	19.55	19.24	19.58	18.23	19.09	19.10	20.19	20.06	19.47
MnO	0.38	0.41	0.36	0.37	0.43	0.40	0.37	0.78	0.94	0.23
MgO	9.48	9.48	9.47	9.72	9.97	8.53	8.65	4.38	5.07	8.46
Na_2O	0.01	0.01						0.01	0.01	
K_2O	9.84	9.83	9.92	9.80	9.70	9.99	9.37	9.68	9.61	9.59
Total	95.91	96.45	96.65	96.56	95.84	96.70	95.38	95.91	97.29	95.79
n	13	16	14	8	18	22	16	7	5	10
Structural Formulae										
Si	2.764	2.756	2.755	2.762	2.718	2.676	2.679	2.756	2.684	2.606
Al	1.236	1.244	1.245	1.238	1.282	1.324	1.321	1.244	1.316	1.394
	4.000	4.000	4.000	4.000	4.000	4.000	4.000	4.000	4.000	4.000
Al	.166	.165	.195	.164	.195	.217	.271	.324	.320	.345
Ti	.163	.165	.164	.156	.179	.220	.182	.173	.182	.179
Fe^{+3}	.122	.125	.122	.125	.116	.119	.120	.308	.298	.093
Fe^{+2}	1.263	1.276	1.249	1.276	1.191	1.236	1.243	1.294	1.270	1.242
Mn	.023	.028	.023	.023	.028	.028	.023	.051	.059	.014
Mg	1.079	1.075	1.071	1.102	1.131	.971	.990	.504	.574	.962
	2.816	2.834	2.824	2.846	2.840	2.791	2.829	2.654	2.703	2.835
Na	.002	.002						.001	.001	
K	.955	.952	.957	.951	.944	.971	.911	.952	.929	.935
	.957	.954	.957	.951	.944	.971	.911	.953	.930	.935
$X^{oct}_{Fe^{2+}}$	.449	.450	.442	.448	.419	.443	.439	.488	.470	.438

Table 18, continued.

	biotite tonalite										biotite-muscovite tonalite			
	SM7	SP2*	SR7	ST2*	ST2*	SW19	SP3*	SW18*	SP186	SA3	SP55	SP55	SP55	SB3*
SiO_2	36.05	35.88	35.19	36.98	37.07	35.13	34.78	35.18	35.12	35.84	35.66	36.05	35.29	35.86
TiO_2	2.84	4.37	2.50	1.64	1.77	3.87	3.61	5.47	3.52	2.28	2.73	2.80	2.77	3.24
Al_2O_3	17.52	15.98	17.46	16.77	16.71	18.07	17.68	16.65	17.88	18.07	17.47	17.39	17.17	16.26
Fe_2O_3	4.12	5.53	5.21	4.70	4.72	3.18	3.91	2.98	5.86	5.19	3.68	3.79	3.81	4.72
FeO	16.91	13.69	16.87	17.11	17.11	16.12	15.72	15.21	14.40	13.66	16.38	16.65	16.77	14.46
MnO	0.39	0.52	0.69	0.57	0.58	0.25	0.41	0.32	0.36	0.36	0.38	0.42	0.43	0.49
MgO	9.30	11.35	9.11	9.58	9.53	9.42	10.50	11.24	10.72	11.93	10.50	10.46	11.00	11.59
Na_2O			0.12								0.01			
K_2O	9.30	11.35	9.11	9.48	9.41	9.95	9.56	10.06	9.38	9.44	9.67	9.22	9.27	9.99
Total	96.82	96.94	96.68	96.83	96.90	95.99	96.17	97.11	97.24	96.77	96.49	96.78	96.51	96.61
n	20	8	20	24	26	10	10	23	8	11	11	10	4	11
Structural Formulae														
Si	2.707	2.672	2.665	2.778	2.783	2.650	2.622	2.623	2.610	2.656	2.683	2.697	2.660	2.686
Al	1.293	1.328	1.335	1.222	1.217	1.350	1.378	1.377	1.390	1.344	1.317	1.303	1.340	1.314
	4.000	4.000	4.000	4.000	4.000	4.000	4.000	4.000	4.000	4.000	4.000	4.000	4.000	4.000
Al	.259	.074	.224	.265	.262	.258	.192	.086	.176	.235	.232	.231	.184	.123
Ti	.160	.244	.143	.093	.099	.202	.204	.307	.197	.127	.154	.157	.156	.182
Fe^{3+}	.232	.310	.297	.265	.267	.181	.223	.167	.328	.291	.208	.213	.217	.267
Fe^{2+}	1.060	.855	1.069	1.074	1.073	1.016	.992	.950	.893	.846	1.031	1.043	1.055	.904
Mn	.023	.027	.036	.032	.032	.018	.027	.018	.018	.022	.018	.023	.023	.031
Mg	1.042	1.262	1.028	1.074	1.064	1.061	1.178	1.250	1.188	1.318	1.176	1.164	1.236	1.296
	2.776	2.772	2.797	2.803	2.795	2.736	2.816	2.778	2.800	2.839	2.819	2.831	2.871	2.803
Na			.018								.002			
K	.929	.913	.910	.903	.902	.961	.924	.959	.893	.891	.931	.881	.887	.954
	.929	.913	.928	.903	.902	.961	.924	.959	.893	.891	.933	.881	.887	.954
$X^{oct}_{Fe^{2+}}$	.382	.308	.382	.383	.384	.371	.352	.342	.319	.298	.366	.368	.367	.323

	biotite-muscovite tonalite		biotite-garnet tonalite				augite-hornblende quartz diorite					
	SB1*	SA251*	SA54*	SA54*	SA54*	FW992	SP179-3*	SP179-2*	SP179-2*	SP179-2*	SP179-2*	SP236*
SiO_2	35.77	37.40	35.25	35.03	35.29	35.78	36.71	37.60	37.48	37.53	37.52	36.61
TiO_2	3.33	3.23	2.77	2.55	2.37	3.69	3.06	3.12	3.09	3.39	3.15	3.18
Al_2O_3	15.83	17.23	19.05	18.57	18.36	16.10	15.74	15.65	15.62	15.69	15.40	14.76
Fe_2O_3	3.89	3.18	3.46	3.29	3.21	6.04	4.54	4.48	4.52	3.73	3.44	5.60
FeO	16.84	17.88	16.99	16.99	16.99	12.68	16.44	16.16	16.16	16.16	16.16	15.13
MnO	0.44	0.28	0.23	0.18	0.16	0.38	0.28	0.29	0.28	0.32	0.31	0.25
MgO	10.81	7.99	9.88	9.55	9.62	11.38	11.30	11.00	11.26	11.51	11.30	11.57
Na_2O							0.04	0.03	0.05	0.06	0.07	
K_2O	9.69	9.32	9.81	9.59	9.52	9.68	9.47	8.88	9.07	9.15	9.21	9.12
Total	96.60	96.51	97.44	95.75	95.52	95.73	97.58	97.21	97.53	97.54	96.56	96.22
n	17	10	20	5	7	10	12	14	17	13	8	5
Structural Formulae												
Si	2.647	2.802	2.626	2.653	2.680	2.688	2.720	2.785	2.772	2.768	2.798	2.751
Al	1.353	1.198	1.374	1.347	1.320	1.312	1.280	1.215	1.228	1.232	1.202	1.249
	4.000	4.000	4.000	4.000	4.000	4.000	4.000	4.000	4.000	4.000	4.000	4.000
Al	.025	.324	.300	.313	.322	.114	.094	.154	.135	.133	.151	.060
Ti	.185	.182	.154	.146	.135	.208	.171	.174	.171	.188	.177	.181
Fe^{3+}	.216	.180	.194	.188	.182	.343	.279	.249	.252	.207	.194	.315
Fe^{2+}	1.039	1.121	1.061	1.074	1.076	.799	1.020	1.002	1.000	.997	1.008	.948
Mn	.040	.018	.013	.014	.009	.018	.018	.018	.018	.022	.019	.018
Mg	1.200	.891	1.097	1.079	1.090	1.273	1.247	1.216	1.240	1.268	1.255	1.295
	2.705	2.716	2.819	2.814	2.814	2.755	2.829	2.813	2.816	2.815	2.804	2.817
Na							.005	.005	.007	.009	.009	
K	.916	.892	.931	.928	.921	.930	.899	.857	.867	.878	.880	.876
	.916	.892	.931	.928	.921	.930	.904	.862	.874	.887	.889	.876
$X^{oct}_{Fe^{2+}}$	.384	.413	.376	.382	.382	.290	.361	.356	.355	.354	.360	.337

2.873 (with tetrahedral site set at 4.000). The substitution of non-divalent cations into the octahedral sites (i.e. Al^{3+}, Fe^{3+}, Ti^{4+}) does not maintain ideal trioctahedral occupancy and is largely responsible for octahedral site deficiency.

The biotites of this study show an extremely limited compositional variation in the interlayer site. K^+ replacement by Na^+ is limited to non-existent. The hornblende-biotite tonalite, the diorite of the Bear Den sill, augite-hornblende quartz diorite, and the diorite from Goat Hill exhibit the greatest amount of Na^+ substitution with $K^+/(K^++Na^+)$ ranging form 1.00 to 0.97. The $K^+/(K^++Na^+)$ ratio of biotites from the more felsic plutonic rocks (porphyritic microcline granite, equigranular granites and tonalites excluding the hornblende-bearing tonalite) is predominantly 1.00. Ca was analyzed but was not detected.

Biotites from the Hardwick Tonalite are plotted in terms of $Fe^{2+}/(Fe^{2+}+Mg)$ and Al(IV) in Figure 21. The biotites of the hornblende-biotite tonalite and biotite-garnet tonalite approximately define the upper and lower limits of Al(IV) and $Fe^{2+}/(Fe^{2+}+Mg)$ ratio with biotites of the biotite tonalite and the biotite-muscovite tonalite in between.

Biotite analyses from the plutonic rocks associated with the Hardwick Tonalite are plotted in terms of $Fe^{2+}/(Fe^{2+}+Mg)$ and Al(IV) in Figure 22. The biotites of the augite-hornblende quartz diorite are similar to the biotites of the augite-hornblende-biotite tonalite. There is little difference between the biotite of the chilled margin of the sill and the interior of the sill. The biotite of the diorite at Goat Hill and the diorite of the Bear Den sill have approximately the same $Fe^{2+}/(Fe^{2+}+Mg)$ ratio, but differ slightly in tetrahedral aluminum.

The biotites from the porphyritic microcline granite, granite at Sheep Rock, granite at Tom Swamp, and the Fitzwilliam Granite define three distinct populations. The porphyritic microcline granite and the granite at Sheep Rock have a similar $Fe^{2+}/(Fe^{2+}+Mg)$ and Al(IV). The biotite of the granite at Tom Swamp has a similar $Fe^{2+}/(Fe^{2+}+Mg)$ but a higher amount of tetrahedral aluminum, while the biotite of the Fitzwilliam Granite has similar amounts of Al(IV) but a vastly higher $Fe^{2+}/(Fe^{2+}+Mg)$ ratio. The Fitzwilliam Granite has the only plutonic biotite with an $Fe^{2+}/(Fe^{2+}+Mg)$ ratio higher than the biotite of the pelitic country rock.

Al(VI), Fe^{3+}, and Ti^{4+} constitute 13 to 30% of the occupied octahedral sites. The normal extent of R^{3+}(Al, Fe^{3+}, and Ti^{4+}) substitution in natural occurring plutonic biotites is approximately one third of the occupied octahedral positions (Foster, 1960). Using Foster's (1960) breakdown of octahedral site occupancy (Figures 23 and 24) coherent groupings of biotite analyses are a result of differences in $Fe^{2+}/(Fe^{2+}+Mg)$ ratio rather than total R^{3+} occupancy.

R^{3+} type substitutions such as $3M^{2+} = \square + 2R^{3+}$ result in vacancies and therefore deviations from trioctahedral mica ideality. Figure 25 is a plot of biotite analyses, with total M^{2+}+Ti+(Si-3) versus 3-(total R^{3+}), modified from Tracy (1978) to include Fe^{3+}. In the insert in Figure 25, the two diagonal lines represent the Tschermak-type substitution [M^{2+}Si = Al(IV)Al(VI)] or Fe^{3+} analogues [M^{2+}Si = Al(IV)Fe^{3+}(VI)] which maintain mica octahedral site stoichiometry. The area between the

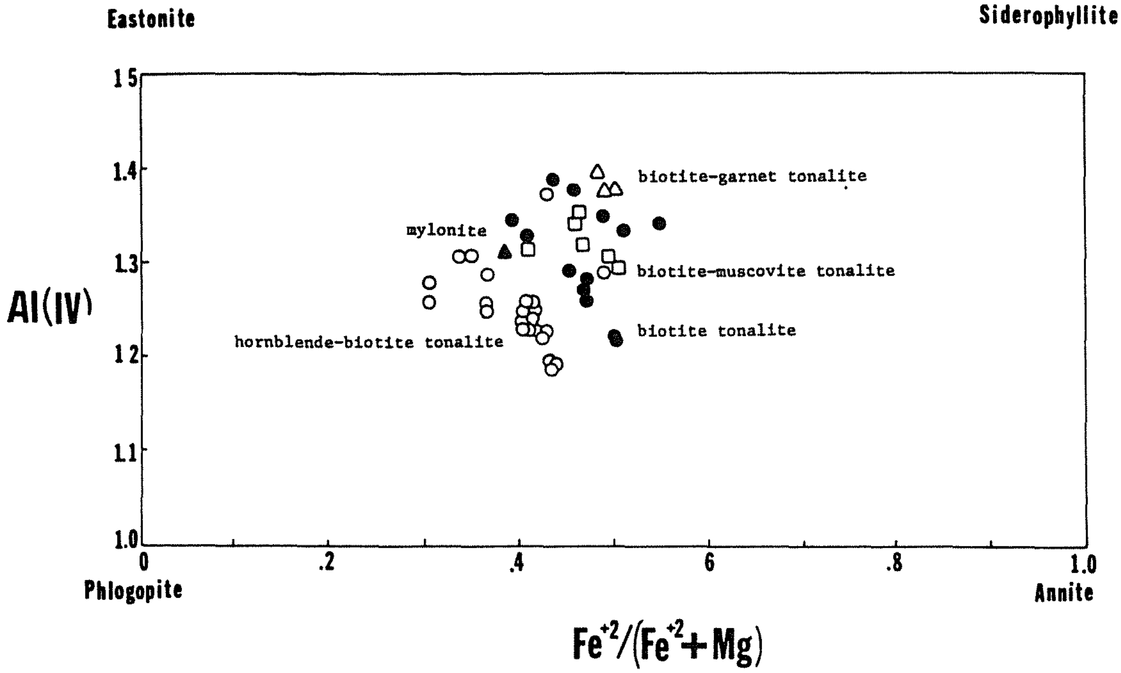

Figure 21. Biotites from the Hardwick Tonalite plotted in terms of end-members Eastonite-Siderophyllite-Phlogopite-Annite.

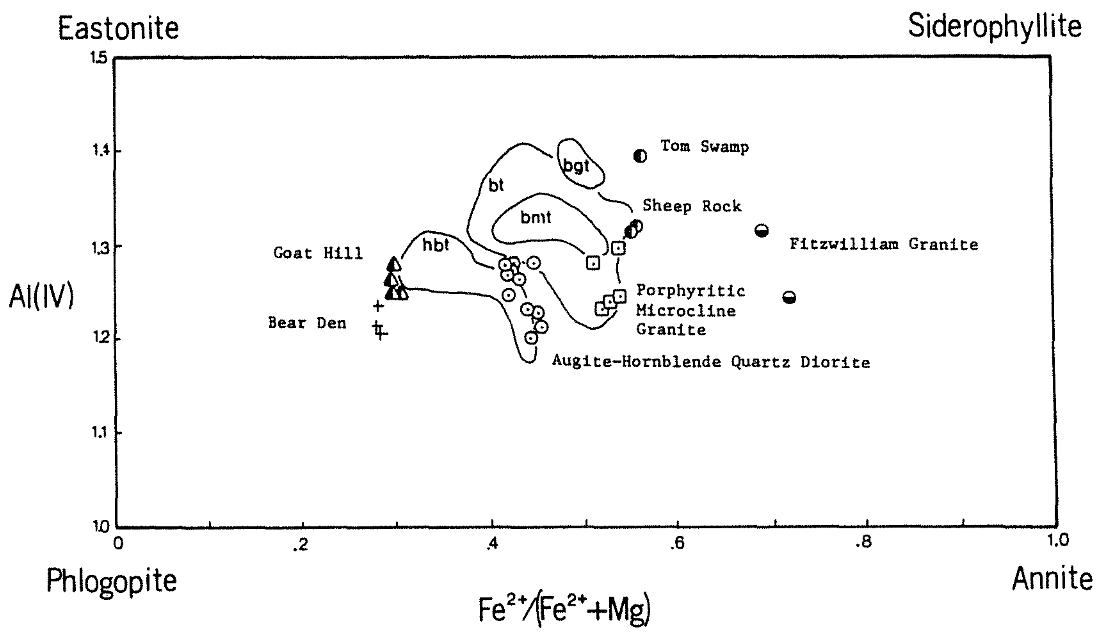

Figure 22. Biotites from the plutonic rocks associated with the Hardwick Tonalite plotted in terms of end members Eastonite-Siderophyllite-Phlogopite-Annite.

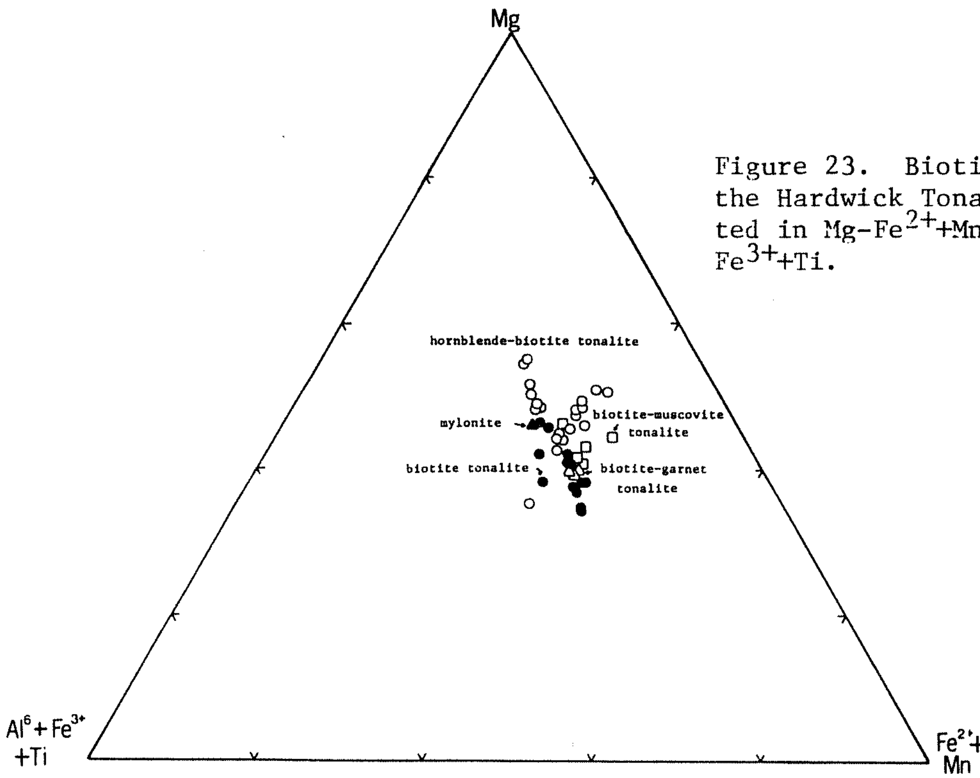

Figure 23. Biotites from the Hardwick Tonalite plotted in Mg-Fe^{2+}+Mn-Al(VI)+Fe^{3+}+Ti.

Figure 24. Biotites from the igneous rocks associated with the Hardwick Tonalite plotted in Mg-Fe^{2+}+Mn-Al(VI) +Fe^{3+}+Ti.

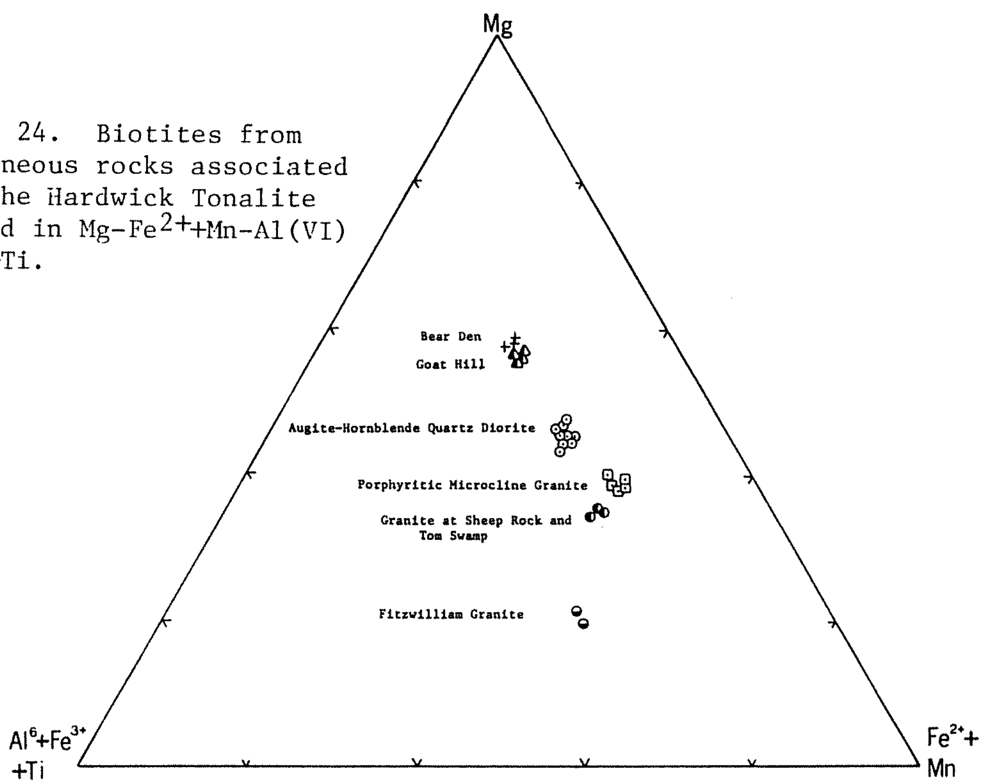

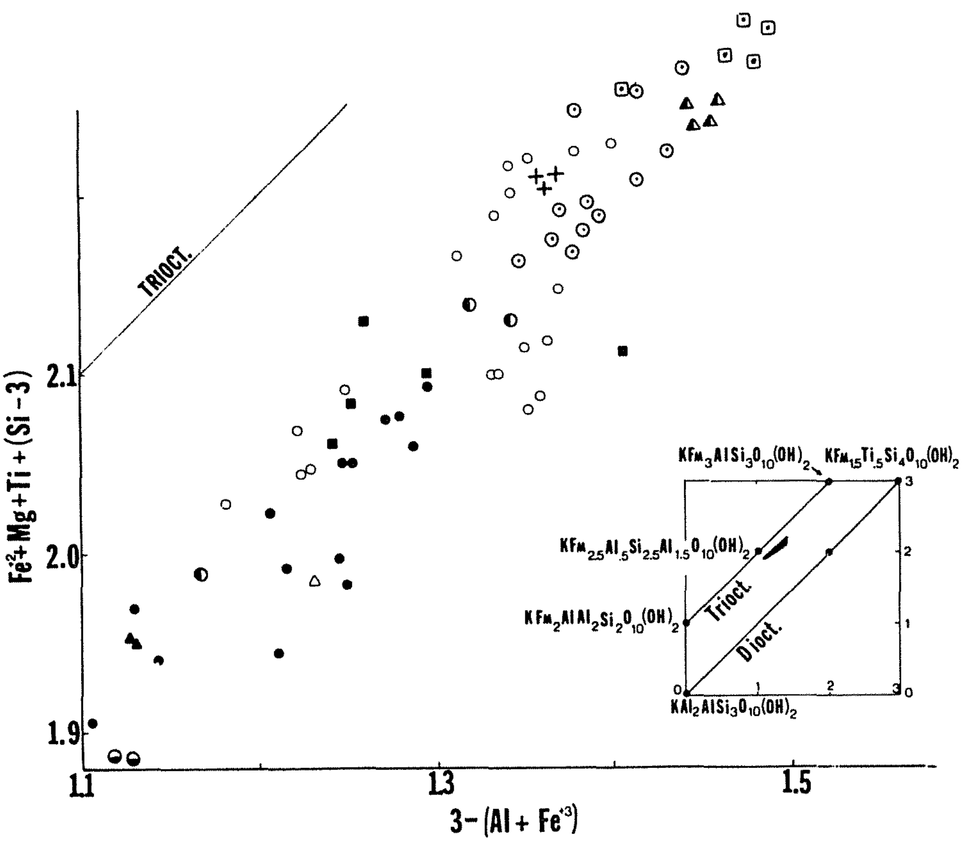

Figure 25. Biotites from the Hardwick Tonalite and associated plutonic rocks plooted in terms of trioctahedral and dioctahedral components after Tracy. Insert shows dioctahedral mica series (muscovite-celadonite) and trioctahedral mica series (biotite-eastonite) with area between the two ideal lines representing the composition field of most micas. Dark area in insert is area of plutonic biotites in this study. Symbols: hornblende-biotite tonalite (○), biotite tonalite (●), biotite-muscovite tonalite (■), biotite-garnet tonalite (▲), mylonite (△), augite-hornblende quartz diorite (⊙), diorite at Goat Hill (◭) and Bear Den (+), Fitzwilliam Granite (◒), porphyritic microcline granite (⊡), and granite at Tom Swamp and Sheep Rock (◐).

trioctahedral mica series and dioctahedral mica series represents the compositional region of most natural micas. The biotite analyses from the Hardwick Tonalite and associated plutonic rocks show divergence from the ideal trioctahedral mica line.

Fe^{3+} in the biotite of the Hardwick Tonalite ranges from 12.8% to 6.0% of the occupied octahedral sites. Those biotites coexisting with hornblende and an FeTi oxide assemblage of magnetite and ilmenite usually have the highest $Fe^{3+}/(Fe^{3+}+Fe^{2+})$ ratio and those biotites coexisting with muscovite and/or garnet and associated with an ilmenite-oxide assemblage have a lower $Fe^{3+}/(Fe^{3+}+Fe^{2+})$ ratio. Biotites from the other plutonic units have the following percent Fe^{3+} octahedral site occupancy: diorite of the Bear Den sill 7%, diorite at Goat Hill 8.5%, augite-hornblende quartz diorite 7.0% to 11.7% with 6.0% in the chilled margin of the sill, porphyritic microcline granite 4.0%, Fitzwilliam Granite 11%, granite at Sheep Rock 4%, and the granite at Tom Swamp 3%.

Ti^{4+} in the biotite of the Hardwick Tonalite ranges from .307 to .091 cations/11 oxygen and this variation is not dependent upon rock type, oxide assemblage or host rock TiO_2. The Ti content of biotite in the other plutonic rocks appears to define a wide spectrum of variation. The biotite of the diorite at Goat Hill has a Ti^{4+} content of .101 to .096 cations/11 oxygen. Chilled margin biotite of the augite-hornblende quartz diorite has a higher Ti content (.241 to .251 cations/11 oxygen) than the biotite from the interior of the sill (.171 to .201 cations/11 oxygens). A number of likely Ti substitutions have been proposed:

$M^{2+}+2Si$ = Ti + 2Al(IV) (Guidotti _et al._, 1977; Tracy, 1978)

2Al(VI) = Ti(VI) + M^{2+} (Czamanske _et al._, 1977)

$2M^{2+} = \square$ + Ti (Czamanske _et al._, 1977)

Ti does not correlate with Al(IV) and Al(VI) and shows a weak correlation with octahedral site vacancy suggesting a complex and variable Ti substitution mechanism (Wones, 1980; Czamanske _et al._, 1981; Hollocher, 1981).

Fe^{3+} and Ti^{4+} substitutions into the octahedral site for the biotites of the Hardwick Tonalite are summarized in Figures 26 and 27. The biotites of the hornblende-bearing or magnetite-bearing tonalites usually have a higher $Fe^{3+}/(Fe^{3+}+Fe^{2+}+Fi^{4+})$ ratio than biotites of garnet- and/or muscovite-bearing or ilmenite-bearing tonalites. Biotite color is also defined by variations in Fe^{2+}, Fe^{3+}, and Ti^{4+}. At low Ti^{4+} contents [$Ti^{4+}/(Ti^{4+}+Fe^{3+}+Fe^{2+})$ less than 0.1] slight increases in Fe^{3+} content change biotite color from red to brown to green. At intermediate Ti^{4+} contents [$Ti^{4+}/(Ti^{4+}+Fe^{3+}+Fe^{2+})$ less than 0.15] and greater than 0.10 increases in Fe^{3+} result in biotite color variations from red to brown. At high Ti^{4+} contents [$Ti^{4+}/(Ti^{4+}+Fe^{3+}+Fe^{2+})$ greater than 0.15] increases in Fe^{3+} result in only red to red brown biotite.

Variations in biotite chemistry in terms of these three components can be explained by differing magmatic f_{O_2} domains within the tonalite and subsolidus decrease in Ti solubility in biotite. Differing magmatic f_{O_2} domains, supported by oxide data and whole rock chemistry, occurred at magmatic temperature T_1 shown in Figure 27. Secondary/recrystallized

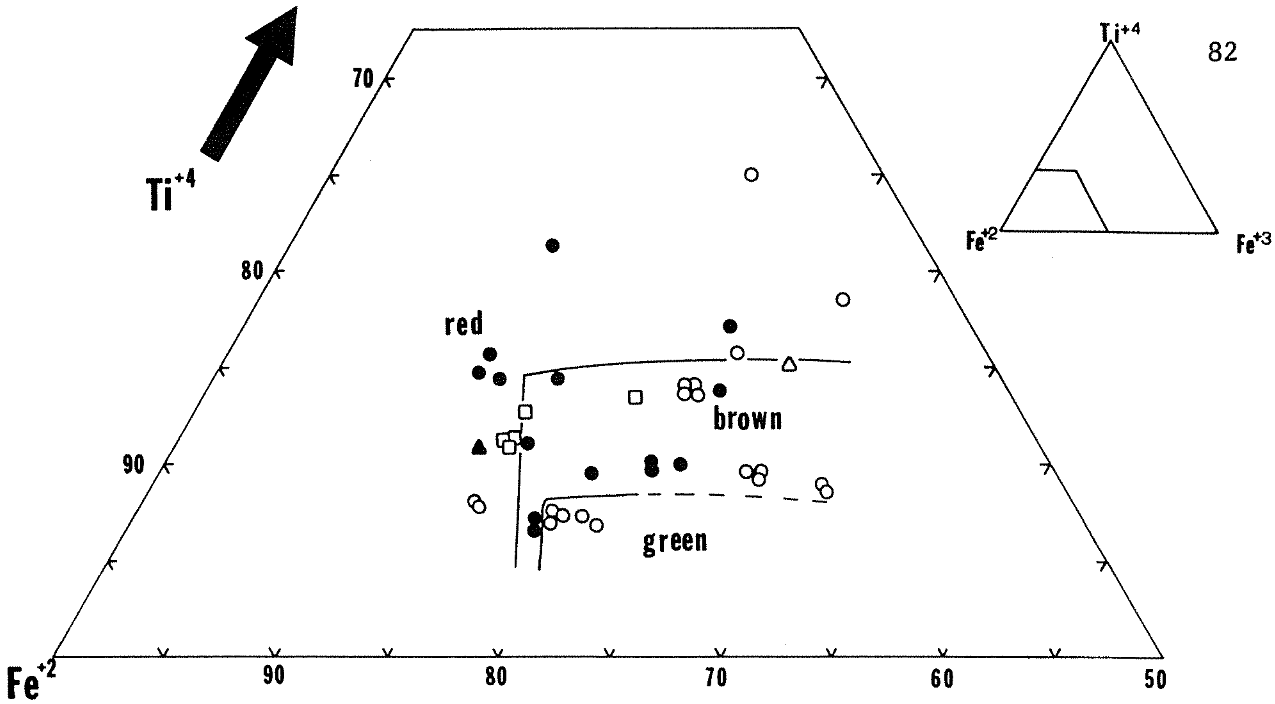

Figure 26. Biotite compositions from the Hardwick Tonalite plotted in terms of Fe^{2+}-Fe^{3+}-Ti^{4+} and contoured with regards to color. Boundaries separating color types are probably not so sharp as presented and fluctuate with varying degrees of vacancies and minor constituent substitution. hornblende-biotite tonalite (○), biotite tonalite (●), biotite-muscovite tonalite (□), biotite-garnet tonalite (▲) and mylonite (△).

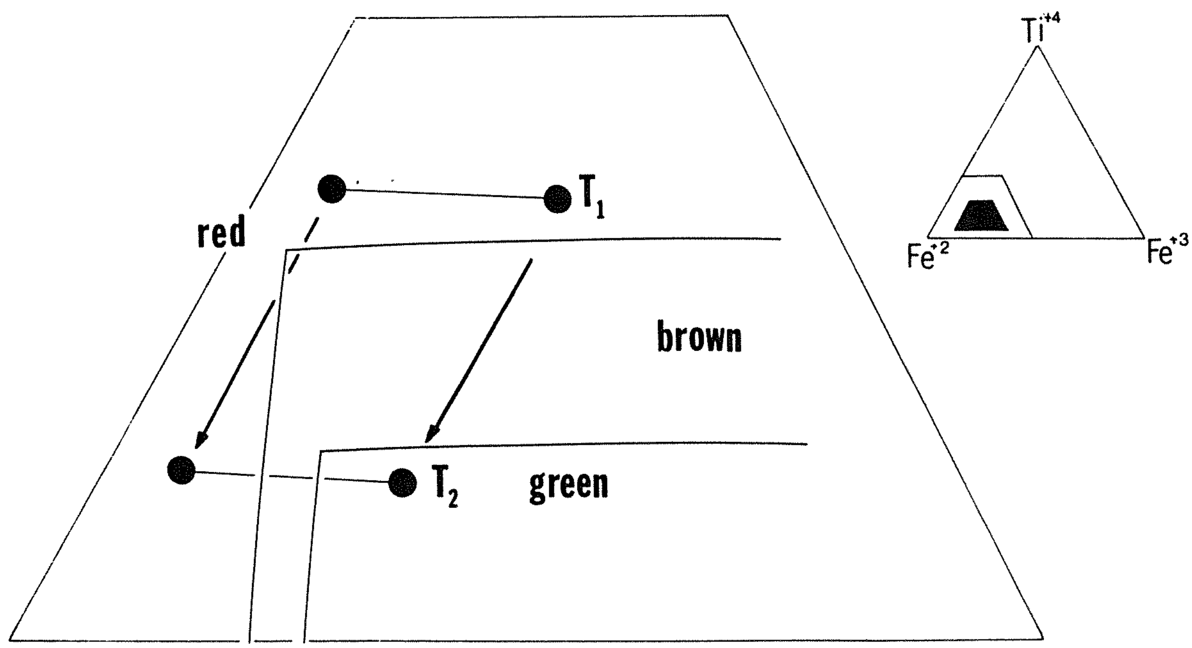

Figure 27. Biotite compositions illustrated in Fe^{2+}-Fe^{3+}-Ti^{4+}. Ti loss occurs during reequilibration. T(temperature)$_1$ is greater than T_2. T_1 approximates magmatic temperatures, whereas T_2 approximates metamorphic reequilibration temperatures.

biotite of the southwestern Japanese batholith (Czamanske et al., 1981) and the Belchertown complex (Ashwal et al., 1980) is distinctively lower in Ti content than the primary, magmatic biotite. Kwak (1968), Guidotti et al. (1974, 1977), and Robinson et al., (1982) demonstrated that the Ti content of biotite in equilibrium with a Ti-saturating phase decreases with decreasing metamorphic grade and temperature. All the biotite of the tonalite coexists with ilmenite and therefore the Ti-saturation limit in these biotites decreases with decreasing temperature. As shown in Figure 27, the decrease in Ti-solubility in biotite during subsolidus reequilibration creates an array of low-Ti biotites between T_1 and T_2. At T_2, only biotites in rocks with a high igneous Fe^{3+} component (i.e. those associated with hornblende and a magnetite-ilmenite oxide assemblage) are green in color (SA160-3). The reaction toward lower Ti (Figure 27) consumes Ti-biotite and FeTi oxides, and produces Fe-richer biotite and sphene.

In addition to Ti^{4+} decreasing with metamorphic reequilibration, variations in the amount of tetrahedral Al appear to be a partial function of metamorphic grade (Figure 28). In metamorhpic zone VI (sillimanite-cordierite-garnet), the biotites of the hornblende-biotite tonalite and biotite tonalite have higher amounts of tetrahedral Al than biotites in the same rock types at a lower metamorphic grades. From metamorphic zone V to zone III, the biotites exhibit an overlapping but gradational decrease in tetrahedral Al. In addition to metamorphic grade, bulk composition is an extremely important factor. Biotite in host rocks with high normative corundum has high Al(VI).

Muscovite

Plutonic muscovite is commonly taken as an indicator of the peraluminous character of plutonic rocks and has been used to put constraints on depth and conditions of crystallization (Althaus et al., 1970; Clark, 1981; Anderson and Rowley, 1981). The petrogenetic constraints imposed by the intersection of muscovite breakdown reactions with the granite solidus are partially based upon assumptions concerning muscovite stoichiometry and the primary igneous nature of the muscovite (Miller et al., 1981). Commonly, plutonic muscovite contains a high percentage of celadonite component $K(Mg,Fe^{2+})AlSi_4O_{10}(OH)_2$ (Maczuga, 1981; Miller et al., 1981; Anderson and Rowley, 1981 and ferri-muscovite component $KFe^{3+}{}_2AlSi_3O_{10}(OH)_2$ (Miller et al., 1981) and to a lesser extent a paragonite component $NaAl_3Si_3O_{10}(OH)_2$, a fluormuscovite component $KAl_3Si_3O_{10}(F)_2$, a Ti-bearing component $KTi_2Al_3SiO_{10}(OH)_2$ (Miller et al., 1981) and a number of trioctahedral mica components. Discrimination between primary and secondary muscovite has been based upon both textural (Tracy, 1974; Miller et al., 1981) and compositional criteria (Miller et al., 1981; Anderson and Rowley, 1981). The criteria of Miller et al (1981) for distinguishing between "P" (primary) and "S" (secondary) muscovite in the Old Woman-Piute Range, Mojave Desert, California and Teacup Granodiorite, south-central Arizona are based upon both textural and compositional characteristics. Texturally, "P" muscovite grains must be: 1) relatively coarse-grained compared to primary mineral phases; 2) subhedral to euhedral, with cleanly terminated form; 3) not raggedly enclosed by or

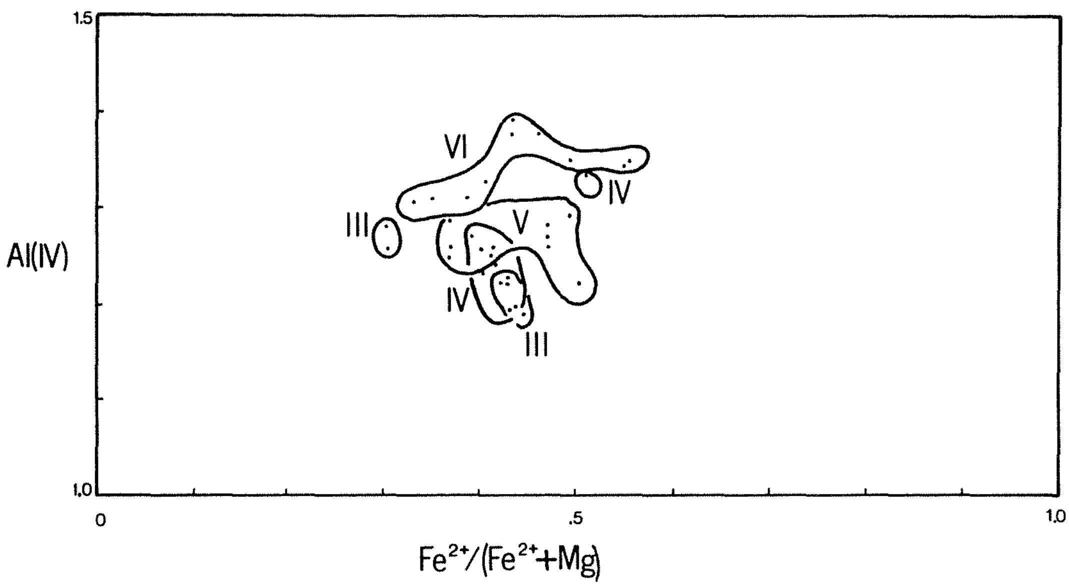

Figure 28. Relationship between Al (IV), $Fe^{2+}/(Fe^{2+}+Mg)$ and metamorphic grade for the biotites of the Hardwick Tonalite. III:sillimanite-muscovite zone, IV:sillimanite-muscovite-K-feldspar zone, V:sillimanite-K-feldspar zone, and VI: sillimanite-cordierite-garnet zone.

enclosing a mineral from which the muscovite may have formed by hydrous alteration (feldspar, garnet, aluminum silicates); and 4) in rock with igneous texture. "P" type muscovites are generally richer in Ti, Na, and Al and poorer in Mg and Si. The chemical characterization of secondary and primary muscovite of the Hardwick Tonalite and associated plutonic rocks is of importance in understanding the origin of the plutonic rocks.

In the Hardwick Tonalite and associated plutonic rocks, muscovite occurs in the biotite-muscovite tonalite, biotite-garnet tonalite, porphyritic microcline granite, and various equigranular granites intruding both metamorphic country rock and tonalite. Muscovite constitutes 0.1 to 6.7 percent of the muscovite-bearing tonalites, 0.2 to 2.9 percent of the porphyritic microcline granite and 0.5 to 6.9 percent of the equigranular granites. Muscovite occurs in four textural habits (Figure 29):

Type 1. Independent, coarse, commonly subhedral, cleanly terminated grains.

Type 2. Coarse, commonly subhedral, cleanly terminated grains closely associated with biotite.

Type 3. Minute, subhedral to anhedral grains interlayered with and cross cutting biotite grains.

Type 4. Ragged, subhedral to anhedral grains associated with plagioclase and K-feldspar and clearly a product of hydrous alteration of feldspar or as possible retrograde rims around garnet (i.e. biotite-garnet tonalite).

Microprobe analyses of muscovite are shown in Tables 19 and 20. Table 20 shows analyses of a single Type 4 muscovite illustrated in Figure 30. In Table 19, cation formulae are based on 11 oxygens and calculated in two ways giving both minimum and maximum values for octahedral site occupancy. Cation calculation (a) assumes all iron as Fe^{2+} giving a maximum trioctahedral mica component. Cation calculation (b) assumes all iron as Fe^{3+} or an octahedral site total of 2 giving a minimum trioctahedral mica component. The minimum trioctahedral component calculation appears to be a closer approximation of natural igneous and metamorphic muscovites (Tracy, 1975; Guidotti, 1973, 1978a,b; Miller _et al._, 1981; Anderson and Rowley, 1981). In Table 19 cation formulae are based on 11 oxygens and assume all iron as Fe^{2+}. The inability of the microprobe to analyze H_2O, Li and F makes it impossible to evaluate vacancies resulting from substitutions of such ions (H_3O^+, Li^+) in the interlayer sites or fluor-muscovite component content.

Interlayer site substitutions in muscovite are commonly made by Na^+ (paragonite end member) and Ca^{2+} (margarite end member). The paragonite substitution is simple $K^+ = Na^+$. The margarite substitution involves a coupled replacement within the interlayer site and tetrahedral site: K+Si(IV) = Ca+Al(IV). Muscovites of the tonalites and granites show little variety in interlayer site composition. There is some replacement of K^+ by Na, but no Ca^{2+}. Limited Ca^{2+} substitution into the muscovite

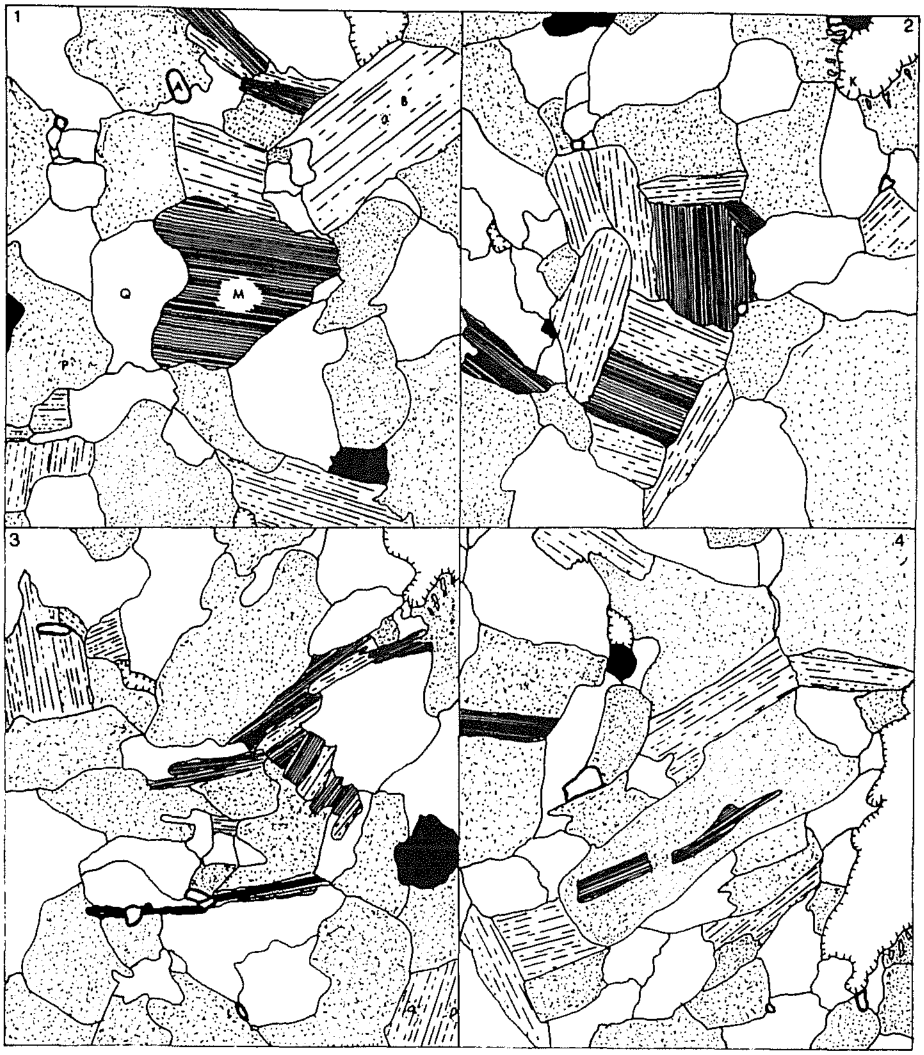

Figure 29. Textural types of muscovite found in the Hardwick Tonalite and associated plutonic rocks. Type 1: independent, coarse, commonly subhedral grains, Type 2: coarse, commonly subhedral grains closely associated with biotite, Type3: minute, subhedral to anhedral grains, interlayered with and cross cutting biotite, and Type 4: ragged grains associated with plagioclase and K-feldspar. The four textural types shown in this figure were observed in specimen SA251.

Table 19. Electron microprobe analyses of muscovite from the Hardwick Tonalite and associated plutonic rocks. Structural formulae for each analyses is calculated in two manners. Calculation (a) assumes all iron to be in the divalent state. Calculation (b) assumes the octahedral total to be 2 cations or all iron as trivalent.

biotite-muscovite tonalite

	SP86	SB-3	SB-3	SB-1	SB-1	SB-1	SA251	SA251
SiO_2	46.34	46.51	46.52	46.67	46.48	46.05	46.71	46.81
TiO_2	1.15	1.02	1.13	1.14	1.09	1.13	0.82	0.65
Al_2O_3	30.81	30.81	29.83	29.64	30.55	30.44	32.09	32.17
FeO*	5.24	5.02	5.47	5.21	5.07	4.87	2.98	3.11
MnO	0.04		0.04	0.02	0.02	0.04	0.02	0.02
MgO	1.50	1.40	1.56	1.48	1.54	1.39	1.59	1.49
Na_2O	0.11	0.24	0.23	0.18	0.18	0.19	0.22	0.17
K_2O	10.53	11.05	10.93	10.99	10.87	10.78	10.64	10.55
Total	95.81	96.05	95.71	95.33	95.80	94.89	95.07	94.99
n	21	10	5	10	6	12	10	6

Structural Formulae

	a	b	a	b	a	b	a	b	a	b	a	b	a	b	a	b
Si	3.138	3.109	3.146	3.118	3.166	3.134	3.183	3.154	3.150	3.123	3.148	3.121	3.142	3.123	3.155	3.137
Al	.862	.891	.854	.882	.834	.866	.817	.846	.850	.877	.852	.879	.854	.877	.845	.863
	4.000	4.000	4.000	4.000	4.000	4.000	4.000	4.000	4.000	4.000	4.000	4.000	4.000	4.000	4.000	4.000
Al	1.598	1.547	1.604	1.555	1.560	1.504	1.567	1.522	1.592	1.543	1.603	1.553	1.695	1.658	1.711	1.680
Ti	.059	.059	.052	.052	.058	.058	.059	.059	.055	.055	.058	.057	.042	.041	.033	.032
Fe^{3+}		.264		.252		.278		.236		.256		.247		.150		.156
Fe^{2+}	.297		.284		.311		.297	.032	.288		.278		.168		.175	
Mn	.002	.002			.002	.002	.001	.001	.001	.001	.002	.002	.001	.001	.001	.001
Mg	.151	.149	.141	.141	.158	.158	.151	.150	.155	.153	.141	.143	.159	.159	.149	.149
	2.107	2.021	2.081	2.000	2.089	2.000	2.075	2.000	2.091	2.008	2.082	2.002	2.065	2.009	2.069	2.018
Na	.016	.016	.030	.032	.031	.032	.024	.024	.024	.024	.025	.024	.029	.029	.022	.024
K	.912	.903	.954	.943	.949	.939	.957	.951	.940	.929	.941	.937	.915	.910	.907	.902
	.928	.919	.984	.975	.980	.971	.981	.975	.964	.953	.966	.961	.944	.939	.929	.926

Texture Type	SP86	SB-3	SB-3	SB-1	SB-1	SB-1	SA251	SA251
	2	1	1	2	2	3	1	1

biotite-muscovite tonalite

	SA251	SA251	SA251	SA251	SA251	SA251	SA251
SiO_2	47.41	46.53	46.96	46.60	47.49	47.12	47.01
TiO_2	0.84	1.12	0.84	0.71	0.27	0.36	0.11
Al_2O_3	31.91	32.68	33.19	32.73	32.27	32.75	33.83
FeO*	2.54	2.78	2.49	2.64	2.74	2.72	2.06
MnO		0.04	0.02	0.02	0.02		0.03
MgO	1.35	1.44	1.38	1.37	1.60	1.55	1.15
Na_2O	0.22	0.23	0.18	0.24	0.26	0.33	0.47
K_2O	11.00	10.70	10.63	10.52	10.78	10.83	10.81
Total	95.27	95.53	95.08	94.83	95.06	95.88	94.84
n	5	10	5	4	19	5	5

Structural Formulae

	a	b	a	b	a	b	a	b	a	b	a	b	a	b
Si	3.182	3.171	3.118	3.103	3.138	3.117	3.137	3.122	3.182	3.167	3.169	3.153	3.150	3.133
Al	.818	.829	.882	.897	.862	.883	.863	.878	.818	.833	.831	.847	.850	.867
	4.000	4.000	4.000	4.000	4.000	4.000	4.000	4.000	4.000	4.000	4.000	4.000	4.000	4.000
Al	1.707	1.688	1.701	1.672	1.753	1.715	1.734	1.707	1.676	1.648	1.729	1.700	1.734	1.706
Ti	.043	.042	.057	.056	.042	.042	.036	.036	.044	.044	.014	.014	.018	.018
Fe^{3+}		.096		.139		.125		.134		.144		.139		.136
Fe^{2+}	.143	.037	.156		.140		.150		.162		.154		.149	
Mn			.002	.003	.002	.002	.002	.002	.001	.001	.001	.001		
Mg	.135	.137	.144	.144	.137	.136	.138	.137	.169	.168	.160	.161	.153	.152
	2.028	2.000	2.060	2.014	2.074	2.020	2.061	2.016	2.052	2.005	2.058	2.015	2.054	2.012
Na	.028	.032	.032	.032	.023	.024	.032	.032	.029	.032	.035	.032	.040	.040
K	.942	.940	.915	.913	.912	.901	.906	.902	.920	.913	.925	.917	.926	.921
	.970	.972	.947	.945	.935	.925	.938	.934	.949	.945	.950	.949	.966	.951

Texture Type	SA251	SA251	SA251	SA251	SA251	SA251	SA251
	2	3	3	3	1	4	4

Table 19, continued.

	biotite-garnet tonalite								porphyritic microcline granite					
	SA54		SA54		SA54		SA54		SA1-1		SA1-1		SP86-1	
SiO_2	46.38		46.94		47.21		46.37		46.28		45.76		47.58	
TiO_2	0.11		0.04		0.59		0.43		0.83		0.88		1.33	
Al_2O_3	33.83		34.19		33.84		34.61		31.25		30.68		33.47	
FeO*	2.06		1.97		2.06		1.78		5.32		5.41		2.10	
MnO	0.03		0.01		0.01		0.01							
MgO	1.15		1.04		1.15		0.87		1.62		1.56		1.36	
Na_2O	0.47		0.38		0.47		0.42		0.09		0.12		0.18	
K_2O	10.81		10.82		10.95		10.89		10.41		10.66		9.91	
Total	94.84		95.39		96.28		95.38		95.80		95.06		95.96	
n	5		5		5		4		10		18		10	
Structural Formulae														
	a	b	a	b	a	b	a	b	a	b	a	b	a	b
Si	3.121	3.106	3.131	3.097	3.127	3.115	3.096	3.086	3.128	3.098	3.129	3.098	3.144	3.131
Al	.879	.894	.869	.903	.873	.885	.904	.914	.872	.902	.871	.902	.856	.869
	4.000	4.000	4.000	4.000	4.000	4.000	4.000	4.000	4.000	4.000	4.000	4.000	4.000	4.000
Al	1.806	1.777	1.821	1.812	1.770	1.750	1.821	1.801	1.619	1.565	1.603	1.544	1.750	1.727
Ti	.006	.006	.002	.002	.030	.030	.022	.022	.043	.042	.045	.045	.062	.061
Fe^{3+}		.105		.098		.104		.088		.268		.277		.105
Fe^{2+}	.116		.110		.114		.099		.301		.308		.115	
Mn	.002	.002			.001	.001	.001	.001					.002	.002
Mg	.115	.117	.104	.103	.113	.115	.087	.088	.163	.161	.160	.159	.135	.134
	2.045	2.007	2.037	2.015	2.028	2.000	2.030	2.000	2.126	2.036	2.116	2.025	2.064	2.029
Na	.061	.064	.050	.048	.060	.063	.054	.056	.008	.008	.008	.008	.023	.024
K	.923	.926	.921	.912	.926	.920	.928	.927	.902	.893	.929	.919	.834	.830
	.984	.990	.971	.960	.986	.983	.982	.983	.910	.901	.937	.927	.857	.854
Textural Type	4		4		4		4		2		2		2	

	granite at Sheep Rock		Fitzwilliam Granite			
	SA68-2		SM4		SM4	
SiO_2	47.48		47.28		47.44	
TiO_2	1.24		0.72		0.85	
Al_2O_3	33.51		31.94		31.72	
FeO*	2.01		3.12		3.28	
MnO			0.03		0.03	
MgO	1.32		1.15		1.12	
Na_2O	0.16		0.13		0.12	
K_2O	10.34		10.76		10.82	
Total	96.06		95.13		95.38	
n	7		10		6	
Structural Formulae						
	a	b	a	b	a	b
Si	3.136	3.124	3.182	3.166	3.188	3.172
Al	.864	.876	.818	.834	.812	.828
	4.000	4.000	4.000	4.000	4.000	4.000
Al	1.746	1.724	1.716	1.688	1.701	1.674
Ti	.062	.061	.036	.036	.042	.043
Fe^{3+}		.103		.136		.139
Fe^{2+}	.111		.176	.024	.185	.030
Mn			.002	.002	.002	.002
Mg	.131	.130	.115	.115	.112	.112
	2.050	2.018	2.045	2.000	2.042	2.000
Na	.024	.024	.017	.017	.015	.015
K	.873	.870	.924	.919	.928	.923
	.897	.894	.941	.936	.943	.938
Texture Type	2		2		2	

n=number of analyses

FeO* total iron as FeO

Table 20. Electron microprobe analyses of a type 4 muscovite from sample SA251 of the biotite-muscovite tonalite. Numbers correspond to location numbers in Figure 30. Structural formulae presented assumes all iron in the divalent state.

	1	2	3	4	5	6	8	9	10	11	12	13	14
SiO_2	47.34	47.01	47.20	46.94	47.28	46.51	47.27	46.53	48.48	47.37	47.26	47.43	47.01
TiO_2	0.36	0.50	0.19	0.10	0.22	0.23	0.78	0.41	0.84	0.20	0.54	0.49	0.10
Al_2O_3	32.75	32.07	32.13	32.69	32.10	32.09	32.10	32.29	32.79	32.29	31.81	31.87	32.81
FeO*	2.72	2.84	2.93	2.45	2.89	2.92	2.68	2.96	2.92	2.74	2.81	2.91	2.54
MnO													
MgO	1.55	1.70	1.78	1.30	1.74	1.69	1.65	1.67	1.73	1.66	1.55	1.55	1.25
Na_2O	0.33	0.28	0.23	0.28	0.21	0.21	0.28	0.25	0.33	0.25	0.29	0.26	0.27
K_2O	10.83	10.79	11.05	10.81	10.28	10.69	11.04	10.71	10.51	10.93	10.72	10.91	10.84
Total	95.88	95.19	95.51	94.57	94.70	94.34	95.80	94.82	97.60	95.44	94.98	95.42	94.82
Structural Formulae													
Si	3.156	3.161	3.168	3.167	3.182	3.156	3.160	3.143	3.169	3.175	3.182	3.183	3.166
Al	.844	.839	.832	.833	.818	.844	.840	.857	.831	.825	.818	.817	.834
	4.000	4.000	4.000	4.000	4.000	4.000	4.000	4.000	4.000	4.000	4.000	4.000	4.000
Al	1.732	1.704	1.711	1.768	1.730	1.724	1.691	1.716	1.697	1.727	1.707	1.704	1.772
Ti	.018	.025	.010	.005	.011	.012	.039	.021	.041	.010	.028	.024	.006
Fe^{2+}	.152	.160	.164	.138	.163	.166	.150	.168	.160	.154	.158	.165	.142
Mn													
Mg	.154	.170	.178	.131	.174	.171	.165	.168	.169	.166	.156	.153	.125
	2.056	2.059	2.063	2.042	2.078	2.073	2.045	2.073	2.067	2.057	2.049	2.046	2.045
Na	.043	.037	.030	.036	.028	.028	.036	.032	.042	.033	.037	.032	.032
K	.922	.926	.947	.931	.882	.926	.942	.924	.877	.935	.921	.935	.931
	.965	.963	.977	.967	.910	.954	.978	.956	.919	.968	.958	.967	.963

	15	16	17	18	19	20
SiO_2	47.54	47.35	46.73	46.52	46.72	47.31
TiO_2	0.14	0.09	0.26	0.88	0.53	0.38
Al_2O_3	32.17	32.61	32.00	32.35	32.21	32.05
FeO*	2.46	2.46	2.78	2.55	2.74	2.67
MnO						
MgO	1.46	1.47	1.63	1.48	1.55	1.49
Na_2O	0.30	0.28	0.27	0.29	0.25	0.37
K_2O	10.79	10.95	10.83	10.88	10.75	10.63
Total	94.87	95.21	94.49	94.95	94.75	94.90
Structural Formulae						
Si	3.196	3.175	3.165	3.136	3.168	3.182
Al	.804	.825	.835	.864	.832	.818
	4.000	4.000	4.000	4.000	4.000	4.000
Al	1.747	1.754	1.722	1.708	1.743	1.722
Ti	.007	.005	.014	.045	.027	.020
Fe^{2+}	.139	.138	.159	.142	.155	.150
Mn						
Mg	.147	.147	.163	.150	.155	.154
	2.040	2.044	2.058	2.045	2.080	2.046
Na	.039	.036	.033	.041	.033	.049
K	.926	.937	.936	.940	.929	.913
	.965	.973	.969	.981	.962	.962

FeO* total iron as FeO

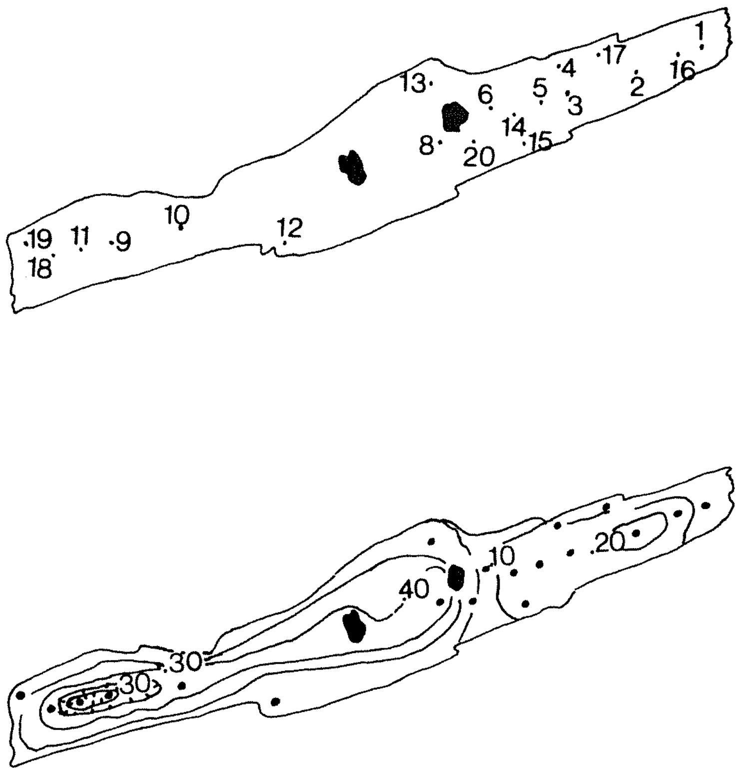

Figure 30. Ti zoning in Type 4 muscovite grain. A. Location of analyses in Table 20. Black grains are ilmenite inclusions. B. Ti zoning in muscovite in units of Ti/11 oxygen x 10. Hatched Ti contour indicates a decrease in Ti zoning.

interlayer site appears to be typical of both high grade metamorphic rocks (Guidotti, 1973; Tracy, 1975) and plutonic rocks (Miller et al., 1981).

Although limited, there are slight and coherent variations in $K^+/(K^++Na^+)$ and the occupancy in the interlayer site of the plutonic muscovites. The $K^+/(K^++Na^+)$ ratio ranges from .991 to .938 (Figure 31) and coincides with the range of metamorphic muscovite from metamorphic zones III and IV in central Massachusetts analyzed by Tracy (1974). Total occupancy in the interlayer site ranges from 85% for a muscovite from an equigranular granite to 98% for a muscovite from a biotite-garnet tonalite (Figure 31). A direct relationship between site occupancy and the $K^+/(K^++Na^+)$ ratio noted in the plutonic muscovites (Figure 31) is not present in the metamorphic muscovites.

The octahedral site in the muscovites is 10% to 24% occupied by Ti, Fe^{3+}, Fe^{2+}, Mn and Mg. The muscovite of the garnet-bearing tonalite has the smallest degree of substitution by these components whereas the muscovite of the porphyritic microcline granite has the largest. The dominant substitutions are Fe^{3+} substitution toward ferri-muscovite and an inverse tschermaks substitution toward celadonite. The ferri-muscovite component contribution is 0% if calculation (a) is used and ranges from 4.4 to 13% if calculation (b) is used. The linear relationship between $Al^{3+}(VI)$ and Fe^{3+} illustrated in Figure 32 suggests Fe^{3+} is substituted into the octahedral site through Fe^{3+} - Al^{3+} and that the ferric iron correction (b) may be a closer approximation than the ferrous iron correction (a). The gap in Figure 32 separates muscovites from the porphyritic microcline granite and most of the biotite-muscovite tonalite (except SA251) from the other plutonic muscovites.

Ti^{4+} can be accommodated into the octahedral site by means of the following substitutions:

(1) $M^{2+}(VI)+Ti^{4+}(VI) = 2Al^{3+}(VI)$ producing $KMTiAlSi_3O_{10}(OH)_2$ end member;

(2) $Ti^{4+}(VI)+Al^{3+}(IV) = Al(VI)+Si^{4+}(IV)$ producing $KTi_2Al_3SiO_{10}(OH)_2$ end member;

The two substitutions maintain charge balance and preserve stoichiometry, and therefore preserve the dioctahedral character of the muscovite. Considering Ti^{4+} substitutions which would maintain the dioctahedral character of the muscovites both Guidotti (1978) and Tracy (1975) concluded that substitution 2 would be less likely to occur because it produces an unbalanced charge distribution between octahedral and tetrahedral layers. The linear relationship between Al(VI) and Ti for the plutonic muscovites of the Hardwick Tonalite and related plutonic rocks (Figure 33) suggest that substitution 1 is most likely.

Textural types 1, 2, and 3 have moderately higher Ti-muscovite component than textural type 4. Ti zoning was not noted in the coarse-grained muscovite, but occurs in textural type 4. Table 20 shows analyses from a zoned type 4 muscovite and Figure 30 illustrates the Ti zoning.

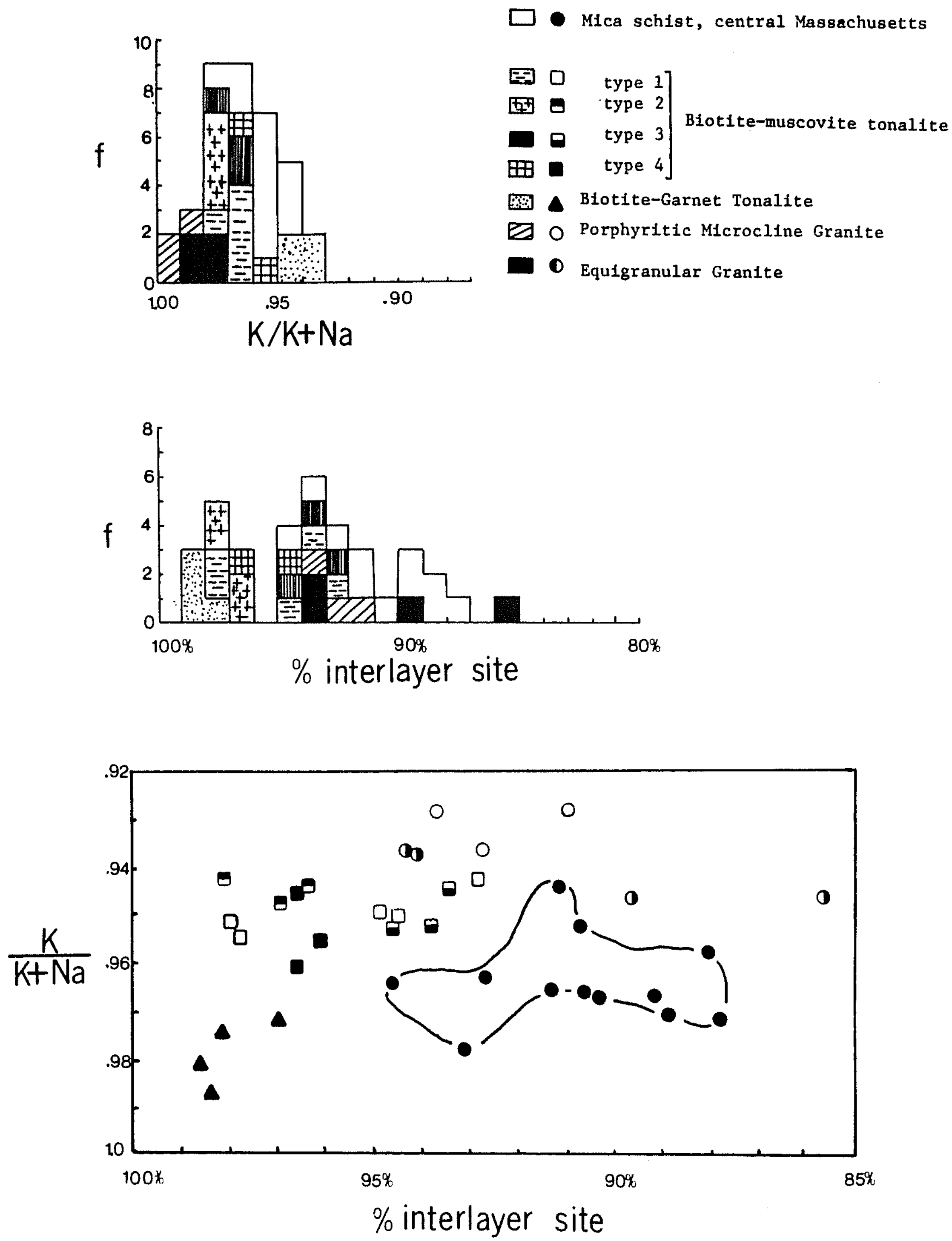

Figure 31. Three diagrams illustrating interlayer site composition and interlayer site occupancy. a) frequency diagram of K/(K+Na) ratio of interlayer site in plutonic muscovite, b) frequency diagram of interlayer site occupancy, c) K/(K+Na) plotted against interlayer site occupancy.

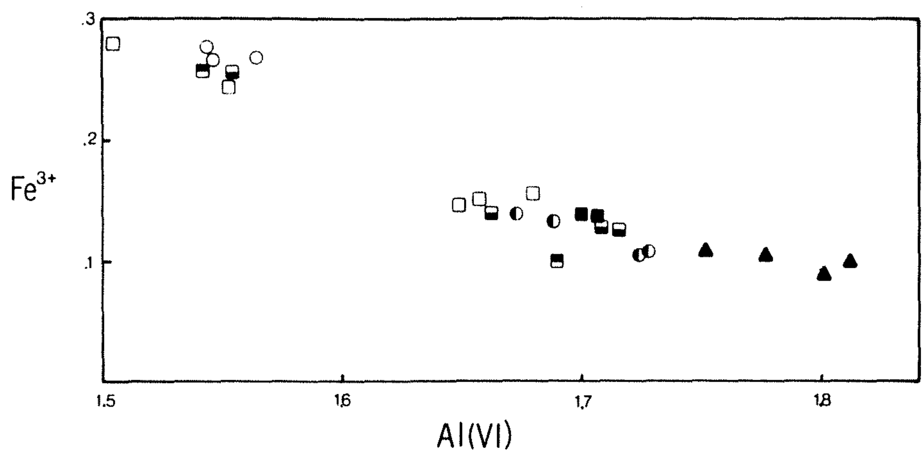

Figure 32. Fe^{3+} plotted against Al(VI) for plutonic muscovites. Symbols used are noted in Figure 31.

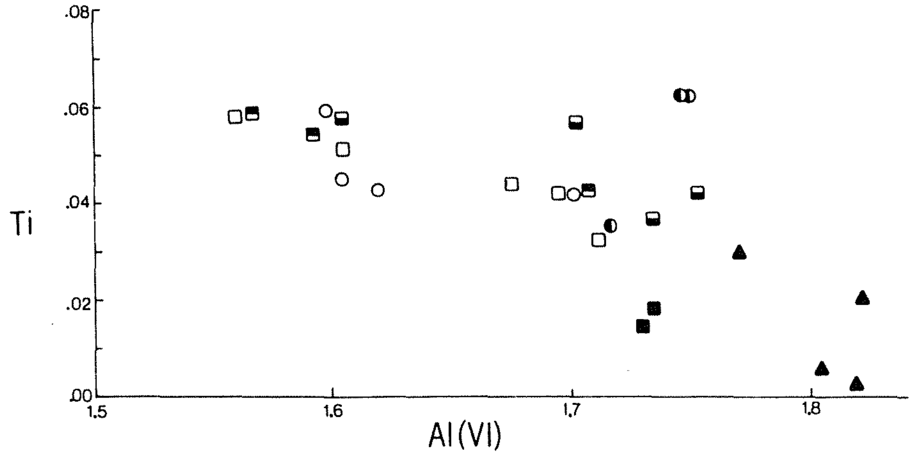

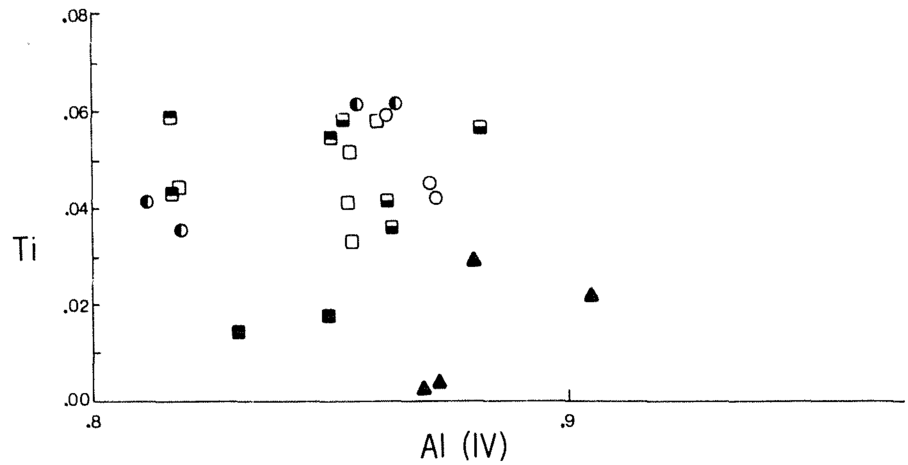

Figure 33. a. Ti/11 oxygen versus Al(VI) for muscovite, b. Ti/11 oxygen versus Al(IV) for muscovite. Symbols are noted in Figure 31.

Divalent cations (Mn, Mg, and Fe) occupy 11% to 22% (calculation a) or 6% to 8% (calculation b) of the octahedral site. Divalent cations may be substituted into the octahedral site by means of an inverse tschermaks substitution ($(Mg, Fe, Mn)^{2+}+Si^{4+} = Al^{3+}(VI)+Al^{3+}(IV)$ toward celadonite, which maintains charge balance and preserves stoichiometry, or a trioctahedral substitution maintaining charge balance but not preserving stoichiometry, i.e. $3M^{2+} = 2Al^{3+}(VI)+\square$. The tioctahedral contribution ranges from 1.4% to 5.9% (a) or 0.0% to 1.8% (b) and therefore suggests the tschermak substitution resulting in solid solution in muscovite toward celadonite is the major divalent cation substitution mechanism. If ferric iron calculation (b) is indeed a closer approximation, the divalent cation in the tschermak substitution is primarily Mg^{2+}.

Figure 34 is a composite graphical representation, after Tracy (1975), of the more probable muscovite substitutions occurring in the plutonic muscovite of the Hardwick pluton and related rocks. In this diagram all muscovites plot either on the ideal dioctahedral mica line or are slightly displaced toward the trioctahedral mica line, indicating either a slight deficiency of Al and Fe^{3+} or an excess of (Fe^{2+}+Mg+Ti+ (Si-3) from ideality.

In Figure 34, muscovite textural types 1 and 2 of the biotite-muscovite tonalite have a slightly to moderately higher celadonite component than the other textural types.

Some of the coarse-grained muscovites (textural types 1 and 2) are zoned from a celadonite-poor core to a celadonite-rich rim. In Figure 34, these core-rim compositions are connected by tie lines. The same type of zoning was noted by Hollocher (1981) in a retrograde metamorphic zone in the Lower Devonian Littleton Formation.

The muscovite compositions of the Hardwick pluton and related rocks deviate quite far from the muscovite end member. This deviation from the muscovite end member is a result of Ti substitution which preserves both charge balance and stoichiometry, an inverse tschermaks substitution toward celadonite and an Fe^{3+} octahedral site substitution. Na interlayer site substitution toward paragonite is minimal and not extremely variable compared to muscovites from other plutonic environments (Miller _et al._, 1981; Anderson and Rowley, 1981). Textural types 1 and 2 are higher in celadonite component than types 3 and 4 and higher in Ti muscovite component than type 4. Textural and compositional differences suggest textural types 1 and 2 are primary plutonic muscovites (Miller _et al._, 1981).

Garnet

Although common in the pelitic country rock into which the plutons were intruded, garnet is not a common phase in the Hardwick Tonalite and associated plutonic rocks. Garnet is present only in the biotite-garnet tonalite and within the chilled margin of the Nichewaug sill of augite-hornblende quartz diorite.

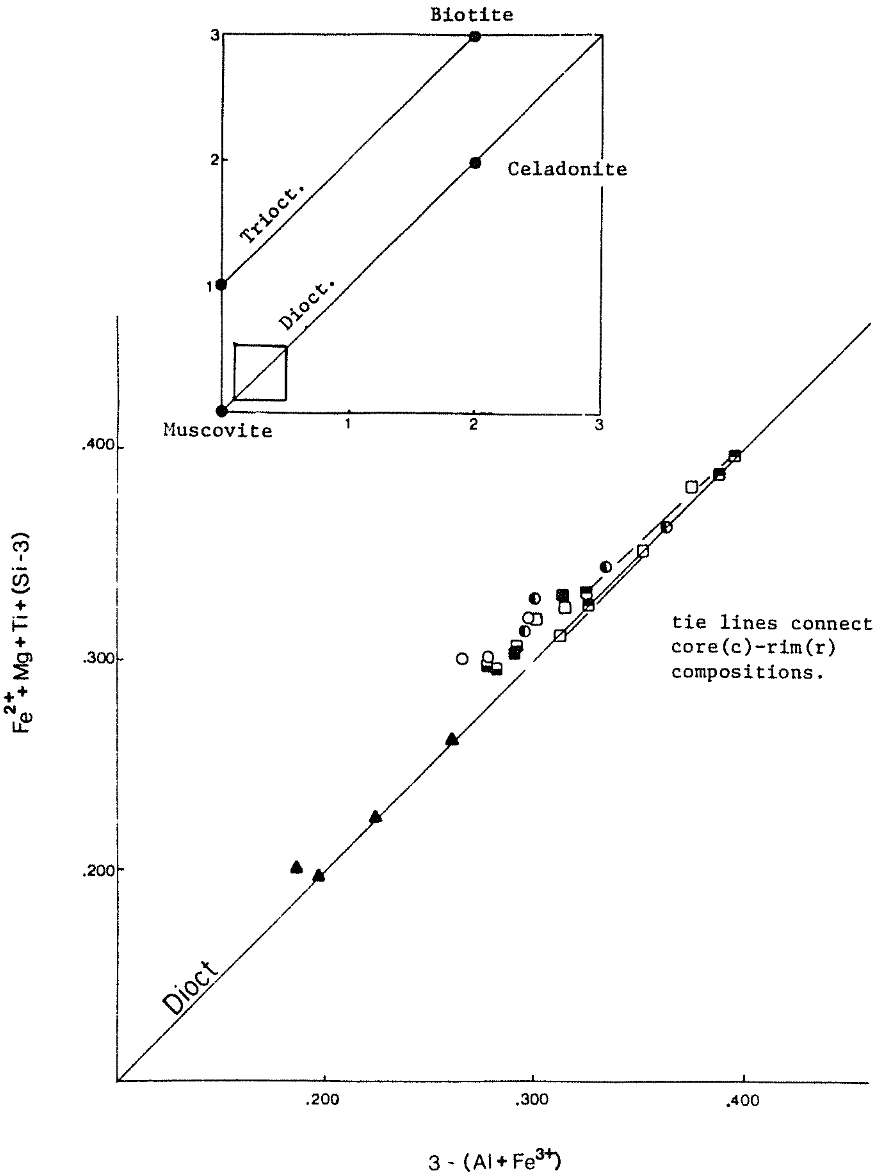

Figure 34. Plot of 3-(Al+Fe^{3+}) versus Fe^{2+}+Mg+Ti+(Si-3) showing the ideal trioctahedral and dioctahedral mica trends (insert). Compositions of muscovites from the Hardwick Tonalite and associated plutonic rocks are plotted in the enlarged area of the insert. All muscovites plotted show only a slight divergence from the ideal dioctahedral line. Muscovites plotted have a maximum Fe^{3+} correction and therefore a minimum trioctahedral component. Symbols are given in Figure 31.

Garnets in the two occurrences are texturally quite distinct. The garnets in the biotite-garnet tonalite are subhedral, equant crystals which are commonly partially rimmed by retrograde muscovite and chlorite and rarely contain inclusions. In contrast, the garnets in the chilled margin of the Nichewaug sill are anhedral, strongly poikilitic to interstitial. Inclusions are numerous and commonly are biotite, quartz and plagioclase.

In addition to textural differences, the garnets from the two units are strikingly different in composition. Table 21 presents electron microprobe analyses for garnets from biotite-garnet tonalite, from the chilled margin of the Nichewaug sill and from Littleton Formation schists. The schist sample was collected less than 30 cm away from the chilled margin sample. Garnets of the biotite-garnet tonalite are almandine-rich with 70 to 77 mole percent $Fe_3Al_2Si_3O_{12}$. Pyrope (12-19%), spessartine (5-7%) and grossular (5%) components are subordinate in amount. The garnets are quite similar to the garnets in the pelitic schists (Table 21). Although almandine-rich, with approximately 58 mole percent Fe_3Al_2-Si_3O_{12}, the garnets of the chilled margin of the Nichewaug sill contain 11 to 13 mole percent pyrope, approximately 12 mole percent spessartine and 17 to 18 mole percent grossular. Compositional differences between these three kinds of garnets are shown in Figure 35.

Garnets of the two garnetiferous igneous units exhibit weak to moderate zoning as illustrated in Figure 35. All analyzed garnets show an increase in the Fe/(Fe+Mg) ratio from core to rim. Such a chemical zoning scheme in garnets of the Littleton Formation was interpreted to be a product of retrograde hydration reactions involving biotite (Tracy et al., 1976; Shearer and Robinson, 1981). The garnets of the garnetiferous plutonic rocks also exhibit spessartine enrichment near the rims. Spessartine enriched rims of granitic garnets have been suggested to reflect crystal growth in a magma with increasing Mn/(Ca+Mg+Fe) (Kistler, et al., 1981). Reequilibration at subsolidus temperatures may also result in MnO enrichment in the garnet rims (Tracy et al., 1976; Clark, 1981).

Clearly, the differences in grossular content between the garnet of the biotite-garnet tonalite and the chilled margin of the sill reflect differences in the bulk composition. The biotite-garnet tonalite has normative corundum and contains 3.53 weight percent CaO. The chilled margin of the sill has normative diopside and contains 6.85 to 6.95 weight percent CaO.

The difference in the spessartine component in the garnets may also be partially attributed to bulk composition. The chilled margin of the sill contains 0.38 weight percent MnO, whereas the biotite-garnet tonalite contains 0.10 weight percent MnO. Experimental evidence of Green (1977) emphasized the effect of MnO on garnet stability. The high Mn/(Mn+Fe+Mg) ratio in the garnet of the chilled margin may have been responsible for its stability in a diopside-normative rock.

The close proximity of the pelitic country rock and the lack of restitic texture or association indicates that these garnets are not

Table 21. Electron microprobe analyses of garnets from the biotite-garnet tonalite, chilled margin of the Nichewaug sill of augite-hornblende quartz diorite and contact aureole in the Littleton Formation surrounding the Nichewaug sill. Each set of analyses are from a single garnet grain.

	biotite-garnet tonalite (SA54)								Nichewaug sill (SP239-3)				
	1	3	23	5	36	37	10	53	1C	1R	2R	1I	2I
SiO_2	37.47	38.05	38.26	38.08	36.52	37.92	36.92	37.61	36.72	36.57	36.87	37.35	37.41
TiO_2	0.01			0.01		0.01	0.01		0.13	0.09	0.12	0.09	0.10
Al_2O_3	21.04	21.03	20.48	21.00	21.19	20.91	20.91	20.47	21.18	21.46	21.38	21.09	21.14
FeO^*	33.90	32.97	33.27	33.23	33.69	33.06	33.89	34.70	26.76	26.66	26.97	26.60	26.57
MnO	2.66	2.54	2.50	2.42	2.50	2.40	2.69	3.14	5.42	5.39	5.62	5.25	5.32
MgO	4.20	4.22	4.14	4.45	5.15	4.54	3.36	3.05	3.37	2.91	3.12	3.28	3.29
CaO	1.75	1.77	1.72	1.77	1.94	1.72	1.76	1.72	6.18	6.27	6.43	6.32	6.24
Total	101.02	100.58	100.37	100.95	100.99	100.55	99.83	100.69	99.76	99.35	100.53	99.98	100.06
n	1	2	1	1	1	1	1	3	4	3	4	4	6
Structural Formulae													
Si site													
Si	2.979	3.019	3.046	3.012	2.910	3.012	2.986	3.019	2.943	2.946	2.948	2.978	2.979
Al	.021				.090		.014		.057	.054	.052	.022	.021
	3.000	3.019	3.046	3.012	3.000	3.012	3.000	3.019	3.000	3.000	3.000	3.000	3.000
Al site													
Al	1.952	1.968	1.923	1.959	1.902	1.953	1.979	1.937	1.945	1.982	1.957	1.961	1.963
Ti									.008	.006	.007	.005	.007
	1.952	1.968	1.923	1.959	1.902	1.953	1.979	1.937	1.953	1.988	1.964	1.966	1.970
M^{2+} site													
Fe^{2+}	2.255	2.189	2.216	2.200	2.246	2.190	2.294	2.330	1.794	1.795	1.798	1.775	1.771
Mn	.179	.171	.169	.163	.169	.161	.185	.213	.368	.367	.380	.355	.359
Mg	.498	.499	.492	.525	.612	.537	.408	.365	.403	.349	.371	.390	.392
Ca	.150	.151	.147	.150	.166	.146	.151	.148	.531	.541	.549	.540	.531
	3.082	3.010	3.024	3.038	3.193	3.034	3.038	3.056	3.096	3.052	3.098	3.060	3.053
Almandine	73.2	72.7	73.3	72.4	70.3	72.2	75.5	76.2	58.0	58.9	58.0	58.0	58.0
Spessartine	5.8	5.7	5.6	5.4	5.3	5.3	6.1	7.0	11.9	12.0	12.3	11.6	11.8
Pyrope	16.2	16.6	16.3	17.3	19.2	17.7	13.4	11.9	13.0	11.4	12.0	12.8	12.8
Grossular	4.8	5.0	4.8	4.9	5.2	4.8	5.0	4.9	17.1	17.7	17.7	17.6	17.4

	contact aureole in the Littleton Formation											
	33	17	18	19	20	21	66	22	23	24	36	35
SiO_2	38.28	38.06	37.36	38.33	38.40	38.03	37.06	37.55	37.49	37.58	38.40	38.17
TiO_2												
Al_2O_3	20.61	21.82	22.25	21.41	21.09	21.44	22.38	22.08	22.18	22.18	20.77	20.50
FeO	32.60	32.33	32.20	32.27	32.41	31.92	32.00	32.18	32.46	32.30	32.30	32.71
MnO	1.70	1.56	1.57	1.66	1.66	1.67	1.67	1.68	1.68	1.76	1.67	1.63
MgO	5.68	6.30	6.51	6.36	6.38	6.37	6.84	6.35	6.19	6.22	5.68	5.64
CaO	0.88	0.97	1.00	0.95	0.91	0.87	0.98	0.93	0.97	1.01	0.86	0.91
Total	99.75	100.04	100.92	100.98	100.85	100.30	100.93	100.78	100.97	101.05	99.68	99.56
n	1	1	1	1	1	1	1	1	1	1	1	1
Structural Formulae												
Si site												
Si	3.039	2.975	2.925	2.995	3.010	2.991	2.923	2.946	2.945	2.944	3.044	3.038
Al		.025	.075	.005		.009	.077	.054	.055	.056		
	3.039	3.000	3.000	3.000	3.010	3.000	3.000	3.000	3.000	3.000	3.044	3.038
Al site												
Al	1;930	1.986	1.980	1.968	1.948	1.980	1.981	1.986	1.997	1.992	1.942	1.925
Ti												
	1.930	1.986	1.980	1.968	1.948	1.980	1.981	1.986	1.997	1.992	1.942	1.925
M^{2+} site												
Fe^{2+}	2.166	2.114	2.111	2.107	2.124	2.101	2.080	2.111	2.118	2.113	2.143	2.179
Mn	.114	.104	.105	.110	.110	.112	.110	.112	.112	.117	.113	.110
Mg	.673	.735	.763	.742	.747	.748	.795	.745	.721	.727	.671	.669
Ca	.075	.082	.084	.076	.077	.074	.082	.079	.081	.084	.073	.078
	3.028	3.035	3.063	3.038	3.058	3.035	3.067	3.046	3.032	3.041	3.000	3.036
Almandine	71.5	69.7	68.9	69.4	69.5	69.2	67.8	69.3	69.9	69.5	71.4	71.8
Spessartine	3.8	3.4	3.4	3.6	3.6	3.7	3.6	3.7	3.7	3.8	3.8	3.6
Pyrope	22.2	24.2	24.9	24.4	24.4	24.7	25.9	24.5	23.8	23.9	22.4	22.0
Grossular	2.5	2.7	2.8	2.6	2.5	2.4	2.7	2.5	2.7	2.8	2.4	2.6

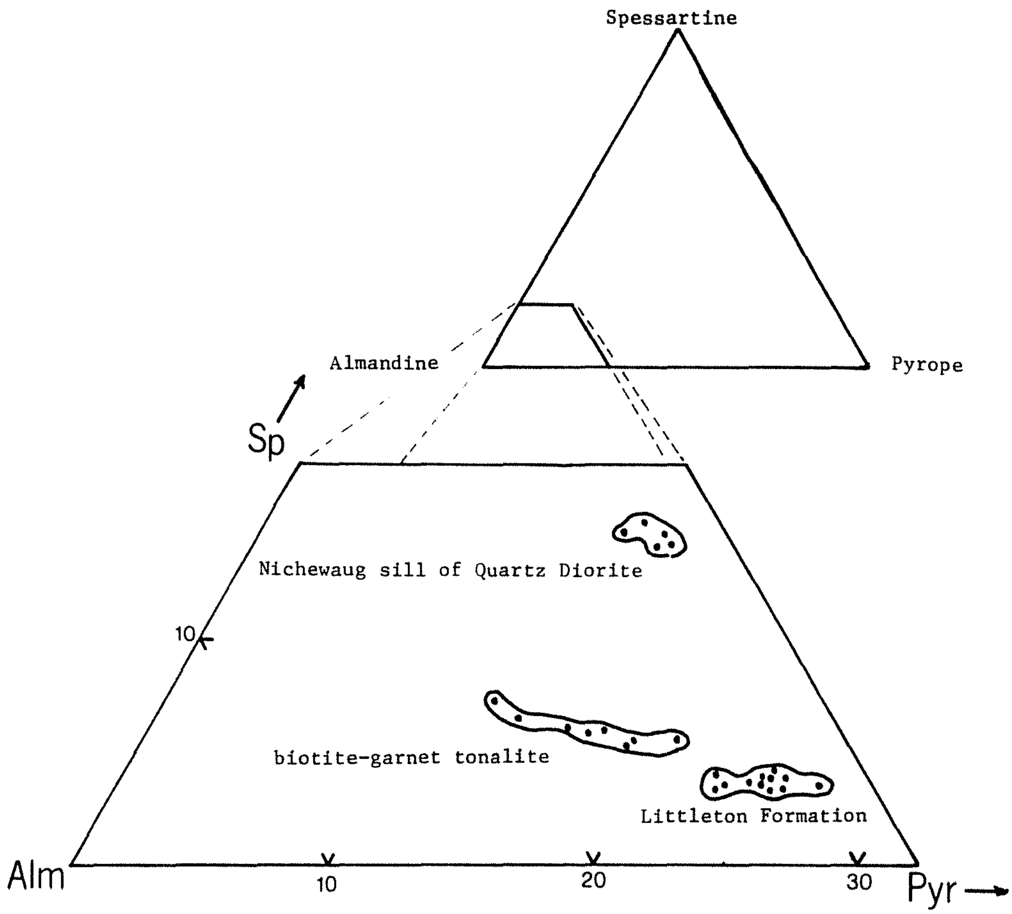

Figure 35. Composition of garnets from the biotite-garnet tonalite, chilled margin of the Nichewaug sill of quartz diorite, and the contact aureole in the gray schist member of the Littleton Formation surrounding the Nichewaug sill represented in terms of end-members spessartine-almandine -pyrope.

xenocrystic refractory residuals of restitic origin. The pyrope-greater-than-spessartine characteristic of these garnets contrasts with garnets of restitic or igneous (non-contamination) origin which commonly have a spessartine component greater than pyrope component (Allan and Clarke, 1981). Contrary to the restitic origin for granitoid garnets suggested by Chappell and White (1974), these garnets are most probably a product of magma contamination with a peraluminous country rock.

Based on plutonic garnets from South Mountain batholith, Nova Scotia, Allan and Clarke (1981) suggested that garnets possessing an anhedral shape and strongly poikilitic texture are more characteristic of growth in a solid state, whereas euhedral to subhedral garnets with grain size similar to coexisting minerals are characterstic of crystallization from a melt. If this textural criterion is used, the garnets of the chilled margin of the sill are a product of growth in the solid state while the garnets of the biotite-garnet tonalite crystallized from a contaminated silicate melt.

Plagioclase

Plagioclase is the dominant mineral common to the tonalites and associated diorites, quartz diorites and granites. The textural character of the plagioclase varies from euhedral to subhedral grains in rocks possessing a relict igneous texture to granoblastic grains in the rocks possessing a metamorphic texture. Representative electron microprobe analyses of plagioclase from the tonalites and associated plutonic rocks are presented in Table 22, and plotted in the ternary feldspar system in Figure 36.

In the tonalite, the plagioclase composition most commonly ranges from sodic andesine to calcic oligoclase. As a result of strong, well developed zoning, plagioclase compositions extend from sodic labradorite in plagioclase cores to sodic oligoclase in plagioclase rims. The orthoclase component in the plagioclase extends up to 2 mole percent. Plagioclase compositions for the tonalite subdivisions overlap considerably. However, the plagioclases of the hornblende-biotite tonalite and the biotite tonalite contain more calcic cores.

Plagioclase in the tonalites that have a relict igneous texture exhibits well developed zoning which is commonly normal in character. Rapid analysis traverses of plagioclase from sample SA100 illustrate that simple oscillatory zoning does occur in the tonalite plagioclase (Figure 37). The plagioclase of the traverse consists of cores with a composition of approximately An_{35}, intermediate zones with compositions ranging from An_{35} to An_{50} and rims with compositions ranging from An_{30}-An_{25}. The calcic, intermediate zone is approximately 0.4 mm in width in the larger grains (3 to 5mm). Granoblastic plagioclase exhibits limited zoning and commonly has a lower proportion of orthoclase component. The general lack of well defined zoning is probably a result of homogenization during metamorphic recrystallization.

The moderately to strongly zoned plagioclase of the augite-hornblende quartz diorite characterizes the relict igneous texture of the rock. Plagioclase zoning is normal from core compositions of $An_{46.1}Ab_{52.6}Or_{1.3}$ to rim compositions of $An_{29.5}Ab_{68.6}Or_{1.9}$ in the coarse-grained interior of the sill. Plagioclase laths in the chilled margin exhibit limited zoning and have compositions similar to cores of plagioclase in the sill's interior. Anhedral to interstitial plagioclase in the matrix of the chilled margin is more sodic with an average composition of $An_{42}Ab_{57.5}Or_{0.5}$. The compositional similarity between the plagioclase cores in the interior of the sill and the plagioclase laths in the chilled margin indicates that that plagioclase was a crystallizing phase prior to intrusion. The larger plagioclase grains in the interior of the sill continued to crystallize on previously nucleated plagioclase laths. Plagioclase from the augite-bearing tonalite within the Hardwick pluton ranges in composition from $An_{38.7}Ab_{60.3}Or_{1.0}$ in the cores to $An_{21.2}Ab_{77.7}Or_{1.1}$ in the rims.

The plagioclase of the Bear Den sill of diorite is poikilitic to interstitial in texture. It is moderately to strongly zoned. Single grains may be zoned from sodic labradorite to sodic oligoclase (Figure 35). Commonly, the plagioclase does not exhibit such a wide compositional variation. Typical plagioclase cores are sodic to intermediate andesine. Zoning is characteristically normal. The orthoclase component in the plagioclase of the Bear Den sill of diorite ranges from 0.1 to 0.9 mole percent and is typically less than 0.4 mole percent.

The plagioclase of the diorite at Goat Hill is normally zoned from approximately $An_{50.4}Ab_{48.3}Or_{1.3}$ to $An_{35.3}Ab_{63.0}Or_{1.7}$ (Figure 36). The orthoclase component ranges from 1.0 to 1.9 mole percent. There appears to be no systematic relationship between the anorthite and orthoclase content. The relict igneous texture suggests these plagioclase compositions are igneous and not a product of metamorphic recrystallization.

Detailed electron microprobe analyses (Table 22) and rapid electron microprobe analyses of plagioclase from the porphyritic microcline granite are plotted in Figure 36. The plagioclases are commonly mildly to moderately zoned from $An_{32.5}Ab_{66.8}Or_{0.7}$ to $An_{13.6}Ab_{85.3}Or_{1.1}$, although the compositional range in the zoning of individual grains rarely extends through this entire compositional spectrum. Granoblastic plagioclase in partially recrystallized microcline porphyritic granite is commonly homogeneous with the composition of calcic oligoclase. Both the zoned and granoblastic plagioclase have an orthoclase component of approximately 0.4 to 1.1 mole percent. Plagioclase inclusions in the potassium feldspar are commonly more sodic than the matrix plagioclase. These inclusions and plagioclase grains adjacent to potassium feldspar are rimmed or partially rimmed by sodic plagioclase. Rapid plagioclase analyses of the sodic plagioclase rims indicates a composition of approximately An_{7-5}. The similarity between the rim composition and plagioclase exsolution in the potassium feldspar and the interfacial relationship of the sodic plagioclase rims with plagioclase and potassium feldspar suggests the rims are of exsolution origin.

Table 22. Electron microprobe analyses of plagioclase from the Hardwick Tonalite and associated plutonic rocks.

	hornblende-biotite tonalite												
	SW12	SW12	SW12	SW12	SA61-2	SA61-2	SA160-3	SA160-3	SA160-3	SA100	SA100	SA100	SA2
SiO_2	60.19	60.09	59.92	60.87	59.14	60.34	60.75	60.51	59.20	60.30	60.56	60.51	57.99
Al_2O_3	25.02	25.11	25.23	25.77	25.67	25.69	25.14	25.22	25.28	25.72	25.82	25.11	26.41
CaO	6.45	6.58	6.47	6.19	7.56	7.05	5.67	6.07	6.62	5.72	5.76	5.68	8.31
BaO	0.09	0.08	0.07	0.07									
Na_2O	7.66	7.66	7.53	7.77	7.92	7.84	8.53	7.99	7.68	8.12	8.03	8.65	6.47
K_2O	0.16	0.16	0.16	0.15	0.10	0.10	0.14	0.17	0.18	0.16	0.22	0.23	0.26
Total	99.57	99.68	99.32	99.83	100.35	100.97	100.23	99.96	99.12	100.18	100.54	100.19	99.44
n	5	2	4	2	3	4	5	2	5	10	3	3	3
Structural Formulae													
Si	2.688	2.683	2.681	2.707	2.635	2.662	2.694	2.690	2.664	2.677	2.678	2.688	2.606
Al	1.318	1.322	1.331	1.299	1.349	1.337	1.314	1.321	1.342	1.346	1.346	1.315	1.399
	4.006	4.005	3.984	3.999	4.012	4.006	4.008	4.011	4.006	4.023	4.024	4.003	4.005
Ca	.309	.315	.310	.295	.361	.334	.269	.289	.312	.272	.274	.272	.400
Ba	.002	.001	.001	.001									
Na	.664	.663	.654	.670	.685	.671	.735	.689	.671	.699	.691	.747	.562
K	.009	.009	.005	.009	.003	.003	.008	.010	.010	.009	.012	.013	.016
	.984	.988	.970	.975	1.049	1.008	1.001	.988	.993	.980	.977	1.032	.978
An	31.5	31.9	32.0	30.3	34.4	33.1	26.6	29.3	31.4	27.8	28.0	26.4	40.9
Ab	67.6	67.2	67.4	68.8	65.3	66.6	72.7	69.7	67.6	71.3	70.7	72.4	57.5
Or	0.9	0.9	0.6	0,9	0.3	0.3	0.7	1.0	1.0	0.9	1.3	1.2	1.6
L	c	c	r	r	i	i	r	i	c	i	i	r	c

n=number of analyses. L=location of analyses within plagioclase grain: c=core, r=rim, i=intermediate, a=average.

	hornblende-biotite tonalite											biotite tonalite	
	SA2	SA2	SA2	SA2	SA2	SA2	SA2	SW21	SW21	SW16	SW16	SW18	SW18
SiO_2	58.66	60.95	60.09	61.69	62.32	62.64	62.71	59.25	59.34	59.88	61.89	55.16	55.77
Al_2O_3	25.99	24.69	24.46	24.35	24.07	24.11	24.10	26.19	25.72	25.47	24.71	28.09	28.28
CaO	7.90	6.08	6.75	5.86	5.55	5.45	5.52	7.34	7.00	7.03	6.00	10.23	10.22
BaO													
Na_2O	6.90	8.01	8.02	8.12	8.24	8:27	8.50	7.51	7.93	7.88	8.11	5.76	5.75
K_2O	0.22	0.23	0.16	0.17	0.25	0.18	0.22	0.25	0.31	0.23	0.24	0.14	0.14
Total	99.67	99.96	99.49	100.19	100.44	100.76	101.05	100.72	100.39	100.49	100.95	99.43	100.16
n	5	5	3	7	7	8	5	6	7	8	4	3	5
Structural Formulae													
Si	2.626	2.710	2.693	2.725	2.750	2.754	2.751	2.631	2.644	2.660	2.722	2.498	2.504
Al	1.372	1.294	1.293	1.275	1.252	1.251	1.248	1.372	1.351	1.335	1.281	1.500	1.497
	3.998	4.004	3.986	4.001	4.002	4.005	3.999	4.003	3.995	3.995	4.003	3.998	4.001
Ca	.379	.288	.323	.279	.263	.256	.258	.350	.335	.334	.283	.497	.492
Ba													
Na	.608	.689	.695	.697	.705	.713	.722	.646	.685	.678	.692	.506	.501
K	.012	.013	.009	.011	.014	.010	.014	.018	.013	.014	.014	.011	.008
	.999	.990	1.027	.987	.982	.979	.992	1.010	1.038	1.025	.989	1.014	1.001
An	37.9	29.1	31.5	28.3	26.8	26.2	26.0	34.7	32.3	32.6	28.6	49.1	49.2
Ab	60.9	69.6	67.7	70.6	71.8	72.8	72.8	64.0	66.0	66.2	70.0	49.9	50.0
Or	1.2	1.3	0.8	1.1	1.4	1.0	1.2	1.3	1.7	1.4	1.4	1.1	0.8
L	i	r	c	i	i	r	r	c	r	c	r	c	c

Table 22, continued.

	biotite tonalite													
	SW18	SW18	SW18	SW18	SW18	SW18	SM7	SM7	SM7	SM7	SP3	SP3	SP3	SP3
SiO_2	55.45	57.05	55.42	56.22	55.55	56.25	60.98	62.43	60.21	61.89	60.58	60.51	61.35	60.53
Al_2O_3	28.22	27.65	28.19	28.14	27.44	27.14	24.86	24.70	24.74	24.89	25.32	25.18	24.37	24.99
CaO	10.32	10.32	10.34	10.11	10.13	9.79	6.32	6.24	6.91	5.64	5.87	5.90	4.76	5.97
BaO							0.02		0.03	0.07				
Na_2O	5.61	5.73	5.73	5.50	5.64	5.96	7.82	7.58	7.86	8.09	8.13	8.06	8.57	8.20
K_2O	0.14	0.12	0.10	0.10	0.12	0.11	0.12	0.13	0.12	0.07	0.17	0.18	0.21	0.14
Total	99.74	100.93	99.78	100.22	99.00	99.32	100.12	101.18	99.87	100.65	100.07	99.85	99.26	99.83
n	2	7	2	4	3	7	3	3	3	4	2	2	4	5
Structural Formulae														
Si	2.500	2.540	2.499	2.521	2.524	2.544	2.704	2.732	2.686	2.731	2.689	2.693	2.737	2.695
Al	1.501	1.452	1.499	1.487	1.471	1.448	1.300	1.275	1.302	1.296	1.325	1.321	1.281	1.312
	4.101	3.992	3.998	4.008	3.995	3.992	4.004	4.007	3.988	4.027	4.014	4.014	4.018	4.007
Ca	.499	.492	.500	.485	.494	.476	.300	.293	.331	.266	.280	.281	.228	.284
Ba										.001				
Na	.490	.492	.501	.480	.497	.523	.673	.652	.680	.693	.699	.695	.740	.707
K	.008	.007	.006	.006	.007	.005	.007	.007	.007	.004	.011	.011	.012	.008
	.997	.991	1.007	.971	.998	1.004	.980	.952	1.018	.964	.990	.987	.980	.999
An	50.1	49.6	49.7	50.0	49.5	47.4	30.6	30.7	32.5	27.6	28.3	28.5	23.2	28.4
Ab	49.1	49.7	49.8	49.4	49.8	52.1	68.7	68.5	66.8	71.9	70.6	70.4	75.5	70.8
Or	0.8	0.7	0.5	0.6	0.7	0.5	0.7	0.8	0.7	0.5	1.1	1.1	1.2	0.8
L	c	c	c	i	i	r	i	i	c	r	c	c	r	c

	biotite tonalite												
	SW19	SW19	SP2	SP186	SP186	SP186	SP186	SA3	SA3	SA3	SA3	SA3	972-50
SiO_2	58.60	59.64	59.32	60.72	60.44	60.55	60.66	59.12	58.49	58.44	57.87	57.45	61.10
Al_2O_3	25.87	25.94	26.81	25.15	24.99	25.28	25.23	26.12	26.82	26.87	26.87	27.10	25.33
CaO	7.04	6.89	7.67	5.76	5.60	5.72	5.72	6.78	7.43	7.41	4.91	8.00	5.87
BaO													
Na_2O	7.80	8.03	7.36	8.09	8.09	8.10	8.03	7.60	7.36	7.32	7.05	7.05	8.34
K_2O	0.23	0.20	0.23	0.30	0.32	0.28	0.30	0.09	0.08	0.07	0.07	0.07	0.24
Total	99.57	100.70	101.39	100.02	99.44	99.93	99.97	100.04	100.22	100.13	99.89	99.67	100.88
n	5	16	7	2	3	2	1	5	10	3	3	3	3
Structural Formulae													
Si	2.630	2.644	2.613	2.697	2.700	2.691	2.671	2.640	2.606	2.604	2.592	2.577	2.693
Al	1.369	1.352	1.393	1.316	1.315	1.325	1.351	1.375	1.408	1.412	1.419	1.434	1.315
	3.999	3.996	4.000	4.013	4.015	4.016	4.022	4.015	4.014	4.016	4.011	4.011	4.008
Ca	.340	.328	.363	.275	.268	.273	.279	.325	.353	.353	.380	.386	.278
Ba													
Na	.680	.693	.630	.704	.703	.700	.688	.660	.658	.632	.614	.615	.715
K	.013	.011	.013	.016	.018	.016	.018	.005	.005	.005	.004	.004	.014
	1.033	1.032	1.006	.995	.989	.989	.985	.990	1.016	.990	.998	1.005	1.007
An	32.9	31.8	36.1	27.6	27.1	27.6	28.3	32.8	34.7	35.7	38.1	38.4	27.6
Ab	65.8	67.2	62.6	70.8	71.1	70.8	69.9	66.7	64.8	63.8	61.5	61.2	71.0
Or	1.3	1.0	1.3	1.6	1.8	1.6	1.8	0.5	0.5	0.5	0.4	0.4	1.4
L	a	a	a	r	r	i	c	r	i	i	c	c	c

Table 22, continued.

	biotite tonalite									biotite-muscovite tonalite				
	972-50	972-50	972-50	SP139	SP139	SP139	SP139	SP139	SP139	SP55	SP55	SP55	SP55	SP10
SiO_2	61.31	61.26	64.87	61.18	60.97	61.27	62.11	61.61	61.13	58.61	58.93	59.18	59.48	59.82
Al_2O_3	25.37	24.88	22.55	23.98	24.31	24.16	24.16	24.51	23.94	26.53	26.16	26.23	26.23	25.03
CaO	5.79	5.62	3.26	7.20	7.10	6.75	6.77	6.77	6.34	7.42	6.92	6.75	7.01	6.95
BaO														0.01
Na_2O	8.26	8.57	9.96	7.59	7.59	7.72	7.95	7.75	8.30	7.30	7.82	7.71	8.04	7.71
K_2O	0.23	0.14	0.14	0.14	0.14	0.16	0.16	0.17	0.15	0.07	0.08	0.09	0.08	0.12
Total	100.96	100.47	100.78	100.10	100.13	100.06	101.17	100.81	99.87	99.93	99.91	99.96	100.85	99.64
n	3	4	3	4	6	5	5	6	2	2	2	3	6	13
Structural Formulae														
Si	2.698	2.709	2.838	2.719	2.709	2.721	2.731	2.718	2.724	2.616	2.632	2.638	2.633	2.675
Al	1.316	1.297	1.164	1.257	1.273	1.265	1.252	1.274	1.258	1.397	1.378	1.378	1.369	1.320
	4.014	4.006	4.002	3.976	3.982	3.986	3.983	3.992	3.982	4.013	4.010	4.016	4.002	3.995
Ca	.272	.266	.153	.345	.339	.320	.317	.318	.302	.354	.330	.321	.332	.333
Ba														
Na	.703	.733	.846	.656	.657	.667	.676	.662	.717	.633	.676	.664	.692	.669
K	.013	.008	.008	.008	.008	.011	.011	.011	.009	.004	.004	.005	.004	.007
	.998	1.007	1.007	1.009	1.004	.998	1.004	.991	1.028	.991	1.010	,990	1.028	1.009
An	27.3	26.4	15.2	34.2	33.8	32.1	31.6	32.1	29.4	35.7	32.7	32.4	32.3	33.0
Ab	70.4	72.8	84.0	65.0	65.4	66.8	67.3	66.8	69.8	63.9	66.9	67.1	67.3	66.3
Or	1.3	0.8	0.8	0.8	0.8	1.1	1.1	1.1	0.8	0.4	0.4	0.5	0.4	0.7
L	c	i	r	c	i	i	r	c	r	c	i	r	r	i

	biotite-muscovite tonalite											biotite-garnet tonalite	
	SP10	SP10	SP10	SP10	SP10	SB1	SB1	SB1	SA251-1	SA251-1	SA251-1	SA54	SA54
SiO_2	59.90	59.85	59.92	59.98	60.10	60.72	61.10	61.20	60.57	61.19	61.37	59.97	60.94
Al_2O_3	24.41	25.02	24.85	25.08	25.03	25.25	24.70	24.41	24.78	25.18	24.32	25.21	24.16
CaO	6.28	6.82	7.17	6.78	7.11	5.85	5.16	4.78	6.03	5.72	4.86	8.46	7.51
BaO	0.01	0.07		0.04									
Na_2O	8.12	8.00	7.02	7.75	7.65	8.35	8.62	8.85	8.10	8.50	8.74	6.89	7.48
K_2O	0.17	0.14	0.12	0.12	0.16	0.13	0.13	0.14	0.14	0.18	0.14	0.06	0.06
Total	98.79	99.90	99.08	99.75	100.04	100.30	99.71	99.38	99.62	100.77	99.43	100.59	100.15
n	3	2	4	3	1	2	2	4	3	2	2	3	9
Structural Formulae													
Si	2.695	2.673	2.687	2.678	2.677	2.691	2.718	2.730	2.701	2.699	2.735	2.655	2.709
Al	1.297	1.318	1.314	1.320	1.315	1.319	1.295	1.283	1.302	1.309	1.278	1.325	1.267
	3.992	3.991	4.001	3.998	3.992	4.000	4.013	4.013	4.003	4.008	4.013	3.980	3.976
Ca	.304	.327	.345	.325	.339	.277	.246	.228	.289	.270	.233	.404	.358
Ba		.001		.001									
Na	.710	.693	.611	.671	.661	.719	.723	.767	.702	.726	.755	.594	.646
K	.010	.008	.007	.007	.009	.008	.008	.008	.008	.011	.008	.003	.003
	1.024	1.029	.963	1.004	1.009	1.004	.977	1.003	.999	1.007	.996	1.001	1.007
An	29.7	31.8	35.8	32.4	33.6	22.6	25.2	22.7	28.9	26.8	23.4	40.4	35.6
Ab	69.3	67.4	63.4	66.8	65.5	71.6	74.0	76.5	70.3	72.1	75.8	59.3	64.2
Or	1.0	0.8	0.8	0.8	0.9	0.8	0.8	0.8	0.8	1.1	0.8	0.3	0.2
L	r	r	c	i	i	c	i	r	c	i	r	c	i

Table 22, continued.

	biotite-garnet tonalite			augite-hornblende quartz diorite										
	SA54	SA54	SA54	SP179	SP179	SP179	SP179	SP179	SP179	SP236	SP236	SP236	SP236	SP236
SiO_2	61.06	60.57	61.10	56.58	55.44	57.92	60.03	55.84	60.16	55.69	54.84	55.83	58.38	59.65
Al_2O_3	24.66	24.84	24.71	28.04	27.63	26.75	24.83	28.01	25.00	27.32	28.10	27.98	27.08	26.18
CaO	6.87	7.74	7.15	9.39	9.60	8.66	6.48	9.60	6.41	9.27	9.83	9.87	8.57	6.78
BaO				0.03	0.04			0.02	0.05	0.06	0.01			0.04
Na_2O	7.75	7.16	7.90	6.54	6.39	7.06	8.14	6.39	8.23	6.69	6.19	6.25	6.86	8.17
K_2O	0.03	0.06	0.04	0.26	0.28	0.24	0.24	0.27	0.34	0.23	0.24	0.23	0.24	0.25
Total	100.37	100.37	100.90	100.84	99.38	100.63	99.72	100.13	100.19	99.26	99.21	100.16	101.13	101.27
n	4	3	3	3	2	5	8	4	3	2	5	2	7	3
Structural Formulae														
Si	2.704	2.688	2.696	2.524	2.514	2.582	2.683	2.511	2.679	2.527	2.491	2.510	2.584	2.640
Al	1.288	1.299	1.285	1.475	1.478	1.406	1.309	1.485	1.313	1.462	1.506	1.483	1.414	1.362
	3.992	3.987	3.981	3.999	3.992	3.988	3.992	3.996	3.992	3.989	3.997	3.993	3.998	4.002
Ca	.327	.368	.339	.449	.467	.414	.311	.463	.306	.451	.478	.476	.408	.320
Ba				.002	.001				.001					.001
Na	.665	.619	.679	.564	.562	.611	.706	.558	.711	.588	.548	.545	.590	.699
K	.002	.003	.002	.015	.016	.014	.013	.016	.019	.013	.014	.013	.013	.014
	.994	.990	1.020	1.030	1.045	1.039	1.030	1.037	1.037	1.053	1.039	1.034	1.011	1.034
An	32.9	37.2	33.2	43.6	44.7	39.8	30.2	44.7	29.5	42.9	46.1	46.0	40.4	31.0
Ab	66.9	62.5	66.6	54.8	53.8	58.8	68.6	53.8	68.6	55.9	52.6	52.7	58.4	67.6
Or	0.2	0.3	0.2	1.6	1.5	1.4	1.2	1.5	1.9	1.2	1.3	1.3	1.2	1.4
L	r	c	r	c	c	i	r	c	r	c	c	c	i	r

	augite-hornblende quartz diorite											Goat Hill diorite
	SP239-3	SP239-3	SP239-3	SP239-3	SP239-3	SP239-3	1083+50	1083+50	1083+50	1083+50	1083+50	FW522
SiO_2	56.32	56.57	56.25	56.60	56.60	56.75	57.37	58.12	61.31	61.37	61.03	54.92
Al_2O_3	28.15	28.36	27.76	27.67	27.66	27.91	27.90	26.71	24.33	24.41	24.51	28.26
CaO	9.71	9.71	9.55	9.56	9.48	8.83	7.89	7.00	4.66	4.40	4.60	9.71
BaO												
Na_2O	6.28	6.14	6.18	6.27	6.34	6.66	6.83	7.48	8.67	9.01	8.82	6.98
K_2O	0.13	0.12	0.12	0.10	0.01	0.11	0.15	0.15	0.22	0.17	0.19	0.22
Total	100.59	100.90	99.89	100.20	100.17	100.26	100.19	99.46	99.39	99.37	99.15	100.09
n	2	2	2	3	2	10	5	2	3	5	5	3
Structural Formulae												
Si	2.519	2.518	2.530	2.537	2.537	2.538	2.560	2.607	2.738	2.736	2.727	2.480
Al	1.482	1.489	1.472	1.461	1.462	1.471	1.468	1.412	1.281	1.282	1.291	1.505
	4.001	4.007	3.992	3.998	3.999	4.009	4.028	4.019	4.020	4.018	4.018	3.985
Ca	.465	.463	.460	.461	.455	.425	.378	.337	.223	.212	.220	.469
Ba												
Na	.542	.530	.541	.544	.550	.581	.590	.652	.751	.777	.768	.613
K	.005	.005	.005	.005	.005	.005	.010	.010	.011	.011	.011	.010
	1.012	.998	1.006	1.010	1.010	1.011	.978	.999	.985	1.000	.999	1.092
An	46.0	46.0	45.7	45.7	45.1	42.0	38.7	33.7	22.6	21.2	22.0	42.9
Ab	53.6	53.1	53.8	53.9	54.5	57.5	60.3	65.3	76.2	77.7	76.9	56.1
Or	0.4	0.5	0.5	0.6	0.4	0.5	1.0	1.0	1.2	1.1	1.1	1.0
L	c	r	c	r	r	a	c	c	i	r	r	c

Table 22, continued.

	Goat Hill Diorite										Bear Den sill of diorite		
	FW522	FW522	FW522	FW522	FW522	FW522	FW522	FW522	FW522	FW522	SP176-3	SP176-3	SP176-3
SiO_2	56.92	57.90	54.31	56.49	58.18	54.68	54.71	57.80	57.17	53.91	59.84	60.35	60.46
Al_2O_3	27.11	26.67	29.01	27.32	26.57	28.13	28.64	26.59	26.79	28.90	25.50	25.83	25.19
CaO	8.59	8.02	10.90	9.18	8.03	11.01	10.33	8.25	8.01	11.08	6.94	6.35	6.04
BaO													
Na_2O	7.45	7.72	5.83	6.97	7.56	5.88	6.11	7.60	7.90	5.94	7.88	8.21	8.55
K_2O	0.24	0.20	0.26	0.29	0.24	0.23	0.28	0.37	0.34	0.26	0.15	0.05	0.06
Total	100.31	100.51	100.31	100.25	100.58	99.93	100.07	100.71	100.21	100.09	100.31	100.79	100.30
n	4	3	5	2	3	2	3	4	4	5	3	2	2
Structural Formulae													
Si	2.553	2.586	2.449	2.540	2.594	2.475	2.468	2.580	2.568	2.440	2.660	2.665	2.683
Al	1.434	1.405	1.542	1.448	1.397	1.501	1.524	1.404	1.418	1.543	1.337	1.344	1.318
	3.987	3.991	3.991	3.988	3.991	3.976	3.993	3.984	3.986	3.983	3.997	4.009	4.001
Ca	.412	.383	.525	.438	.383	.533	.499	.384	.380	.538	.331	.300	.287
Ba													
Na	.646	.665	.509	.605	.654	.511	.537	.654	.679	.522	.679	.700	.736
K	.014	.011	.015	.016	.014	.013	.016	.021	.019	.015	.009	.003	.003
	1.072	1.059	1.049	1.059	1.051	1.057	1.052	1.059	1.078	1.075	1.019	1.003	1.026
An	38.4	36.2	50.1	41.4	36.4	50.4	47.4	36.3	35.3	50.0	32.5	29.9	28.0
Ab	60.3	62.8	48.5	57.1	62.2	48.3	51.1	61.8	63.0	48.6	66.6	69.8	71.7
Or	1.3	1.0	1.4	1.5	1.4	1.3	1.5	1.9	1.7	1.4	0.9	0.2	0.3
L	i	r	c	i	r	c	r	c	r	c	c	c	i

	Bear Den sill of diorite											
	SP176-3	SP176-3	SP176-3	SP176-2	SP176-2	SP176-2	SP176-2	SP176-2	SP176-2	SP176-2	SP176-2	SP176-2
SiO_2	62.99	64.93	65.31	56.81	59.58	62.57	62.54	65.68	58.72	60.88	60.59	65.54
Al_2O_3	23.46	22.80	21.88	27.96	26.13	24.26	24.19	21.54	25.76	25.28	25.23	21.96
CaO	4.84	2.99	2.80	9.95	7.82	5.11	4.85	2.36	7.84	6.25	6.18	2.47
BaO												
Na_2O	9.23	9.96	10.39	6.44	7.04	8.87	8.96	10.73	7.65	8.22	8.27	10.55
K_2O	0.03	0.06	0.04	0.05	0.07	0.06	0.08	0.06	0.05	0.05	0.07	0.06
Total	100.55	100.74	100.42	101.19	100.64	100.87	100.63	100.37	100.02	100.68	100.34	100.58
n	2	3	3	2	1	3	2	3	1	2	3	3
Structural Formulae												
Si	2.775	2.837	2.864	2.525	2.639	2.748	2.751	2.880	2.626	2.688	2.686	2.867
Al	1.218	1.175	1.131	1.465	1.365	1.256	1.255	1.114	1.358	1.316	1.319	1.132
	3.993	4.012	3.995	3.990	4.004	4.004	4.006	3.994	3.984	4.004	4.005	3.999
Ca	.228	.139	.132	.473	.370	.240	.230	.111	.376	.297	.293	.116
Ba												
Na	.788	.846	.885	.555	.607	.755	.766	.912	.661	.706	.709	.893
K	.001	.003	.002	.003	.004	.003	.005	.003	.003	.003	.004	.003
	1.017	.988	1.019	1.031	.981	.998	1.001	1.026	1.041	1.007	1.006	1.002
An	22.4	14.1	13.0	45.9	37.7	24.1	23.0	10.8	36.1	29.5	29.1	11.6
Ab	77.5	85.6	86.9	53.8	61.9	75.7	76.5	88.9	63.5	70.1	70.5	89.1
Or	0.1	0.3	0.1	0.3	0.4	0.2	0.5	0.3	0.4	0.4	0.4	0.3
L	i	r	r	c	c	i	i	r	c	i	i	r

Table 22, continued.

	Bear Den sill of diorite					porphyritic microcline granite								
	SP176-2	SP176-2	SP176-1	SP176-1	SP176-1	SP86	SP86	SP86	SA1	SA1	SA1	SA1	SA1	SA1
SiO_2	63.95	64.36	57.29	61.27	64.21	61.56	61.96	62.01	65.03	62.82	62.49	60.95	60.53	60.97
Al_2O_3	23.02	22.31	26.37	24.10	23.14	24.53	24.08	24.35	22.55	22.83	23.45	24.52	24.44	23.62
CaO	4.11	2.48	10.09	6.54	4.04	5.68	5.75	5.69	2.99	3.54	4.26	5.52	5.44	4.79
BaO					0.03	0.10		0.07						
Na_2O	9.78	10.03	5.50	7.62	9.22	8.57	8.32	8.36	10.33	10.06	9.79	9.17	9.34	9.48
K_2O	0.06	0.07	0.04	0.06	0.04	0.17	0.19	0.16	0.21	0.18	0.08	0.13	0.12	0.12
Total	100.92	99.25	99.29	99.59	100.55	100.61	100.30	100.64	101.11	99.43	100.07	99.99	99.87	98.98
n	2	2	5	6	5	4	5	5	5	5	2	2	15	4
Structural Formulae														
Si	2.802	2.851	2.584	2.729	2.812	2.720	2.741	2.734	2.838	2.797	2.768	2.702	2.701	2.738
Al	1.190	1.166	1.402	1.265	1.195	1.278	1.256	1.266	1.161	1.199	1.225	1.288	1.285	1.251
	3.992	4.017	3.986	3.994	4.007	3.998	3.997	4.000	3.999	3.996	3.993	3.990	3.987	3.989
Ca	.192	.117	.488	.313	.190	.269	.273	.269	.140	.169	.202	.264	.260	.231
Ba					.001	.002		.001						
Na	.832	.862	.481	.659	.784	.735	.714	.715	.875	.869	.841	.792	.808	.826
K	.003	.004	.002	.003	.002	.009	.011	.009	.011	.010	.004	.007	.007	.007
	1.027	.983	.971	.975	.977	1.016	.998	.994	1.026	1.048	1.047	1.063	1.075	1.064
An	18.7	11.9	50.3	32.1	19.5	26.6	27.4	27.1	13.6	16.1	19.3	24.8	24.2	21.7
Ab	81.0	87.7	49.5	67.6	80.3	72.6	71.5	72.0	85.3	82.9	80.3	74.5	75.2	77.6
Or	0.3	0.4	0.2	0.3	0.2	0.8	1.1	0.9	1.1	1.0	0.4	0.7	0.6	0.7
L	r	r	c	i	r	r	c	i	r	r	i	c	c	c

	granite at Sheep Rock		granite at Tom Swamp							Fitzwilliam Granite		
	SA68	SA68	Z93	Z93	Z93	Z93	Z93	Z93	Z93	SM4	SM4	SM4
SiO_2	61.72	61.21	62.74	61.83	61.94	62.12	62.18	61.96	62.70	62.01	62.31	63.29
Al_2O_3	24.30	24.08	23.42	24.40	23.95	23.75	24.02	24.53	24.00	24.23	24.13	23.28
CaO	5.64	5.69	4.62	4.54	4.72	4.71	4.59	4.72	4.48	4.70	4.63	4.10
BaO												
Na_2O	8.24	8.36	8.95	9.22	8.81	8.81	9.00	9.08	8.88	8.63	8.78	9.51
K_2O	0.15	0.15	0.23	0.18	0.14	0.21	0.20	0.27	0.22	0.16	0.16	0.19
Total	100.05	99.49	99.96	100.18	99.56	99.60	100.00	100.56	100.28	99.73	100.01	100.37
n	5	5	4	4	4	10	4	5	2	2	8	4
Structural Formulae												
Si	2.735	2.731	2.779	2.736	2.754	2.762	2.754	2.733	2.766	2.750	2.756	2.790
Al	1.270	1.267	1.223	1.273	1.256	1.245	1.254	1.276	1.248	1.266	1.257	1.210
	4.005	3.998	4.002	4.009	4.010	4.007	4.008	4.009	4.014	4.016	4.013	4.000
Ca	.268	.272	.218	.215	.224	.224	.218	.223	.212	.224	.220	.193
Ba												
Na	.708	.723	.767	.792	.759	.759	.772	.779	.758	.741	.754	.811
K	.008	.008	.013	.012	.008	.012	.011	.015	.012	.011	.011	.011
	.984	1.003	.998	1.019	.991	.995	1.001	1.017	.982	.976	.985	1.015
An	27.2	27.1	21.9	21.1	22.6	22.5	21.8	21.9	21.6	22.9	22.3	19.0
Ab	72.0	72.1	76.8	77.7	76.6	76.3	77.1	76.6	77.2	75.9	76.5	79.9
Or	0.8	0.8	1.3	1.2	0.8	1.2	1.1	1.5	1.2	1.2	1.2	1.1
L	c	r	c	c	c	i	r	r	r	c	i	r

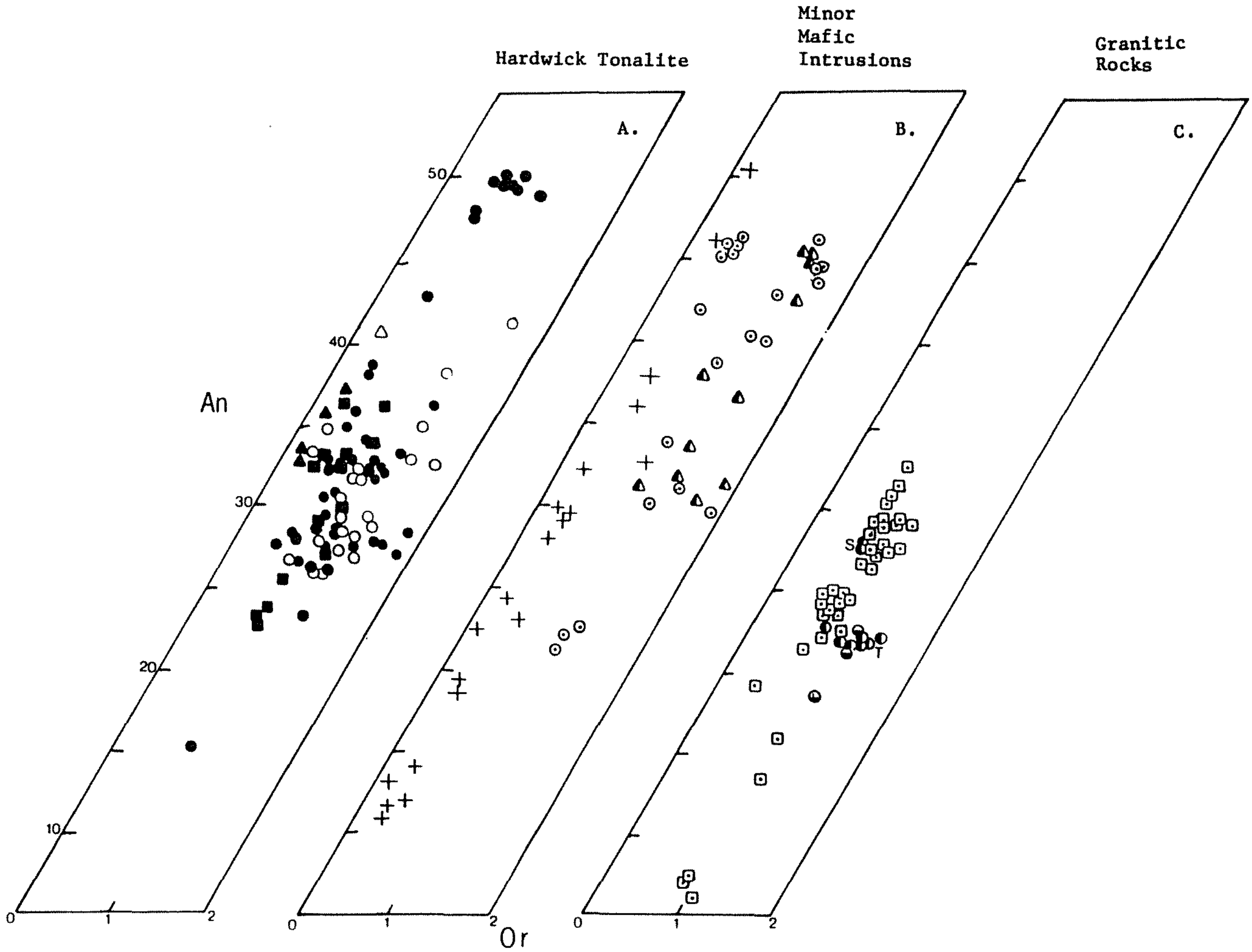

Figure 36. Plagioclase from (A) the Hardwick Tonalite: hornblende-biotite tonalite (○), biotite tonalite (●), biotite-muscovite tonalite (■), biotite-garnet tonalite (▲); (B) minor mafic intrusions: augite-hornblende quartz diorite (⊙), diorite at Goat Hill (◭), diorite at Bear Den Sill (+); and (C) associated granitic rocks: porphyritic microcline granite (⊡), Fitzwilliam Granite (◒), granites at Tom Swamp (◐T) and Sheep Rock (◐S) plotted in ternary system An-Ab-Or.

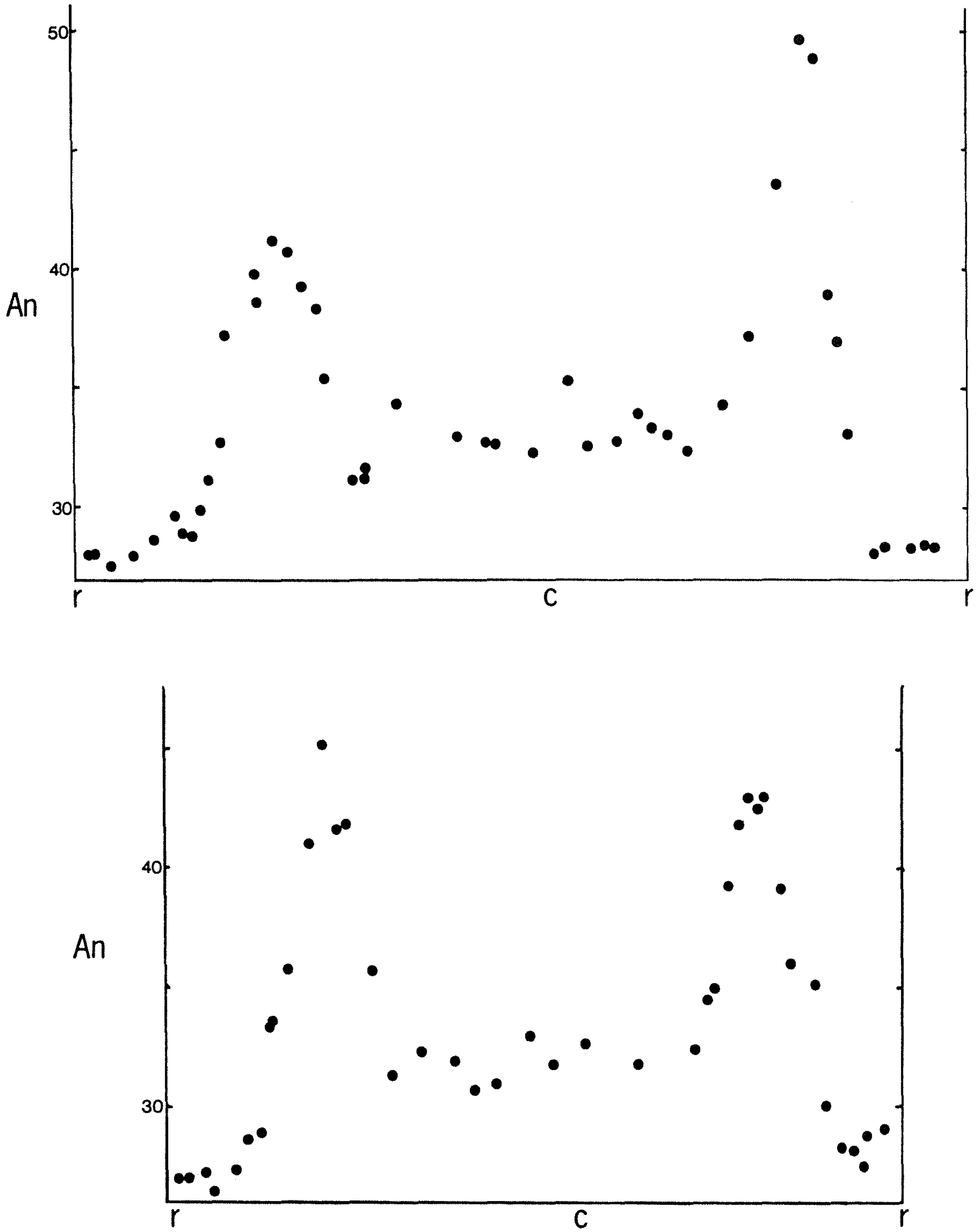

Figure 37. Rapid analysis traverses of two plagioclase grains from sample SA100. (scale: 1.5inches=1mm)

Electron microprobe analyses of plagioclase from the equigranular biotite-muscovite granites from Sheep Rock, Tom Swamp and Fitzwilliam Granite are shown in Table 22 and plotted in Figure 36. The limited amount of analyses suggest the plagioclase of the granites at Sheep Rock and Top Swamp exhibit limited compositional zoning. Plagioclase compositions for these two granites are intermediate to calcic oligoclase. Although microprobe analyses suggest limited zoning, optical determinations suggest zoning is perhaps moderately developed in some grains. Electron microprobe analyses of plagioclase of the Fitzwilliam Granite, on the other hand, indicate moderate zoning is well developed. Plagioclase compositions are calcic to intermediate oligoclase with rim compositions of sodic oligoclase. The orthoclase component in the three granites ranges from 0.8 to 1.6 mole percent. Albite rims occur on some plagioclase grains included in or adjacent to large potassium feldspar grains.

In summary, plagioclases in rocks possessing a relict igneous texture are moderately to strongly zoned and with increasing metamorphic recrystallization the plagioclase becomes more homogeneous. The variation in orthoclase component appears to be partially dependent upon recrystallization and this dependency obscures any relationship between orthoclase and anorthite component variations.

Potassium Feldspar

Potassium feldspar is commonly anhedral to interstitial orthoclase in the augite-hornblende quartz diorite and in the more mafic members of the Hardwick Tonalite, and interstitial to euhedral microcline in the granites and in the more felsic members of the Hardwick Tonalite. As determined from electron microprobe analyses, the potassium feldspars exhibit an extremely narrow range of compositional variability. As shown in Table 23, the orthoclase component varies from $Or_{91.5}$ to $Or_{86.4}$. Also shown in Table 23 are estimates of host/exsolution ratios used in determination of bulk potassium feldspar compositions. With respect to the orthoclase component there is no difference in potassium feldspar composition between units. These compositions appear to be typical of metamorphic potassium feldspars (Evans and Guidotti, 1966; Hollocher, 1980; Tracy 1975). The degree of development of microperthitic texture is variable from less than 5% to 25% plagioclase exsolution and is variable within individual grains and between units. The exsolved plagioclase shows limited variability in composition from An_5 to An_8, suggesting that the composition is solvus-controlled. Compositions of exsolution lamellae were determined by electron microprobe and the Michel-Levy extinction angle method.

The potassium feldspars were numerically rehomogenized from estimates of host/exsolution ratios and determinations of host/exsolution compositions to obtain bulk potassium feldspar compositions. These compositional reconstructions are shown in Figure 38. With the reconstructions, the potassium feldspar compositional variability increases and approaches approximate igneous compositions. The orthoclase of the augite-hornblende quartz diorite (Figure 38) has a calculated bulk composition between

Table 23. Electron microprobe analyses of potassium feldspars from the Hardwick Tonalite and associated plutonic rocks. Also included in table is the percent plagioclase exsolution in the potassium feldspars used in the reconstructions in Figure 48.

	hornblende-biotite tonalite							biotite tonalite					
	SA160-3	SA160-3	SA160-3	SW12	SA2	SA2	SA2	SM7	SM7	SM7	SM7	SP139	SP139
SiO_2	63.93	63.76	63.53	64.31	63.75	63.03	63.80	64.62	64.37	65.12	64.37	64.43	64.37
Al_2O_3	18.97	18.99	19.15	18.66	19.68	19.05	19.56	18.62	18.71	18.50	18.73	18.99	18.58
CaO								0.04	0.03	0.05	0.04	0.07	0.03
BaO	2.06	2.14	2.42	0.76	1.42	1.46	1.42	0.68	0.66	0.43	0.71	1.67	1.48
Na_2O	0.98	0.91	0.99	0.97	1.25	1.26	1.26	0.88	0.91	0.80	0.94	0.90	0.91
K_2O	14.77	14.80	14.77	14.94	15.19	14.95	14.83	15.11	14.97	15.16	15.31	15.56	15.49
Total	100.71	100.60	100.86	99.64	101.33	100.22	100.90	99.95	99.65	100.06	100.10	101.62	100.86
n	10	5	5	5	2	5	6	4	4	4	2	2	3
Structural Formulae													
Si	2.964	2.961	2.950	2.984	2.935	2.946	2.943	2.988	2.984	3.000	2.979	2.962	2.977
Al	1.036	1.040	1.049	1.020	1.068	1.050	1.064	1.015	1.023	1.005	1.022	1.030	1.013
	4.000	4.001	3.999	4.004	4.003	4.006	4.007	4.003	4.011	4.005	4.001	3.992	3.990
Ca								.002	.001	.003	.002	.004	.001
Ba	.036	.039	.045	.014	.025	.028	.025	.012	.011	.008	.013	.030	.028
Na	.089	.084	.089	.089	.111	.112	.111	.079	.084	.072	.084	.083	.083
K	.875	.876	.876	.886	.891	.893	.870	.892	.886	.892	.904	.913	.911
	1.000	.999	1.010	.989	1.029	1.034	1.007	.985	.982	.975	1.003	1.030	1.023
An								0.2	0.1	0.3	0.2	0.4	0.1
Ab	8.9	8.4	8.8	9.0	10.8	10.8	11.0	8.0	8.6	7.4	8.4	8.1	8.1
Or	87.5	87.7	86.7	89.6	86.6	86.4	86.4	90.6	90.2	91.5	90.1	88.6	89.1
Cn	3.6	3.9	4.5	1.4	2.4	2.7	2.5	1.2	1.1	0.8	1.3	2.9	2.7
percent Ab exsolution	18%	18%	18%	10%	15%	15%	15%	25%	25%	25%	25%	4%	4%

	biotite tonalite						augite-hornblende quartz diorite							
	SP3	972+50	972+50	SR7	SR7	SR7	SP179	SP179	SP179	SP179	SP236	SP236	SP236	SP236
SiO_2	62.71	63.41	63.22	62.44	62.51	62.34	63.20	62.64	62.43	62.34	62.56	62.16	62.87	62.87
Al_2O_3	19.32	19.37	19.29	19.91	19.68	20.14	19.52	19.17	19.26	19.65	20.04	20.19	19.98	19.36
CaO	0.01	0.03	0.03				0.03	0.02	0.03	0.03	0.02	0.03	0.04	0.03
BaO	1.05	1.01	0.83	2.50	2.47	2.36	1.88	2.23	1.83	2.17	1.60	2.09	1.70	1.95
Na_2O	0.94	0.82	1.03	1.00	0.97	1.03	0.87	0.75	0.80	0.71	0.77	0.77	0.84	0.82
K_2O	15.57	15.30	15.33	14.58	14.50	14.54	15.45	15.38	15.73	15.25	15.68	15.66	15.49	15.50
Total	99.59	99.94	99.73	100.43	100.13	100.41	100.95	100.19	100.08	100.15	100.67	100.90	100.92	100.53
n	4	3	8	4	4	3	6	3	3	2	8	4	4	5
Structural Formulae														
Si	2.937	2.949	2.945	2.916	2.925	2.908	2.928	2.937	2.929	2.946	2.948	2.935	2.945	2.933
Al	1.066	1.062	1.060	1.096	1.085	1.108	1.071	1.060	1.066	1.069	1.065	1.069	1.062	1.065
	4.003	4.011	4.005	4.012	4.000	4.016	3.999	3.997	3.995	4.015	4.013	4.004	4.007	3.998
Ca		.001	.001	.002	.001	.002	.001	.001	.002	.001	.001	.002	.002	.002
Ba	.019	.020	.014	.045	.045	.042	.034	.041	.033	.041	.027	.038	.035	.035
Na	.084	.073	.095	.090	.090	.095	.079	.068	.071	.064	.069	.070	.074	.075
K	.929	.905	.913	.870	.866	.863	.918	.920	.937	.890	.909	.908	.894	.920
	1.022	.999	1.023	1.005	1.000	1.000	1.033	1.030	1.043	.996	1.006	1.018	1.005	1.033
An		0.1	0.1				0.2	0.1	0.2	0.1	0.1	0.2	0.2	0.2
Ab	8.2	7.3	9.3	9.0	9.0	9.5	7.6	6.6	6.8	6.4	6.9	6.9	7.3	7.3
Or	90.9	90.6	89.2	86.5	86.5	86.3	88.9	89.3	89.8	89.4	90.3	89.2	89.0	89.1
Cn	1.9	2.0	1.4	4.5	4.5	4.2	3.3	4.0	3.2	4.1	2.7	3.7	3.5	3.4
percent Ab exsolution	25%	5%	5%	5%	5%	5%	20%	20%	20%	20%	25%	25%	25%	25%

Table 23, continued.

	porphyritic microcline granite SA1	SA1	SA1	SA1	SP86	SP86	SP86
SiO_2	64.78	64.56	64.40	64.62	65.27	65.96	64.47
Al_2O_3	18.66	18.68	18.75	18.96	18.58	18.58	18.55
CaO						0.03	0.04
BaO	0.68	0.51	0.76	0.98	0.48	0.53	0.52
Na_2O	0.86	1.32	0.73	0.82	0.78	1.07	1.03
K_2O	15.57	14.77	15.75	14.83	15.01	14.30	14.68
Total	100.55	99.74	100.39	100.21	100.15	100.47	99.29
n	10	3	3	4	5	2	4
Structural Formulae							
Si	2.985	2.975	2.988	2.981	3.002	3.012	2.993
Al	1.014	1.026	1.011	1.032	1.007	1.000	1.015
	3.999	4.001	4.000	4.013	4.009	4.012	4.008
Ca						.002	.002
Ba	.012	.009	.014	.018	.008	.010	.010
Na	.077	.120	.064	.074	.072	.095	.093
K	.916	.882	.919	.873	.879	.834	.869
	1.005	1.011	.997	.965	.959	.941	.974
An						0.2	0.2
Ab	7.7	11.9	6.4	7.7	7.5	10.1	9.6
Or	91.1	87.2	92.2	90.4	91.7	88.6	89.2
Cn	1.2	0.9	1.4	1.9	0.8	1.1	1.0
percent Ab exsolution	25%	25%	25%	25%	5%	5%	5%

	granite at Sheep Rock SA68	SA68	SA68	SA68	SA68	SA68	Tom Swamp granite Z93	Fitzwilliam Granite SM4
SiO_2	64.72	64.11	64.31	65.27	64.92	64.98	64.76	64.37
Al_2O_3	18.42	18.75	18.66	18.58	18.86	18.93	18.38	18.51
CaO		0.01		0.03				
BaO	0.32	0.97	0.76	0.49	0.30	0.30	1.12	0.55
Na_2O	0.93	1.20	0.97	0.89	1.04	1.01	0.91	1.13
K_2O	15.45	14.65	14.94	15.01	15.65	15.97	15.31	15.03
Total	99.84	99.69	99.64	100.27	100.77	100.89	100.48	99.59
n	5	2	1	1	3	1	4	3
Structural Formulae								
Si	2.995	2.997	2.984	3.001	2.980	2.977	2.992	2.987
Al	1.005	1.027	1.021	1.006	1.021	1.023	1.002	1.013
	4.000	4.004	4.005	4.007	4.001	4.000	3.994	4.000
Ca				.002				
Ba	.006	.018	.014	.009	.005	.005	.019	.011
Na	.083	.108	.088	.078	.094	.090	.083	.100
K	.912	.868	.885	.881	.914	.934	.905	.892
	1.001	.994	.987	.970	1.013	1.029	1.007	1.003
An				0.2				
Ab	8.3	10.9	8.9	8.1	9.3	8.8	8.2	10.0
Or	91.1	87.3	89.7	90.8	90.2	90.7	89.9	88.9
Cn	0.6	1.8	1.4	0.9	0.5	0.5	1.9	1.1
percent Ab exsolution	4%	4%	4%	4%	4%	4%	28%	5%

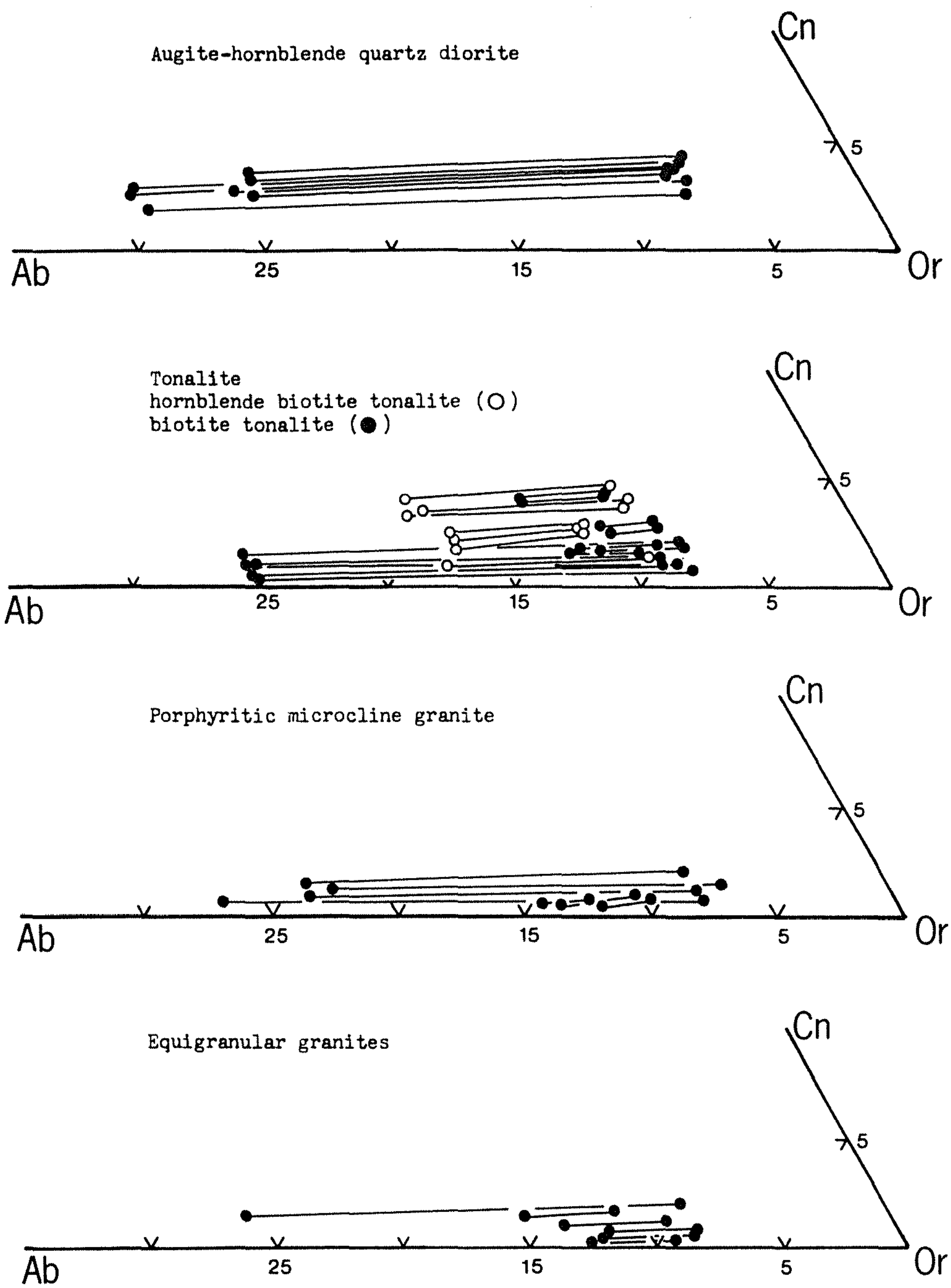

Figure 38. Potassium Feldspar analyses from the Hardwick Tonalite and associated plutonic rocks plotted in Ab-Or-Cn. Tie-lines connect microprobe analyses (Or-rich) with bulk feldspar analyses calculated by integrating host and exsolution (Ab-rich).

Or_{75} and Or_{70}. The potassium feldspar of the Hardwick Tonalite has a wide range of bulk potassium feldspar compositions from Or_{88} to Or_{75}. The bulk orthoclase of the hornblende-bearing tonalite is intermediate in composition with respect to that range with compositions of Or_{83} to Or_{80}. The microcline of the porphyritic microcline granite shows a range in composition from Or_{90} to Or_{73}. The augen-shaped microclines in those porphyritic granites that possess a well developed metamorphic texture have bulk compositions with a higher orthoclase component than the rectangular microcline in those porphyritic granites that possess a poorly developed metamorphic texture. Microcline from the Fitzwilliam Granite and the Sheep Rock Granite ranges in bulk composition from Or_{88} to Or_{85}. Only the Tom Swamp Granite (Z93) has microcline with a bulk composition of Or_{75}.

The celsian feldspar component in these potassium feldspars varies from 0.5 to 4.5 mole percent. The celsian component is highest in the augite-hornblende quartz diorite and hornblende-biotite tonalite and decreases as the rock composition becomes more felsic. Although Ba is strongly partitioned into the potassium feldspar host during exsolution, Figure 38 shows that exsolution cannot account for all the Ba variation. The Ba variation is a function of bulk composition and not a function of exsolution concentration. Although not substantiated by detailed structural ordering data, the celsian content also appears to decrease from orthoclase to microcline (Figure 38). Afonina and Shmakin (1970) claimed that Ba substitution inhibited ordering in potassium feldspar. Rhodes (1969) found no significant correlation between Ba content and potassium feldspar ordering in Australian granites, but illustrated a Ba decrease in the potassium feldspar as whole as rock compositions changed from granodiorite to leucocratic granite. The possible correlations of Ba content of potassium feldspars of the Hardwick Tonalite and associated plutonic rocks with potassium feldspar ordering and whole rock composition appear not to be dependent upon low temperature reequilibration or differences in grade of metamorphism.

Oxides

Ilmenite or rutile-hematite intergrowths after ilmenite occur in abundance as accessory minerals in all rocks of the Hardwick pluton and associated plutonic rocks except the equigranular granites and the Bear Den sill of diorite. The ilmenite commonly forms euhedral to subhedral laths or anhedral grains rimmed by sphene. Exsolution lamellae of titanohematite in the ilmenite host range from 0 to 15% in amount. In the hornblende-biotite tonalite, augite-hornblende quartz diorite and Goat Hill diorite a magnetite-ilmenite assemblage is very common. The magnetite-ilmenite assemblage may also occur in biotite tonalite and porphritic microcline granite. Magnetite in all these associations is homogeneous.

Ilmenite and hematite microprobe analyses are presented in Table 24 and plotted in Figure 39. Magnetite microprobe analyses are presented in Table 25. Oxide weight percents and structural formulae of the ilmenite, hematite and magnetite have been recalculated in the basis of two,

Table 24. Electron microprobe analyses of ilmenite and hematite from the Hardwick Tonalite and associated plutonic rocks. Oxide weight percent and structural formulae calculated on the basis of 2 cations and 3 oxygens. MgO was analyzed and was found to be zero in all cases.

	hornblende-biotite tonalite											
	SA160-3	SA160-3	SA160-3	SA100	SA100	SA100	SA100h	SW12	SW12	SW12	SW12	SW12h
TiO_2	50.30	50.11	50.67	48.49	47.58	47.96	10.96	44.94	46.24	47.02	47.46	0.15
Fe_2O_3	4.55	4.83	3.82	7.63	9.56	8.75	78.33	14.75	12.92	11.42	10.76	100.67
FeO	38.14	37.82	38.60	33.51	37.63	38.11	9.32	36.13	37.21	37.49	37.94	0.05
MnO	6.99	7.14	6.87	9.96	5.08	4.94	0.52	4.21	4.32	4.72	4.67	0.08
Total	99.97	99.90	99.96	99.59	99.85	99.76	99.13	100.03	100.68	100.65	100.83	100.95
n	10	10	8	16	6	7	2	2	2	8	5	4
Structural Formulae												
Ti	.957	.954	.964	.927	.909	.923	.218	.859	.877	.892	.898	.003
Fe^{3+}	.043	.046	.036	.073	.091	.077	.782	.141	.123	.108	.102	.997
Fe^{3+}	.043	.046	.037	.073	.092	.078	.781	.141	.123	.108	.102	.997
Fe^{2+}	.807	.801	.816	.713	.799	.815	.207	.768	.785	.791	.798	.001
Mn	.150	.153	.147	.214	.109	.107	.012	.091	.092	.101	.100	.002
Hematite %	4.3	4.6	3.7	7.3	9.2	7.8	78.1	14.1	12.3	10.8	10.2	99.7
Ilmenite %	80.7	80.1	81.6	71.3	79.9	81.5	20.7	76.8	78.5	79.1	79.8	0.1
Pyrophanite %	15.0	15.3	14.7	21.4	10.9	10.7	1.2	9.1	9.2	10.1	10.0	0.2
oxide assemblage	i	i	i	m+i	m+i	m+i	m+i	m+i	m+i	m+i	m+i	m+i
(Hem/Hem+Ilm)x100	1	1	1	10	10	10		2	4	8	8	

	hornblende-biotite tonalite							biotite tonalite				
	SW21	SW21h	SW16	SP65	SP65	SP65	SA4	SP2	SP2	SP2h	SR7	SR7
TiO_2	45.38	13.20	47.15	47.73	48.15	46.01	51.01	47.33	45.89	12.82	49.29	48.74
Fe_2O_3	13.41	76.53	10.17	9.04	8.41	11.68	3.02	10.32	12.68	77.18	6.99	7.08
FeO	38.79	11.64	37.43	38.02	38.11	36.88	39.76	38.45	37.06	11.14	37.12	36.72
MnO	1.97	0.22	4.89	4.82	5.12	4.44	6.08	4.04	4.14	0.38	7.10	7.01
Total	99.55	101.59	99.65	99.61	99.78	99.01	99.87	100.14	99.77	101.52	100.50	99.55
n	10	2	8	6	4	5	5	10	10	3	6	6
Structural Formulae												
Ti	.871	.256	.903	.913	.920	.887	.971	.902	.879	.249	.934	.932
Fe^{3+}	.129	.744	.097	.087	.080	.113	.029	.098	.121	.751	.066	.068
Fe^{3+}	.129	.744	.097	.087	.080	.113	.029	.098	.122	.751	.066	.068
Fe^{2+}	.828	.251	.797	.809	.810	.791	.841	.815	.789	.241	.782	.781
Mn	.043	.005	.106	.104	.110	.096	.130	.087	.089	.008	.152	.151
Hematite %	12.9	74.4	9.7	8.7	8.0	11.3	2.9	9.8	12.2	75.1	6.6	6.8
Ilmenite %	82.8	25.1	79.7	80.9	81.0	79.1	84.1	81.5	78.9	24.1	78.2	78.1
Pyrophanite %	4.3	0.5	10.6	10.4	11.0	9.6	13.0	8.7	8.9	0.8	15.2	15.1
oxide assemblage	m+i	m+i	m+i	m+i	m+i	m+i	i	m+i	m+i	m+i	i	i
(Hem/Hem+ilm)x100	6%	6%	1%					8%			1%	1%

	biotite tonalite						biotite-muscovite tonalite				
	SW18	ST2	ST2	ST2	SP139	SW15	SB1	SA251-1	SA251-1	SA251-1	SA251-1
TiO_2	49.49	51.86	51.73	51.57	50.16	47.47	48.75	52.52	52.55	52.17	52.23
Fe_2O_3	6.25	1.75	1.87	1.81	6.12	8.83	6.66	0.99	1.09	1.57	1.81
FeO	40.63	39.66	40.72	40.12	38.49	38.81	38.62	43.29	43.01	42.82	42.98
MnO	3.81	6.72	5.97	6.48	6.51	3.85	5.13	3.82	4.01	4.00	3.89
Total	100.18	99.99	100.29	99.98	101.28	98.97	99.17	100.66	100.81	100.59	100.94
n	7	8	10	10	6	10	5	3	10	7	3
Structural Formulae											
Ti	.941	.982	.979	.978	.942	.915	.936	.991	.990	.985	.983
Fe^{3+}	.059	.018	.021	.022	.058	.085	.064	.009	.010	.015	.017
Fe^{3+}	.059	.018	.021	.022	.058	.085	.064	.010	.011	.015	.017
Fe^{2+}	.859	.838	.852	.840	.804	.832	.825	.908	.903	.899	.900
Mn	.082	.144	.127	.138	.138	.083	.111	.082	.085	.085	.083
Hematite %	5.9	1.8	2.1	2.2	5.8	8.5	6.4	1.0	1.1	1.5	1.7
Ilmenite %	85.9	83.8	85.2	84.0	80.4	83.2	82.5	90.8	90.3	89.9	90.0
Pyrophanite %	8.2	14.5	12.7	13.8	13.8	8.3	11.1	8.2	8.6	8.6	8.3
oxide assemblage	i	i	i	i	i+m	i	i	i	i	i	i
(Hem/Hem+Ilm)x100	2%	2%	2%	2%	8%	4%					

Table 24, continued.

	biotite-muscovite tonalite			biotite-garnet tonalite		augite-hornblende quartz diorite						
	SA251-1	SP55	SB1	SA54	SA54	SP236	SP236	SP236	SP236	SP179	SP179	SP179
TiO_2	52.54	51.09	50.12	50.84	50.36	50.30	49.72	50.22	50.24	48.91	49.16	49.32
Fe_2O_3	1.06	5.61	5.27	2.93	3.81	4.32	6.42	5.07	4.89	7.28	6.55	6.11
FeO	43.17	39.95	37.13	42.92	42.33	40.62	40.62	41.29	41.12	39.67	49.62	39.80
MnO	3.96	5.91	7.82	2.75	2.91	4.54	4.02	3.80	3.99	4.24	4.51	4.48
Total	100.76	100.56	100.35	99.43	99.41	99.78	100.78	100.39	100.25	100.10	99.83	99.71
n	2	8	10	8	8	1	1	3	4	5	5	6
Structural Formulae												
Ti	.990	.948	.950	.972	.964	.959	.939	.952	.954	.931	.938	.942
Fe^{3+}	.010	.052	.050	.028	.036	.041	.061	.048	.046	.069	.062	.058
Fe^{3+}	.010	.052	.050	.028	.036	.041	.060	.048	.047	.069	.062	.059
Fe^{2+}	.905	.825	.783	.913	.901	.861	.854	.871	.868	.839	.841	.845
Mn	.084	.123	.167	.059	.063	.097	.086	.081	.085	.091	.097	.096
Hematite %	1.0	5.2	5.0	2.8	3.6	4.1	6.0	4.8	4.7	6.9	6.2	5.9
Ilmenite %	90.6	82.5	78.3	91.3	90.1	86.1	85.4	87.1	86.8	83.9	84.1	84.5
Pyrophanite %	8.4	12.3	16.7	5.9	6.3	9.7	8.6	8.1	8.5	9.1	9.7	9.6
oxide assemblage	i	i	i	i+r	i+r	m+i	m+i	m+i	m+i	m+i	m+i	m+i
(Hem/Hem+Ilm)x100		1%				1%	1%	1%	1%	6%	6%	6%

	augite-hornblende quartz diorite	Goat Hill Diorite				
	SP239-1	FW522	FW522h	FW522h	FW522	FW522
TiO_2	51.48	47.03	12.89	13.73	48.15	47.27
Fe_2O_3	1.49	11.06	76.03	74.05	10.07	10.66
FeO	44.02	39.87	11.32	12.04	41.05	40.16
MnO	2.70	1.08	0.11	0.14	1.01	1.05
Total	99.62	99.81	100.51	100.13	100.98	99.88
n	3	6	5	6	2	2
Structural Formulae						
Ti	.986	.894	.253	.270	.905	.898
Fe^{3+}	.014	.105	.745	.729	.095	.102
Fe^{3+}	.015	.106	.746	.729	.096	.102
Fe^{2+}	.938	.843	.248	.263	.858	.849
Mn	.047	.023	.002	.003	.021	.022
Hematite %	1.5	10.6	74.6	72.9	9.6	10.2
Ilmenite %	93.8	86.8	25.2	26.8	88.0	87.1
Pyrophanite %	4.7	2.6	0.4	0.3	2.4	2.7
oxide assemblage	i	m+i	m+i	m+i	m+i	m+i
(Hem/Hem+Ilm)x100		15			15	15

n = number of analyses.

h in sample number indicates analyses of hematite exsolution in ilmenite.

oxide assemblage: i = ilmenite, m = magnetite, r = rutile.

(Hem/Hem+Ilm) x 100 = percent hematite exsolution in ilmenite.

	porphyritic microcline granite						granite at sheep rock	Littleton Form.
	SA1	SA1	SA1	SP86	SP86	SP86	SA68	Met140
TiO_2	45.64	45.66	47.00	48.56	48.36	48.08	49.52	51.49
Fe_2O_3	12.99	13.00	10.75	6.93	7.75	8.33	5.82	0.79
FeO	35.53	35.55	36.73	38.25	38.70	39.22	39.59	45.75
MnO	4.88	4.86	4.77	5.18	4.67	3.95	4.86	0.54
Total	99.05	99.07	99.26	98.93	99.47	99.58	99.84	98.57
n	3	3	2	2	8	2	7	15
Structural Formulae								
Ti	.875	.875	.897	.933	.926	.920	.943	.992
Fe^{3+}	.125	.125	.103	.067	.074	.080	.057	.008
Fe^{3+}	.125	.125	.103	.067	.074	.080	.057	.008
Fe^{2+}	.768	.768	.792	.821	.825	.835	.838	.980
Mn	.107	.107	.104	.112	.101	.085	.104	.012
Hematite %	12.5	12.5	10.3	6.7	7.4	8.0	5.7	0.8
Ilmenite %	76.8	76.8	79.3	82.1	83.5	83.5	83.9	98.0
Pyrophanite %	10.7	10.7	10.4	11.2	10.1	8.5	10.4	1.2
oxide assemblage	m+i	m+i	m+i	i	i	i	i	i
(Hem/Hem+Ilm)x100	1	1	1					

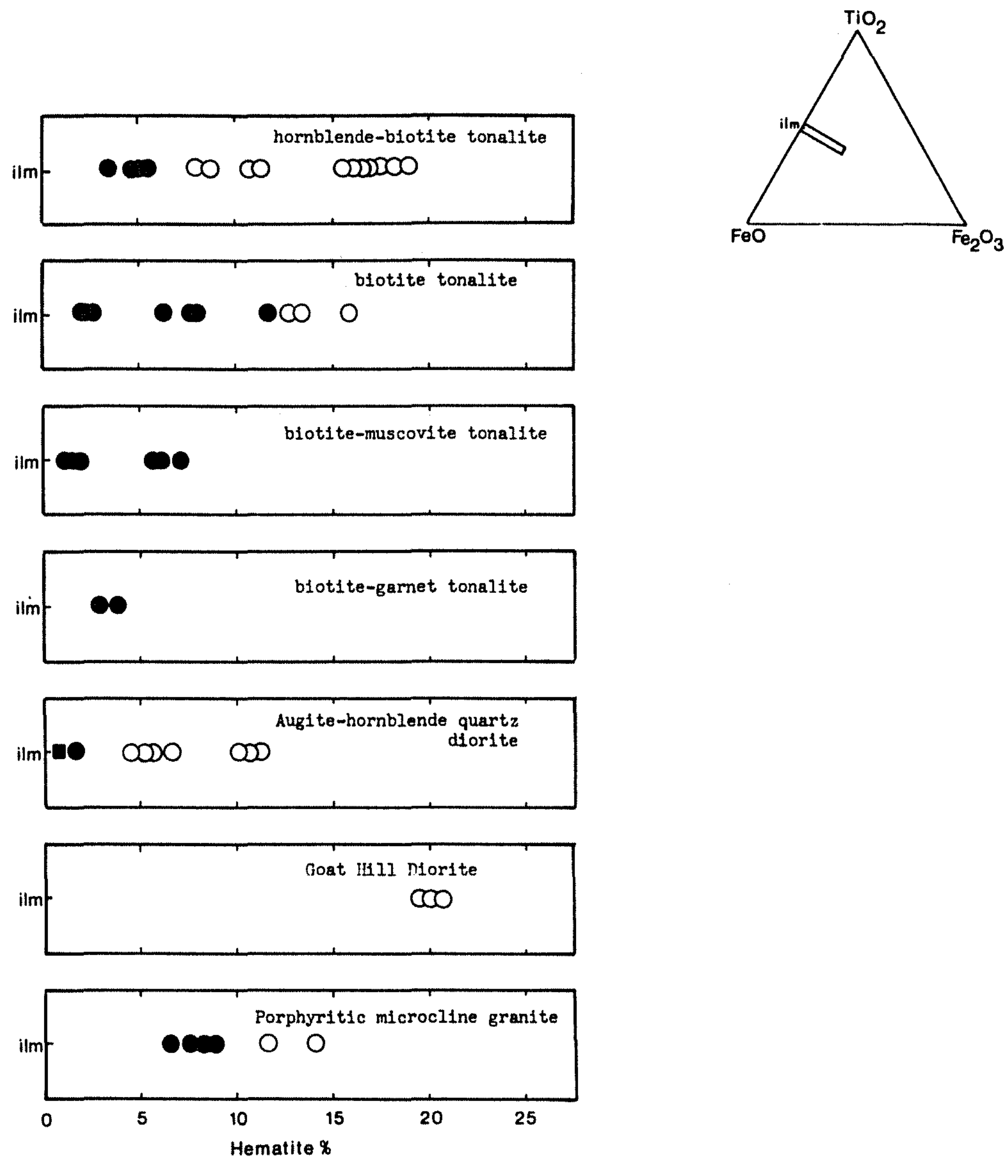

Figure 39. Ilmenite compositions from the Hardwick Tonalite and associated plutonic rocks. Ilmenite with magnetite (○), ilmenite (●), ilmenite in Littleton Formation surrounding the Nichewaug Sill (■).

Table 25. Electron microprobe analyses of magnetite from the hornblende-biotite tonalite and tonalite mylonite (FW992). Structural formulae based on 3 cations.

	hornblende-biotite tonalite						tonalite mylonite
	SA160-3	SA160-3	SA160-3	SA100	SP65	SP65	FW992
TiO_2	0.10	0.25	0.17	0.14	0.02	0.06	0.14
Fe_2O_3	68.45	68.97	68.35	68.58	68.57	69.05	68.47
FeO	30.94	31.40	31.01	30.84	30.87	31.13	31.03
MnO	0.03	0.07	0.05	0.26	0.01	0.04	0.03
Total	99.51	100.69	99.58	99.82	99.48	100.27	99.67
n	4	10	6	8	10	4	10
Structural Formulae							
Fe^{2+}	1.002	1.005	1.003	.995	1.000	1.000	1.003
Fe^{3+}	1.994	1.986	1.990	1.993	1.999	1.997	1.992
Ti	.003	.007	.005	.004	.001	.002	.004
Mn	.001	.002	.001	.001		.001	.001
Magnetite %	99.7	99.3	99.5	99.6	99.9	99.8	99.6
Ulvospinel %	0.3	0.7	0.5	0.4	0.1	0.2	0.4

two, and three cations respectively, to account for iron in the ferric state. Figure 39, is a plot of reintegrated or homogeneous ilmenite projected on to the TiO_2-FeO-Fe_2O_3 plane from $MnTiO_3$ as suggested by Lindsley and Spencer (1982). Figure 40 shows reintegrated or homogeneous ilmenite plotted on $FeTiO_3$-$MnTiO_3$-Fe_2O_3.

Ilmenite of the Hardwick Tonalite contains between 1.0 and 14.1% hematite component and between 4.3 and 21.4% pyrophanite component. Upon reintegration of exsolved titanohematite and projection from pyrophanite, the hematite component (hematite/(hematite+ilmenite)) ranges from approximately 1.1 to 19%. The hematite component decreases in the sequence hornblende-biotite tonalite (19 to 6%), biotite tonalite (16 to 2%), biotite-muscovite tonalite (7 to 1%) and biotite-muscovite-garnet tonalite (4 to 2%). Ilmenite with a hematite component of greater than 8% commonly coexists with magnetite. The magnetite contains less than 0.7% Usp. The sequence of decreasing hematite solid solution in the ilmenite and the disappearance of magnetite from the oxide assemblage suggests a decrease in f_{O_2} from the hornblende-bearing tonalite to muscovite- and garnet-bearing tonalite.

Hornblende-biotite tonalite in close proximity to inclusions of pyrrhotite schist of the Partridge Formation (SA4) exhibits atypical low hematite components in the ilmenite, and magnetite is absent from the oxide assemblage. The hematite component in the ilmenite increases with distance (to 25 meters) from the inclusion (SA160).

The enriched pyrophanite component in the ilmenite of the Hardwick Tonalite may be accounted for by the model suggested by Czamanske and Mihalik (1972) for oxidizing magma environments or by the Mn enrichment of residual, more SiO_2-rich magmas in a reducing magma environment. The lack of correlation between hematite and pyrophanite components in the ilmenite and between the pyrophanite component and SiO_2 content of the host rock suggests that the two proposed magmatic models cannot account for the pyrophanite content and variation in the ilmenite of the Hardwick Tonalite. Exsolution of titanohematite would enrich the host ilmenite in Mn because D(ilm/hem)/Mn is greater than 1, but a correlation between percent exsolution and pyrophanite content does not exist and the amount of hematite exsolution is usually low. Lower values for pyrophanite component in the biotite-garnet tonalite are a result of the preference of Mn for garnet over ilmenite.

Ilmenite of the augite-hornblende quartz diorite exhibits a variation in the hematite component from 1.5 mole percent at the chilled margin of the sill to 5.9 mole percent in the interior of the sill (Figure 39). Titanohematite exsolution in the ilmenite ranges from 0 to 6% and upon integration and projection from pyrophanite, the hematite/hematite + ilmenite ratio ranges from 1.6 to 11.2%. Magnetite is associated with ilmenite in all oxide assemblages except in the chilled margin. Plotted in Figure 39, is the composition for ilmenite in the Littleton Formation gray schist in contact with the sill at the chilled margin (Met140). The low hematite component of the chilled margin ilmenite seems to be the result of lower f_{O_2} at the contact with the reduced schist.

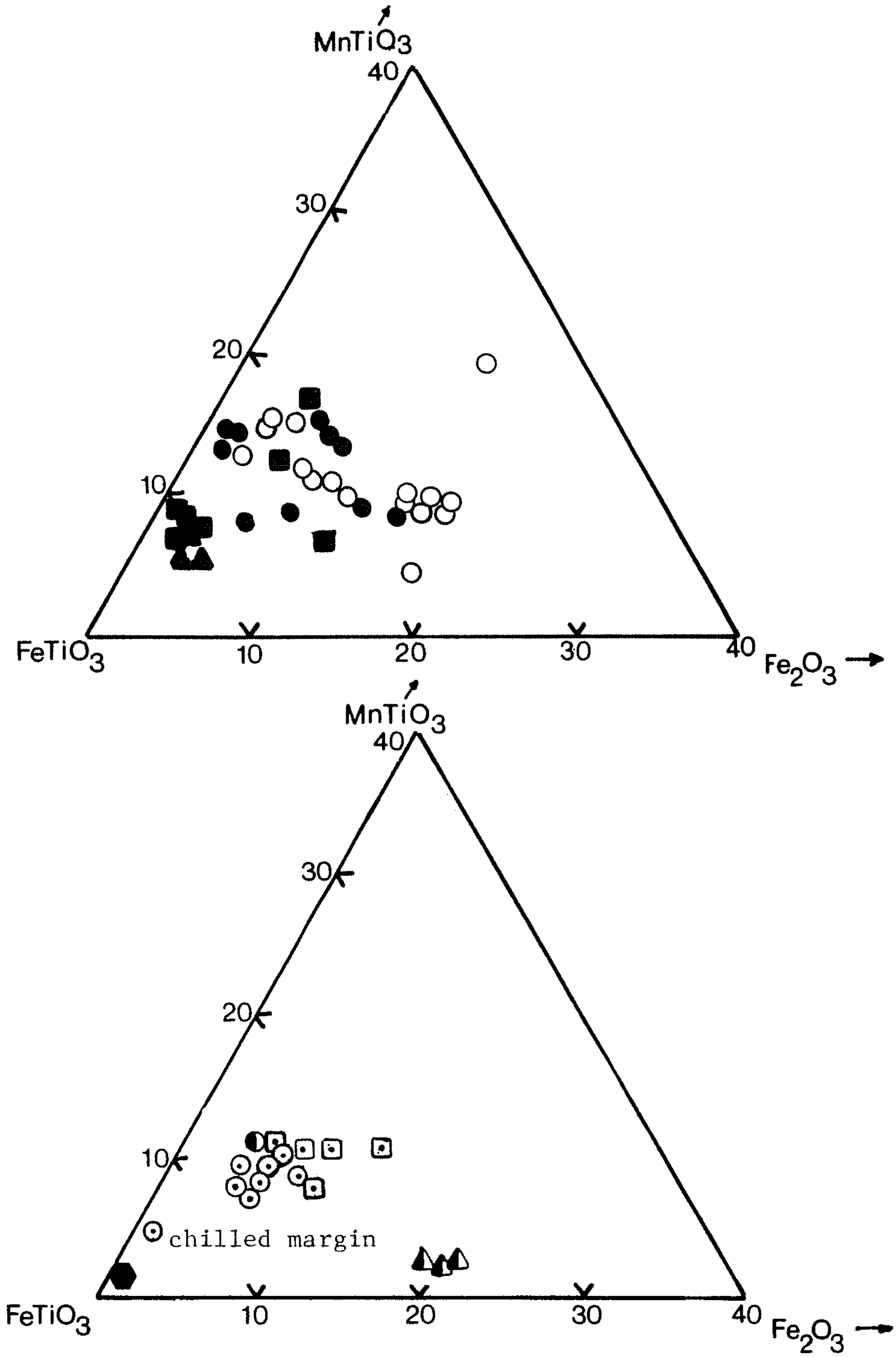

Figure 40. Reintegrated or homogeneous ilmenites plotted on $FeTiO_3$-$MnTiO_3$-Fe_2O_3. (a) Hardwick Tonalite with hornblende-biotite tonalite (○), biotite tonalite (●), biotite-muscovite tonalite (■), and biotite-garnet tonalite (▲). (b) associated plutonic rocks with augite-hornblende quartz diorite (⊙), Goat Hill Diorite (◭), porphyritic microcline granite (⊡), and Sheep Rock granite sill (◐). Ilmenite from Littleton Formation (⬢).

The pyrophanite component in the ilmenite ranges from 8.1% to 9.7% in the interior of the sill to 4.7% at the chilled margin. The Mn depletion in the ilmenite of the chilled margin is simply related to the presence of garnet accomodating Mn in the chilled margin.

In the Goat Hill diorite, ilmenite coexists with magnetite and shows coarse titanohematite exsolution to 15%. The hematite component ranges from 9.5 to 10.6% and the pyrophanite component even with extensive exsolution averages only 2.2%. Reintegrated and recalculated, the bulk ilmenite contains 19.5 to 20.6% hematite component. This contrasts with the ilmenites of the Hardwick Tonalite, which are Mn enriched and contain lower amounts of hematite solid solution, and the ilmenites of the Belchertown pluton (Ashwal, 1974) which are even more depleted in Mn and contain a much more extensive hematite solid solution.

In the porphyritic microcline granite, ilmenite is typically the only oxide phase, but coexists with magnetite in sample SA1. Titanohematite exsolution in the ilmenite is rare to absent. The hematite component is higher in the ilmenite coexisting with magnetite (12.5 to 10.3%), than ilmenite not associated with magnetite (6.7 to 8.0%). These ilmenites, like the ilmenite of the Hardwick Tonalite, are enriched in Mn with 8.15 to 11.2% pyrophanite component.

The equigranular granites contain sparse, homogeneous ilmenite. Ilmenite is the only primary oxide phase in the granites. Ilmenite from sample SA68 is the only oxide analyzed from the equigranular granite (Table 24). Hematite component is relatively low (5.7%) and pyrophanite enriched (10.4%).

Sphene

The presence or absence of sphene in granites has been used to infer sedimentary (S-type) or igneous (I-type) source material (Chappell and White, 1974; Hine *et al.*, 1978) and to reflect differences in oxygen fugacities in S-type and I-type source material (Ivanova and Butuzova, 1978).

Sphene is present in the hornblende-biotite tonalite and locally in the biotite tonalite as euhedral to subhedral grains associated with magnetite. Where present in the biotite-garnet tonalite, biotite-muscovite tonalite, porphyritic microcline granite and commonly in the biotite tonalite, the sphene is anhedral, occurs as rims around ilmenite or partial rims around biotite, or contains ilmenite inclusions. It has been suggested that the euhedral sphene is primary, whereas the anhedral, rim sphene is a retrograde product (Ashwal, 1974; Shearer, 1981; D.R. Wones, 1981, personal communication) or a result of prograde metamorphism (Rao *et al.*, 1973).

The ideal formula for sphene is $CaTiSiO_5$. In the tetrahedral site, Al may substitute for Si with a possible compensation by hydroxyl for oxygen substitution. Two types of coupled, charge-balancing and stoichiometry-preserving substitutions are possible to enable Al^{3+} (and Fe^{3+})

Table 26. Electron microprobe analyses of sphene from the Hardwick Tonalite.

	hornblende-biotite tonalite: euhedral											biotite tonalite: euhedral	
	SA61-1	SA61-1	SA61-1	SA61-1	SP65-1	SP65-1	SP65-1	SP65-1	SA160-3	SA160-3	SA160-3	SP139	SP139
SiO_2	29.19	29.24	28.72	29.46	28.66	28.45	28.45	28.79	29.06	29.59	29.55	29.37	29.86
TiO_2	39.02	39.06	39.08	39.10	38.09	38.14	38.51	38.24	37.37	37.63	37.12	38.20	38.18
Al_2O_3	1.10	1.18	1.12	1.17	1.48	1.44	1.44	1.41	1.41	1.19	1.27	1.31	1.16
FeO	0.88	1.09	0.86	1.06	1.12	1.10	1.08	1.11	1.66	1.41	1.84	1.37	1.43
MnO	0.10	0.14	0.07	0.16	0.25	0.27	0.21	0.20	0.16	0.09	0.10	0.24	0.21
MgO													
CaO	28.23	27.75	28.20	27.85	28.31	28.28	28.47	27.84	27.72	28.21	28.01	28.21	28.55
Na_2O													
Total	98.52	98.46	98.05	98.80	97.91	97.68	98.09	97.62	97.38	98.12	97.89	98.70	99.39
n	4	3	7	3	6	5	6	8	9	6	3	5	5
Structural Formulae													
Si site													
Si	.973	.974	.963	.978	.964	.959	.955	.969	.981	.990	.993	.978	.987
Al	.027	.026	.037	.022	.036	.041	.045	.031	.019	.010	.007	.022	.013
	1.000	1.000	1.000	1.000	1.000	1.000	1.000	1.000	1.000	1.000	1.000	1.000	1.000
Ti site													
Ti	.978	.979	.985	.976	.964	.968	.973	.968	.949	.947	.938	.957	.950
Al	.017	.020	.007	.024	.023	.017	.013	.026	.037	.037	.050	.029	.032
Fe	.025	.030	.024	.030	.031	.031	.030	.030	.043	.039	.042	.038	.040
Mn	.003	.004	.003	.005	.008	.008	.006	.006	.004	.002	.003	.007	.006
Mg													
	1.023	1.033	1.019	1.035	1.033	1.024	1.022	1.030	1.033	1.015	1.043	1.031	1.028
Ca site													
Ca	.978	.991	1.013	.990	1.020	1.023	1.024	1.003	1.003	1.012	1.009	1.007	1.012
Na													
	.978	.991	1.013	.990	1.020	1.023	1.024	1.003	1.003	1.012	1.009	1.007	1.012

	biotite tonalite: euhedral				biotite-muscovite tonalite: anhedral									
	SP139	SP139	SP139	SP139	SA251-1	SA251-1	SA251-1	SA251-1	SA251-1	SA251-1	SB-1	SB-1	SB-1	SB-1
SiO_2	29.21	29.43	29.55	29.61	29.56	29.63	29.93	29.76	29.66	29.88	29.81	30.03	29.49	29.96
TiO_2	37.90	38.51	38.47	37.40	37.23	36.97	37.72	37.60	36.21	37.42	36.08	36.36	35.89	36.44
Al_2O_3	1.29	1.11	1.16	1.27	2.33	2.57	2.30	2.46	2.93	2.17	3.10	3.12	3.05	3.09
FeO	1.42	1.27	1.29	1.63	0.43	0.62	0.66	0.51	0.89	0.65	1.03	1.02	1.03	1.08
MnO	0.20	0.22	0.24	0.26	0.08	0.11	0.09	0.10	0.15	0.16	0.10	0.12	0.07	0.16
MgO														
CaO	27.83	28.32	28.70	28.14	28.79	28.45	27.93	27.51	28.66	28.46	28.51	28.50	28.37	28.66
Na_2O														
Total	97.85	98.86	99.41	98.31	98.42	98.35	98.63	97.94	98.50	98.72	98.63	99.15	97.90	99.39
n	5	7	5	3	5	5	5	5	3	3	3	2	2	6
Structural Formulae														
Si site														
Si	.981	.979	.978	.990	.981	.984	.990	.989	.985	.989	.988	.989	.985	.986
Al	.019	.021	.022	.010	.019	.016	.010	.011	.015	.011	.012	.011	.015	.014
	1.000	1.000	1.000	1.000	1.000	1.000	1.000	1.000	1.000	1.000	1.000	1.000	1.000	1.000
Ti site														
Ti	.957	.964	.958	.941	.930	.924	.939	.940	.905	.931	.900	.901	.901	.901
Al	.032	.023	.023	.040	.072	.085	.080	.085	.100	.074	.109	.110	.105	.106
Fe	.040	.035	.036	.046	.013	.018	.019	.014	.025	.018	.029	.029	.029	.029
Mn	.006	.006	.006	.007	.003	.003	.003	.003	.004	.005	.003	.004	.003	.005
Mg														
	1.035	1.028	1.023	1.034	1.028	1.030	1.041	1.042	1.034	1.028	1.041	1.044	1.038	1.041
Ca site														
Ca	1.002	1.010	1.019	1.009	1.025	1.014	.990	.980	1.020	1.010	1.013	1.006	1.016	1.011
Na														
	1.002	1.010	1.019	1.009	1.025	1.014	.990	.980	1.020	1.010	1.013	1.006	1.016	1.011

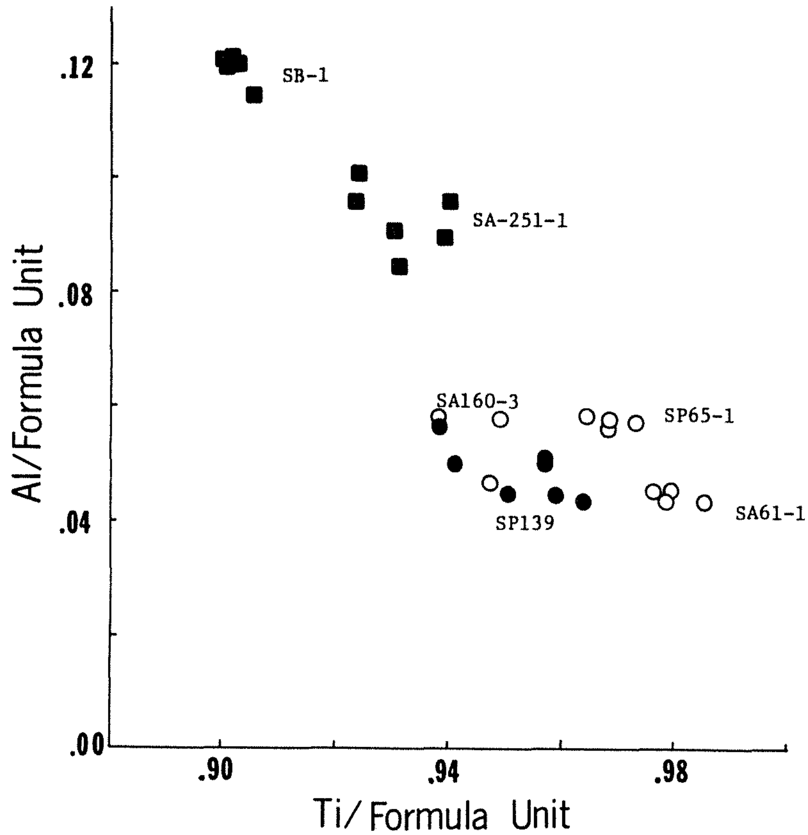

Figure 41. Ti/formula unit plotted against Al/formula unit for sphene from the hornblende-biotite tonalite (○), biotite tonalite (●), and biotite-muscovite tonalite (■).

to substitute for Ti^{4+}. One type of substitution involves a coupled anion-cation substitution such as $Al^{3+} + X^- = Ti^{4+} + O^{2-}$ where $X=OH^-$, F^-, Cl^-. A second type of substitution involves a REE entry into the Ca site: $(REE)^{3+} + Al^{3+} = Ca^{2+} + Ti^{4+}$.

Table 26 shows analyses from euhedral sphene (SA61-1, SP65-1, SA160-3, and SP139) and anhedral rim sphene (SA25101 and SB-1). Na_2O and MgO were analyzed but were not detected. Structural formulae in the table were calculated based on 5 oxygens. The high cation totals in the Ti site suggest that iron is in both the trivalent and divalent oxidation state.

Figure 41 shows a highly correlated inverse relationship between Al^{3+} and Ti^{4+}. Two distinct populations of sphene occur, high Ti, euhedral sphene which commonly coexists with magnetite and low Ti, anhedral rim sphene. Hollocher (1981) stressed the importance of a $(TiO)^{2+} = (AlOH)^{2+}$ substitution mechanism in some retrograde sphenes. D.R. Wones (1981, personal communication) has suggested that a $(TiO)^{2+} = (AlF)^{2+}$ substitution mechanism occurs and has found that primary plutonic sphene is commonly Al and F poor and secondary sphene is commonly Al and F enriched. Such an evalution of these plutonic sphenes would suggest that the euhedral sphene may be primary or only partially requilibrated.

DISCUSSION OF IGNEOUS AND METAMORPHIC PHASE RELATIONSHIPS

The Hardwick Tonalite and associated plutonic rocks contain mineral assemblages which have requilibrated at subsolidus temperatures to varying degrees. Evaluation of phase relationships within these assemblages is pertinent to understanding genetic history.

ACF Relationships

Chappel (1978) and White and Chappell (1977) successfully repesented "I- and S-type" granitoid mineralogy and chemistry in ACF diagrams, where $A=Al_2O_3-Na_2O-K_2O$, C=CaO and F=FeO+MgO+MnO. "I-type" granitoids are defined by the area plagioclase-biotite-hornblende, whereas the "S-type" granitoids are defined by the area plagioclase-biotite-muscovite or plagioclase-biotite-cordierite. The plagioclase-biotite tie line separates the two regions, although because of variations in the A/(A+F) ratio of the biotite, the plagioclase-biotite assemblage defines an intermediate area and not a single tie line.

Analyses of hornblende, biotite, and muscovite from the Hardwick Tonalite and associated plutonic rocks are plotted in Figures 42 and 43, respectively. The plagioclase-biotite-hornblende assemblage contains biotite with a low A/(A+F) ratio. Within individual rock units, increases in the A/(A+F) ratio in biotite is accompanied by a similar increase in hornblende, although tie lines of different units intersect. The plagioclase-biotite assemblage contains biotite which has a A/(A+F) ratio

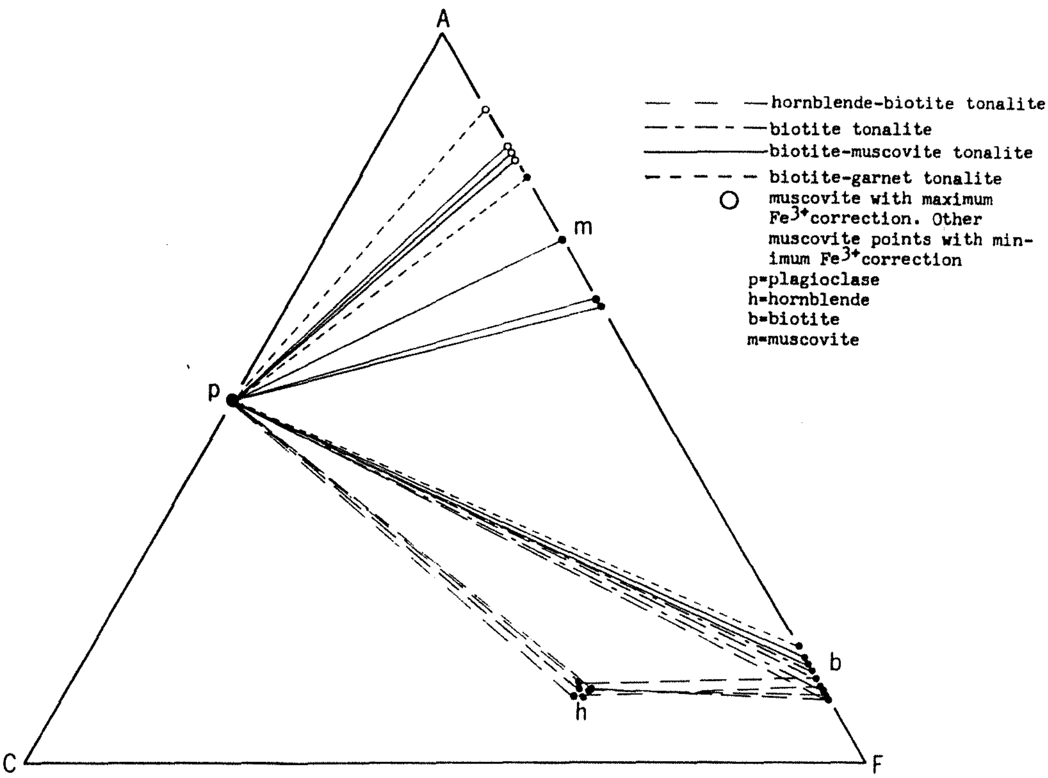

Figure 42. ACF plot of hornblende (h), biotite (b), and muscovite (m) from the Hardwick Tonalite.

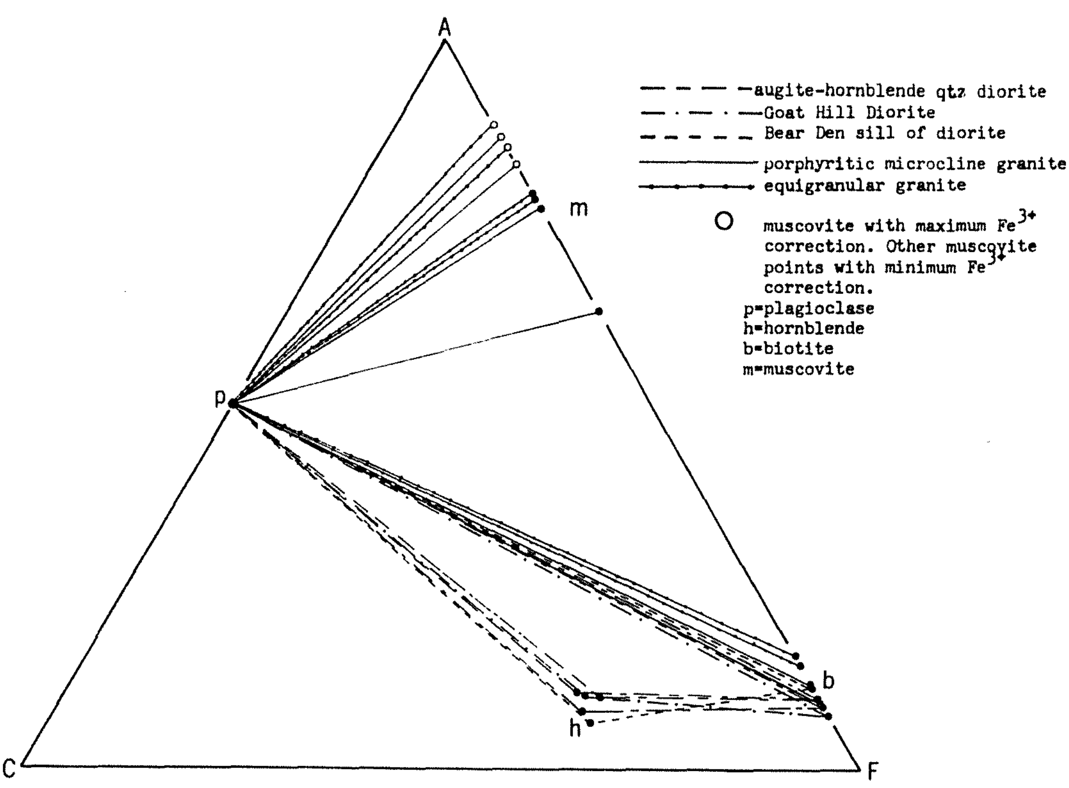

Figure 43. ACF plot of hornblende (h), biotite (b), and muscovite (m) from the igneous rocks associated with the Hardwick Tonalite.

equal to or greater than the high A/(A+F) biotite of the plagioclase biotite-hornblende assemblage. The small area defined by the plagioclase-biotite assemblage contains greater than 60% of the Hardwick Tonalite. The plagioclase-biotite-muscovite assemblage is defined by biotite with A/(A+F) ratios equal to or greater than the biotite of the plagioclase-biotite assemblage. Muscovite has a large celadonite component which increases, correspondingly, with changes in the A/(A+F) ratio in the biotite.

Plagioclase-biotite-cordierite assemblages noted by Chappell and White (1974) and Speer (1981) were not observed in these plutonic rocks.

With increasing SiO_2 in the host rock, rock compositions move from the plagioclase-biotite-hornblende region through the plagioclase-biotite regions and into the plagioclase-biotite-muscovite region of the ACF diagram. Chappell and White (1974) suggested that this pattern reflected different source compositions manifesting differences in time and situation of residence in the weathering cycle. Long time residence in the weathering cycle increased the Al and depleted the Ca content of the protosource material. The genesis of a sequence of "I and S-type" plutonic rocks in a single intrusive unit must be the result of mixing of metaluminous and peraluminous end-members. Alternative models to account for Ca depletion and Al enrichment with increasing SiO_2 have been proposed and include fractional crystallization of hornblende (Abbott, 1981; Cawthorn et al., 1976), different degrees of partial melting of a mildly peraluminous source (Nabelek et al., 1981), in situ contamination by country rock (Goad and Cerný, 1981) and the interaction between residual magma and subsolidus rocks and hydrothermal fluids (Muecke and Clarke, 1981). In addition to igneous processes, metamorphic crystallization and hydration of plutonic rock with a metaluminous mineralogy could produce a plutonic rock with an apparent "intermediate" or "peraluminous" mineralogy. With the formation of epidote (anorthite + hornblende = epidote + more Al-rich biotite) such a mineralogical transformation is possible, that would fool the observer and belie the true chemical nature of the rock. Epidote stability and the previously mentioned Al variations in biotite are observed in the Hardwick Tonalite and the Belchertown pluton (Ashwal et al., 1979). The recrystallization, however, only accounts for different mineralogies in the same bulk composition and not variations in the bulk composition.

Igneous Crystallization

Evaluation of igneous mineral equilibria is made difficult by varied subsolidus reequilibration. Representative analyses of mafic minerals from the Hardwick Tonalite and associated plutonic rocks are plotted in a quartz-saturated AFM projection from feldspar as modified by Abbott (1981) and Nesbitt and Cramer (1981) to include amphibole. The modification subtracts K_2O, Na_2O and CaO from the apex. The annite-phlogopite join (A=0) separates the peraluminous region (A greater than 0) in the projection.

As shown in Figures 44 and 45, biotite coexisting with amphibole commonly has a higher $Mg/(Mg+Fe^{2+}+Mg)$ ratio (greater than 0.55) and a

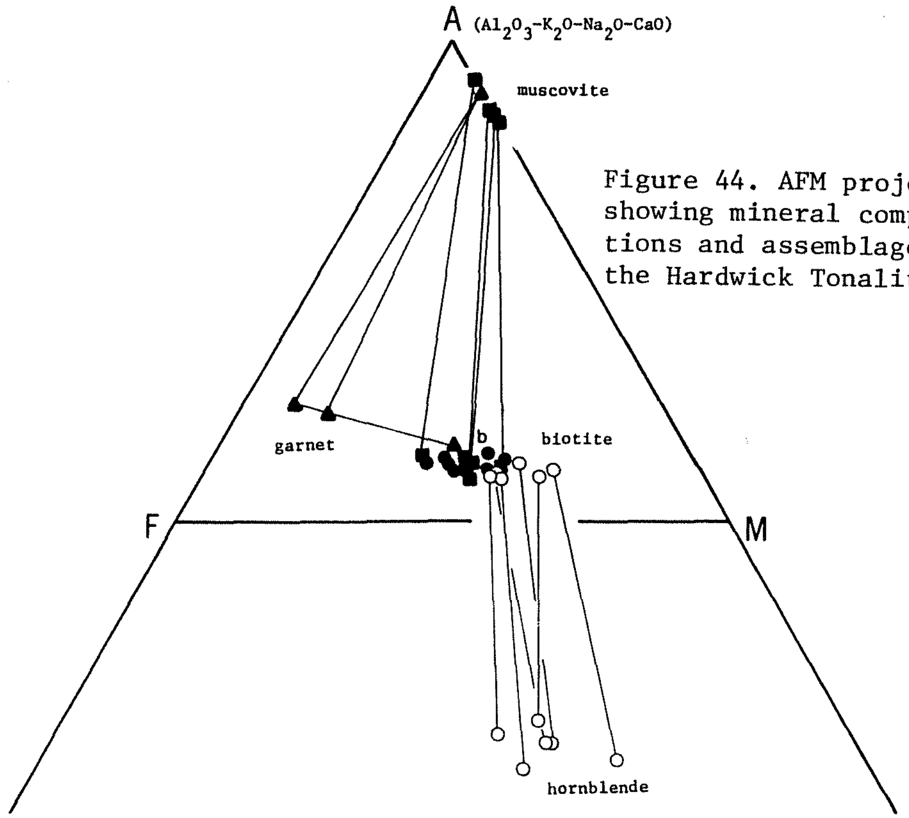

Figure 44. AFM projection showing mineral compositions and assemblages for the Hardwick Tonalite.

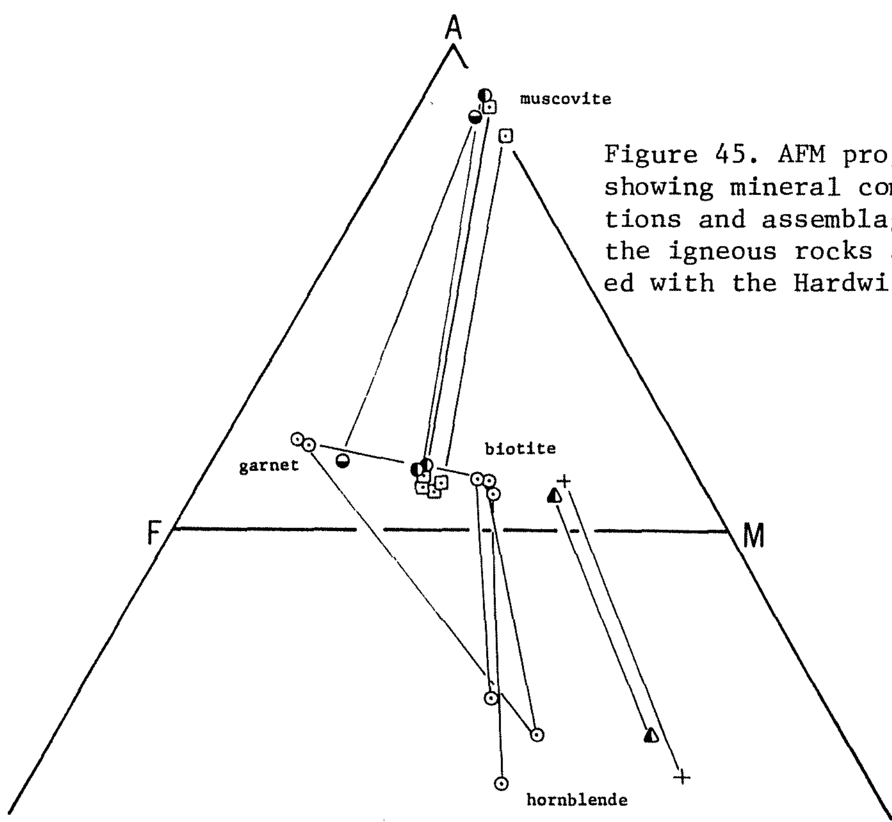

Figure 45. AFM projection showing mineral compositions and assemblages for the igneous rocks associated with the Hardwick Tonalite.

lower $Al/(Al+Fe^{2+}+Mg)$ ratio (less than 0.10) than biotite which does not coexist with amphibole. Although obscured to some degree by subsolidus reequilibration, the termination of amphibole-biotite coexistence in the plutonic rocks may be interpreted as a cessation of amphibole crystallization at an $Mg/Mg+Fe^{2+}$ ratio of 0.55. As shown in Figure 46, the cessation of amphibole crystallization may be the result of the transformation of the liquidus boundary between biotite and amphibole stability fields from cotectic (liquid = amphibole + biotite) in the metaluminous region of the projection to peritectic (amphibole + liquid = biotite) in the peraluminous region of the projection (Figure 46a). The theoretical aspects of the transformation from an even to an odd topology have been discussed by Abbott (1981).

The point of the cotectic to peritectic transformation is partially dependent upon the f_{O2} of the magmatic environment. An oxidized magmatic environment would expand the amphibole field to higher $Mg/(Mg+Fe^{2+})$ at A=0 (Figure 46b)

The overlap of the $Mg/(Mg+Fe^{2+})$ ratio in biotite of the hornblende-, biotite-, and muscovite-bearing tonalites may be the result of contamination by a peraluminous material, driving magma compositions off the liquidus field boundary and into the biotite stability field (Figure 46c) Biotites in these hybrid rocks would have a higher eastonite-siderophyllite component. A contaminated assemblage containing hornblende, biotite, and garnet is shown in Figure 45. The stability of garnet with hornblende may be the result either of an assemblage not in equilibrium due to the chilled nature of the contamination zone or of Ca or Mn in the garnet which stabilized and expanded the garnet field closer to the metaluminous boundary.

In the AFM projection, muscovite coexisting with biotite is plotted (Figures 44 and 45). Plotted muscovites are based on the maximum ferric iron correction previously mentioned. Muscovites in all assemblages, except in the Fitzwilliam Granite, plot along the A-M join. With decreasing $Mg/(Mg+Fe^{2+})$ in the biotite, the coexisting muscovite plots closer to the A apex of the projection. The biotite of the Fitzwilliam Granite has an extremely low $Mg/(Mg+Fe^{2+})$ ratio and coexists with a muscovite plotting off the A-M join. Biotite- and biotite-muscovite-bearing plutonic rocks may represent melts that have left the biotite-hornblende liquidus as a result of its peritectic character, as a result of contamination by a more aluminous component, or by partial melting in a more aluminous source.

Uncommon garnet assemblages in the Hardwick Tonalite and associated plutonic rocks suggests it is more common for the crystallizing tonalite-granite magma to stay in the biotite field. Only with extreme contamination by an aluminous component does the composition reach the biotite-garnet liquidus boundary (Abbott, 1981). Biotite coexisting with garnet commonly has a higher degree of Al-Al substitution.

Metamorphic Reequilibration

Although metamorphic recrystallization does form non-magmatic phases such as secondary amphibole, secondary sphene, secondary muscovite and

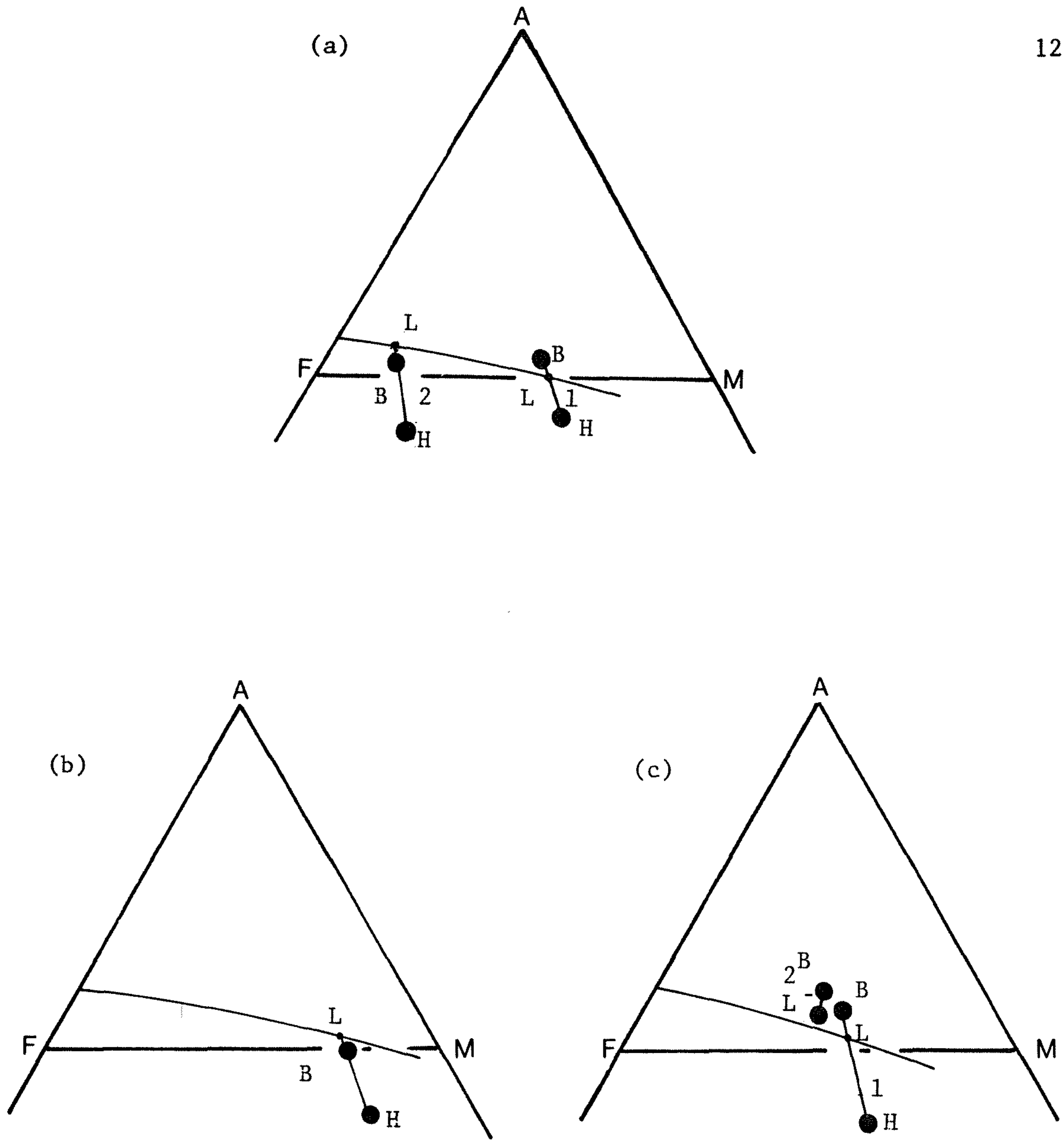

Figure 46. Schematic phase relationships between hornblende (H), biotite (B), and liquid (L). Liquidus boundary separates the biotite and hornblende fields. (a) assuming a biotite composition on the A side of the F-M join phase relationship at 1 is L=B+H and phase relationship at 2 is L+H=B. (b) higher f_{O_2} will extend the amphibole field to higher $Mg/(Mg+Fe^{2+})$ at A = 0. (c) contamination of L(1) by a peraluminous material may drive liquid composition from liquidus field boundary into the biotite stability field (L=2).

epidote, much of the subsolidus equilibrium involves reequilibration of the chemistries of magmatic phases. These variations in mineral chemistries have been previously noted in the discussion of the individual minerals.

Phase relations among biotite, oxides and sulphides with varying reequilibration can be evaluated on a SiO_2 and K-feldspar projection of TiO_2-FeO-Fe_2O_3 (Figure 47). Figures 47A to 47C represent compositions of decreasing biotite Ti content which has been correlated to decreasing temperature. At a single temperature (and biotite Ti content) biotite with the highest $Fe^{3+}/(Fe^{3+}+Fe^{2+}+Ti)$ ratio coexists with magnetite and an ilmenite with a high hematite component. The biotites in these oxide assemblages are associated with metaluminous silicate assemblages. With decreasing $Fe^{3+}/Fe^{3+}+Fe^{2+}+Ti$ in the biotite, magnetite disappears from the oxide assemblage, the hematite solid solution in the ilmenite is reduced and the silicate assemblage becomes more aluminous. With decreasing temperature and decreasing Ti content in the biotite, the biotite and ilmenite coexisting with magnetite exhibit a decrease in Fe^{3+}. Magnetite in all samples is nearly stoichiometric with a maximum of 0.7% Usp component.

With decreasing temperature, Ti solubility in biotite and hematite solid solution in ilmenite decreases. The development of secondary sphene may be approximated by the discontinuous reaction:

ilmenite + Ti-biotite + andesine =

sphene + Ti-poor biotite + oligoclase

and represented in Figure 48A. The decrease in Ti in the biotite and the anorthite component in plagioclase is of a continuous nature, rather than a discontinuous one, suggesting the simplified continuous reaction represented in Figure 48B. The continuous movement of the biotite-plagioclase tie-line changes the shape of the plagioclase-sphene-biotite-ilmenite volume. The plagioclase-sphene-biotite plane gradually moves toward the bulk composition, resulting in the decrease of the modal amount of ilmenite. A second subsolidus reaction suggested by Figure 48 is:

ilmenite + Ca plagioclase + K-feldspar + quartz + H_2O =

biotite + Na plagioclase + sphene

Such a reaction may account for the high amount of biotite and sphene in strongly reequilibrated tonalites. The reaction also accounts for the homogenous character of the plagioclase in the reequilibrated tonalites.

Coexisting sulfide-oxide-biotite assemblages can be graphically represented in the system Fe-Ti-S-O. The TiO_2-Fe-S-Fe_2O_3 portion of that system is illustrated in Figure 49. At both high and low Ti content in biotite corresponding to high igneous and lower metamorphic conditions, the sequence of mineral assemblages from the high oxygen

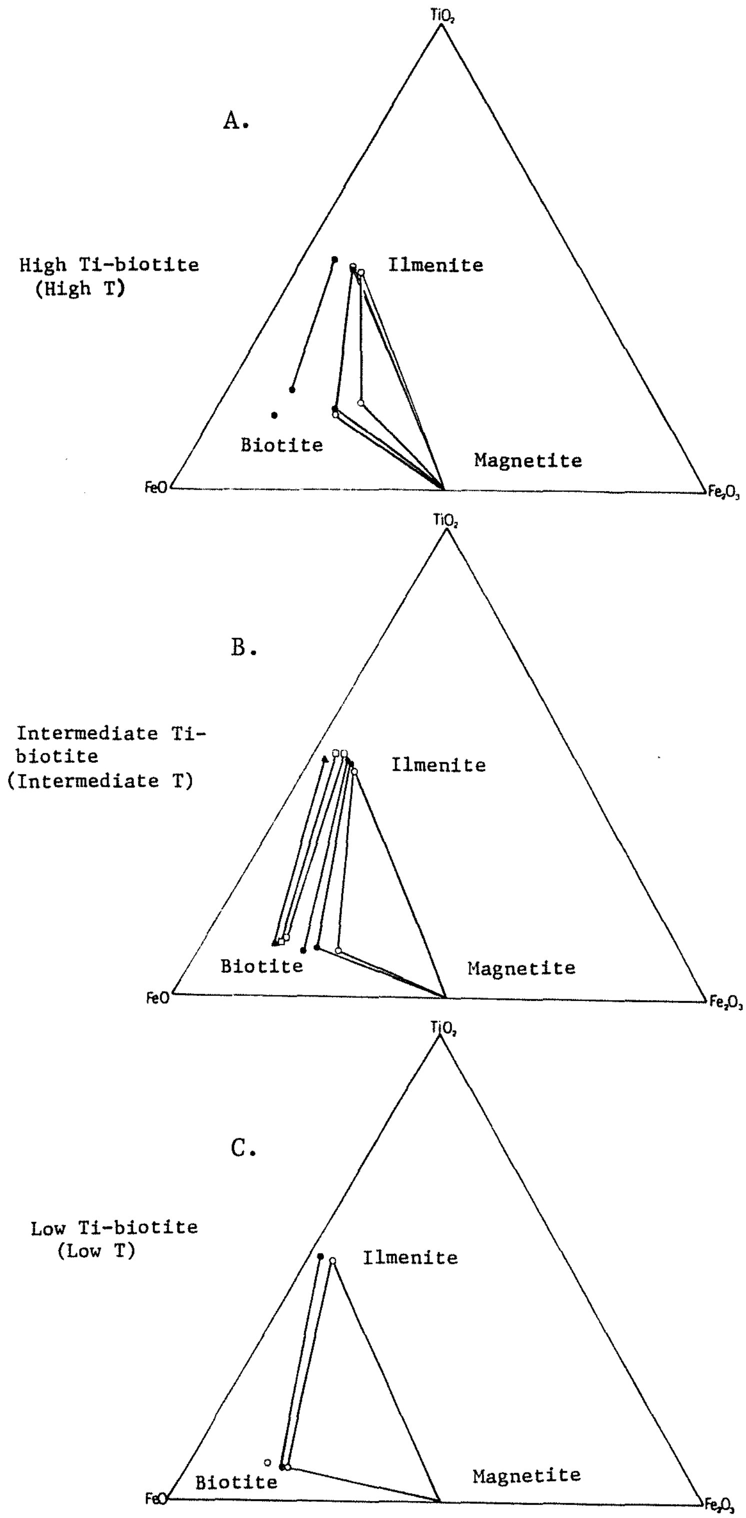

Figure 47. Variations in mineral assemblage and chemistry for magnetite-ilmenite and biotite evaluated in a quartz and K-feldspar projection onto TiO_2-FeO-Fe_2O_3. Figures A to C represent compositions of decreasing biotite Ti content which has been correlated to decreasing temperature.

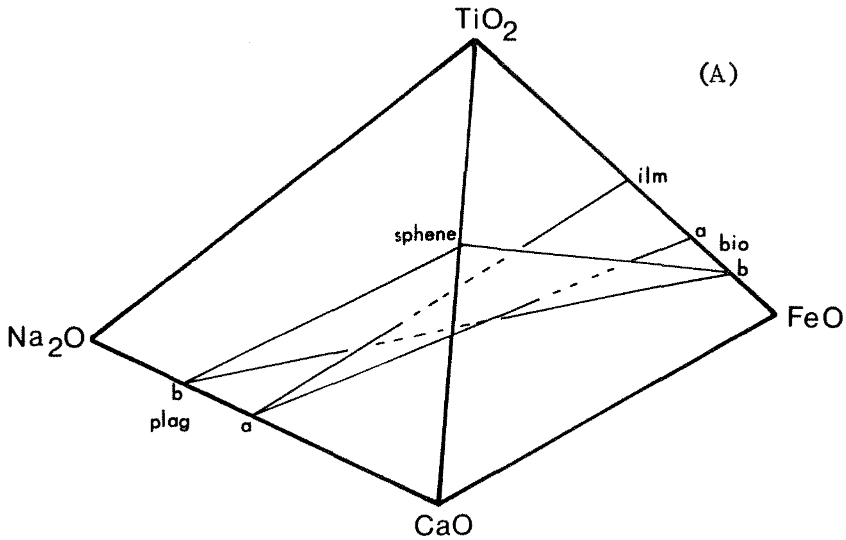

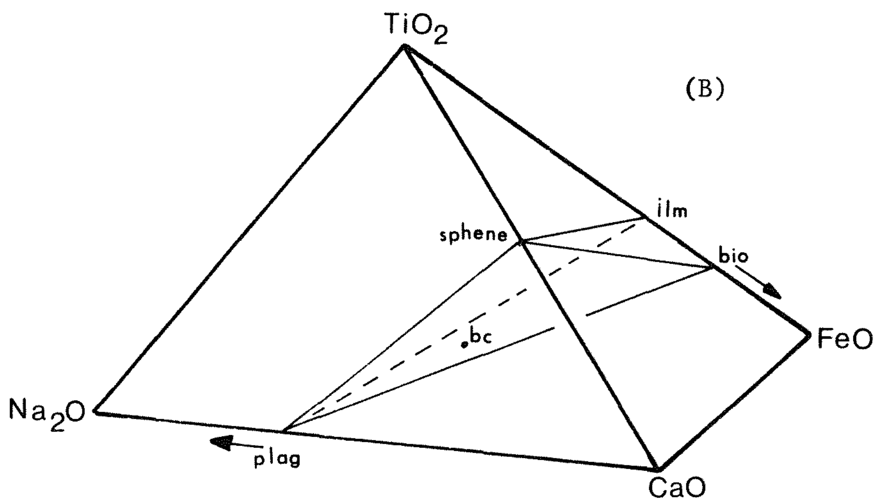

Figure 48. Representation of subsolidus tonalite reactions in the system Na_2O-CaO-FeO-TiO_2(+SiO_2, +K_2O, +H_2O). (A) discontinuous reaction illustrating the development of sphene, Ti-poor biotite and Ca-poor plagioclase. (a) biotite moves toward (b) biotite and (a) plagioclase moves toward (b) plagioclase with subsolidus reequilibration. (B) simplified continuous reaction illustrating increase in modal sphene, increase in albite component in plagioclase and decrease in Ti content in biotite. Text discusses reactions.

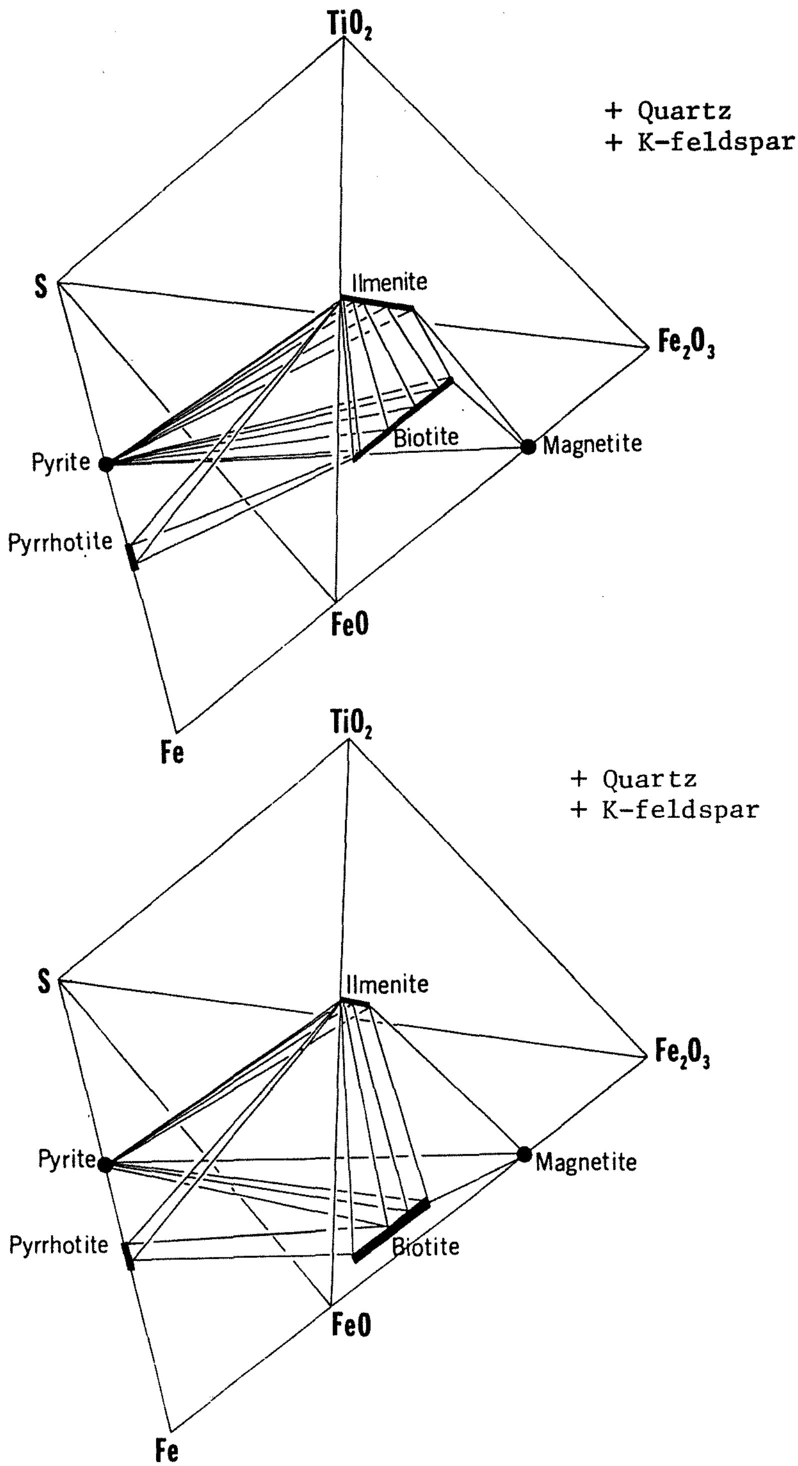

Figure 49. Sulfide-oxide-biotite assemblage for the Hardwick Tonalite graphically represented in the TiO_2-Fe-S-Fe_2O_3 portion of the Fe-Ti-S-O system. (a) This diagram represents the high-Ti biotite assemblage (high temperature). (b) This diagram represents the low-Ti biotite assemblage (low temperature).

portion of the system to the low oxygen portion of the system is as follows:

1) pyrite - magnetite - hematite-rich ilmenite - Fe^{3+}-rich biotite,

2) pyrite - ilmenite with intermediate hematite component - Fe^{3+} intermediate biotite,

3) pyrite - pyrrhotite - ilmenite with low hematite component - Fe^{3+}-poor biotite

4) pyrrhotite - ilmenite with extremely limited hematite component - very-low-Fe^{3+} biotite.

The sequence of assemblage 1 through 2 coincides with the metaluminous to peraluminous composition sequence. Assemblage 3 is associated with contacts between tonalite and highly reduced schist inclusions of the Partridge Formation. Assemblage 4 is not observed in the tonalites. The tonalite whole rock oxygen content inhibits graphite stability (graphite plotted at negative oxygen) in these assemblages. The effect of metamorphic reequilibration on these assemblages producing biotite with less Ti is shown in Figure 49B.

The stability of plutonic muscovite within regions of the Hardwick Tonalite overprinted with metamorphic zone V (sillimanite-K-Feldspar) and VI (sillimanite-cordierite-garnet) conditions warrants further discussion. The stability of muscovite in the tonalite, in contrast to muscovite breakdown in the neighboring pelitic schist, may be the result of differing $Mg/(Mg+Fe^{2+})$ ratios. AFM projections in Figures 44 and 45 illustrate that muscovite has a higher $Mg/(Mg+Fe^{2+})$ ratio than coexisting biotite. The pelitic schists exhibit the same relationship (Tracy, 1975). Compared to the muscovite-biotite pairs in the pelitic rocks, the tonalite pairs have a higher $Mg/(Mg+Fe^{2+})$ ratio (Figure 50). The higher $Mg/(Mg+Fe^{2+})$ ratio in the tonalite as compared to the pelitic schist, might result in an extension of muscovite stability to higher temperatures.

ESTIMATES OF T-f_{O_2} RELATIONS

Feldspar Geothermometry

The percent albite component in the plagioclase is plotted against the percent albite component of the coexisting alkali feldspar in Figure 51. The alkali feldspar compositions plotted are host-exsolution integrated bulk compositions. Upon this is superimposed Stormer's (1975) feldspar geothermometer calibrated to 5 kbar.

With increasing host rock SiO_2 content (Analyses presented in the following section: Geochemistry of the Hardwick Tonalite), the albite component increases in plagioclase and decreases in the alkali feldspar. The overlap between and within rock types is attributed to plagioclase zoning, feldspar reequilibration, and errors in the alkali feldspar

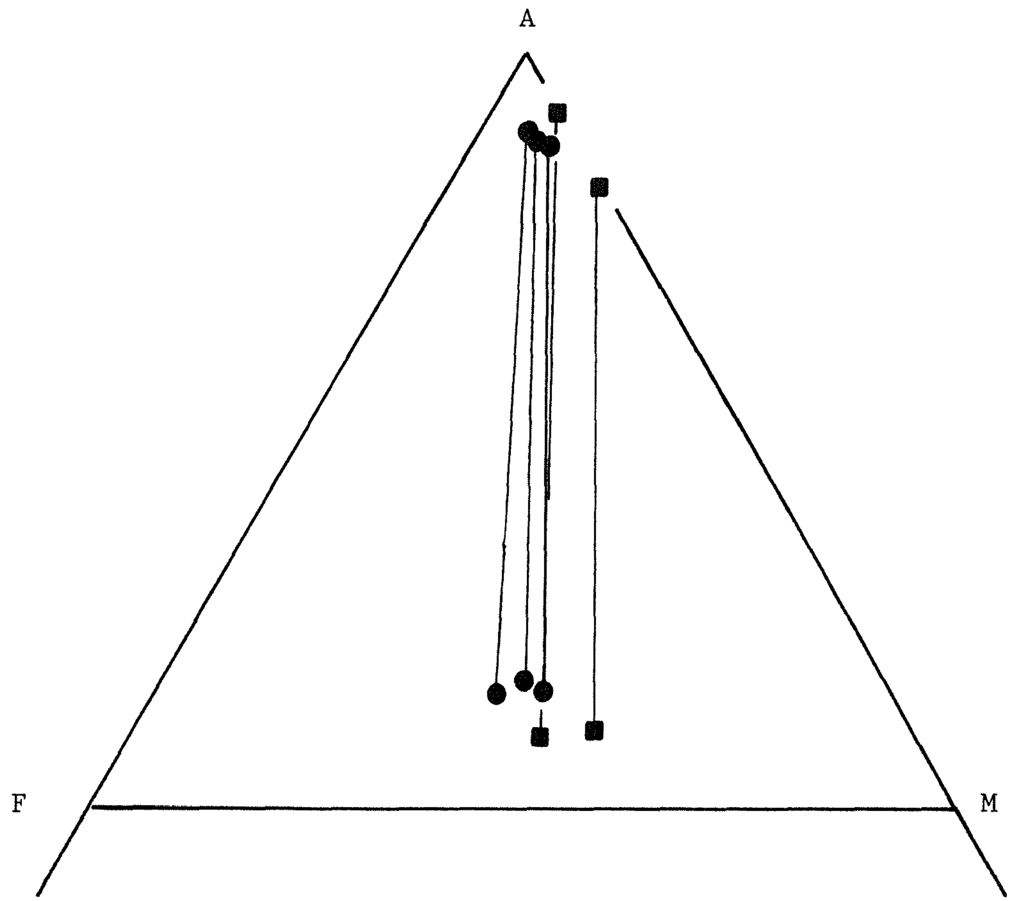

Figure 50. AFM plot of coexisting muscovite and biotite from the biotite-muscovite tonalite within metamorphic zone VI (square) and Quabbin Reservoir area (circle). Quabbin Reservoir analyses are from Tracy (1978) and include samples M34, B35, and 595C.

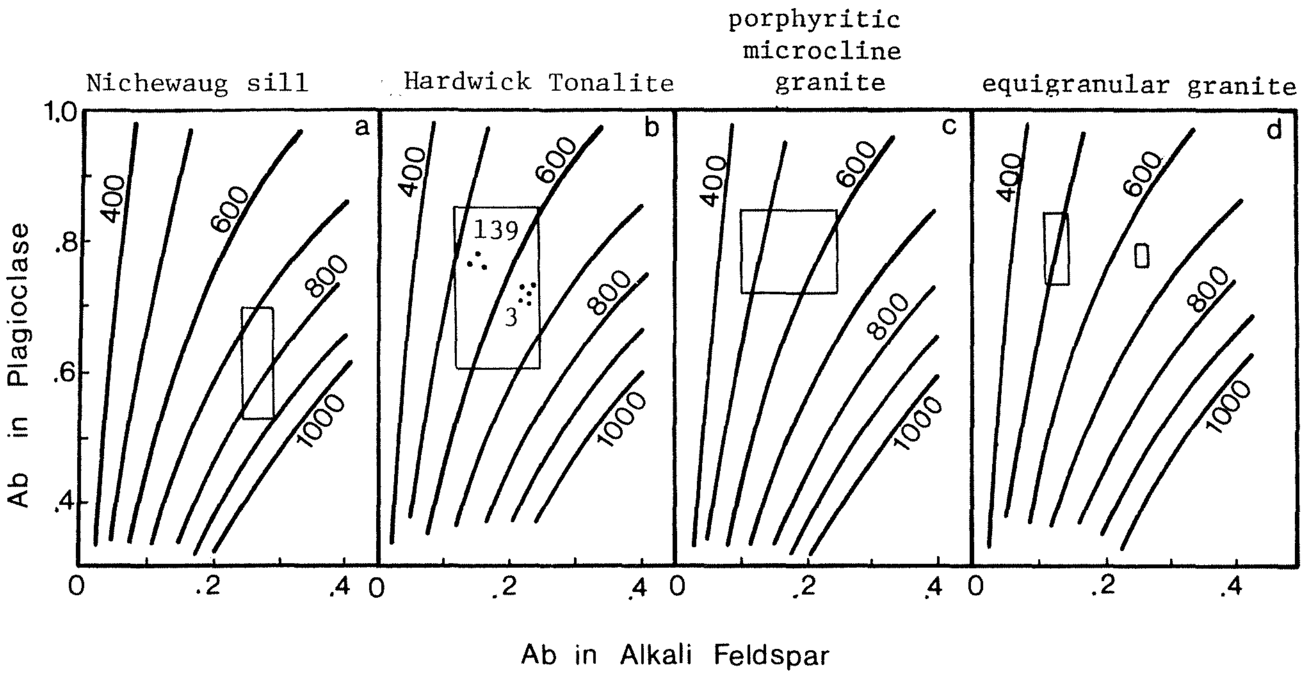

Figure 51. Ab in plagioclase plotted against Ab in alkali feldspar. Boxes illustrate range of rock type variability. Plotted in the Hardwick Tonalite diagram (b) are data points for a tonalite with relict igneous texture (SP3) and a tonalite with a metamorphic mineral assemblage and texture (SP139). The feldspar geothermometer of Stormer (1975) is superimposed.

integration. Temperatures derived from the geothermometer are as follows: augite-hornblende quartz diorite 700-900°C, Hardwick Tonalite 500-700°C, porphyritic microcline granite 450-650°C, Fitzwilliam Granite and the granite at Sheep Rock 450-550°C and the granite at Tom Swamp 640°C. Temperatures for most of the feldspar pairs suggest that solidus compositional relationships were not retained. In addition to giving low temperatures, many of the bulk alkali feldspar compositions are not capable of being in equilibrium with granitic melt. Alkali exchange with residual magmatic or later metamorphic fluids must have occurred. The feldspar pairs of the augite-hornblende quartz diorite, the granite at Tom Swamp and the Hardwick Tonalite indicate that alkali exchange and reequilibration was variable.

Estimates of f_{O2} from Biotite-Oxide Phase Relations

Petrographic observations and mineral chemistries suggest variations of relative oxygen fugacities within the Hardwick Tonalite and associated plutonic rocks. Biotite and oxide equilibria have been used in a number of studies to estimate f_{O2} in plutonic rocks and an endeavor is made here to estimate the f_{O2} for the differing rock types. Estimates of approximate magmatic f_{O2} must be calculated with great care, selecting only biotite and oxide analyses which come the closest to approaching magmatic compositions.

Dodge _et al_. (1969) related Sierra Nevada batholith biotite compositions to three common oxygen buffers, magnetite-hematite, Ni-NiO and fayalite-magnetite-quartz, in the ternary diagram Fe^{2+}-Fe^{3+}-Mg. Biotites from the Hardwick Tonalite plot between the Ni-NiO and magnetite-hematite buffers (Figure 52a). The biotites of the hornblende-biotite tonalite generally plot at high f_{O2} near the magnetite-hematite buffer, whereas the biotites of the muscovite- and garnet-bearing tonalite generally plot near the Ni-NiO buffer. The biotite of the biotite tonalite is commonly at intermediate f_{O2}. Biotites from the plutonic units associated with the tonalites are plotted in Figure 52B and exhibit a range of f_{O2} between the fayalite-magnetite-quartz buffer and the magnetite-hematite buffer.

Estimates of f_{O2} determined in the manner of Dodge _et al_. (1969) assume that biotite stability is primarily dependent upon Mg, Fe^{3+}, and Fe^{2+} octahedral site occupancy. Wones (1973) and Czamanske and Wones (1973) have shown that biotite stability is also dependent upon total octahedral site characteristics and F/(F+OH) ratio. Czamanske and Wones calculated the upper stability limit of biotite using the following equation:

$$-1/2 \log f_{O2} = (7409/T) + 4.25 - \log f_{H2O} + 3 \log X_{Fe^{2+}} + 2 \log X_{OH} - \log a_{KAlSi_3O_8} - \log a_{Fe_3O_4}$$

T is temperature in degrees K. P_{total} is assumed equal to P_{H2O}. The relationship between P_{H2O} and f_{H2O} is from Burnham _et al_. (1969) as suggested by Czamanske _et al_. (1977, 1981) and Czamanske and Wones

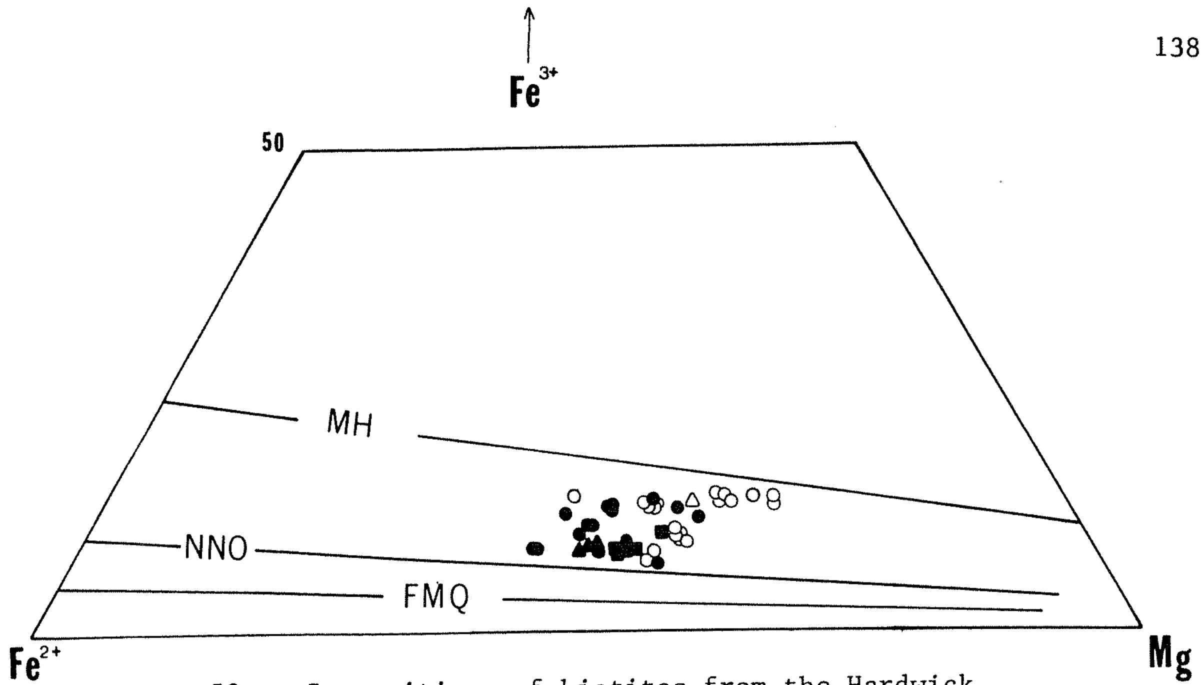

Figure 52a. Compositions of biotites from the Hardwick Tonalite plotted in the ternary diagram Fe^{2+}, Fe^{3+}, Mg. Magnetite-hematite (MH), fayalite-magnetite-quartz (FMQ) and Ni-NiO (NNO) buffers are projected into system.

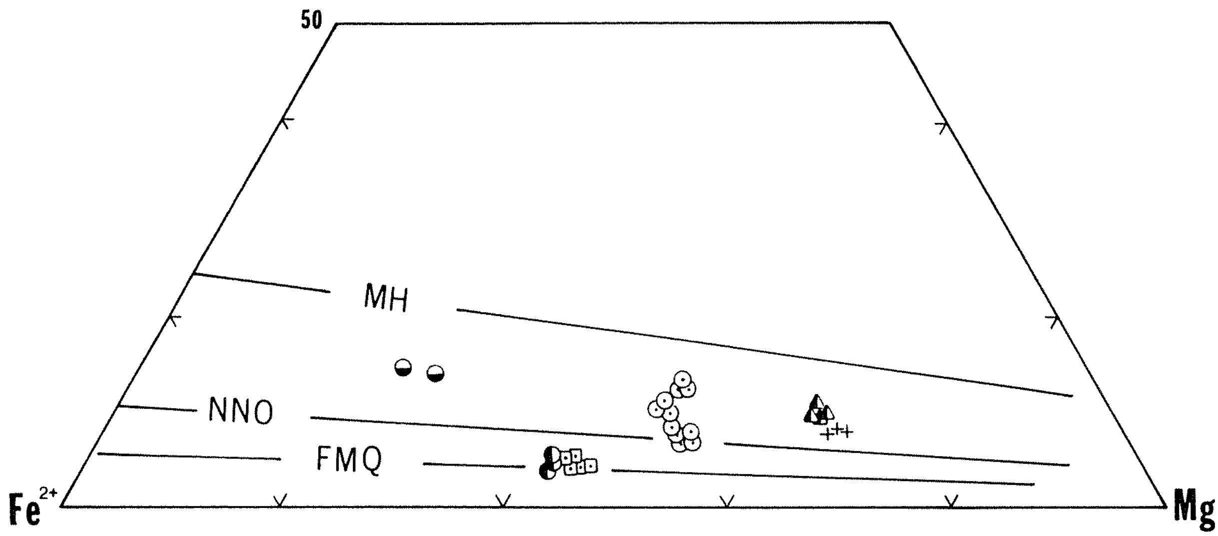

Figure 52b. Compositions of biotites from the plutonic rocks associated with the Hardwick pluton. MH, FMQ, and NNO buffers projected into system. Augite-hornblende quartz diorite (⊙), diorite from Goat Hill (▲) and Bear Den Sill (+), porphyritic microcline granite (⊡), granites from Sheep Rock and Tom Swamp (◐), and Fitzwilliam Granite (◒).

(1973). P_{H_2O} was set equal to 5 kbar. $X_{Fe^{2+}}$ is equal to the ratio of the number of Fe^{2+} cations to total number of occupied octahedral sites. F was not determined in these biotites. X_{OH} = OH/(OH+F) was set equal to .91. This value is comparable to X_{OH} values in biotites from similar plutonic rocks (Czamanske et al., 1977, 1981; Wones, 1981; Ashwal et al., 1979). The activity of $KAlSi_3O_8$ between 0.75 and 1.00 and equal to 0.50 for $X_{KAlSi_3O_8}$ between .27 and .75 between 600° and 800° (Waldbaum and Thompson, 1969). The activity of Fe_3O_4 is taken as 1.0 for magnetite-bearing rocks and as 0.2 for magnetite-absent rocks as suggested by Czamanske et al, (1981). The $a_{Fe_3O_4}$ option of 1.0 versus 0.2 lowers the stability curve 0.70 log units.

The upper limits of biotite stability for selected biotites of the Hardwick Tonalite are compared with three common oxygen buffers, magnetite-hematite, Ni-NiO and fayalite-magnetite-quartz, in Figure 53. At magmatic temperatures (700-900°C), the stability curves for the biotite show a range of f_{O_2} between the metaluminous, magnetite-bearing tonalite and the peraluminous, ilmenite-bearing tonalite that reaches a maximum of 3 orders of magnitude.

The upper limits of stability have been estimated for the biotite of the augite-hornblende quartz diorite, the Goat Hill Diorite, the Bear Den sill of diorite, the porphyritic microcline granite and the equigranular granites (Figure 54). At magmatic temperatures, the stability curves for the biotite of the Goat Hill Diorite and the Bear Den sill of diorite are between the Ni-NiO and the magnetite-hematite buffers. The stability curve for the biotite of the augite-hornblende quartz diorite is at the Ni-NiO buffer with the biotite of the chilled margin displaced to lower f_{O_2} values. This displacement is primarily a result of the absence of magnetite in the oxide assemblage and therefore an activity of Fe_2O_3 = 0.2 was used in the calculations. The stability curves of the biotite from the various granites plot at or lightly above the FMQ buffer at granitic magmatic temperatures (650-750°C).

In summary, biotite and oxide equilibria suggest that the Hardwick Tonalite and associated plutonic rocks crystallized at or above the FMQ buffer, with the range extending to f_{O_2} between the Ni-NiO and magnetite-hematite buffers. These estimates fall within the calc-alkaline envelope suggested by Haggerty (1975). The estimated f_{O_2} for the various rock types falls within both "I"- and "S-type" f_{O_2} regions suggested by Wones (1981), but above the upper f_{O_2} limits of the graphite-bearing country rock.

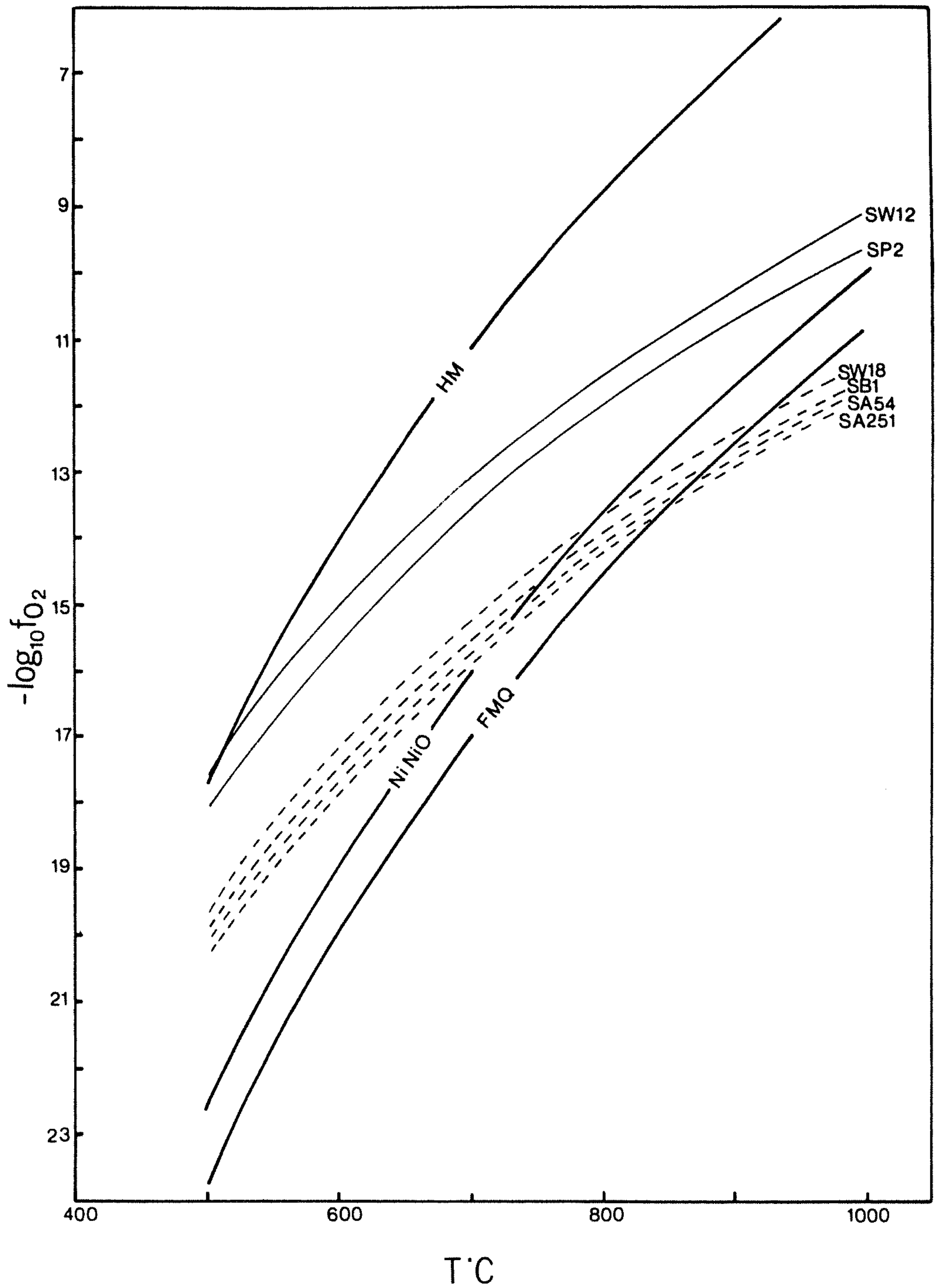

Figure 53. Stability curves for the biotites of the Hardwick Tonalite plotted in T°C versus $-\log_{10} f_{O_2}$. Solid stability curves represented biotite coexisting with both magnetite and ilmenite. HM, NiNiO and FMQ buffers are also plotted.

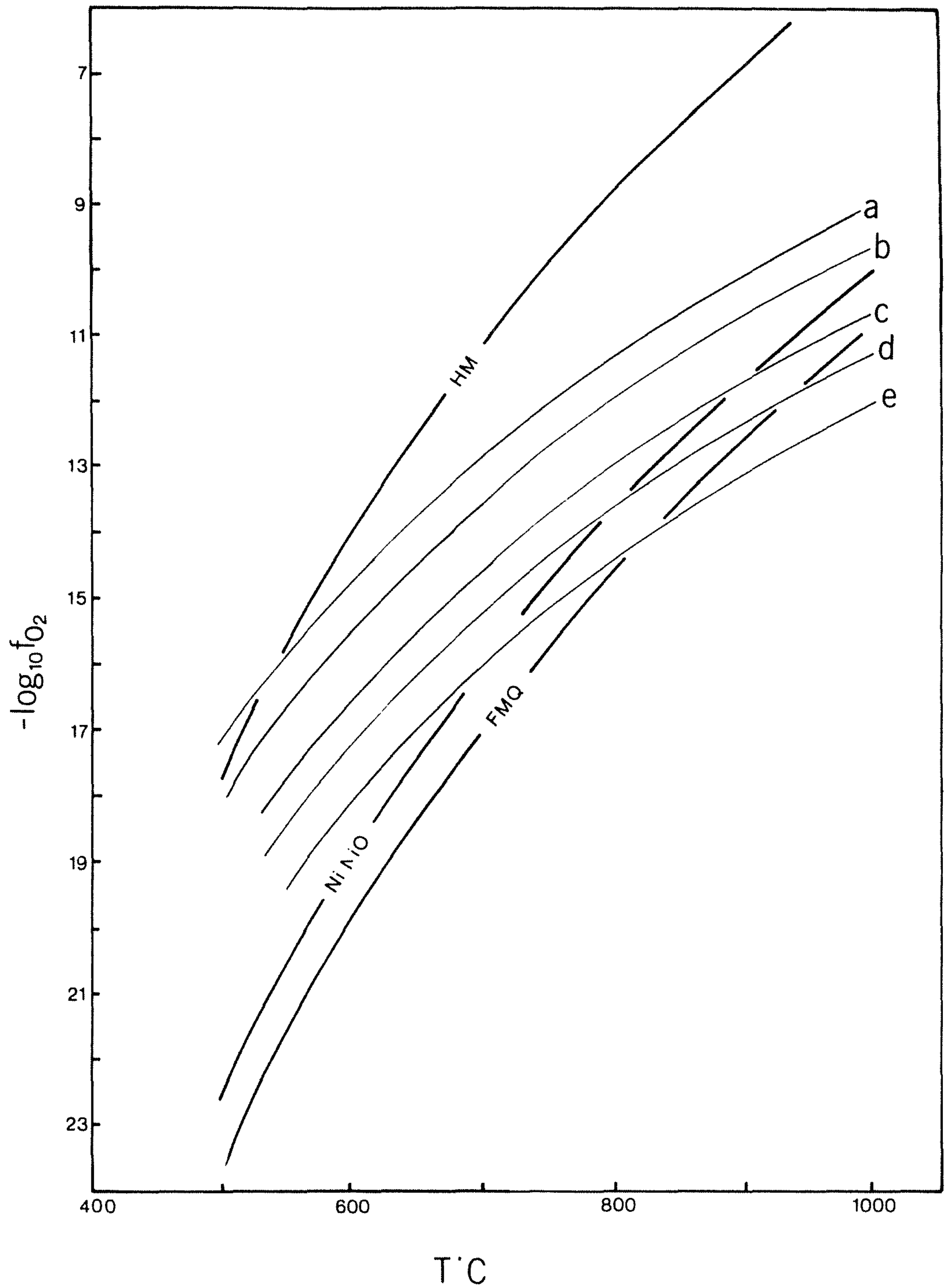

Figure 54. Stability curves for biotite of plutonic rocks associated with the Hardwick Tonalite in T°C versus $-\log_{10} f_{O_2}$. (a) Bear Den Sill of diorite, (b) Goat Hill Diorite, (c) Nichewaug Sill of augite-hornblende quartz diorite, (d) chilled margin of Nichewaug Sill, and (e) granites.

PART II

GEOCHEMISTRY OF THE HARDWICK TONALITE

ABSTRACT

The Hardwick Tonalite is a member of the Acadian (Devonian) New Hampshire Plutonic Series and is the largest Acadian pluton in Massachusetts, with an estimated surface area of approximately 300 km^2. It intrudes a sequence of metamorphosed Middle Ordovician, Silurian, and Lower Devonian clastic sedimentary rocks of the Merrimack synclinorium and is situated within the central Massachusetts Acadian metamorphic high. The pluton forms an irregular west-dipping syntectonic sheet which appears generally to occupy an isoclinal stratigraphic syncline in the Devonian Littleton Formation. Locally, however, the tonalite is in direct contact with the Augen Gneiss Member of the Ordovician Partridge Formation.

The tonalite has been subdivided into four petrographic types: hornblende-biotite tonalite, biotite tonalite, biotite-muscovite tonalite, and biotite-garnet tonalite. The distribution of these types defines a mineralogical zoning in the sheet from hornblende-biotite tonalite and biotite tonalite in the interior to biotite-muscovite tonalite and biotite-garnet tonalite at the perimeter. Accompanying this outward metaluminous to peraluminous mineralogical zoning, is an outward decrease in the oxidation state.

The SiO_2 content of the tonalite varies from 52 to 66% and is negatively correlated to TiO_2, Fe_2O_3, MgO, CaO, FeO, and P_2O_5. Al_2O_3, MnO, Na_2O and K_2O exhibit a weak to virtually non-existent correlation with SiO_2. The $Na_2O/(Na_2O+K_2O)$ ratio of the tonalites ranges from 0.55 to 0.33 and does not appear to be dependent upon rock type. The distribution of of Na_2O and K_2O in the tonalite does not correspond to the "I- and S-type" characterization observed in the granitoids of eastern Australia and elsewhere, although the distribution discriminates between the tonalites and the pelitic country rocks. The ratio $Al/[K+Na+(Ca/2)]$ ranges from .73 to 1.24 and, after a large P_2O_5 (apatite) correction, corundum is still present in the normative mineralogy of the majority of the tonalites. Corresponding with the metaluminous to peraluminous mineralogical zoning, the tonalite sheet is zoned from a diopside-normative interior to a corundum-normative perimeter. The tonalites define a distinctively calc-alkaline trend.

The hornblende-biotite tonalite, biotite tonalite and biotite-muscovite tonalite contrast with the biotite-garnet tonalite and the local metamorphosed sedimentary rocks in being enriched in the moderately lithophile elements, light rare earth elements (LREE) and high field strength (HFS) elements. Comparison of variations in Rb-Sr, K-Rb, Ba-Rb and Ba-Sr with fractional crystallization vectors constructed from mineral/melt distribution coefficients, and LREE and HFS element differences between the biotite-garnet tonalite and other tonalites suggests the following conclusions: 1) hornblende fractionation accounts for the geochemical variability in the hornblende-biotite tonalite, 2) melting in a heterogeneous source area accounts for the geochemical variation between the hornblende-biotite tonalite, biotite tonalite and biotite-muscovite tonalite, and 3) in situ contamination is responsible for the formation of the biotite-garnet tonalite. The heterogeneous source area consisted of two interlayered end-members: a metalluminous, oxidized member, and a

peraluminous, reduced member. The metaluminous, oxidized member may correspond to oxidized and partially altered basalt or andesite whereas the peraluminous, reduced member may correspond to a graywacke-argillite sequence, both deep within the Acadian subduction complex and probably unrelalated to the enclosing sedimentary sequence.

INTRODUCTION

The Devonian Hardwick Tonalite is a north-south trending quasiconcordant syntectonic plutonic sheet (Figure 55) located within the central Massachusetts metamorphic high where pelitic schists carry assemblages characteristic of the sillimanite-muscovite, sillimanite-muscovite - K-feldspar, sillimanite - K-feldspar, and sillimanite - K-feldspar-garnet-cordierite zones (Tracy et al., 1976).

The "Hardwick granite" (type locality in Hardwick, Massachusetts) was interpreted by Emerson (1898, 1917) to be a series of intrusive sheets composed predominantly of a black granite gneiss. It was assigned a late- or post-Carboniferous age. In southern New Hampshire, Fowler-Billings (1949) assigned a lower Devonian age to the Spaulding Quartz Diorite which is of a similar character and probably a northern extension of the Hardwick Tonalite. Subsequent mapping by Fitzgerald in the Royalston quadrangle (1960), Mook in the Athol quadrangle (1967), D'Onfro in the Templeton quadrangle (1974), Field in the Ware quadrangle (1975) and Tucker in the Barre quadrangle (1977) defined the relationship between the Hardwick pluton and the region's deformational history and stratigraphy. Nielson et al. (1976) examined the relationship between the Spaulding Quartz Diorite and the region's deformational history. Lyons and Livingston (1977) derived a whole rock age of 410 million years for the Spaulding Quartz Diorite. Petrography and mineralogy of the tonalite and associated plutonic rocks has been examined by Shearer (1979, 1980, 1981, 1983).

GEOLOGIC SETTING

The Hardwick Tonalite is intruded into a sequence of metamorphosed clastic sedimentary rocks and subordinate volcanics of the Merrimack synclinorium. To the west, the Merrimack synclinorium is bounded by the Bronson Hill anticlinorium and to the east by the Milford anticlinorium (Hall and Robinson, 1982). The Bronson Hill anticlinorium consists of a series of en echelon gneiss domes mantled by amphibolites, mica schists, quartzites and calc-silicate rocks. The stratigraphic sequence in the Bronson Hill anticlinorium has been described by Billings (1937, 1956), Robinson (1967a,b, 1979) and Thompson et al. (1968). The Milford anticlinorium contains metamorphic rocks of Late Precambrian and younger ages. Gneisses in the core of the Milford anticlinorium have been correlated to those in the Pelham dome of the Bronson Hill anticlinorium (Field, 1975; Hall and Robinson, 1982).

Figure 55. Generalized bedrock geologic map of central Massachusetts showing major stratigraphic and plutonic units.

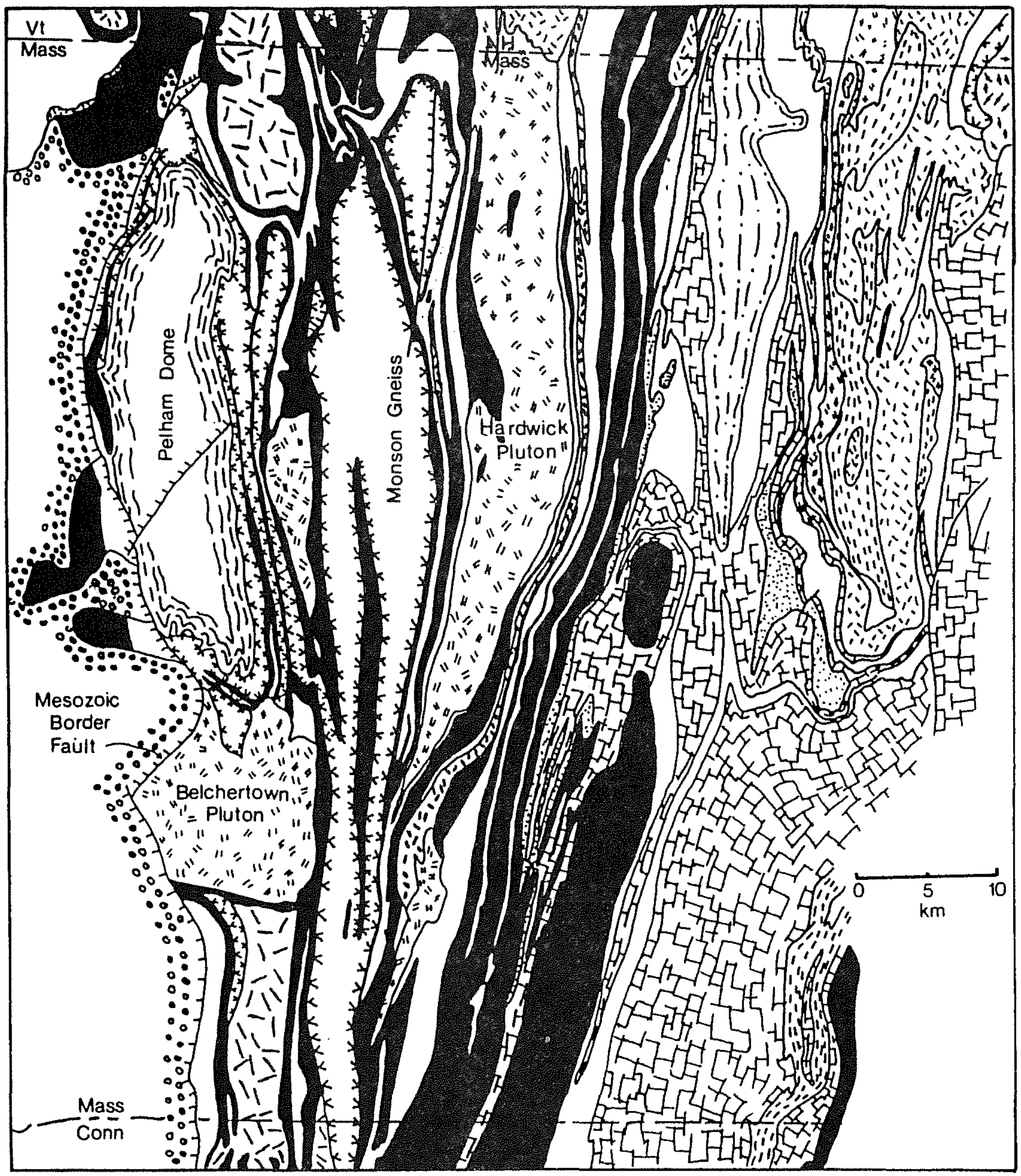

Lower Jurassic-Upper Triassic — Conglomerate, sandstone, shale, and basalt.

Upper Pennsylvanian — Weakly foliated biotite granite.

Devonian — Weakly foliated muscovite granite. Foliated muscovite granite gneiss. Coys Hill Granite. Granodiorite, quartz diorite, tonalite, gabbro.

Lower Devonian — Littleton, Erving, and Waits River Formations.

Silurian — Paxton Formation-sulfidic schist where separately mapped. Paxton Formation Granulite member. Clough Quartzite in western portion of map, Paxton Formation schist and quartzite members in central and eastern portion of map.

Middle Ordovician — Ammonoosuc Volcanics and Partridge Formation. Tatnic Hill Formation in southeastern portion of map.

Ordovician — Massive gneiss of plutonic origin in cores of domes.

Ordovician Late Precambrian? — Monson and related layered gneisses.

Late Precambrian — Dry Hill and related gneisses, schists and quartzites.

Major normal faults with hatches on downthrown side.

The stratigraphic sequence in the Merrimack synclinorium can be divided into two major divisions: (1) a sequence of Middle Ordovician metamorphosed sedimentary and volcanic rocks and (2) a sequence of Silurian and Lower Devonian metamorphosed sedimentary and volcanic rocks.

The Middle Ordovician of the Merrimack synclinorium is represented by the Partridge Formation. The Partridge Formation is typically a pyrrhotite-graphite-mica schist which weathers to a "rusty" yellow brown color. Lenticular pods of calc-silicate one-half to two meters long and several centimeters thick occur within the sequence. In the lower portion of the Partridge Formation, the rusty schist is interbedded with mafic and felsic volcanics. An Augen Gneiss Member of the Partridge Formation is commonly in contact with the western edge of the Hardwick Tonalite, but its stratigraphic location within the Partridge Formation is not known.

The sequence of Silurian and Lower Devonian sedimentary and volcanic rocks unconformably overlies the Middle Ordovician sequence. The Silurian in the Merrimack synclinorium is represented by the Fitch Formation in the extreme western portion of the synclinorium and the Paxton Formation which is the major Silurian unit in the central and eastern portion of the synclinorium. It has been argued that the Paxton Formation is the eastern equivalent of the Fitch Formation (Field, 1975). In the immediate vicinity of the Hardwick Tonalite, the Fitch Formation is typically a pyrrhotite-graphite calc-silicate rock. The Lower Devonian Littleton Formation overlies the Fitch Formation and Paxton Formation. The Littleton Formation is dominated by gray graphite pelitic schist, but also contains minor feldspar gneiss and orthopyroxene gneiss members. The gneisses have been interpreted as felsic and mafic volcanics (Field, 1975).

Most of the plutonic rocks of the Merrimack synclinorium within central Massachusetts are southern extensions of the Acadian New Hampshire Plutonic Series (Billings, 1956; Nielson et al., 1976). The plutons form either syntectonic, concordant to quasi-concordant sheets or late- to post-tectonic, discordant plutons of uncertain shape. The former intrusive style is dominant and the contrasting styles are probably a function of relative temperature and rheologic differences between the intruding magma and the country rock and deformational stage in which the intrusion occurred (Nielson et al., 1976).

Plutonic rocks account for 21% by area of the rocks exposed in the Bronson Hill anticlinorium and the Merrimack synclinorium in central Massachusetts. Of this 21%, gabbro-diorite makes up 5%, tonalite-granodiorite-monzodiorite, 53%; and granite 42%. These plutonic rocks are compositionally strongly bimodal with a high frequency of plutonic rocks with 59% and 71% SiO_2. The Hardwick Tonalite is a major contributor to the first peak.

In many of the plutonic rocks of the Bronson Hill anticlinorium and the Merrimack synclinorium, the igneous texture has been replaced with a metamorphic texture and mineralogy developed during Acadian deformations and metamorphism. The metamorphic effects on texture and mineralogy of some of the plutonic rocks have been described by Ashwal et al. (1979), Maczuga (1981), and Shearer (1982). The sequence of Acadian deformation in central Massachusetts as interpreted by Robinson (1967a,b), Field (1975), Tucker (1977), Robinson (1979) and Hall and Robinson (1982) consists of four phases: (1) Recumbent, isoclinal, westward-directed nappe folding of large amplitude (tens of kilometers). Several plutonic sheets including the Hardwick Tonalite were intruded prior to or during this structural stage. The Spaulding Quartz Diorite in New Hampshire is thought to have been intruded into the Littleton Formation early in the deformational history, but after the intrusion of the Kinsman Quartz Monzonite (Nielson et al., 1976). A low pressure "contact" metamorphism possibly resulting from the intrusion of the plutonic sheets is suggested by aggregates of sillimanite that appear to be pseudomorphs after andalusite (Tracy and Robinson, 1980) and by a relict contact aureole (Shearer and Robinson, 1980). (2) Recumbent backfolding of the isoclinal folds developed in stage 1. During this stage in the deformation, metamorphic grade in the immediate area of the Hardwick Tonalite reached sillimanite-muscovite grade at the northwest margin of the tonalite and sillimanite-cordierite-garnet grade at the southeast margin of the tonalite. Isograds lie at oblique angles to and cut across the tonalite. Rocks previously exposed to a low pressure metamorphism attained peak metamorphic conditions of up to 700°C and 6.3 kbars. Mylonites found at the margins and southern end of the tonalite were formed late in this stage of the deformational history. (3) Formation of gneiss domes in the Bronson Hill anticlinorium and development of northeast-trending minor folds and mineral lineations near the Hardwick pluton. (4) Formation of a series of broad open folds about north-trending axes. The relationship between the deformational history, the metamorphism and the plutonism in the Merrimack synclinorium and the Bronson Hill anticlinorium in central Massachusetts is outlined schematically in Figure 56.

GEOLOGICAL RELATIONS AND PETROGRAPHY OF THE HARDWICK TONALITE

The Hardwick pluton is the largest Acadian pluton in central Masschusetts, covering an area of approximately 300 km^2 and having a minimum estimated volume of 1200 km^3. The pluton forms an irregular west-dipping sheet which appears to occupy an isoclinal stratigraphic syncline in the Devonian Littleton Formation. This apparent positioning within a single stratigraphic horizon had led earlier observers to suggest that the Hardwick Tonalite was in reality ultrametamorphosed volcanics in the Littleton Formation (Page, 1967). Locally, however, on the northwest side of the intrusion the Hardwick Tonalite is in direct contact with the Augen Gneiss Member of the Ordovician Partridge Formation (Figure 57) and contains an extensive suite of inclusions of Partridge, Fitch and Littleton Formations. In addition to the cross-cutting relationships, chilled and contaminated margins, a relict contact aureole (Shearer and Robinson, 1980) and limited recognizable Littleton Formation volcanics suggest the origin of the tonalite is indeed intrusive.

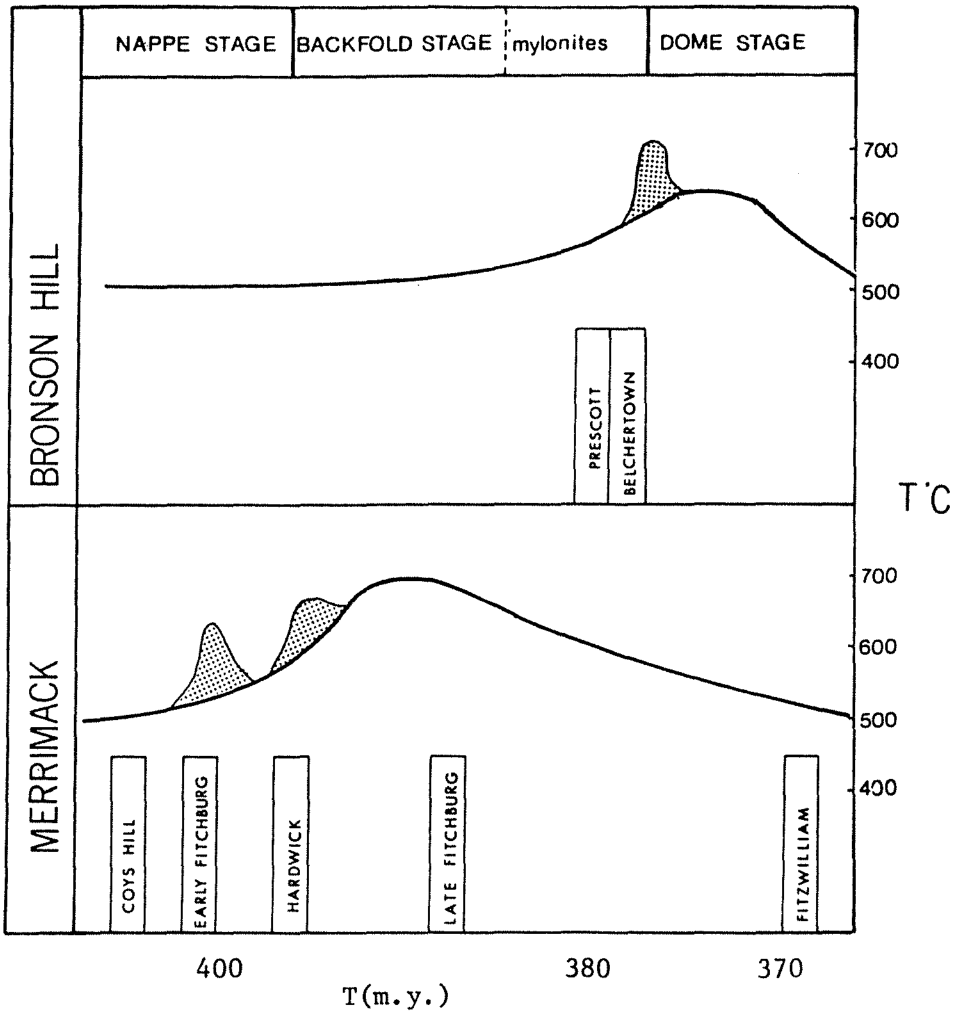

Figure 56. Schematic outline of the relationship between deformational history, regional metamorphism, and plutonism in the Merrimack synclinorium and the Bronson Hill anticlinorium in central Massachusetts. Dotted peaks represent thermal pulses during intrusion of plutons. Estimates of metamorphic temperatures are from Tracy et al. (1976) and Shearer and Robinson (1980).

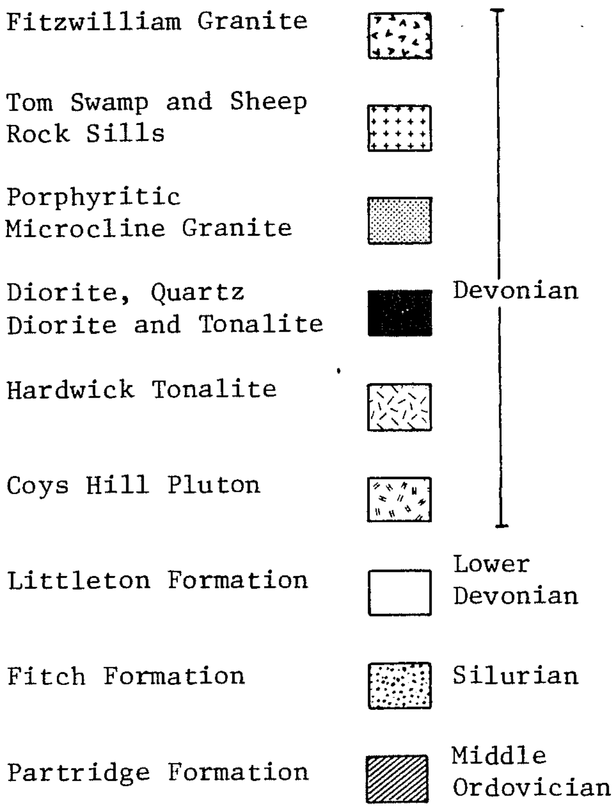

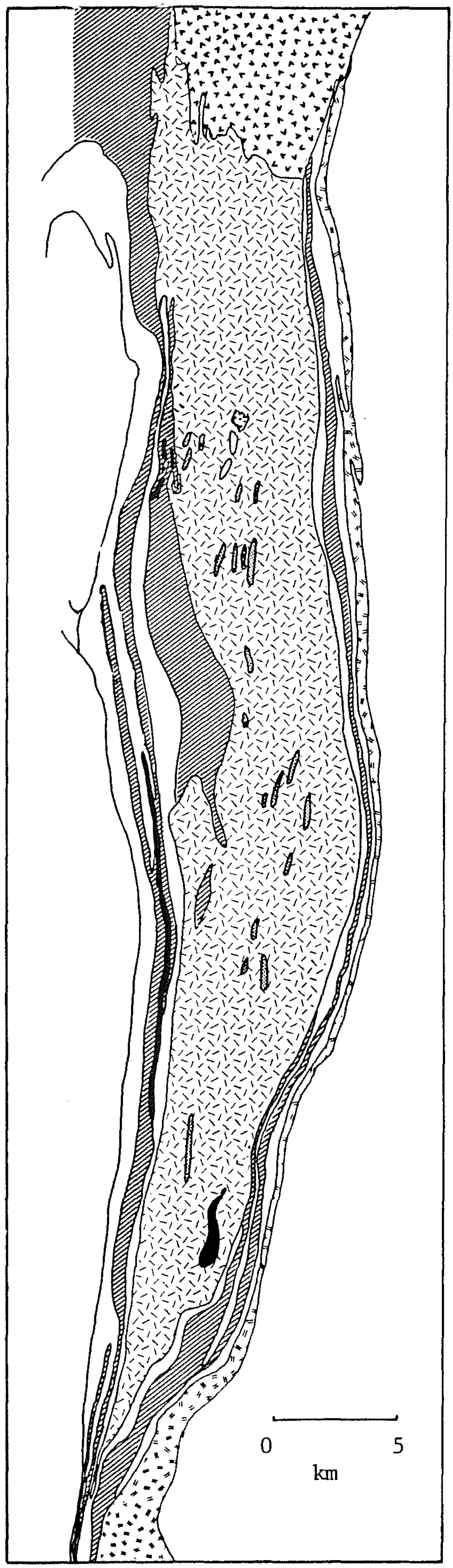

Figure 57. Distribution of rock types within the Hardwick pluton and surrounding plutons.

A plot of modal quartz, plagioclase and potassic feldspar in the Hardwick Tonalite (Figure 58), shows that these rocks are classified as tonalites, quartz diorites and granodiorites by the IUGS nomenclature (Streckeisen, 1973). The tonalite sheet, which appears to represent a single intrusive pulse, has been subdivided into four types: hornblende-biotite tonalite, biotite tonalite, biotite-muscovite tonalite and biotite-garnet tonalite. The distribution of these types defines a zoning from hornblende-biotite tonalite and biotite tonalite in the interior of the pluton to discontinuous muscovite- and garnet-bearing tonalites at the margins (Figure 59).

Accompanying the metaluminous to peraluminous mineralogical zoning in the pluton, there is a variation in oxide assemblage and oxide composition. The hornblende-biotite tonalite and some of the biotite tonalite have an oxide assemblage of magnetite and ilmenite. The ilmenite has a hematite component of up to 18%. As the character of the silicate mineralogy changes from metaluminous to peraluminous, magnetite disappears from the oxide assemblage and the hematite component in the ilmenite decreases. Biotite and oxide data (Shearer, 1983) suggest the metaluminous rocks crystallized at an f_{O2} at or above the NiNiO buffer and the peraluminous rocks between the FMQ buffer and the NiNiO buffer at magmatic temperatures of between 700-900°C (Shearer, 1981, 1982, 1983).

In rocks containing a relict igneous texture, clusters of biotite, hornblende and/or muscovite define a glomeroporphyritic texture, the plagioclase is strongly zoned (An_{50-30}), and quartz and potassic feldspar are commonly interstitial. Apatite, allanite, sphene, and oxides are common accessory minerals, although primary sphene is absent in the muscovite- and garnet-bearing tonalites. The modal apatite content for the hornblende-biotite tonalite ranges from 0.9 to 3.5%, for the biotite tonalite between 0.5 and 2.9%, for the biotite-muscovite tonalite between 0.1 and 2.2% and for the biotite-garnet tonalite between 0.00 and 0.3%. Modal analyses show that apatite is not evenly distributed, but associated with the mafic clusters - a common characteristic of I-type granites (Hine et al., 1978). Point-counted determinations of the ratio of apatite in mafic clusters against apatite associated with felsic minerals range from 5/1 to 3/1.

Much more commonly, the primary igneous texture is partially to totally obscured by the Acadian deformational-metamorphic overprint. The tonalites are moderately to strongly foliated and a new subsolidus mineral assemblage is developed. In the reequilibrated to recrystallized mineralogy, epidote and sphene form reaction rims around allanite and ilmenite, respectively. Primary igneous zoning in plagioclase is partially to totally erradicated and primary mineral chemistries are reequilibrated to subsolidus temperatures (e.g. biotite becomes depleted in Ti).

Based on the mineralogical zoning in the Hardwick Tonalite, Shearer (1981, 1983) suggested that the magmatic evolution of the tonalite requires the mixing of an oxidized, metaluminous component ["I-type" source material of Chappel and White (1974)] with a reduced, peraluminous component ["S-type" source material of Chappell and White (1974)]

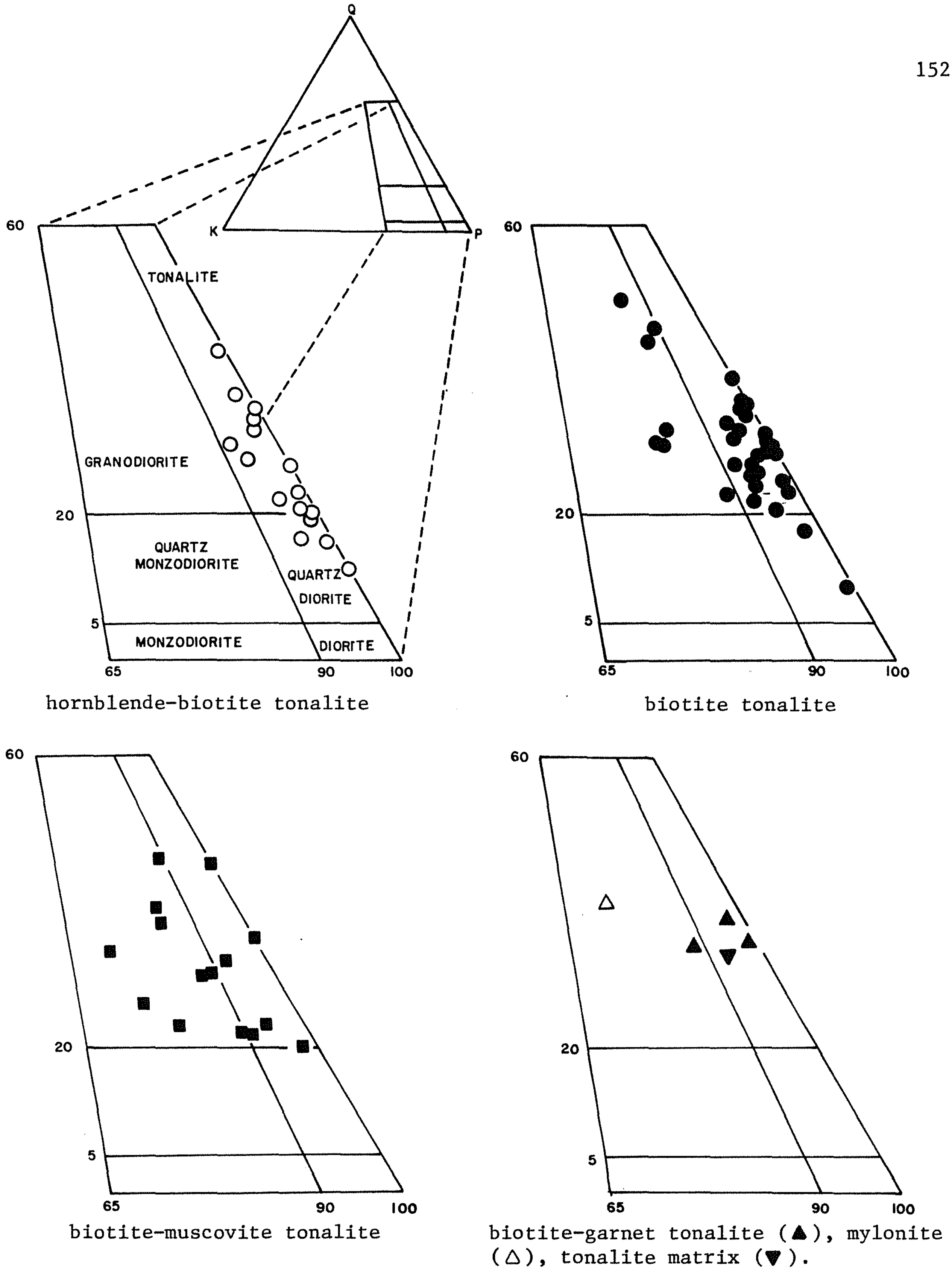

Figure 58. Quartz-Plagioclase-K-Feldspar plot of modes of the various rock types of the Hardwick Tonalite.

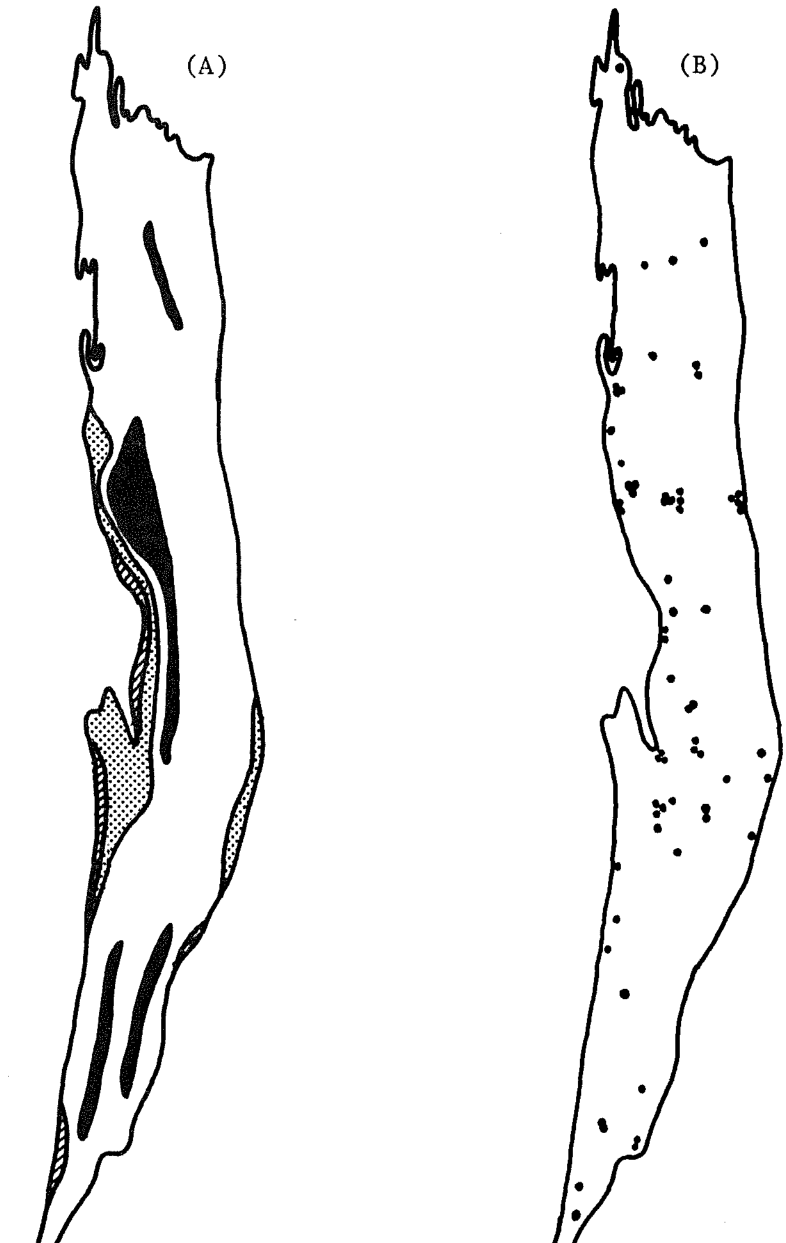

Figure 59. A. Rock type distribution within the Hardwick Tonalite. Black: hornblende-biotite tonalite, white: biotite tonalite, dotted: biotite-muscovite tonalite, stripe: biotite-garnet tonalite. B. sample locations

during or after initial melting of the source material. In addition, the glomeroporphyritic texture of the tonalites, the ambiguity between apatite solubility experiments (Watson, 1979, 1980) and the modal amount of apatite in the Hardwick Tonalite and the high tonalite liquidus temperatures indicated by the melting experiments of Wyllie et al. (1976), Stern and Wyllie (1973), Stern et al. (1975) and Huang and Wyllie (1973, 1974, 1981) suggests the tonalite was intruded as a mixture of melt and refractory residual minerals rather than a tonalite liquid (Shearer, 1983). Geochemical evaluation of the Hardwick Tonalite further defines and clarifies these processes and materials.

SAMPLING AND ANALYTICAL PROCEDURES

Seventy-one samples of the Hardwick Tonalite were strategically chosen for whole rock chemical analyses based upon insight derived from three summers of detailed mapping within the Athol and Petersham quadrangles in Massachusetts and reconnaissance in the Templeton, Ware, Bare, Royalston, Winchendon quadrangles in Massachusetts and the Mt. Monadnock quadrangle in New Hampshire. In addition to the tonalite, collections were made of the Augen Gneiss Member of the Partridge Formation and the pelitic schists of the Littleton Formation that occur as inclusions within the pluton or lie along contacts with the pluton. The analyses of local non-plutonic rocks may aid in the interpretation of possible source material and/or contamination processes.

Major element whole rock analyses were done on fused glass discs and irradiated by a chromium target X-ray tube under vacuum. The glass discs were made by fusing the sample with lithium tetraborate in proportions such that a maximum efficiency in sensitivity and elimination of matrix effects is achieved (Norrish and Chappell, 1967; Norrish and Hutton, 1969). Major elements analyzed by this method were SiO_2, TiO_2, Al_2O_3, total Fe as FeO, MnO, MgO, CaO, K_2O and P_2O_5. Trace elements were analyzed in two groups and done on pressed powder pellets with boric acid base. Rb, Sr, Ga, Th, Pb, and Y were determined using a molybdenum target X-ray tube without a vacuum. Nb, Zr, Zn, Ni, Cr, V, Ba, Ce and La were determined using a gold target X-ray tube under vacuum. Corrections made for non-linear background, element interferences (Norrish and Chappell, 1969) and mass absorption coefficients were estimated from Mo and Au compton peaks following modifications of the method of Reynolds (1975).

Ferrous iron was determined titrimetrically to distinguish between FeO and Fe_2O_3 (Maxwell, 1968). Na_2O was determined using a IL443 flame photometer with an Li internal standard.

ANALYTICAL RESULTS

Table 27 is a compilation of major and trace element analyses and CIPW norms for the Hardwick Tonalite. Those for the local country rock are shown in Table 28.

Table 27. Whole rock analyses for the major and trace elements and calculated CIPW norms for the Hardwick Tonalite.

	hornblende-biotite tonalite											
Sample	A100-1	A100-2	A100-3	P65-1A	P65-1B	W16	W21	R6	W12-1	W12-2	A61-1A	A61-1B
SiO_2	57.38	57.17	57.29	54.83	55.30	55.45	57.10	58.06	58.34	58.46	52.60	52.71
TiO_2	2.62	2.56	2.57	2.27	2.35	2.37	2.13	1.83	2.20	2.17	2.11	2.11
Al_2O_3	15.01	15.03	15.03	15.16	15.33	15.79	16.00	14.80	15.47	15.39	15.39	15.25
Fe_2O_3	2.47	2.56	2.55	2.98	2.85	2.77	2.73	2.12	2.74	2.52	3.57	3.52
FeO	6.33	6.30	6.30	6.24	6.33	6.59	5.47	6.68	4.65	4.73	5.84	5.80
MnO	0.22	0.23	0.23	0.24	0.21	0.22	0.15	0.22	0.16	0.19	0.18	0.19
MgO	3.35	3.39	3.41	4.18	4.28	3.14	3.40	4.48	3.18	3.30	6.07	6.04
CaO	5.22	5.30	5.10	5.50	5.64	5.28	5.18	4.37	4.84	4.99	6.98	6.92
Na_2O	2.38	2.40	2.46	2.91	2.95	3.18	3.08	1.75	2.52	2.41	2.27	2.29
K_2O	3.34	3.29	3.24	3.08	3.09	3.09	3.55	3.72	4.38	4.16	2.82	2.79
P_2O_5	1.09	1.20	1.09	1.20	1.27	1.18	0.97	0.85	1.03	1.14	0.94	1.05
volatile loss	0.67	0.54	0.59	0.87	0.76	0.86	nd	0.76	0.33	0.40	0.84	0.95
total	100.08	99.97	99.86	99.46	100.36	99.92	99.76	99.46	99.84	99.86	99.54	99.32
$Fe^{3+}/(Fe^{3+}+Fe^{2+})$	.26	.27	.27	.30	.29	.30	.31	.23	.34	.33	.36	.35
Al/[K+Na+(Ca/2)]	.87	.87	.89	.84	.82	.87	.86	.99	.87	.88	.79	.79
Q	14.76	14.68	14.77	8.77	8.63	9.25	9.96	16.16	13.08	14.27	6.11	6.54
Or	19.74	19.44	19.15	18.20	18.26	18.26	20.98	21.98	25.88	24.58	16.67	16.49
Ab	20.14	20.31	20.82	24.62	24.96	26.91	26.06	14.81	21.32	20.39	19.21	19.38
An	19.49	19.24	18.89	19.21	19.46	19.26	19.35	16.68	17.96	18.05	23.48	23.09
C	0.34	0.47	0.55			0.16		1.78		0.31		
Di				0.83	1.01		0.52				4.45	4.05
En				0.26	0.32		0.17				1.63	1.48
Fs				0.14	0.17		0.09				0.50	0.45
Wo				0.43	0.52		0.27				2.32	2.11
Hy	14.01	14.10	14.14	15.70	15.95	14.13	12.76	19.06	10.86	11.59	17.61	17.72
En	8.34	8.44	8.49	10.15	10.34	7.82	8.30	11.16	7.92	8.22	13.49	13.56
Fs	5.67	5.65	5.65	5.55	5.61	6.31	4.46	7.90	2.94	3.37	4.13	4.16
Mt	3.58	3.71	3.70	4.32	4.13	4.02	3.96	3.07	3.97	3.65	5.18	5.10
Il	4.98	4.86	4.88	4.31	4.46	4.50	4.05	3.48	4.18	4.12	4.01	4.01
Ap	2.38	2.62	2.38	2.62	2.78	2.58	2.12	1.86	2.25	2.49	2.08	2.08
volatile loss	0.67	0.54	0.59	0.87	0.76	0.86	nd	0.76	0.33	0.40	0.84	0.95
total	100.09	99.97	99.86	99.45	100.40	99.92	99.76	99.64	99.84	99.86	99.62	99.62
Trace Elements (in ppm)												
Y	31	32	32	25	24	22			29	30	30	31
Sr	846	849	850	955	964	1051	1308	566	1380	1389	1156	1175
Rb	87	87	87	97	98	101			114	112	76	75
Ba	1127	1134		1222	1229	1415	2025	1106	1903	1858	1527	1530
Th	16	16	16	20	19	23			23	23	13	13
Pb	39	38	38	30	29	30			37	37	26	25
Ga	23	22	22	24	24	26			24	24	21	21
Nb	34	32		25	25	33	26	28	27	27	24	23
Zr	271	267		302	300	637	601	453	357	362	414	408
Zn	150	152		147	141	169	136	170	147	142	124	124
Ni	44	45		47	45	21	29	39	39	37	107	104
Cr	71	75		179	181	68	93	180	83	80	179	172
V	89	96		132	131	141	131	120	116	107	154	152
La	62	62		98	98	163	183	111	112	118	97	100
Ce	121	125		219	210	309	323	231	202	215	176	169

Table 27, continued.

Sample	hornblende-biotite tonalite				biotite tonalite						
	A61-1C	A160-3-1	A160-3-2	A160-3-3	W1-1	W1-2	A3-2A	A3-2B	P3-1	P3-2	W18
SiO_2	52.75	56.28	56.16	56.32	61.97	62.01	56.52	56.52	61.54	61.50	58.26
TiO_2	2.09	2.06	2.08	2.03	1.51	1.52	2.20	2.24	1.65	1.59	2.44
Al_2O_3	15.35	15.06	15.01	14.98	16.17	15.93	15.31	15.34	16.06	16.01	15.72
Fe_2O_3	3.66	2.96	3.01	2.88	0.90	0.85	2.26	2.20	1.29	1.30	1.27
FeO	5.75	4.78	4.80	4.84	5.51	5.48	5.97	6.00	5.19	5.22	6.80
MnO	0.19	0.18	0.19	0.17	0.09	0.15	0.16	0.19	0.12	0.14	0.17
MgO	5.90	3.94	3.99	3.96	2.24	2.32	3.58	3.71	2.46	2.43	3.36
CaO	6.83	5.70	5.76	5.65	3.20	3.31	4.94	5.00	3.71	3.77	5.48
Na_2O	2.32	3.46	3.36	3.46	2.62	2.69	2.39	2.44	3.28	3.30	1.84
K_2O	2.71	4.04	3.87	3.87	3.75	3.68	3.32	3.33	3.54	3.38	3.11
P_2O_5	1.02	1.05	1.12	1.09	0.60	0.64	1.02	1.07	0.73	0.76	1.17
volatile loss	0.90	1.07	1.10	1.13	0.64	0.61	0.94	1.01	0.63	0.65	nd
total	99.36	100.58	100.45	100.38	99.20	99.19	98.65	99.01	100.40	100.04	99.62
$Fe^{3+}/(Fe^{3+}+Fe^{2+})$	.37	.36	.36	.35	.12	.12	.26	.25	.18	.18	.15
Al/[K+Na+(Ca/2)]	.80	.74	.74	.74	1.14	1.13	.93	.92	1.00	1.01	.96
Q	6.98	5.61	6.54	6.22	20.44	20.10	13.95	13.53	16.43	16.84	18.36
Or	16.02	23.88	22.81	22.87	22.16	21.75	19.62	19.68	20.92	19.92	18.38
Ab	19.63	29.28	28.43	29.28	22.17	22.76	20.22	20.39	27.76	27.92	15.57
An	23.47	13.63	14.47	13.91	12.35	12.66	18.51	18.51	14.11	14.23	20.31
C					3.28	2.88	1.00	.99	1.66	1.72	1.88
Di	3.53	6.79	6.02	6.18							
En	1.30	2.44	2.17	2.19							
Fs	.39	.81	.71	.77							
Wo	1.85	3.54	3.14	3.22							
Hy	17.44	9.82	10.30	10.37	12.63	12.91	14.61	15.16	12.09	12.20	16.09
En	13.40	7.37	7.76	7.67	5.58	5.78	8.92	9.24	6.13	6.05	8.27
Fs	4.05	2.45	2.54	2.70	7.05	7.13	5.69	5.92	5.96	6.15	7.72
Mt	5.31	4.29	4.36	4.18	1.30	1.23	3.28	3.19	1.87	1.88	1.84
Il	3.97	3.91	3.95	3.86	2.87	2.89	4.25	4.18	3.13	3.02	4.63
Ap	2.23	2.29	2.45	2.38	1.31	1.40	2.23	2.34	1.60	1.66	2.56
volatile loss	0.90	1.07	1.10	1.13	0.64	0.61	0.94	1.01	0.63	0.65	nd
total	99.47	100.58	100.44	100.38	99.15	99.19	98.17	98.98	100.20	100.04	99.62

Trace Elements (in ppm)

Sample	A61-1C	A160-3-1	A160-3-2	A160-3-3	W1-1	W1-2	A3-2A	A3-2B	P3-1	P3-2	W18
Y	31	31	31	31	24	24	27	27			38
Sr	1168	1556	1540	1543	572	580	719	721			1427
Rb	75	126	126	125	145	143	123	125			104
Ba	1458	2060	2046		1448	1460	1185		1237		2508
Th	13	24	23	23	23	23	21	21			19
Pb	26	35	35	37	32	33	22	22			37
Ga	20	21	22	22	24	24	23	24			23
Nb	23	26	25		25	26	26		25		28
Zr	399	407	394		511	505	320		558		714
Zn	125	153	147		131	137	153		146		171
Ni	110	41	39		15	15	38		20		43
Cr	167	82	96		55	61	109		59		88
V	142	125	121		97	98	127		102		137
La	100	142	135		71	71	123		158		
Ce	180	221	233		140	142	212		295		312

Table 27, continued.

	biotite tonalite											
Sample	A45	P139-21	P139-22	P139-23	M1-1-1	M1-1-2	T2-1	T2-2	T2-3	Wi-1-2	W19	A40
SiO_2	59.03	58.88	58.50	58.47	59.11	59.36	60.19	60.18	60.18	61.19	64.76	56.90
TiO_2	1.92	2.25	2.23	2.20	1.95	1.92	1.88	1.85	1.86	1.46	1.01	2.62
Al_2O_3	15.83	15.57	15.50	15.41	15.69	15.61	15.86	15.78	15.78	15.59	15.96	14.58
Fe_2O_3	1.55	2.00	1.97	2.00	1.50	1.60	1.46	1.35	1.43	1.08	1.03	3.03
FeO	5.94	5.89	5.99	5.88	5.53	5.50	5.37	5.20	5.37	4.83	5.22	5.74
MnO	0.17	0.19	0.20	0.20	0.20	0.20	0.13	0.14	0.13	0.12	0.09	0.24
MgO	2.77	3.19	3.24	3.18	2.68	2.64	3.06	3.09	3.10	2.16	2.14	3.27
CaO	4.46	4.63	4.57	4.57	4.57	4.49	4.14	4.16	4.17	4.90	3.06	5.20
Na_2O	2.24	2.82	2.81	2.79	2.81	2.76	2.53	2.60	2.57	1.79	2.98	2.22
K_2O	3.79	3.80	3.81	3.80	3.66	3.64	4.60	4.56	4.48	3.67	2.53	3.61
P_2O_5	0.90	1.02	1.00	0.99	0.95	0.96	0.90	0.93	0.91	0.98	0.10	1.01
volatile loss	0.91	0.60	0.60	0.65	0.65	0.65	0.74	0.70	0.70	0.87	0.65	1.03
total	99.51	100.83	100.42	100.14	99.30	99.33	100.86	100.54	100.68	98.44	99.53	99.45
$Fe^{3+}/(Fe^{3+}+Fe^{2+})$	.19	.23	.23	.23	.20	.20	.19	.19	.19	.17	.15	.32
Al/[K+Na+(Ca/2)]	.99	.91	.90	.90	.93	.93	.95	.94	.93	.97	1.20	.86
Q	17.01	13.20	12.44	13.00	14.62	15.53	14.08	13.88	14.17	17.40	24.95	14.98
Or	22.40	22.46	22.52	22.46	21.63	21.51	27.18	26.95	26.48	21.81	14.95	21.33
Ab	18.96	23.86	23.78	23.61	23.78	23.36	21.41	22.00	21.75	24.96	25.22	18.79
An	16.83	16.97	16.79	16.85	17.09	16.63	15.25	15.17	15.34	15.39	14.59	19.16
C	1.87	0.60	0.60	0.53	0.84	1.04	1.13	1.01	1.08	1.10	2.97	
Di												0.57
En												0.18
Fs												0.10
Wo												0.29
Hy	13.67	13.76	14.13	13.80	12.74	12.55	13.41	13.33	13.57	11.17	12.56	12.02
En	6.90	7.94	8.07	7.92	6.67	6.57	7.62	7.70	7.72	5.38	5.33	7.96
Fs	6.77	5.82	6.06	5.88	6.07	5.98	5.79	5.64	5.85	5.79	7.23	4.06
Mt	2.25	2.90	2.86	2.90	2.17	2.32	2.12	1.96	2.07	1.57	1.49	4.39
Il	3.75	4.25	4.24	4.18	3.70	3.65	3.57	3.51	3.53	2.77	1.92	4.98
Ap	1.97	2.23	2.19	2.16	2.08	2.10	1.97	2.03	1.99	1.40	0.22	2.21
volatile loss	0.91	0.60	0.60	0.65	0.65	0.65	0.74	0.70	0.70	0.87	0.65	1.03
total	99.51	100.83	100.13	100.14	99.30	99.33	100.86	100.54	100.68	98.44	99.53	99.45
Trace Elements (in ppm)												
Y	28	35	35	35	31	32	30	29	30	26		30
Sr	902	882	886	883	699	713	1304	1362	1316	766	438	1177
Rb	125	136	135	137	135	132	120	121	122	140		117
Ba	1732	1218	1257	1250	1327	1350	2397	2423		1321	780	1899
Th	23	19	19	19	26	27	24	27	27	25		14
Pb	29	30	29	29	38	34	44	43	42	33		28
Ga	24	24	25	24	24	23	23	23	23	23		23
Nb	27	34	33	33	29	29	25	24	24	23	17	29
Zr	590	231	204	201	565	588	627	581	592	526	252	402
Zn	147	150	150	150	138	136	124	134	130	124	109	143
Ni	26	36	36	36	11	12	40	37	37	11	26	36
Cr	68	98	87	86	49	49	84	80	80	52	61	74
V	113	124	124	130	117	117	124	118	115	99	83	141
La	217	108	112	113	137	136		165	171	135	28	103
Ce	361	220	228	225	255	252	263	291	287	258	60	103

Table 27, continued.

	biotite tonalite										
Sample	R7	P322	B2	P186	A402	R5	M7-1	M7-1	W22-1	W22-1	P2
SiO_2	58.59	58.10	57.28	59.66	60.72	59.47	64.16	64.23	59.46	59.50	56.99
TiO_2	2.20	1.90	1.99	1.83	1.90	1.66	1.25	1.31	2.29	2.20	2.14
Al_2O_3	15.10	16.30	15.68	15.83	15.74	15.94	15.69	15.48	16.55	16.48	15.97
Fe_2O_3	1.88	2.22	2.45	2.13	1.71	1.82	1.02	1.04	1.32	1.41	2.42
FeO	6.51	5.71	6.06	5.24	5.65	5.44	4.52	4.50	5.77	5.80	6.05
MnO	0.23	0.17	0.19	0.16	0.16	0.17	0.11	0.11	0.12	0.14	0.20
MgO	2.84	3.54	3.82	2.38	2.62	2.80	1.91	1.94	2.32	2.23	3.29
CaO	4.86	4.74	4.69	4.05	4.30	4.17	3.40	3.32	4.39	4.33	4.91
Na_2O	2.53	2.61	2.31	3.28	3.20	2.73	2.72	2.79	3.01	3.06	2.48
K_2O	3.60	3.32	3.37	3.54	3.51	3.80	3.99	4.00	2.72	2.59	3.14
P_2O_5	0.99	0.86	0.98	0.85	0.89	0.75	0.58	0.57	1.01	1.00	0.88
volatile loss	0.39	nd	nd	0.71	nd	nd	0.59	0.63	0.60	0.60	0.73
total	99.73	99.74	98.81	99.67	100.40	99.35	99.94	99.92	99.56	99.34	99.20
$Fe^{3+}/(Fe^{3+}+Fe^{2+})$	.21	.26	.27	.27	.21	.23	.17	.17	.17	.18	.23
Al/[K+Na+(Ca/2)]	.89	.99	.99	.95	.93	1.01	1.04	1.03	1.03	1.05	.98
Q	14.69	14.69	14.89	14.62	15.02	15.08	21.86	21.65	18.53	18.94	14.65
Or	21.28	19.62	19.92	20.92	20.75	22.46	23.58	23.64	16.07	15.31	18.56
Ab	21.41	22.09	19.55	27.76	26.08	23.10	23.02	23.61	25.47	25.89	20.99
An	18.29	18.46	17.51	15.09	16.10	16.28	13.46	13.12	15.84	15.60	19.18
C	0.34	1.65	1.82	1.07	0.78	1.37	1.96	1.75	2.85	2.93	1.46
Di											
En											
Fs											
Wo											
Hy	14.26	13.81	15.67	11.07	12.65	13.03	10.35	10.28	11.72	11.67	14.14
En	7.07	8.82	9.51	5.93	6.52	6.97	4.76	4.83	5.78	5.55	8.19
Fs	7.19	4.99	6.16	5.15	6.12	6.06	5.60	5.45	5.95	6.11	5.95
Mt	2.74	3.94	3.55	3.09	2.49	2.64	1.48	1.51	1.91	2.04	3.51
Il	4.18	3.61	3.78	3.48	3.61	3.15	2.37	2.49	4.35	4.18	4.06
Ap	2.16	1.88	2.14	1.86	1.94	1.64	1.27	1.25	2.21	2.19	1.92
volatile loss	0.49	nd	nd	0.71	nd	nd	0.59	0.63	0.60	0.60	0.73
total	99.73	99.74	98.81	99.67	100.40	98.75	99.94	99.92	99.56	99.34	99.20
Trace Elements (in ppm)											
Y						31	31	32			27
Sr	800	692	934	600		804	406	400	1350	1341	679
Rb						121	154	154			103
Ba	1635	1450	1255	1321		1465	1179	1170	2976	2986	1424
Th						23	31	32			20
Pb						35	36	35			29
Ga						23	23	21			24
Nb	32	29	22	28		28	24	23	31	30	26
Zr	614	578	398	478		512	544	530	723	730	410
Zn	145	160	153	142		135	108	105	145	152	148
Ni	22	21	35	11		20	14	10	12	10	26
Cr	55	73	119	45		66	48	40	14	8	93
V	125	122	126	110		111	84	86	135	136	142
La	334	128	133	134		158	133	134	139	139	
Ce	498	253	265	266		272	263	253	239	253	218

Table 27, continued.

	biotite tonalite					biotite-muscovite tonalite						
Sample	P146	R4	A13	P87	R2-1	R2-2	M5	B3	P265-1	P265-2	P265-3	P55
SiO_2	59.56	59.88	56.89	58.95	62.70	62.75	63.09	65.69	62.24	62.37	62.29	58.69
TiO_2	1.74	1.79	2.18	1.86	1.29	1.25	1.29	0.75	1.63	1.54	1.65	1.99
Al_2O_3	16.18	15.30	15.73	15.80	15.06	14.89	15.39	15.37	15.56	15.51	15.54	15.87
Fe_2O_3	1.96	2.73	2.16	2.13	1.44	1.46	0.96	1.06	1.40	1.45	1.51	1.38
FeO	5.55	4.80	6.88	5.17	4.15	4.17	4.85	3.52	4.91	4.89	4.96	6.12
MnO	0.15	0.17	0.17	0.16	0.14	0.15	0.12	0.09	0.12	0.13	0.12	0.16
MgO	2.91	2.50	4.38	2.76	3.07	3.11	1.87	2.14	2.51	2.47	2.43	2.96
CaO	4.13	4.27	4.47	3.81	4.41	4.37	3.27	2.87	3.34	3.36	3.43	5.01
Na_2O	3.30	2.99	2.74	2.80	2.93	2.95	2.73	2.69	2.60	2.71	2.63	2.49
K_2O	2.90	4.02	4.00	2.53	2.85	2.81	4.37	3.92	3.80	3.72	3.59	2.99
P_2O_5	0.82	0.81	0.94	0.64	0.81	0.82	0.52	0.24	0.65	0.69	0.71	0.95
volatile loss	0.80	nd	nd	nd	0.70	0.75	0.66	0.78	0.42	0.46	0.46	nd
total	99.98	99.26	99.73	98.98	99.55	99.48	99.12	99.13	99.22	99.30	99.32	98.61
$Fe^{3+}/(Fe^{3+}+Fe^{2+})$	.24	.34	.22	.27	.24	.24	.14	.20	.20	.20	.22	.17
Al/[K+Na+(Ca/2)]	1.00	1.00	.99	.93	.95	.94	1.01	1.12	1.07	1.06	1.07	.97
Q	15.44	14.50	14.45	14.14	20.70	20.79	19.18	24.26	20.87	20.74	21.64	16.79
Or	16.14	23.76	21.69	23.64	16.84	16.61	25.83	23.17	22.46	21.98	21.22	17.67
Ab	27.92	25.32	15.15	23.19	24.79	24.96	23.10	22.76	22.00	22.93	22.26	21.07
An	15.67	16.42	18.55	16.65	17.12	16.86	13.17	12.83	12.75	12.61	12.84	19.27
C	1.85	0.01	2.02	0.86	0.88	0.82	1.34	2.00	2.50	2.40	2.62	1.48
Di												
En												
Fs												
Wo												
Hy	13.22	10.15	18.47	11.83	12.21	12.41	10.86	9.83	11.64	11.63	11.41	14.48
En	7.25	6.23	10.91	6.87	7.65	7.74	4.66	5.33	6.25	6.15	6.05	7.37
Fs	5.98	3.92	7.57	4.96	4.56	4.67	6.20	4.50	5.39	5.48	5.36	7.11
Mt	2.84	3.96	3.13	3.09	2.09	2.12	1.39	1.54	2.03	2.10	2.19	2.00
Il	3.30	3.40	4.14	3.53	2.45	2.37	2.45	1.44	3.10	2.92	3.13	3.78
Ap	1.79	1.77	2.14	2.05	1.77	1.79	1.14	0.52	1.42	1.51	1.55	2.08
volatile loss	0.80	nd	nd	nd	0.70	0.75	0.66	0.78	0.46	0.46	0.46	nd
total	99.98	99.26	99.73	98.98	99.55	99.48	99.12	99.13	99.22	99.30	99.32	98.61
Trace Elements (in ppm)												
Y	20	31	29	30			29	10	18	17	18	29
Sr	837	715	592	907			399	1067	828	830	829	1040
Rb	139	125	157	140			158	112	128	128	129	141
Ba	1000	1409	979	1692	1716		1211	1645	1541			1640
Th	33	22	20	20			29	8	26	23	25	24
Pb	25	36	23	32			36	29	27	27	27	22
Ga	25	23	22	28			22	20	23	22	23	24
Nb	18	26	24	29	18		23	12	17			26
Zr	423	448	398	585	298		541	225	542			454
Zn	148	137	165	150	90		111	106	120			142
Ni	26	26	55	22	94		14	42	24			20
Cr	86	49	147	62	79		43	92	67			79
V	115	108	132	108	98		84	76	105			141
La	163	345	114	164	116		112	73				147
Ce	163	500	211	233	216		189	33	314			271

Table 27, continued.

	biotite-muscovite tonalite									biotite-garnet tonalite			mylonitized tonalite
Sample	A250-1	A251	B1	P233-1	P233-2	P233-3	A19	A119	T3	A54-1	A54-2	P43	FW922
SiO_2	63.59	62.51	61.20	59.21	59.29	59.19	63.21	60.55	62.49	62.92	63.21	63.64	55.84
TiO_2	1.34	1.48	1.55	1.64	1.67	1.67	1.34	1.70	1.70	0.92	0.90	0.73	1.80
Al_2O_3	15.83	15.27	16.45	16.61	16.63	16.64	15.56	15.49	14.49	17.80	17.89	18.13	17.69
Fe_2O_3	1.04	1.16	1.12	1.51	1.47	1.43	0.90	1.41	1.70	0.99	1.03	0.83	2.13
FeO	4.69	5.14	5.01	5.39	5.23	5.35	4.80	5.89	6.58	5.40	5.41	5.17	4.86
MnO	0.12	0.14	0.13	0.13	0.15	0.15	0.10	0.17	0.82	0.10	0.10	0.14	0.09
MgO	1.98	2.25	2.42	2.79	2.77	2.77	1.82	2.73	2.73	2.36	2.39	2.05	2.80
CaO	3.63	3.81	3.76	3.85	3.96	3.98	3.19	3.97	3.83	3.53	3.59	3.10	4.09
Na_2O	3.05	2.80	2.80	2.85	2.81	2.81	2.75	2.98	2.01	3.27	3.09	2.68	3.22
K_2O	2.91	2.53	4.27	3.86	3.97	3.99	4.46	2.95	2.76	2.56	2.72	4.15	5.46
P_2O_5	0.58	0.64	0.71	0.72	0.77	0.83	0.58	0.76	0.64	0.14	0.10	0.09	1.11
volatile loss	0.67	0.62	0.54	0.60	0.60	0.60	0.57	nd	0.68	0.41	nd	nd	0.79
total	99.43	98.35	99.96	99.17	99.32	99.44	99.28	98.60	100.44	100.40	100.43	100.65	99.87
$Fe^{3+}/(Fe^{3+}+Fe^{2+})$	.17	.17	.17	.20	.21	.19	.14	.17	.19	.14	.14	.13	.29
Al/[K+Na+(Ca/2)]	1.07	1.07	1.03	1.04	1.03	1.03	1.03	1.01	1.10	1.22	1.22	1.24	.96
Q	22.83	23.78	16.00	14.43	14.40	14.19	19.31	18.02	25.30	19.84	20.22	19.56	4.15
Or	17.20	14.95	25.23	22.81	23.46	23.58	26.36	17.43	16.31	15.13	16.12	24.46	32.21
Ab	25.81	23.69	23.69	24.17	23.78	23.78	23.27	25.22	17.01	27.67	26.29	22.53	27.25
An	14.00	15.14	14.48	14.87	15.12	14.86	12.42	15.23	15.24	16.69	17.24	14.46	13.76
C	2.31	2.38	1.93	2.29	2.17	2.25	1.66	1.81	2.61	3.53	3.62	3.93	1.45
Di													
En													
Fs													
Wo													
Hy	10.69	11.90	11.98	13.13	12.81	13.12	10.58	13.96	16.19	13.64	13.79	13.02	11.33
En	4.93	5.60	6.03	6.95	6.90	6.90	4.53	6.80	6.80	5.88	6.00	5.10	6.97
Fs	5.76	6.30	5.96	6.18	5.91	6.22	6.05	7.16	9.39	7.77	7.79	7.92	4.36
Mt	1.51	1.68	1.62	2.19	2.13	2.07	1.30	2.04	2.46	1.44	1.39	1.16	3.09
Il	2.54	2.81	2.94	3.11	3.17	3.17	2.54	3.23	3.23	1.75	1.67	1.37	3.42
Ap	1.27	1.40	1.55	1.57	1.68	1.81	1.27	1.66	1.40	0.31	0.24	0.20	2.43
volatile loss	0.67	0.62	0.54	0.60	0.60	0.60	0.57	nd	0.68	0.41	nd	nd	0.79
total	99.43	98.35	99.96	99.17	99.32	99.44	99.28	98.60	100.44	100.40	100.49	100.69	99.87
Trace Elements (in ppm)													
Y	26	22	31	24	26	25	25	30		24	23		
Sr	470	614	838	805	807	802	428	521	501	222	218		3026
Rb	153	121	140	132	130	134	169	135		106			
Ba	1273	1350	1566	2037			1280	978	1024	286	419		4026
Th	32	33	19	31	33	32	36	31		6			
Pb	32	24	33	35	35	35	37	25		22			
Ga	23	22	23	24	24	24	24	23		21			
Nb	25	18	22	24			24	27	19	11	10		17
Zr	591	644	497	619			575	552	333	161	158		711
Zn	128	132	126	142			126	132	110	95	98		135
Ni	15	20	24	24			13	27	25	22	19		15
Cr	53	67	67	68			45	78	31	39	43		23
V	89	104	104	122			88	105	130	73	101		130
La	129	118	89	84			102	109	59	17	19		155
Ce	237	232	178	252			203	293	121	33	43		276

Table 28. Whole rock analyses for the major and trace elements and calculated CIPW norms for samples of the Gray Schist Member of the Littleton Formation and the Augen Gneiss Member of the Partridge Formation.

	Littleton Formation					Partridge Formation		
Sample	Met140A	Met140B	Met140C	P398-1	P398-2	P280	A66-1	A66-2
SiO_2	59.05	59.04	59.29	55.03	54.84	66.42	68.93	68.41
TiO_2	1.52	1.51	1.51	1.49	1.45	0.99	0.73	0.72
Al_2O_3	19.42	19.44	19.47	21.96	21.89	15.77	16.13	15.98
Fe_2O_3	2.12	2.10	2.17	1.57	1.61	1.03	0.57	0.60
FeO	9.10	9.15	9.14	9.00	9.02	4.79	3.99	3.87
MnO	0.33	0.34	0.35	0.15	0.15	0.11	0.06	0.06
MgO	3.92	4.02	4.01	2.99	2.96	1.90	1.35	1.43
CaO	0.49	0.49	0.49	0.11	0.10	1.61	1.43	1.41
Na_2O	0.38	0.42	0.40	0.66	0.64	2.06	2.24	2.26
K_2O	2.68	2.67	2.69	5.60	5.54	2.89	4.10	3.99
P_2O_5	0.10	0.10	0.11	0.08	0.06	0.07	0.17	0.17
volatile loss	0.98	0.98	0.98	0.82	0.82	0.96	0.82	0.70
total	100.09	100.26	100.61	99.46	99.08	99.39	100.52	99.60
$Fe^{3+}/(Fe^{3+}+Fe^{2+})$	.17	.17	.17	.14	.14	.16	.12	.12
Al/[K+Na+(Ca/2)]	4.43	4.33	4.44	2.98	3.02	1.70	1.47	1.47
Q	33.99	33.58	33.93	19.33	19.47	32.32	32.94	32.75
Or	15.84	15.78	15.90	33.09	32.74	17.55	24.23	23.58
Ab	3.22	3.55	3.38	5.58	5.42	19.97	18.96	19.12
An	1.84	1.84	1.78	0.08	0.14	7.68	6.09	6.00
C	15.22	15.18	15.25	14.79	14.79	5.96	5.77	5.75
Di								
En								
Fs								
Wo								
Hy	22.82	23.22	23.13	20.49	20.49	11.43	9.12	9.09
En	9.76	10.01	9.99	7.45	7.37	4.80	3.36	3.56
Fs	13.06	13.21	13.15	13.05	13.12	6.63	5.76	5.53
Mt	3.07	3.04	3.15	2.28	2.33	1.49	0.83	0.87
Il	2.88	2.87	2.87	2.83	2.75	1.88	1.39	1.37
Ap	0.22	0.22	0.24	0.17	0.13	0.15	0.37	0.37
volatile loss	0.98	0.98	0.98	0.82	0.82	0.96	0.82	0.70
total	100.09	99.26	99.61	99.46	99.08	99.39	100.52	99.60
Trace Elements (in ppm)								
Y	45	45	46	38		18	18	22
Sr	69	69	70	110	105	121	121	286
Rb	125	125	125	200		165	164	123
Ba	420	681	612	862	864	445	591	589
Th								14
Pb								26
Ga	27	27	29	30		20	21	24
Nb	23	22	22	22	23	17	16	16
Zr	228	233	233	239	246	301	229	235
Zn	175	176	170	173	167	100	81	78
Ni	62	61	61	49	52	20	10	7
Cr	95	140	138	135	139	50	48	37
V	137	213	201	179	178	92	72	71
La	10	17	17	24	24	34	41	41
Ce	26	41	40	57	56	75	88	87

Major Element Characteristics

The SiO_2 content of the tonalite varies from 53 to 66% with a maximum frequency at approximately 59% SiO_2 (Figure 60). Within this range, the hornblende-biotite tonalite occurs at low values of SiO_2, the muscovite- and garnet-bearing tonalites occur at high values of SiO_2 and the biotite tonalite occurs at intermediate and overlapping values of SiO_2. The correlation between SiO_2 and other major and minor oxides is shown in Table 29. There is a strong negative correlation between SiO_2 and TiO_2, Fe_2O_3, MgO, CaO, and P_2O_5, a moderate negative correlation between SiO_2 and FeO, and a weak to virtually nonexistent correlation between SiO_2 and Al_2O_3, MnO, Na_2O and K_2O.

The $Na_2O/(Na_2O+K_2O)$ ratio of the tonalites ranges from 0.55 to 0.33 and appears to be independent of rock type (Figure 61a). This ratio does, however, discriminate between the tonalite and the metamorphosed sedimentary country rock with the country rock possessing lower $Na_2O/(Na_2O+K_2O)$ ratios (Figure 61b). The distribution of Na_2O and K_2O in the tonalites does not correspond to the "I- and S-type" characterization observed in the Berridale batholith (White et al., 1977) and the Kosciusko batholith (Hine et al., 1978) in eastern Australia. This lack of correspondence appears to be typical for the granitoids in central Massachusetts (Maczuga, 1981; Robinson and Shearer, 1981).

Although more potassic than the "I-type" granitoids from eastern Australia (Chappell and White, 1974) and the Sierra Nevada (Wones, (1980), the Hardwick Tonalites have similar CaO contents. These CaO contents appear to be typical of plutonic and volcanic rock produced in convergent tectonic environments (Wones, 1980; Maaloe and Petersen, 1981). The characteristic P_2O_5 content for most of the tonalites is anomalously high compared to the previously mentioned granitoids and the metamorphic country rock analysed in this study. A restitic origin for the apatite is suggested (Watson, 1979, 1980).

The ratio Al/(K+Na+(Ca/2)) ranges from .73 to 1.24 (Figure 62a) and encompasses both the "I- and S-type" character of the granitoids of eastern Australia (Chappell and White, 1974). After a large P_2O_5 correction for apatite, corundum is present in the normative mineralogy of most of the tonalites (Figure 62b). Based upon 71 analyses, the Hardwick Tonalite appears to be zoned from a diopside normative interior to a corundum normative perimeter (Figure 63). This zoning pattern corresponds with the metaluminous to peraluminous mineralogical zoning (Shearer, 1983). In rocks not possessing a peraluminous mineralogy, i.e. hornblende-biotite tonalite and biotite tonalite, the Al-Al substitution in biotite contributes to the amount of corundum in the norm.

The relationship between tonalite geochemistry and mineralogy can be partially represented in an ACF diagram (Figure 64). "I-type" granitoids are defined by the area plagioclase-biotite-hornblende, whereas the "S-type" granitoids are defined by the area plagioclase-biotite-muscovite or plagioclase-biotite-cordierite (Chappell and White, 1974; Chappell, 1978). The plagioclase-biotite tie line separates the two regions, although because of the A/(A+F) ratio of the biotite, the plagioclase-biotite assemblage defines an intermediate area and not a single tie line. The plot illustrates the gradational and overlapping

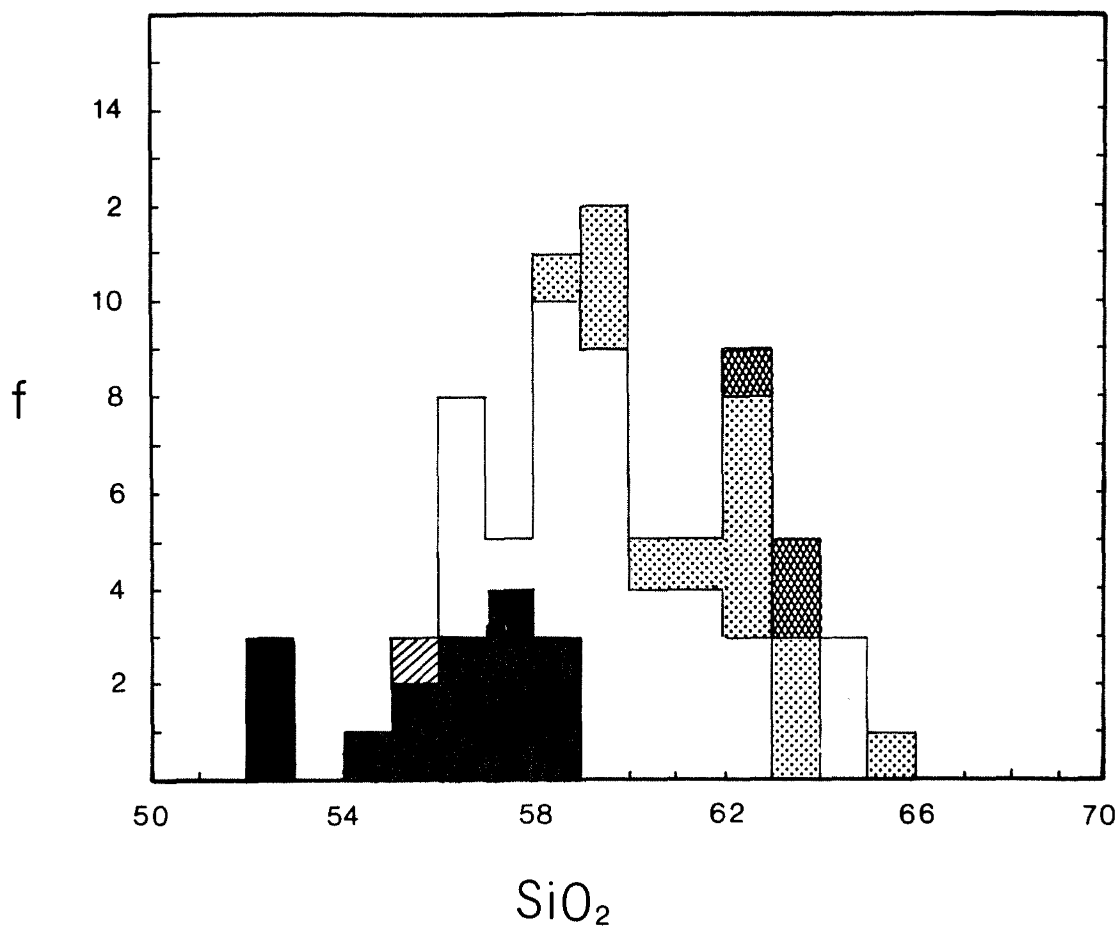

Figure 60. Frequency diagram of the SiO_2 content in subdivisions of the Hardwick Tonalite. hornblende-biotite tonalite (black) biotite tonalite (white), biotite-muscovite tonalite (dotted), biotite-garnet tonalite (cross-hatched), mylonite (diagonal lines)

Table 29. Correlation coefficient matrix for the major elements in the Hardwick Tonalite. Correlation coefficients with absolute values more than 0.85 are underlined.

	SiO_2	TiO_2	Al_2O_3	Fe_2O_3	FeO	MgO	MnO	CaO	Na_2O	K_2O	P_2O_5
SiO_2	1.00										
TiO_2	-0.80	1.00									
Al_2O_3	0.16	-0.20	1.00								
Fe_2O_3	-0.88	0.68	-0.39	1.00							
FeO	-0.55	0.68	-0.11	0.32	1.00						
MgO	-0.85	0.53	-0.33	0.87	0.42	1.00					
MnO	-0.20	0.31	-0.45	0.29	0.46	0.22	1.00				
CaO	-0.92	0.73	-0.36	0.89	0.45	0.91	0.24	1.00			
Na_2O	0.20	-0.29	0.34	-0.13	-0.49	-0.37	-0.34	-0.22	1.00		
K_2O	0.08	-0.06	0.15	-0.11	-0.35	-0.22	-0.24	-0.26	0.04	1.00	
P_2O_5	-0.82	0.90	-0.29	0.69	0.49	0.58	0.22	0.77	-0.16	0.06	1.00

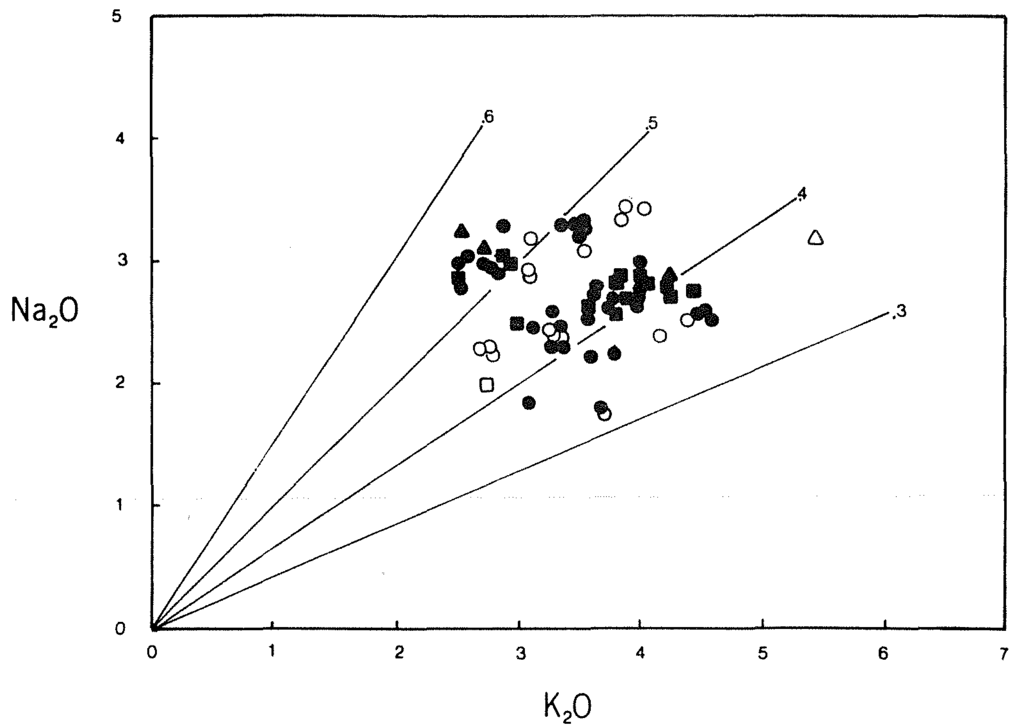

Figure 61a. Plot of Na_2O versus K_2O for the various rock types of the Hardwick Tonalite. hornblende-biotite tonalite: open circles, biotite tonalite:dark circles, biotite-muscovite tonalite:dark squares, biotite-garnet tonalite:dark triangles, and tonalite mylonite:open triangle. Lines representing Na_2O/Na_2O+K_2O ratios are plotted.

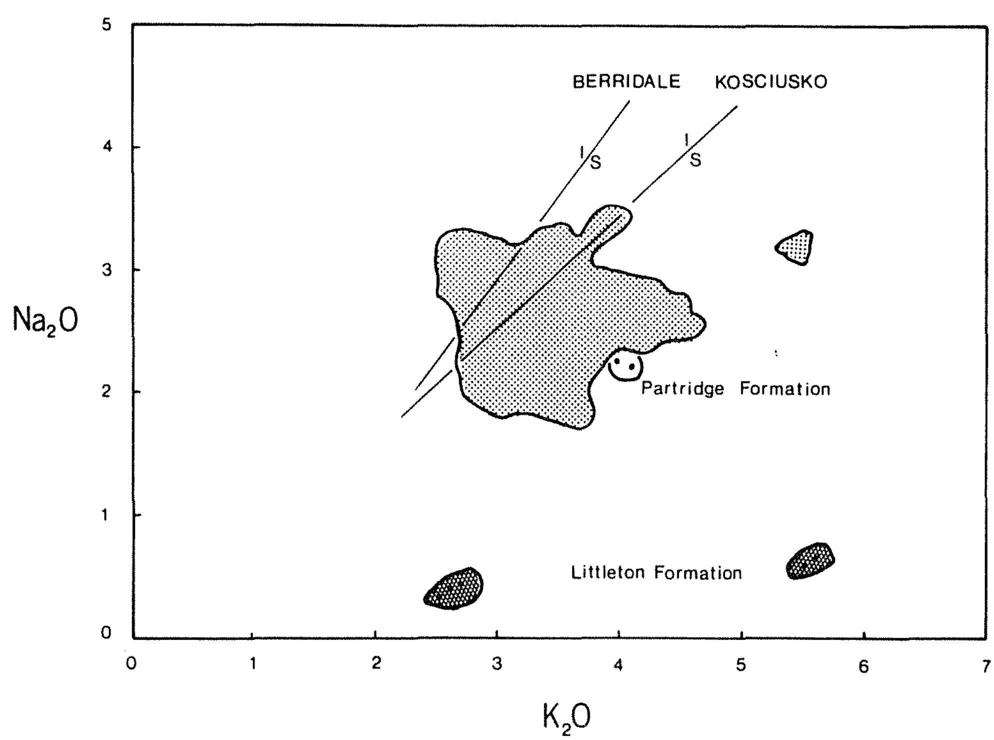

Figure 61b. Distribution of Hardwick Tonalite in Na_2O and K_2O compared to local metamorphic rocks and I and S granitoids.

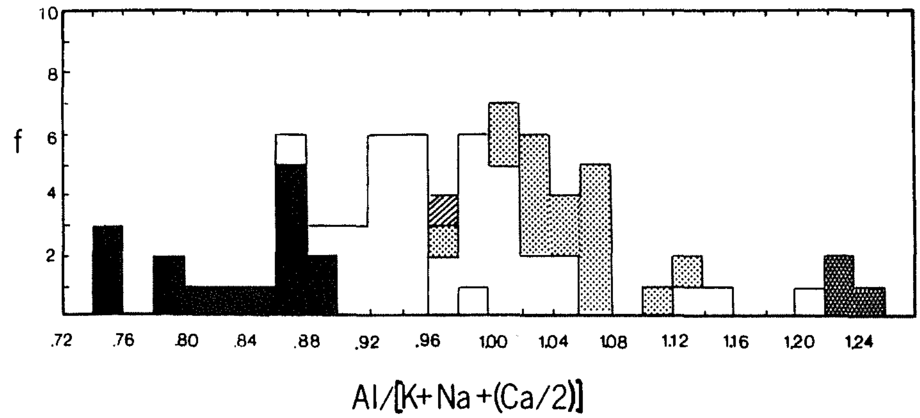

Figure 62a. Frequency diagram illustrating variation in Al/K+Na+(Ca/2) within the Hardwick Tonalite and with rock type. f=frequency, hornblende-biotite tonalite (black) biotite tonalite (white), biotite-muscovite tonalite (dotted) biotite-garnet tonalite (cross hatched) mylonite (stripe)

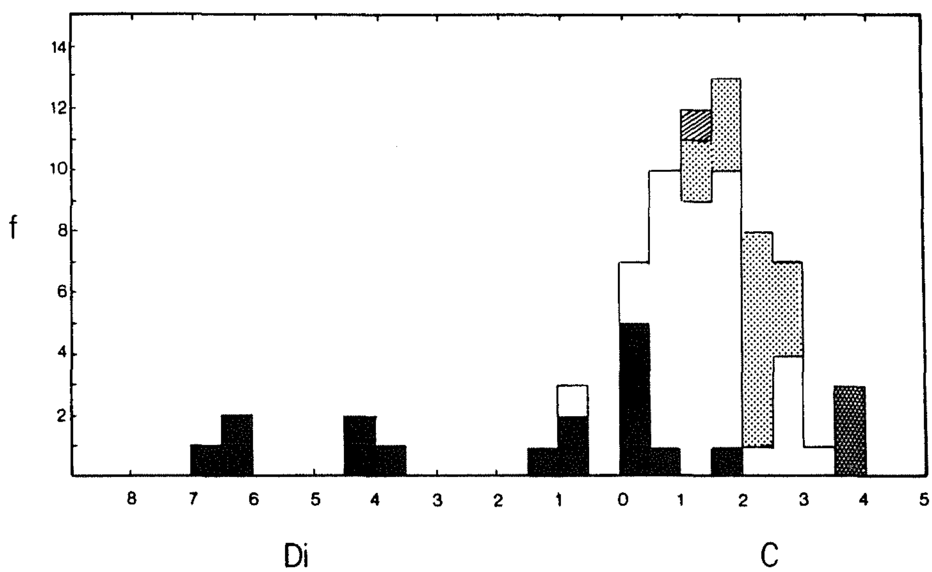

Figure 62b. Frequency diagram illustrating the variation in normative diopside (Di) and corundum (C) within the Hardwick Tonalite and with rock type.

Figure 63. Hardwick Tonalite contoured with % normative diopside and corundum. Dotted pattern: 8% diopside to 1% corundum, white: 1% to 2% corundum, and black: greater than 2% corundum.

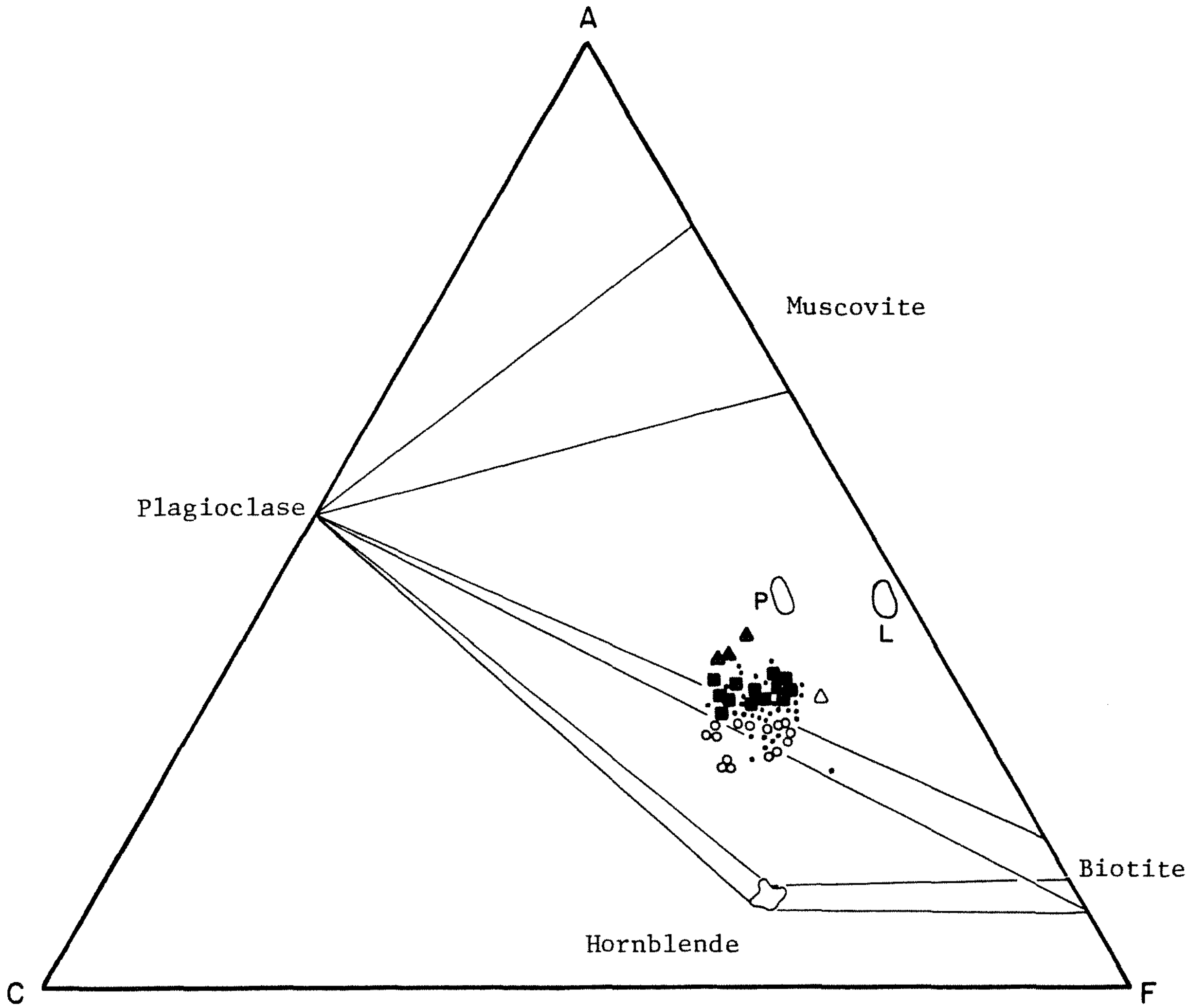

Figure 64. Whole rock analyses of the Hardwick Tonalite, Littleton Formation (L) and Partridge Formation (P) plotted in a ACF diagram. Microprobe analyses of hornblende, biotite and muscovite from the Hardwick Tonalite are also plotted. Rock type symbols: hornblende-biotite tonalite (○), biotite tonalite (●), biotite-muscovite tonalite (■), biotite-garnet tonalite (▲), tonalite mylonite (△).

mineralogical-geochemical character of the rocks, which range from a hornblende-biotite-plagioclase assemblage to a biotite-muscovite-plagioclase assemblage. A majority of the analyses plot within the plagioclase-biotite and biotite-muscovite-plagioclase fields.

In an Alk-total Fe-MgO plot, the trend of the tonalites is distinctively calc-alkaline in nature (Figure 65). Similar to the southern California batholith (Figure 65) and other intrusions of modern continent-ocean convergence zones, the tonalite exhibits a relative alkali enrichment accompanied by an iron depletion. There is a considerable amount of overlap, although the hornblende-biotite tonalites are usually higher in MgO and lower in alkalies than the other tonalite units.

Trace Element Characteristics

Hornblende-biotite tonalite, biotite tonalite and biotite-muscovite tonalite contrast with the biotite-garnet tonalite and the local metamorphic country rocks in being strongly enriched in the moderately lithophile elements (LIL) such as Sr and Ba, the LREE such as La and Ce, and the high field strength (HFS) trace elements Zr and Nb. Such enrichments correspond with high K_2O, P_2O_5 and TiO_2 contents in the major element analyses.

Differences in the LIL elements between the tonalite subdivisions and the analyzed metamorphic rocks are illustrated in plots of Rb against Sr (Figure 66a), Rb against K_2O (Figure 67a), Rb against Ba (Figure 68a) and Sr against Ba (Figure 69a). In Figure 66a, the hornblende-biotite tonalite defines a near linear distribution at a near constant ($\approx$0-1), magmatically more primitive Rb/Sr ratio. The metamorphic country rocks plot at higher Rb/Sr ratios and the biotite tonalites, biotite-muscovite tonalites and biotite-garnet tonalites plot between these extremes. Figures 67a to 69a show that the biotite tonalite, biotite-muscovite tonalites and garnet-biotite tonalites occupy a similar position between the fields for country rock and the hornblende-biotite tonalites, although Rb/Ba and Sr/Ba show some exceptions.

In Figure 70, Rb, K, Sr, P, Nb, Zr and Ti in the tonalites and the Augen Gneiss Member of the Partridge Formation are normalized to Littleton Formation schist sample Met 140A. Normalized patterns for the hornblende-biotite tonalite, biotite tonalite and biotite-muscovite tonalite are typified by P, Sr, and Zr enrichments. In addition to the previously noted differences in K and Rb, the biotite and biotite-muscovite tonalites are also commonly enriched in Zr compared to the hornblende-biotite tonalite. The biotite-garnet tonalite and the augen gneiss of the Partridge Formation contrast with the other tonalites with only slight enrichments of Sr and P and depletions of Nb, Zr and Ti.

The hornblende-biotite tonalite, biotite tonalite and biotite-muscovite tonalite are strongly enriched in LREE with La 200 to 580 times chondritic abundance and Ce 150 to 400 times chondritic abundance. This contrasts with the LREE of the biotite-garnet tonalite which has an La content of

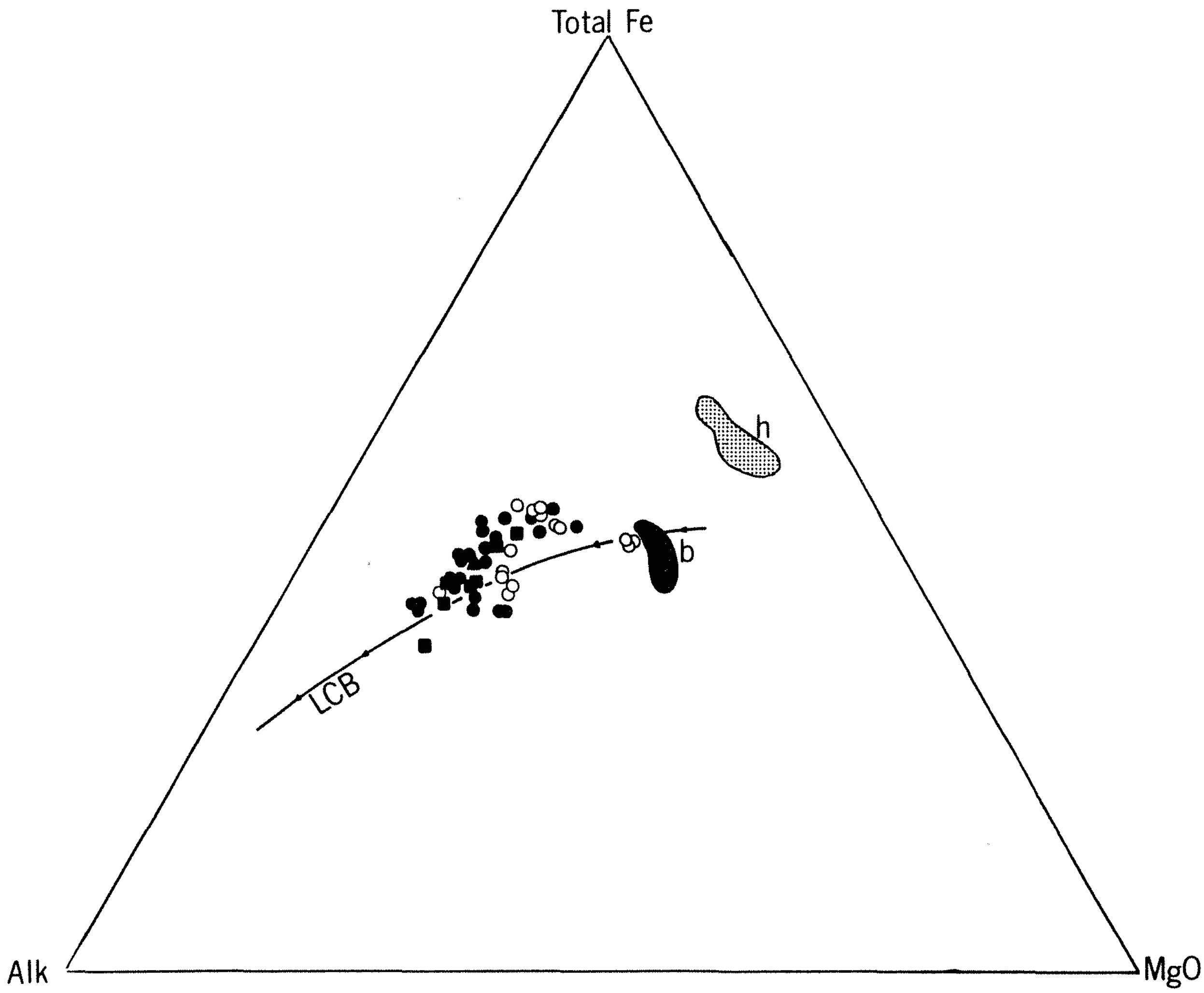

Figure 65. Hardwick Tonalite analyses plotted within a AFM diagram. Also plotted are microprobe analyses of biotite (b) and hornblende (h) from the tonalite and a generalized AFM trend of the lower California batholith (LCB).

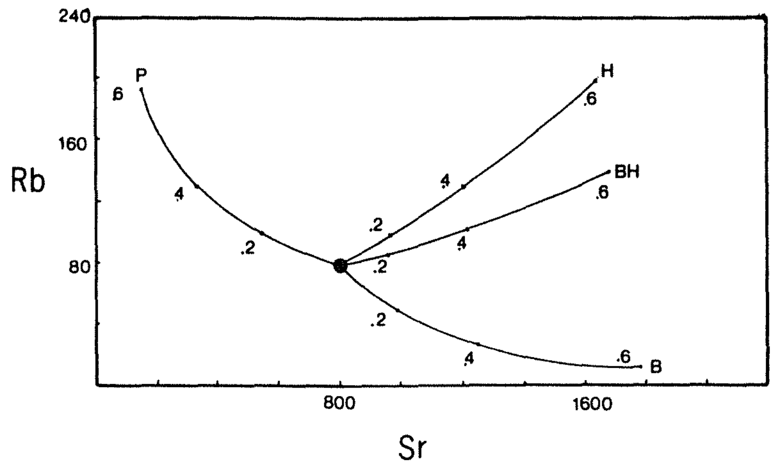

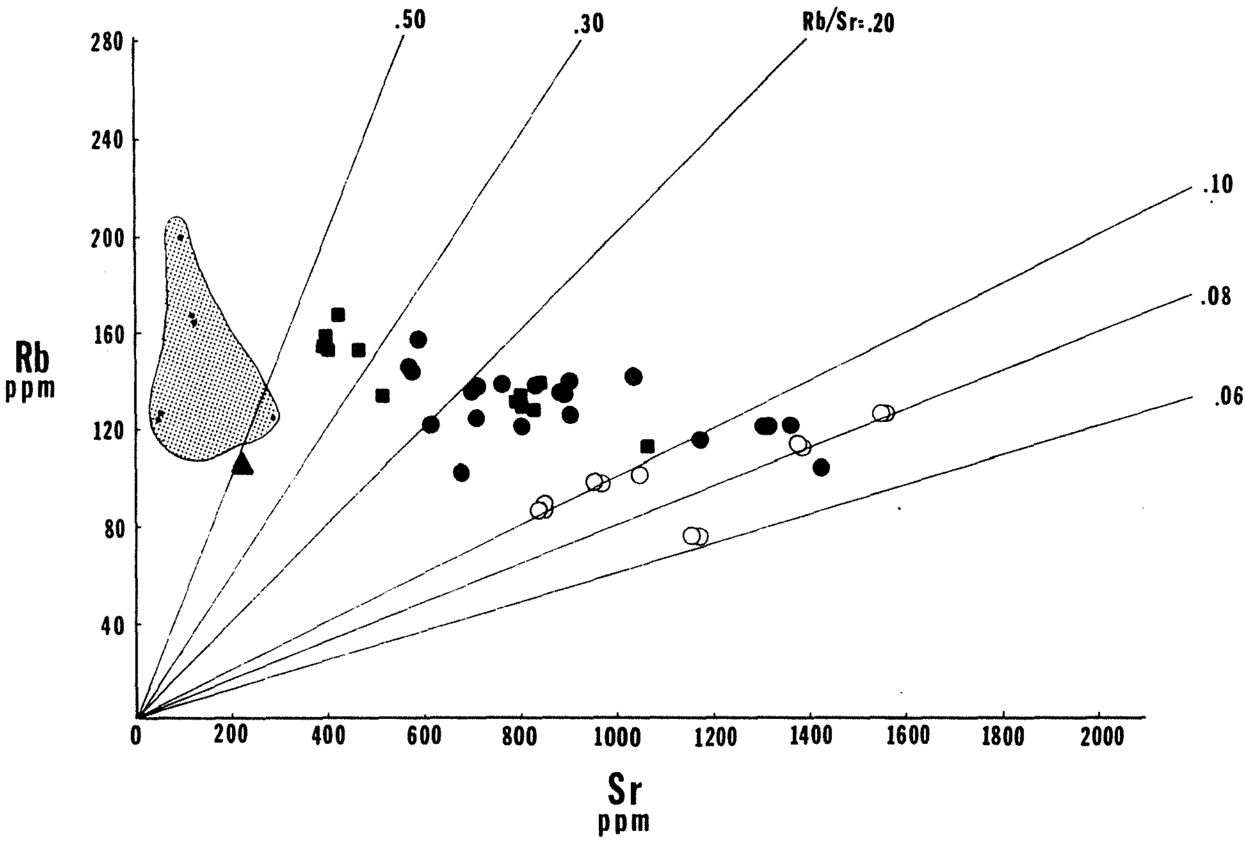

Figure 66. (a) Plot of Rb versus Sr for the Hardwick Tonalite and local metamorphic rocks (dotted shading). (b) insert, plot of vectors which indicate the change in Rb and Sr with fractional removal of biotite (B), hornblende (H), hornblende and biotite in a biotite/biotite + hornblende ratio of 0.33 (BH) and plagioclase (P). Symbols (also in Figures 67, 68, 69) hornblende-biotite tonalite (○), biotite tonalite (●), biotite-muscovite tonalite (■), and biotite-garnet tonalite (▲).

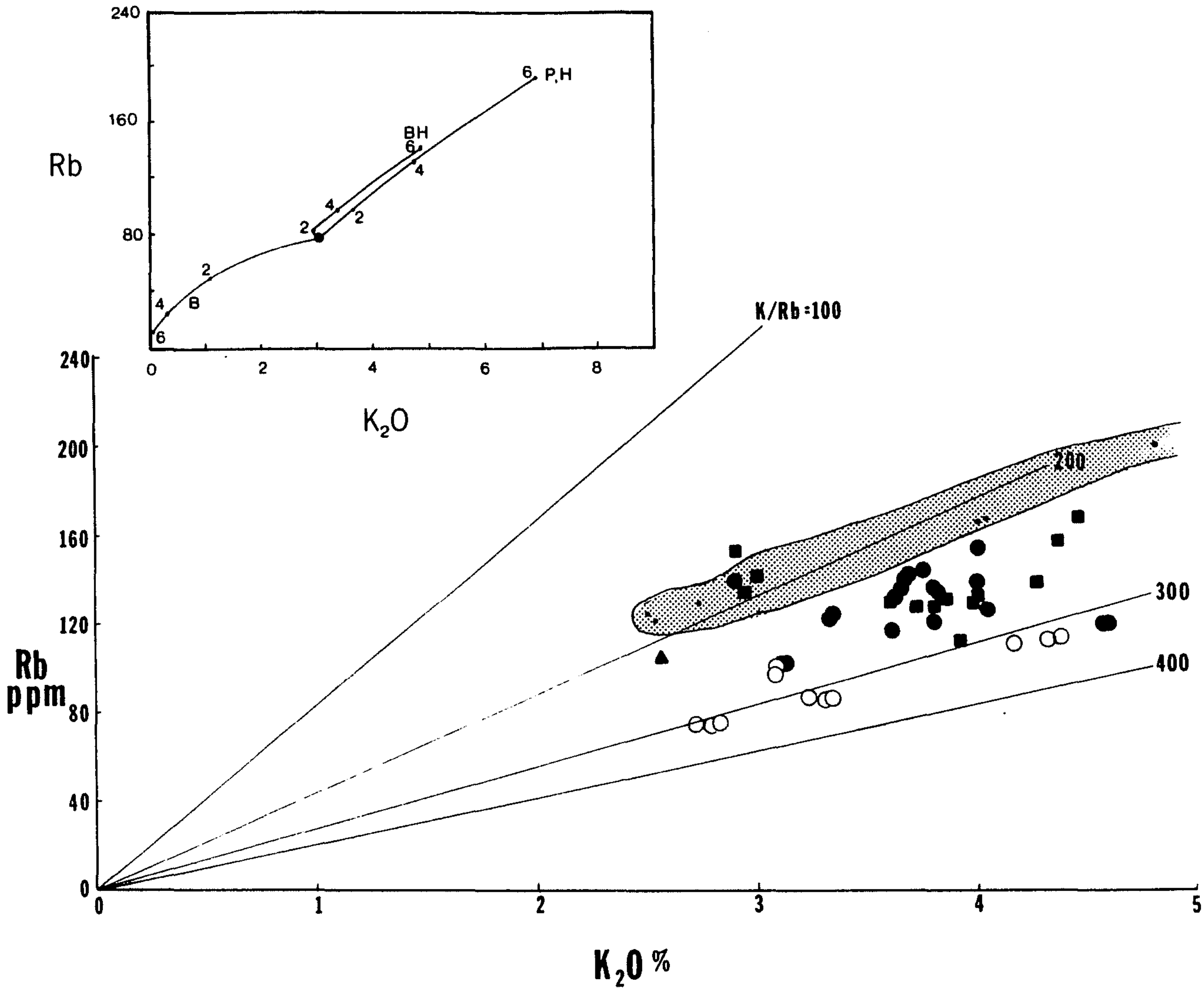

Figure 67. (a) Plot of Rb versus K_2O for the Hardwick Tonalite and local metamorphic rocks (dotted shading). (b) insert, plot of vectors which indicate the change in Rb and K_2O with fractional removal of biotite (B), hornblende (H), hornblende and biotite in a biotite/biotite+hornblende ratio of 0.33 (BH) and plagioclase (P).

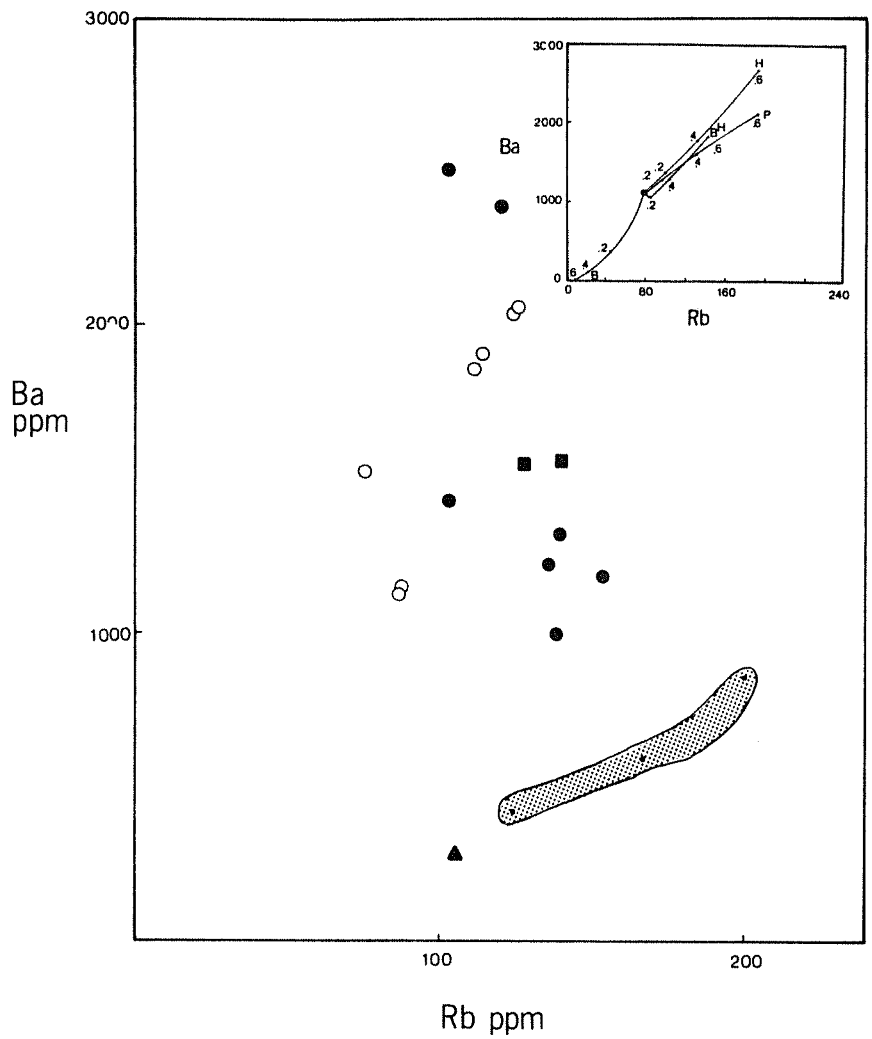

Figure 68. (a) Plot of Rb versus Ba for the Hardwick Tonalite and local metamorphic rocks (dotted shading). (b) insert, plot of vectors which indicate the change in Rb and Ba with fractional removal of biotite (B), hornblende (H), hornblende and biotite in a biotite/biotite + hornblende ratio of 0.33 (BH) and plagioclase (P).

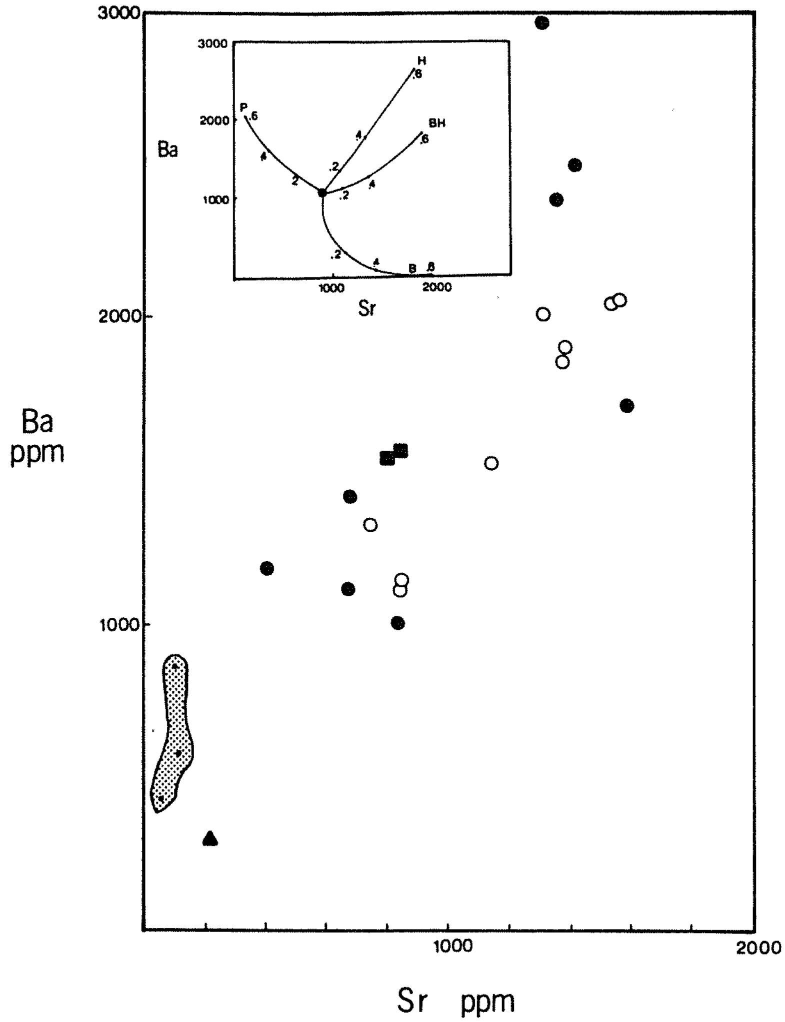

Figure 69. (a) Plot of Sr versus Ba for the Hardwick Tonalite and local metamorphic rocks (dotted shading). (b) insert, plot of vectors which indicate change in Sr and Ba with the fractional removal of biotite (B), hornblende (H), hornblende and biotite in a biotite/biotite+hornblende ratio of 0.33 (BH) and plagioclase (P).

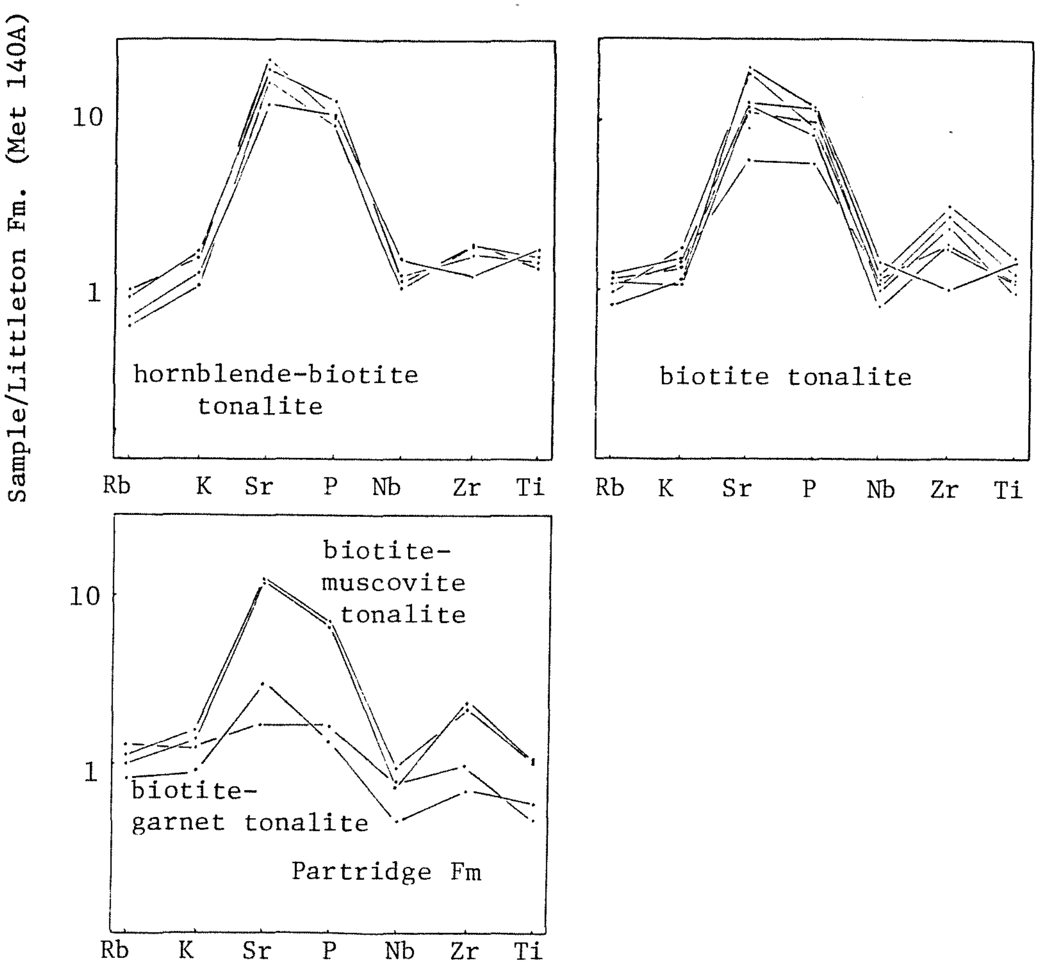

Figure 70. Pl t of Rb, K, Sr, P, Nb, Zr, and Ti from the tonalites normalized to L'ttleton schist sample Met 140A.

53 times chondritic abundance and a Ce content of 40 times chondritic abundance. In the metamorphic country rock, the schist of the Littleton Formation has a La content of 30 to 76 times chondritic abundance and a Ce content of 33 to 70 times chondritic abundance while the Augen Gneiss Member of the Partridge Formation has a Ce content of 108 times chondritic abundance. La content in the Augen Gneiss Member was not determined.

In summary, the trace element data has identified two groups of tonalites which have different geochemical characteristics. The hornblende-tonalite, biotite tonalite and much of the biotite-muscovite tonalite are enriched in many of the incompatible elements such as the LIL, LREE and the HFS. The biotite-garnet tonalite and some of the biotite-muscovite tonalite (e.g. M5, A19) have high Rb contents, but are relatively depleted in most of the other incompatible elements and have an affinity to the local metamorphic rocks, particularly the augen gneiss.

DISCUSSION

The plot of SiO_2 against normative corundum/diopside in Figure 71 shows a trend of increasing SiO_2 with decreasing normative diopside/increasing normative corundum. The plot differentiates the tonalite subdivisions into a diopside normative-low SiO_2 division which includes primarily hornblende-biotite tonalite, a corundum-normative intermediate SiO_2 division which consists primarily of biotite tonalite, and a corundum-normative high SiO_2 division which consists primarily of the muscovite- and garnet-bearing tonalites. A bend in the distribution occurs at 57% SiO_2 and 1% normative corundum. This trend appears to be typical of calc-alkaline intrusions (Stephens and Halliday, 1979) and has been attributed to epidote fractionation (E-an Zen, personal communication), amphibole fractionation (Ringwood, 1974; Cawthorn and O'Hara, 1976; Cawthorn et al., 1976; Abbott, 1981), contamination of a diopside normative magma by aluminous sediments during ascent or emplacement (Presnall and Bateman, 1973; Brown, 1973; Hildreth, 1981), partial melting in a diopside normative source with variable amounts of amphibole in the residual (Helz, 1976), vapor transfer of alkalis (Luth et al., 1964) and partial melting in a heterogeneous source which contains both metaluminous and peraluminous materials (Shearer, 1981, 1982).

Fractional Crystallization

Fractionation of a diopside normative phase would produce a peraluminous magma from a metaluminous parent magma. In Figure 72a, magmatic phases in the tonalite are plotted and compared to the tonalite trend. Epidote was not considered due to its metamorphic origin in the tonalite. The fractional removal of biotite and hornblende in a biotite/biotite + hornblende ratio of .33 is the best approximation of the tonalite trend (Figure 72B). Fractional removal of plagioclase in addition to biotite and hornblende would also produce a similar trend, but at lower biotite/biotite + hornblende ratios.

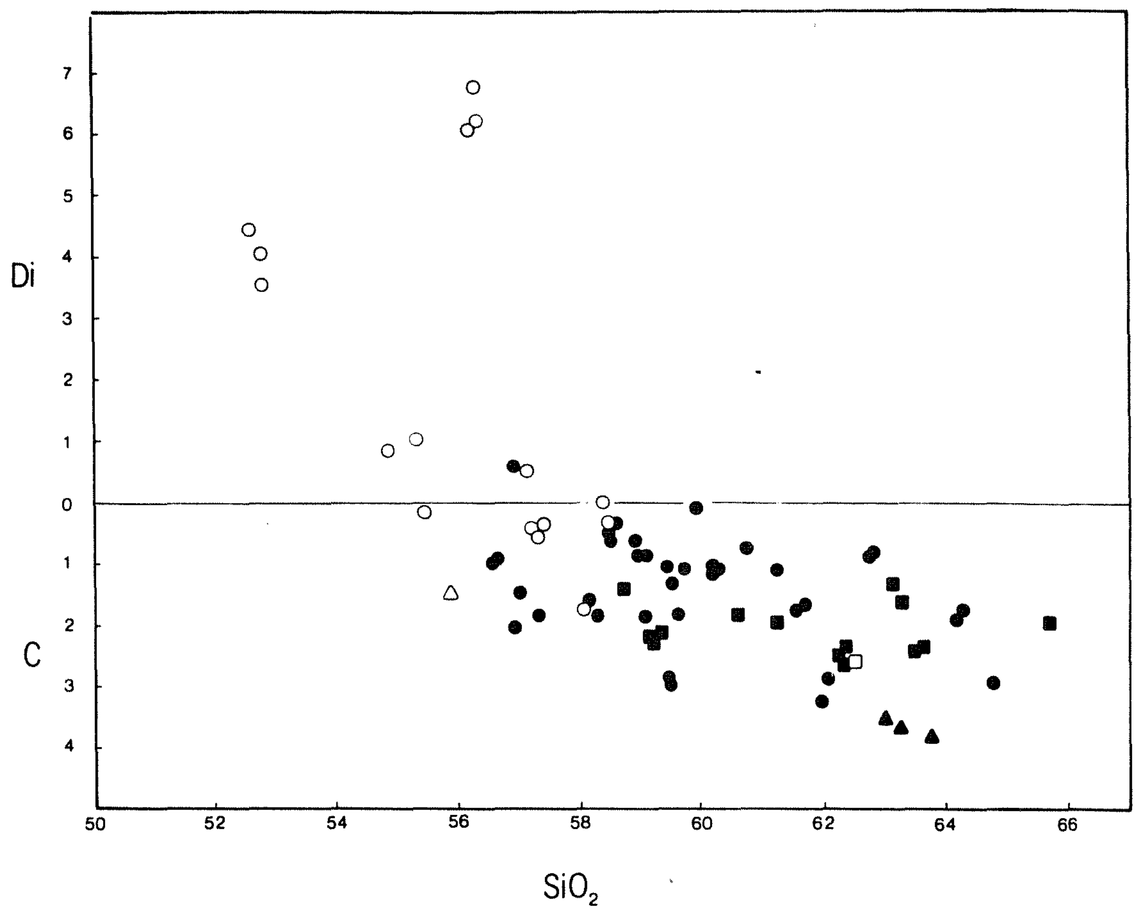

Figure 71. Plot of normative diopside (Di) and normative corundum (C) versus weight percent SiO_2 for the Hardwick Tonalite. hornblende-biotite tonalite (○), biotite tonalite (●), biotite-muscovite tonalite (■), biotite-garnet tonalite (▲), mylonite (△), tonalite matrix in an "intrusive breccia" (□).

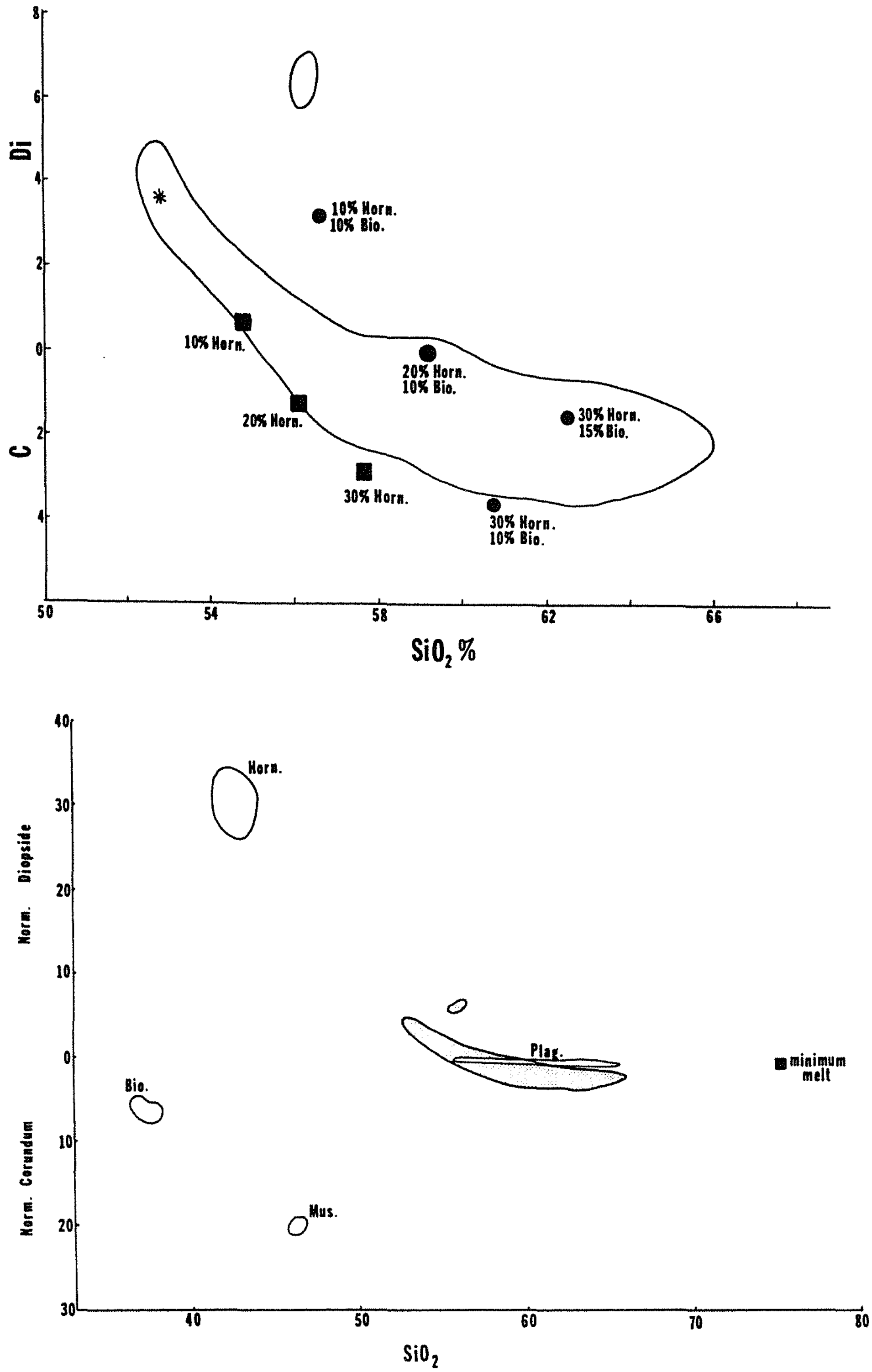

Figure 72. (a) Plot of normative diopside and normative corundum versus weight percent SiO_2 for the Hardwick Tonalite and magmatic mineral phases in the tonalite. Also plotted is the composition of a minimum melt derived from an "S-type" source (Chappell and White, 1974). (b) Model for the Hardwick Tonalite variability in normative mineralogy and SiO_2 by fractional removal of horn-blende and/or biotite from a hypothetical parent magma(*).

Evaluation of variations of Rb/Sr, K/Rb, Ba/Rb and Ba/Sr ratios with consideration of mineral/melt distribution coefficients allows appraisal of the previously mentioned processes. Mineral/melt distribution coefficients for biotite, hornblende, plagioclase and potassic feldspar (Hanson, 1978; Arth, 1976) were used as suggested by Hanson (1978) to evaluate fractional cystallization. In a plot of Rb against Sr (Figure 66b), the hornblende-biotite tonalites define a trace element distribution commensurate with hornblende fractionation or the removal of hornblende and minor amounts of biotite. Vectors constructed from feldspar/melt distribution coefficients suggest plagioclase dominated fractionation could account for the trace element array of biotite and biotite-muscovite tonalites in the Rb/Sr diagram. K-Rb (Figure 67b), Ba-Rb (Figure 68b) and Ba-Sr (Figure 69b) exhibit a similar hornblende fractionation pattern for the hornblende-biotite tonalite, but are not compatible with plagioclase fractionation for the production of the other tonalites.

Contradicting the hornblende fractionation model, tonalite modes show the biotite/(biotite + hornblende) ratios exceed 0.60 and usually are greater than 0.80 (Figure 73). This suggests either that tonalites with biotite/(biotite + hornblende) ratios of less than 0.33 are not exposed at present erosional levels or that hornblende fractionation is not responsible for the total compositional variation in the tonalite.

In summary, the array of tonalite compositions can be explained by fractional removal of hornblende + biotite ± plagioclase from a metaluminous melt and contamination or mixing of that melt with a peraluminous material.

Contamination With a Peraluminous, Reduced Component

The plot of an oxidation index ($2Fe_2O_3/(2Fe_2O_3 + FeO)$) against normative corundum/diopside in Figure 74 shows a trend of increasing "reduction" with increasing normative corundum. This geochemical variation is shown by the metaluminous to peraluminous variations in the silicate mineralogy and the accompanying transition from a magnetite-ilmenite-sphene assemblage to an ilmenite assemblage. Although varying the degree of partial melting and thereby the amount of amphibole in the residual of a metaluminous source may result in melts of variable normative mineralogy (Helz, 1976), variations in f_{O_2} should not necessarily result.

The analyzed samples of the Littleton and Partridge Formations contain high amounts of corundum in their norms and have oxidation indices equal to the more reduced tonalites (Figure 75). According to Chappell and White (1974) melts derived from sedimentary source material contain greater than 1% normative corundum. Melts derived from pelitic rocks similar to those analyzed in this study contain up to 8% normative corundum (Thompson and Tracy, 1978). The aluminous character of the melts that could be derived from the country rocks indicate they could not have been the parent material, although the country rock may have been a contributing contaminant.

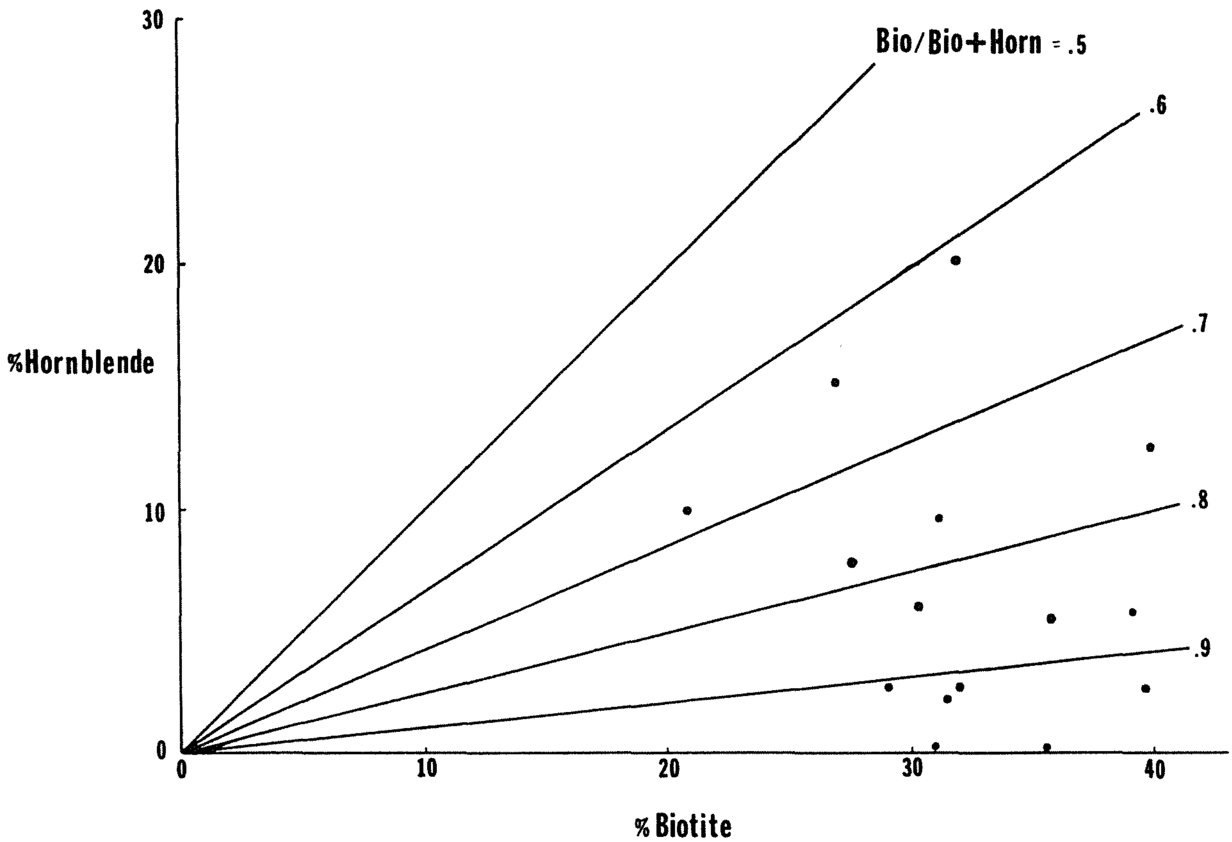

Figure 73. Plot of modal hornblende versus modal biotite for the hornblende-biotite tonalite.

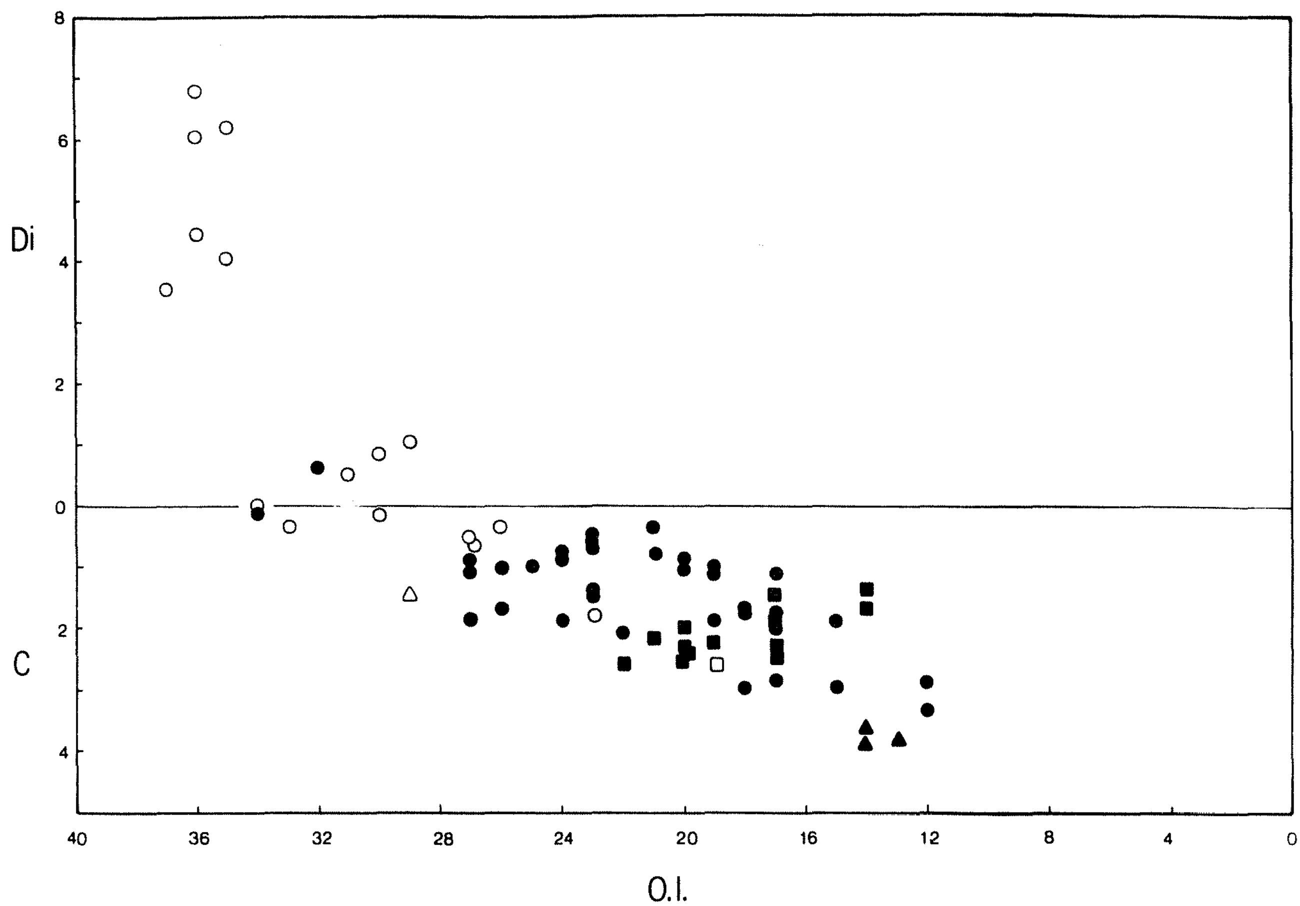

Figure 74. Plot of an oxidation index (O.I.=$Fe^{3+}/(Fe^{3+} + Fe^{2+})$ versus normative diopside (Di) and corundum (C) for the Hardwick Tonalite. hornblende-biotite tonalite (○), biotite tonalite (●), biotite-muscovite tonalite (■), biotite-garnet tonalite (▲), mylonite (△), tonalite matrix in "intrusive breccia" (□).

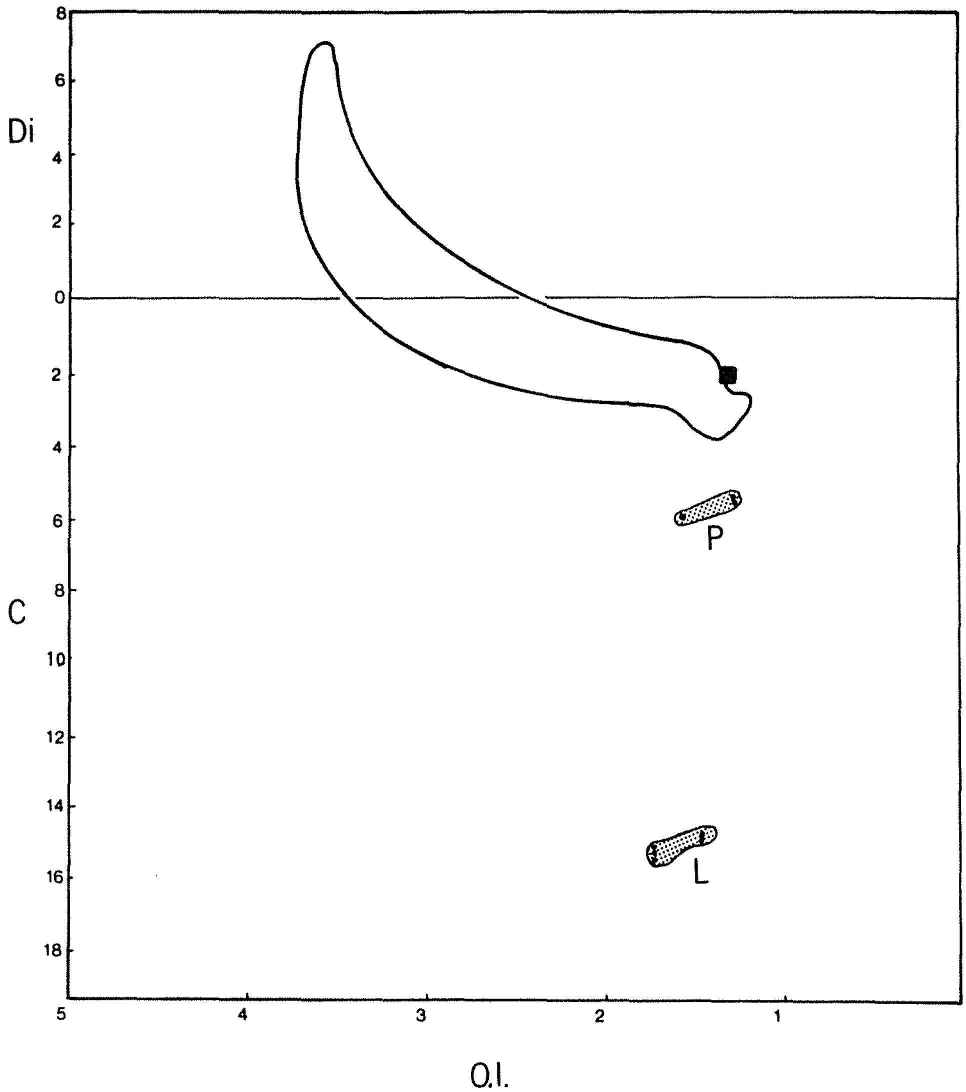

Figure 75. Comparison of the variation in the oxidation index (I.O.) and normative diopside (Di) and corundum (C) of the Hardwick Tonalite with the Littleton (L) and Partridge (P) Formations and a minimum melt derived from a "S-type" source (shaded square).

The mixing of a diopside-normative, hornblende-bearing material/melt with corundum-normative material/melt producing an array of tonalites of intermediate compositions is supported by the Rb, Ba, Sr and K_2O plots (Figures 66, 67, 68, 69). The effect of hornblende fractionation with contamination from a peraluminous component is schematically summarized in Figure 76.

The mixing of a diopside-normative, oxidized melt with a corundum-normative reduced melt/material can produce many of the geochemical characteristics of the Hardwick Tonalite. The mixing may have occurred either in situ or within the source region.

In situ Contamination Versus Mixing Within Source Region

Discrimination between the two mixing models can be partially evaluated with the present data. Two geochemically distinct tonalite groups can be distinguished. The biotite-garnet tonalite is characteristically similar geochemically to the metamorphic country rock (Figure 70), particularly the augen gneiss of the Partridge Formation. In addition to this similarity, the close proximity to the tonalite-country rock contact suggests in situ contamination was a major factor in the genesis of the biotite-garnet tonalite. Hornblende-biotite, biotite, and biotite-muscovite tonalites are characteristically enriched in HFS elements (Figure 70), LREE, and some LIL elements such as Sr (Figure 70) indicating a small country rock mixing component. Particularly evident is the the enrichment of Zr from hornblende-biotite to the biotite and biotite-muscovite tonalite. Mixing of a hornblende-biotite tonalite with a country rock component would have the opposite effect. In addition, the ratio of hornblende-biotite tonalite : biotite tonalite : biotite-muscovite tonalite: biotite-garnet tonalite at the present erosional level (11:77:9:3) suggests a high proportion of peraluminous-reduced material was added to the hornblende-biotite tonalite to produce the intermediate tonalites. Melting in a heterogeneous source region could perhaps be more efficient in mixing a high proportion of two end-members than in situ contamination.

The metaluminous to peraluminous zoning from the interior to the perimeter is partially an effect of the tonalite-country rock interaction at the immediate contact, but the zoning may also be attributed to compositional gradients during initial melting (Wones, 1980). The zoning character is the reverse of many of the Sierra Nevada plutons (Bateman and Chappell, 1979); Wones, 1980).

Oxidized Metaluminous Source

The oxidized-metaluminous and reduced-peraluminous sources indicated by the major element analyses correspond with the "I- and S-type" sources, respectively, of Chappell and White (1974). Although the SiO_2 and CaO contents and the high K/Rb and low Rb/Sr ratios are suggestive of a basaltic source for the metaluminous tonalites, the high K_2O, Rb, Sr, Ba and LREE contents compared to the average Archaean basalt (Hart et al.,

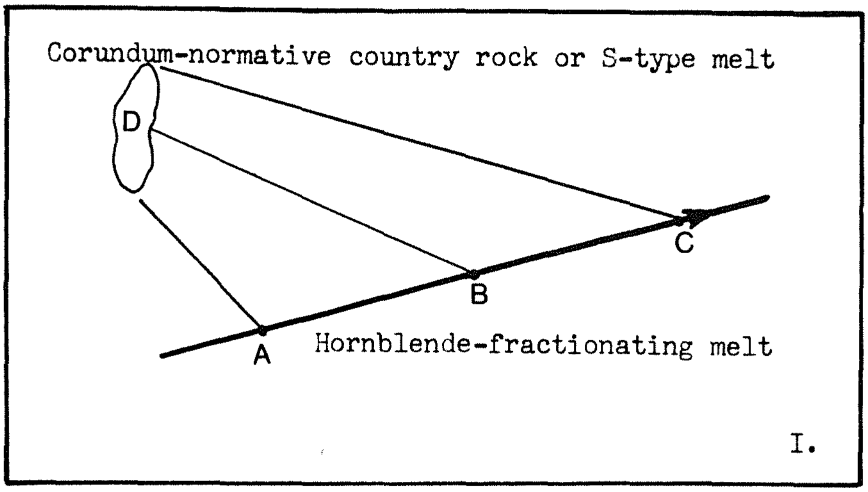

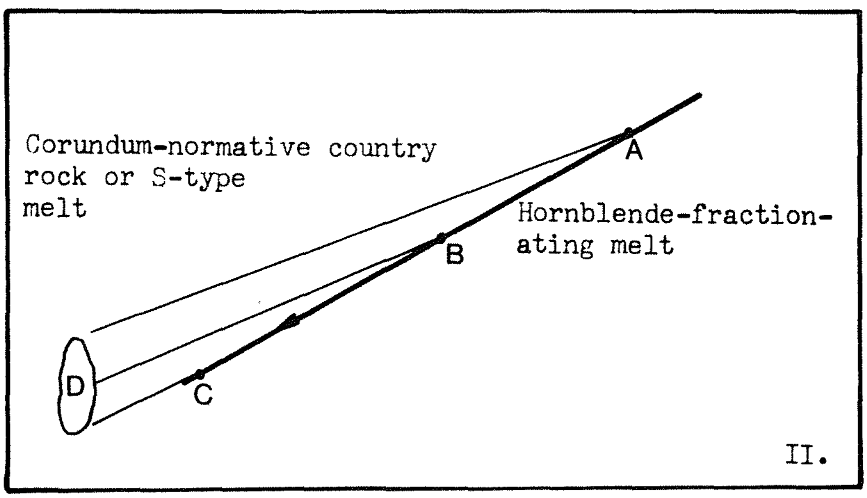

Figure 76. Illustration of trace element variability resulting from the contamination or mixing of a hornblende fractionating melt (A, B, C) with country rock or a minimum melt derived from an "S-type" source. Example I is analogous to Rb versus Sr and example II is somewhat similar to Ba versus Sr.

1970) indicate that neither a basaltic liquid modified by fractional crystallization nor partial melts derived from a basaltic source rock are acceptable parent material for the tonalite (Hanson, 1978).

Although trace element data suggests a basaltic or even a primitive andesitic source may not be suitable as a source for the metaluminous tonalite, basalt or andesite enriched in incompatible elements through participation in the weathering cycle or in sea water alteration is an acceptable alternative. Bohlhe et al. (1981) noted phosphate and Sr enrichment during sea water alteration of basalts. Involvement in a weathering environment would lower the $Na_2O/(Na_2O+K_2O)$ ratio (Chappell and White, 1974), and increase the HFS element content (Hine et al., 1978; White, personal communication). The commonly mobile LIL elements (e.g. Sr, Rb) could be transported during low temperature hydrothermal alteration or weathering of the volcanics (Tarney and Saunders, 1979).

Reduced Peraluminous Source

The reduced, peraluminous source for the tonalites contrasts with the country rock surrounding the Hardwick Tonalite by being enriched in many of the LIL and HFS elements, capable of yielding melts within the range of 1 to 3% normative corundum and having an f_{O_2} exceeding the stability limit for graphite-bearing assemblages. A graywacke-argillite sequence may fulfill these qualifications.

During partial melting, LIL elements are commonly partitioned into the melt, whereas HFS elements are retained in the residuum by minor phases such as ilmenite, sphene, allanite, rutile, zircon, apatite, etc. Therefore HFS elements are low in granitoid melts approaching the minimum melting composition. The anomalously high HFS element content suggests an extremely high degree of partial melting was involved or these minor phases were incorporated as restites in the melt. The high LREE content in the tonalite, the glomeroporphyritic texture, the high modal amount of apatite and the high crustal temperatures (>900°C) needed to produce a melt of tonalitic composition (Wyllie, 1977) suggest the probability of restite incorporation to enrich the melt in HFS elements.

In summary, the compositional variability in the Hardwick Tonalite is predominantly the result of partial melting of a heterogeneous, crustal source region consisting of an interlayered sequence of altered and/or weathered mafic to intermediate volcanics, graywacke (with a volcanic component) and argillite. Limited and variable homogenization resulted in the formation of domains of different f_{O_2} and aluminous character. Fractional redistribution of hornblende, minor biotite and accessory minerals such as apatite, sphene, magnetite and ilmenite caused the compositional variability in the hornblende-biotite tonalite. In situ contamination of the tonalite by the local metamorphic rocks resulted in the formation of the biotite-garnet tonalite along the margins of the intrusions.

Implications Concerning Tectonic Setting

The incompatible element enrichment in the Hardwick Tonalite contrasts with the typical geochemical characteristics of calc-alkaline volcanics and plutonics associated with Andean type, convergent tectonic environments (Hawksworth, 1979). The geochemical characteristics of the tona lites are similar to the high-K calc-alkaline plutonic complexes which occur in both subduction and interplate tectonic settings (Hawksworth, 1979).

A tectonic synthesis of southern New England by Robinson and Hall (1980) suggests the Acadian orogeny and accompanying plutonism was a result of Siluro-Devonian convergence between the "Bronson Hill" and "Avalon" plates. In this model, the main subduction is of deep crust and mantle of the Avalon plate. Subduction of interlayered mafic to intermediate volcanics and "clastic sediments" may have provided the thermal energy necessary to generate tonalite melt/crystal magma. In addition, mafic magmas produced along the subduction zone during convergence and injected into the lower crust, crystallized and partially melted the lower crust through heat transfer. The involvement of mafic magmas in the Acadian plutonism and metamorphism is suggested by the presence of mafic plutonic rocks in zones of extremely high metamorphism in central Massachusetts.

REFERENCES CITED

Abbott, R.N., 1981, AFM liquidus projections for magmas, with special reference to hornblende, biotite, and garnet: Can. Mineral., 19, 103-111.

Albee, A.L., and Ray, Lily, 1970, Correction factors for electron probe microanalysis of silicates, oxides, carbonates, phosphates, and sulfates: Ana. Chem., 42, 1408-1414.

Allan, B.D., and Clarke, D.B., 1981, Occurrence and origin of garnets in the South Mountain batholith, Nova Scotia: Can. Mineral., 19, 19-25.

Anderson, J.L., 1980, Mineral equilibria and crystallization conditions in the late Precambrian Wolf River rapakivi massif, Wisconsin: Am. J. Sci., 280, 298-332.

_____, and Rowley, M.C., 1981, Synkinematic intrusion of peraluminous and associated metaluminous granitic magmas, Whipple Mountains, California: Can. Mineral., 19, 83-101.

Arth, J.G., 1976, Behavior of trace elements during magmatic processes - A summary of theoretical models and their applications: J. Res. U.S. Geol. Survey, 4, 41-47.

Ashwal, L.D., 1974, Metamorphic hydration of augite-orthopyroxene monzodiorite to hornblende granodiorite gneiss, Belchertown batholith, west-central Massachusetts: M.S. thesis, University of Massachusetts, Amherst, 117 p.

_____, Leo, G.W., Robinson, Peter, Zartman, R.E., and Hall, D.J., 1979, The Belchertown Quartz Monzodiorite pluton, west-central Massachusetts: A syntectonic Acadian intrusion: Am. J. Sci., 279, 936-969.

Bence. A.E., and Albee, A.L., 1968, Empirical correction factors for the electron microanalysis of silicates and oxides: J. Geol., 76, 382-403.

Billings, M.P., 1956, Regional metamorphism of the Littleton-Moosilaukee area. New Hampshire: Geol. Soc. America Bull., 48, 463-566.

_____, 1956, The geology of New Hampshire, part II- bedrock geology: New Hampshire Planning and Development Commission, 203 p.

Bohlke, J.K., Honnorez, J., Honnorez-Guerstein, B.-M., Muehlenbacks, K., and Petersen, N., 1981, Heterogeneous alteration of the upper oceanic crust: correlation of rock chemistry, magnetic properties and O isotope ratios with alteration patterns in basalt from site 396B, DSDP: J. Geophy. Res., 9, 7935-7956.

Bowles. J.F.W., 1977, A method of tracing the temperature and oxygen fugacity histories of complex magnetite-ilmenite grains: Mineral. Mag. 41, 103-109.

Brown, G.C., 1973, Evolution of granitic magmas at destructive plate margins: Nature Phys. Sci., 241, 26-28.

Cawthorn, R.G., and O'Hara, M.J., 1976, Amphibole fractionation in calc-alkaline magma genesis: Am. J. Sci., 276, 309-328.

_____, Strong, D.F., and Brown, P.A., 1976, Origin of corundum normative intrusive and extrusive magmas: Nature, 259, 102-104.

Chappell, B.W., 1978, Granitoids from the Moonbi district, New England batholith, eastern Australia: J. Geol. Soc. Austr., 25, 267-283.

_____, and White, A.J.R., 1974, Two contrasting granite types: Pacific Geol., 8, 173-174.

Clarke, D.B., 1981, The mineralogy of peraluminous granites: a review: Can. Mineral., 19, 3-17.

Czamanske, G.K., and Mihalik, P., 1972, Oxidation during magmatic differentiation, Finnmarka complex, Oslo area, Norway, 1, The opaque oxides: J. Petrol., 13, 493-509.

_____, and Wones, D.R., 1973, Oxidation during magmatic differentiation, Finnmarka complex, Oslo area, Norway, 2, The mafic silicates: J. Petrol., 14, 349-380.

_____, and Wones, D.R., and Eichelberger, J.C., 1977, Mineralogy and petrology of the intrusive complex of the Pling Range, New Hampshire: Am. J. Sci., 277, 1073-1123.

_____, Ishihara, Shunso, and Atkin, S.A., 1981, Chemistry of rock-forming minerals of the Cretaceous-Paleocene batholith in Southwestern Japan and implications for Magma genesis: Jour. of Geophy. Res., 86, 10431-10469.

Dixon, H.R., 1968, Bedrock geology of the Danielson Quadrangle, Connecticut. U.S. Geological Survey Geological Map, GQ-696.

Dodge, F.C.W., Papike, J.J., and Mays, R.E., 1968, Hornblendes from granitic rocks of the central Sierra Nevada batholith, California: J. Petrology, 9, 378-410.

_____, Smith, V.C., and Mays, R.E., 1969, Biotites from granitic rocks of the central Sierra Nevada batholith: J. Petrol., 10, 250-271.

Emerson, B.K., 1898, Geology of old Hampshire County, Massachusetts: U.S. Geol. Survey Monograph 29, 790 p.

_____, 1917, Geology of Massachusetts and Rhode Island: U.S. Geol. Survey Bulletin 597, 289 p.

Ernst, W.G., 1963, Significance of phengitic micas from low-grade schists: Am. Mineral., 48, 1357-1373.

Evans, B.W., and Guidotti, C.V., 1966, The sillimanite-potash feldspar isograd in western Maine, U.S.A.: Contr. Mineral. Petrology, 12, 25-62.

Fahlquist, Frank, 1935, Geology of region in which Quabbin Aqueduct and Quabbin Reservoir are located: appendix to report of chief Engineer, Annual Report of the Metropolitan District Water Supply Commission, Commonwealth of Massachusetts, Public Document No. 147.

Field, M.T., 1975, Bedrock geology of the Ware area, central Massachusetts: (Ph.D. thesis) Contribution No. 22, Geology Department, University of Massachusetts, Amherst, 186 p.

Fitzgerald, R.T., 1960, The geology of the Royalston quadrangle: M.S. thesis, University of Massachusetts, Amherst, 72 p.

Foster, M.D., 1960, Interpretation of the composition of trioctahedral mica: U.S. Geol. Surv. Prof. Pap., 354-B, 48 p.

Fowler-Billings, Katherine, 1949, Geology of the Monadnock region of New Hampshire: Geol. Soc. America Bull., v. 60, p. 1249-1280.

Goad, B.E., and Cerný, Peter, 1981, Peraluminous pegmatitic granites and their pegmatite aureoles in the Winnipeg River district, southeastern Manitoba: Can. Mineral., 19, 177-194.

Green, T.H., 1977, Garnet in silicic liquids and its possible use as a P-T indicator: Contr. Mineral Petrology, 65, 59-67.

Grew, E.S., 1970, The geology of the Pennsylvanian and pre-Pennsylvanian rocks of the Worchester area, Massachusetts: Ph.D. thesis, Harvard Univeristy, Cambridge, Massachusetts, 263 p.

Guidotti, C.V., 1973, Compositional variation of muscovite as a function of metamorphic grade and assemblage in metapelites from N.W. Maine: Contr. Mineralogy Petrology, 42, 33-41.

_____, 1974, Transition from staurolite to sillimanite zone, Rangly Quadrangle, Maine: Geol. Soc. Am. Bull., 85, 475-490.

_____, Cheney, J.T., and Conatore, P.D., 1975, Coexisting cordierite biotite + chlorite from the Rumford Quadrangle, Maine: Geology, 3, 147-148.

_____, and Sassi, F.P., 1976, Muscovite as a petrogenetic indicator mineral in pelitic schists: Neues Jahrbuchfuer Mineralogie Abhandlungen, 127, 97-142.

_____, Cheney, M.T., and Guggenheim, Stephen, 1977, Distribution of titanium between coexisting muscovite and biotite in pelitic schists from northwestern Maine: Am. Mineral, 62, 438-448.

_____, 1978a, Muscovite and K-feldspar from two-mica Adamellite in northwestern Maine: composition and petrogenetic implications: Am. Mineral., 63, 750-753.

_____, 1978b, Compositional variation of muscovite in medium- to high grade metapelites of northwestern Maine: Am. Mineral, 68, 878-884.

Guthrie, J.O., 1972, Geology of the northern portion of the Belchertown intrusive complex: University of Massachusetts Geology Department Contribution No. 8, 110 p.

_____, and Robinson, Peter, 1967, Geology of the northern portion of the Belchertown intrusive complex, in New England Intercollegiate Geol. Conf., 59th Ann. Mtg., Amherst, Mass., Guidebook for the field trips in the Connecticut Valley of Massachusetts: 143-153.

Hall, D.J., 1973, Geology and geophysics of the Belchertown batholith, west-central Massachusetts, Ph.D. thesis, University of Massachusetts, 110 p.

Hall, L.M., and Robinson, Peter, 1982, Stratigraphic - tectonic subdivisions of southern New England, pp. 15-41 in St. Julieu, Pierre, and Beland, Jacques, Editors, Major Structural Zones and Faults of the Northern Appalachians. The Geological Association of Canada, Spec. Pap. 24, 280 p.

Hanson, G.N., 1978, The application of trace elements to the petrogenesis of igneous rocks of granitic composition: Earth Planet. Sci. Lett., 38, 26-43.

Hart, S.R., Brooks, Christopher, Krogh, T.E., Davis, G.L., and Nava, D., 1970, Ancient and modern volcanic rocks: a trace element model: Earth Planet. Sci. Lett., 10, 17-28.

Helz, R.T., 1976, Phase relations of basalts in their melting range at P_{H_2O} = 5kb. II. Melt compositions: J. Petrology, 17, 139-193.

Hepburn, J.C., 1976, Preliminary bedrock geologic map of the Sterling Quadrangle, U.S. Geol. Survey, open file report.

Hildreth, Wes, 1981, Gradients in silicic magma chambers: Implications for lithospheric magmatism: J. Geophy. Res., 86, 10153-10192.

Hine, R., Williams, I.S., Chappell, B.W., and White, A.J.R., 1978, Contrasts between I- and S-type granitoids of the Kosciusko batholith: Journal of the Geol. Soc. of Aus., 25, 219-234.

Hollocher, K.T., 1981, Retrograde metamorphism of the Lower Devonian Littleton Formation in the New Salem Area, west-central Massachusetts: M.S. thesis, University of Massachusetts, Amherst, 268 p.

Huang, W.L., and Wyllie, P.J., 1973, Melting relations of muscovite-granite to 35 kbar as a model for fusion of metamorphosed subducted oceanic sediments: Contrib. Mineral. Petrology, 42, 1-14.

_____, and _____, 1974, Melting relations of muscovite with quartz and sanidine in the system K_2O-Al_2O_3-SiO_2H_2O to 30 kilobars and an outline of paragonite melting relations: Am. J. Sci., 274, 378-395.

_____, and _____, 1981, Phase relationships of S-type granite with H_2O to 35 kilobars: The Harney Peak muscovite-granite from South Dakota: J. Geophy. Res., 86, 10414-10529.

Ishihara, Shunso, 1977, The magnetite-series and ilmenite-series granitic rocks: Min. Geol. Tokyo, 27, 293-305.

_____, 1978, Metallogenesis of the Japanese island arc system: J. Geol. Soc. London, 135, 389-406.

_____, 1979, Lateral variation of magnetic susceptibility of the Japanese granitoids: J. Geol. Soc. Japan, 85, 509-523.

Ivanova, G.F., and Butuzova, Ye. G., 1968, Distribution of tungsten, tin, and molybdenum in the granites of Eastern Transbaykalia: Geochem. Int., 5, 572-583.

Kwak, T.A.P., 1958, Ti in biotite and muscovite as an indication of metamorphic grade in almandine amphibolite facies rocks from Sudbury, Ontario: Geochim. et Cosmochim. Acta, 32, 1222-1229.

Labotka, T.C., 1980, Petrology of a medium-pressure regional metamorphic terrane, Funeral Mountain, California: Am. Mineral., 65, 670-689.

Leake, B.E., 1978, Nomenclature of amphiboles: Can. Mineral., 16, 501-520.

Lindsley, D.H., and Spencer, K.J., 1982, Fe-Ti oxide geothermometry: reducing analyses of coexisting Ti-magnetite (Mt) and Ilmenite (Ilm): EθS, 63, 471.

Luth, W.C., Jahns, R.H., and Tuttle, O.F., 1964, The granite system at pressures of 4 to 10 kilobars: J. Geophy. Res., 69, 759-773.

Maaloe, Sven, and Petersen, T.S., 1981, Petrogenesis of oceanic andesites: J. Geophy. Res., 86, 10273-10286.

Maczuga, D.E., 1981, The petrology and geochemistry of the Fitchburg Plutonic Complex, central Massachusetts: M.S. thesis, University of Massachusetts, Amherst, 128 p.

Maxwell, J.A., 1968, Rock and Mineral Analysis, Interscience, New York, 584 p.

McNamara, M.J., 1965, The lower greenschist facies in the Scottish Highlands: Geologiska Foreningens i Stockholm Forhandliger, 87, 347-389.

Miller, C.F., Stoddard, E.F., Bradfish, L.J., and Dollase, W.A., 1981, Composition of plutonic muscovite: genetic implications: Can. Mineral., 19, 25-34.

Mook, A.L., 1967, Petrography of the Athol Quadrangle, Massachusetts: U.S. Geol. Survey open file report.

Muecke, G.K., and Clarke, D.B., 1981, Geochemical evolution of the South Mountain batholith, Nova Scotia: rare-earth-element evidence: Can. Mineral. 19, 133-146.

Nabelek, P.I., Papike, J.J., and White, C., 1981, The geochemical evolution of the Notch Peak granite stock, Utah: EθS, 62, 435.

Nielson, D.L., Clark, R.G., Lyons, J.B., Englund, E.J., and Borns, D.J., 1976, Gravity models and mode of emplacement of the New Hampshire Plutonic Series, in Lyons, P.C., and Brownlow, A.H., eds., Studies in New England Geology: Geol. Sco. Amer. Mem., 146, 301-318.

Osberg, P.H., 1979, Geologic relationships in south-central Maine, in Skehan, J.W., and Osberg, P.H., eds., The Caledonides in the U.S.A., Weston Observatory, Department of Geology and Geophysics, Boston College, Weston, Massachuseetts, 37-62.

Page, L.R., 1968, Devonian Plutonic Rocks in New England, in E-an Zen, W.S. White, J.B. Hadley and J.B. Thompson, eds., Studies of Appalachian Geology: Northern and Maritime, Wiley, 271-383.

Peper, J.D., and Pease, M.H., 1975, Geology of the Brimfield area, Massachusetts, U.S. Geol. Survey open file report, 75-50.

Peper, J.D., and Wilson F.A., 1978, Reconnaissance bedrock geologic map of the Fitchburg Quadrangle and part of the Ashby Quadrangle north-central Massachusetts: U.S. Geol. Survey Misc. Field Studies Map MF-959.

Presnall, D.C., and Bateman, P.C., 1973, Fusion relations in the system $NaAlSi_3O_8$-$CaAl_2Si_2O_8$-$KAlSi_3O_8$-SiO_2-H_2O and generation of granitic magmas in the Sierra Nevada batholith: Geol. Soc. Amer. Bull., 84, 3181-3202.

Rao, C.N.R., 1961, Kinetics and thermodynamics of the crystal structure transformation of spectroscopically pure anatase to rutile: Can. J. Chem., 36, 498-500.

Rhodes, J.M., 1969, The geochemistry of a granite-gabbro association at Hartley, New South Wales: Ph.D. thesis, Australian National University Canberra, Australia, 315 p.

Ringwood, A.E., 1974, The petrological evolution of island arc systems: J. Geol. Soc. London, 130, 183-204.

Robinson, Peter, 1967a, Gneiss domes and recumbent folds of the Orange area, west-central Massachusetts: _in_ New England Intercollegiate Geol. Conf., 59th Ann. Mtg. Guidebook, Amherst, Massachusetts, 17-47.

_____, 1967b, Geology of the Quabbin Reservoir area, central Massachusetts: _in_ New England Intercollegiate Geol. Conf., 59th Ann. Mtg., Guidebook, Amherst, Massachusetts, 114-127.

_____, 1979, Bronson Hill anticlinorium and Merrimack synclinorium in central Massachusetts, p. 126-150, _in_ Skehan, J.W., and Osberg, P.H., eds., The Caledonides in the U.S.A., Geological Excursions in the Northeast Appalachians, Project 27, Caledonide Orogen 1979, Weston, Massachusetts, 250 p.

_____, and Hall, L.M., 1980, Tectonic synthesis of southern New England: _in_ Wones, D.R., ed., The Caledonides in the USA, 73-82.

_____,Tracy, R.J., Hollocher, K.T., and Dietsch, C.S., 1982, High grade Acadian regional metamorphism in south-central Massachusetts: _in_ Guidebook for field trips in Connecticut and south-central Massachusetts, New England Intercollegiate Geol. Conf., University of Connecticut, Storres, Connecticut, p. 289-339.

Rogers, John, 1972, Latest Precambrian (post-Greenville) rocks of the Appalachian region: Amer. J. Sci., 272, 507-520.

Ross, Malcolm, and Huebner, J.S., 1975, A pyroxene geothermometer based on composition-temperature relationships of naturally occurring orthopyroxene, pigeonite and augite: Intern. Conf. Geothermometry Geobarometry (abstr.), Penn. State Univ., Univ. Park, PA.

Seifert, Friedrich, 1970, Low-temperature compatibility relations of cordierite in haplopelites of the system K_2O-MgO-Al_2O_3-SiO_2-H_2O: J. Pet., 11, 73-99.

Shearer, C.K., 1980, Petrology of the Hardwick pluton, central Massachusetts: Geol. Soc. Amer., Abstracts with Programs, 12, 82.

_____, 1981, Hardwick pluton: The occurrences of "S-type" and "I-type" granitoids in a single intrusive unit: EΘS, 62, 436.

_____, 1983, The petrography, mineral chemistry and geochemistry of the Hardwick Tonalite and associated igneous rocks, central Massachusetts: Ph.D. thesis University of Massachusetts, Amherst, 265 p.

_____, and Robinson, Peter, 1980, Constant temperature regional metamorphism of an H_2O activity gradient in a preexisting contact aureole, Petersham, Massachusetts: EΘS, 61, 389.

Skehan, J.W., Murray, D.D., Palmer, A.R., Smith, A.T., and Belt, E.S. 1978, Significance of fossiliferous Middle Cambrian rocks of Rhode Island to the history of the Avalonian microcontinent: Geology (Boulder), 6, 694-698.

Stephen, W.E., and Halliday, A.N., 1979, Compositional variation in the Galloway plutonics: in Atherton, M.P., and Tarney, J., eds., Origin of Granite Batholiths: Geochemical Evidence, Shiva, 9-17.

Stern, C.R., and Wyllie, P.J., 1973, Water-saturated and undersaturated melting relations of a granite to 35 kilobars: Earth Planet. Sci. Lett., 18, 163-167.

_____, Huang, W.L., and Wyllie, P.J., 1975, Basalt-andesite-rhyolite-H_2O: Crystallization intervals with excess H_2O and H_2O-under-saturated liquidus surfaces to 35 kilobars with implications for magma genesis: Earth Planet. Sci. Letter., 28, 189-196.

Streckeisen, A.L., 1973, Plutonic rocks-classification and nomenclature recommended by the I.U.G.S. subcommission on the systematics of igneous rocks: Geotimes, 18, 26-30.

Stormer, J.C., Jr., 1975, A practical two-feldspar geothermometer, Am. Mineral., 60, 667.

Tarney, J. and Saunders, A.D., 1979, Trace element constraints on the origin of cordilleran batholiths: in Atherton, M.P., and Tarney, J., eds., Origin of Granite Batholiths: Geochemical Evidence, Shiva, 90-105.

Thompson, A.B., and Tracy, R.J., 1977, Anatectic melting reactions in pelitic rocks: Am. Geophys. Union Trans., 58, 520.

Thompson, J.B., 1977, Phengitic dioctahedral micas in metamorphosed pelites: EθS, 58, 992.

_____, Robinson, Peter, Clifford, T.N., and Trask, N.J., Jr., 1968, Nappes and gneiss domes in west-central New England: in Zen, E-an, White, W.S., Hadley, J.B., and Thompson, J.B., eds., Studies of Appalachian geology, northern and maritime: Wiley, 203-218.

Tracy, R.J., 1975, High grade metamorphic reactions and partial melting in pelitic schists, Quabbin Reservoir area, Massachusetts: Ph.D. thesis, Univ. Massachusetts, Amherst, 127.

_____, 1978, High grade metamorphic reactions and partial melting in pelitic schist, west-central Massachusetts: Am. Jour. Sci., 278, 150-178.

_____, Robinson, Peter, and Thompson, A.B., 1976, Garnet composition and zoning in the determination of temperature and pressure of metamorphism, central Massachusetts: Am. Mineral., 61, 762-775.

_____, and Robinson, Peter, 1980, Evolution of metamorphic belts: information from detailed petrologic studies: in Wones, D.R., ed., The Caledonides in the USA, 189-195.

Tsusue, A., and Ishihara, Shunso, 1974, The iron-titanium oxides in the granitic rocks of southwest Japan: Min. Geol. Tokyo, 24, 13-30.

Tucker, R.D., 1977, Bedrock geology of the Barre area, central Massachusetts: M.S. thesis, Contribution No. 30, Department of Geology, University of Massachusetts, Amherst, 132 p.

Van Der Plas, L., 1965, A chart for judging the reliability of point-counting results: Am J. of Sci., 263, 87-90.

Velde, Bruce, 1965, Phengite micas: synthesis, stability and natural occurrence: Amer. J. Sci., 263- 886-913.

_____, 1967, Si^{+4} content of natural phengites: Contr. Mineral. Petrology, 14, 250-258.

Walbaum, D.R., and Thompson, J.B., 1969, Mixing properties of sanidine crystalline solutions, IV, Phase diagrams from equations of state: Am. Mineral., 54, 1274-1298.

Watson, E.B., 1979, Apatite saturation in basic to intermediate magmas: Geophys. Res. Letters, 6, 937-940.

_____, 1980, Apatite and phosphorus in mantle source regions: an experimental study of apatite/melt equilibria at pressures to 25 kbars: Earth Planet. Sci. Lett., 51, 322-335.

_____, and Capobianco, C.J., 1981, Phosphorus and the rare earths in granites: an assessment of the role of apatite: Geochim. Cosmochim. Acta, 45, 2349-2358.

Wenk, Eduard, 1970, Distribution of Al between coexisting micas in metamorphic rocks from the central Alps: Contrib. Mineral. Petrology, 26, 50-61.

White, A.J.R., and Chappell, B.W., 1977, Ultrametamorphism and granitoid genesis: Tectonophysics, 43, 7-22.

_____, Williams, I.S., and Chappell, B.W., 1977, Geology of the Berridal, 1:100,000 sheet (8625): Memoir of the Geological Survey of New South Wales, 138.

Wones, D.R., 1980, Contributions of crystallography, mineralogy and petrology to the geology of the Lucerne pluton, Hancock country, Maine, Am. Mineral. 65, 411-437.

_____, 1980, A comparison between granitic plutons of New England, U.S.A. and the Sierra Nevada batholith, California: in Wones, D.R., ed., The Caledonides in the USA, 123-130.

_____, 1982, Amphiboles in the igneous environment: in Veblen, D.R., and Ribbe, P.H., eds., Mineral. Soc. Amer. Reviews in Mineralogy 9B, 355-390.

_____, and Eugster, H.P., 1965, Stability of biotite: experiment, theory, and application: Amer. Mineral., 50, 1228-1278.

Wyllie, P.J., Huang, W.L., Stern, G.R., and Maaloe, Sven, 1976, Granitic magmas: possible and impossible sources, water contents and crystallization sequences: Can. J. Earth Sci., 13, 1007-1019.

Zen, E-an, 1968, Introduction in Zen, E-an, White, W.S. Hadley, J.B. and Thompson, J.B., eds., Studies of Appalachian Geology, Northern and Maritime: Wiley, 475 p.

APPENDIX

SUMMARY OF THE GEOCHEMISTRY OF THE PLUTONIC ROCKS ASSOCIATED WITH THE HARDWICK TONALITE

INTRODUCTION

Analyses for major and trace elements were done not only on the Hardwick Tonalite and local metamorphosed sedimentary rocks of the Littleton and Partridge Formations, but on plutonic rocks that are spatially but not necessarily genetically associated. Major and trace element analyses of the Bear Den sill of diorite, augite-hornblende quartz diorite from the Nichewaug sill, Goat Hill Diorite, porphyritic microcline granite and equigranular granites are presented in Table 30.

These whole rock analyses will be combined with petrographic and mineralogical data previously presented in this thesis to form the basis of two additional papers to be prepared at a future date. The first paper will focus on the mafic plutonic rocks associated with the Hardwick Tonalite. The second paper will focus on the porphyritic microcline granite also closely associated with the Hardwick Tonalite. A brief summary and discussion of geochemical characteristics of these plutonic rocks follows.

BEAR DEN SILL OF HORNBLENDE DIORITE

Major Element Geochemistry

The hornblende diorite has an SiO_2 content of between 52.12 and 52.52 weight percent and is silica oversaturated with 4.23 to 7.82% normative quartz. The diorite is metaluminous with the Al/[Na+K+(Ca/2)] ration ranging from 0.78 to 0.85. After a large P_2O_5 correction, diopside (3.78 to 0.52%) is present in the normative mineralogy in all but specimen SA176-33 (0.16% corundum). The oxidation index $[2Fe_2O_3/(2Fe_2O_3+FeO)]$ of the diorite ranges from 0.32 to 0.46. The K_2O content is typically greater than 3% and the $Na_2O/(K_2O+Na_2O)$ ratio ranges from 0.30 to 0.41. Biotite is the major contributor to the high K_2O content at such low SiO_2 contents.

Trace Element Geochemistry

Compared to the local metamorphosed sedimentary rocks, the diorite is depleted in Rb, enriched in Sr, Ba, LREE and Ni. The Rb/Sr ratio ranges from 0.043 to 0.050. The K/Rb ratio ranges from 400 to 550. Typical ratios for Archean basalts are Rb/Sr=0.034 and K/Rb=356 (Hart et al., 1970). The The Ba/Rb ratio for the diorite is 20 and the Sr/Ba ratio is 1.07. The Rb/Sr ratio is lower in the hornblende diorite than in the local metamorphosed sedimentary rocks and the Hardwick Tonalite, whereas the K/Rb, Ba/Rb and Sr/Ba ratios are higher in the hornblende diorite than in the local metamorphosed sedimentary rocks and most of the Hardwick Tonalite.

Table 30. Whole rock analyses for major and trace elements and calculated CIPW norms for samples of the plutonic rocks associated with the Hardwick Tonalite.

	Bear Den Sill of diorite					Nichewaug Sill of augite-hornblende quartz diorite					
Sample	A176-31	A176-32	A176-33	A176-2	A176-1	P236-1	P236-2	P236-3	P239-1A	P239-1B	1153+50
SiO_2	52.32	52.39	52.45	52.62	52.12	53.73	53.67	53.65	52.76	52.80	55.62
TiO_2	2.30	2.31	2.28	2.18	2.22	2.79	2.86	2.86	2.86	2.83	2.17
Al_2O_3	14.74	14.88	14.88	14.98	15.04	15.37	15.41	15.43	15.70	15.61	15.31
Fe_2O_3	2.47	2.39	2.51	1.81	3.04	2.33	2.36	2.33	1.97	1.96	1.00
FeO	7.72	7.64	7.60	7.31	7.23	7.43	7.51	7.40	9.27	9.15	7.73
MnO	0.23	0.24	0.22	0.25	0.24	0.32	0.32	0.31	0.38	0.39	0.20
MgO	6.17	6.18	6.30	6.15	5.83	3.78	3.73	3.70	4.59	4.50	4.78
CaO	6.42	6.36	6.25	6.34	6.65	6.16	6.31	6.11	6.85	6.95	5.64
Na_2O	1.45	1.44	1.50	2.23	2.28	2.43	2.46	2.46	2.26	2.28	2.86
K_2O	3.41	3.38	3.21	3.29	3.21	3.16	3.05	3.19	1.84	1.87	1.87
P_2O_5	1.16	1.15	1.20	1.19	1.19	1.50	1.55	1.42	1.53	1.55	1.29
volatile loss	0.89	1.01	0.87	1.05	0.92	0.61	0.64	0.57	nd	nd	nd
total	99.28	99.37	99.27	99.40	99.97	99.61	99.86	99.43	100.01	99.89	99.47
$Fe^{3+}/(Fe^{3+}+Fe^{2+})$	.22	.22	.23	.18	.27	.22	.22	.22	.16	.17	.11
Al/[K+Na+(Ca/2)]	.83	.85	.86	.80	.77	.83	.82	.83	.87	.85	.85
Q	7.13	7.34	7.82	4.04	4.23	8.93	9.06	8.78	9.75	9.60	7.44
Or	20.15	19.98	18.97	19.44	18.97	18.67	18.02	18.85	10.87	11.05	16.96
Ab	12.27	12.19	12.69	18.87	19.29	20.65	20.82	20.82	19.12	19.29	24.20
An	23.64	24.16	23.95	21.15	21.32	21.65	22.00	21.64	24.99	25.37	20.40
C			0.16						0.83	0.54	0.02
Di	1.13	0.52		2.69	3.79	0.06	0.16	0.27			
En	0.35	0.16		0.83	1.21	0.02	0.04	0.07			
Fs	0.20	0.09		0.48	0.63	0.01	0.04	0.06			
Wo	0.58	0.26		1.38	1.95	0.03	0.08	0.13			
Hy	23.58	23.83	24.22	22.80	20.23	17.09	16.94	16.60	22.81	22.44	22.06
En	15.02	15.23	15.69	14.48	13.31	9.40	9.25	9.14	11.43	11.21	11.90
Fs	8.57	8.60	8.53	8.32	6.92	7.69	7.69	7.46	11.38	11.24	10.16
Mt	3.58	3.47	3.64	2.62	4.41	3.38	3.42	3.38	2.86	2.84	1.45
Il	4.37	4.39	4.33	4.14	4.22	5.30	5.41	5.43	5.43	5.37	4.12
Ap	2.53	2.51	2.62	2.60	2.60	3.30	3.39	3.10	3.34	3.39	2.82
volatile loss	0.89	1.01	0.87	1.05	0.92	0.61	0.64	0.57	nd	nd	nd
total	99.28	99.37	99.27	99.40	99.97	99.64	99.86	99.43	100.01	99.90	99.47
Trace Elements (in ppm)											
Y	24	24	24	32	35	35	37	35			
Sr	1119	1169	1131	1354	1382	1562	1571	1563			
Rb	51	50	50	68	67	66	64	67			
Ba	1043						1244				
Th	9	9	9	14	13	13	14	14			
Pb	26	29	29	26	27	33	34	33			
Ga	19	17	17	22	21	24	23	24			
Nb	15						24				
Zr	269						423				
Zn	125						134				
Ni	274						25				
Cr	654						43				
V	136						124				
La	66						93				
Ce	133						188				

Table 30, continued.

	Goat Hill Diorite				Porphyritic Microcline Granite							
Sample	W522-2	W522-3	W4-10	W4-11	A1-1	A1-2	P56-1	P56-2	A3-4A	A3-4B	A160-1	P78-1
SiO_2	54.79	54.44	56.40	56.36	64.76	64.61	64.57	64.83	68.41	68.32	66.49	70.07
TiO_2	1.87	1.91	2.14	2.15	1.17	1.16	1.15	1.15	0.72	0.72	1.02	0.63
Al_2O_3	14.96	14.85	15.58	15.53	15.77	15.68	15.88	15.79	15.17	15.21	15.77	14.84
Fe_2O_3	2.93	3.16	1.02	0.93	0.41	0.32	0.37	0.53	0.87	0.92	0.53	0.23
FeO	6.69	6.61	7.68	7.73	4.22	4.20	3.99	3.95	2.54	2.50	3.80	2.73
MnO	0.19	0.21	0.18	0.18	0.11	0.10	0.08	0.09	0.07	0.07	0.21	0.05
MgO	7.05	6.93	4.79	4.85	1.75	1.67	1.64	1.66	0.97	0.96	1.37	0.75
CaO	6.44	6.45	5.47	5.42	3.06	2.97	2.84	2.90	2.12	2.09	2.79	1.56
Na_2O	1.91	2.03	2.25	2.25	3.12	3.05	2.70	2.71	2.14	2.18	3.11	3.13
K_2O	2.03	2.04	2.67	2.69	4.52	4.56	5.14	4.84	5.48	5.52	4.80	5.45
P_2O_5	0.80	0.78	1.29	1.21	0.53	0.54	0.54	0.56	0.30	0.34	0.52	0.25
volatile loss	nd	nd	0.59	0.60	0.68	0.60	nd	nd	0.64	nd	nd	0.57
total	99.66	99.41	100.06	99.90	100.10	99.46	98.90	99.01	99.43	98.83	100.40	100.26
$Fe^{3+}/(Fe^{3+}+Fe^{2+})$	.47	.49	.21	.19	.16	.13	.16	.21	.39	.40	.21	.14
Al/[K+Na+(Ca/2)]	.87	.86	.94	.94	1.01	1.02	1.05	1.06	1.14	1.14	1.03	1.07
Q	10.60	10.01	12.93	12.56	18.90	19.33	19.63	20.96	28.45	28.20	20.93	25.41
Or	12.00	12.06	15.78	15.90	26.71	26.95	30.38	28.60	32.39	32.62	28.37	32.21
Ab	16.16	17.18	19.04	19.04	26.40	25.81	22.85	22.93	18.11	18.45	26.32	25.49
An	26.25	25.38	19.55	19.77	12.06	11.56	10.91	11.09	8.75	8.37	10.78	6.27
C			1.82	1.67	1.32	1.49	1.88	2.03	2.51	2.58	1.51	1.49
Di	0.80	1.63										
En	0.28	0.56										
Fs	0.11	0.22										
Wo	0.41	0.85										
Hy	24.30	23.24	21.99	22.29	10.04	9.88	9.36	9.22	5.30	5.16	8.67	5.74
En	17.28	16.69	11.93	12.08	4.36	4.16	4.08	4.13	2.42	2.39	3.41	1.87
Fs	7.02	6.54	10.06	10.21	5.68	5.72	5.27	5.08	2.89	2.77	5.25	3.88
Mt	4.25	4.58	1.48	1.35	0.59	0.46	0.54	0.77	1.26	1.33	0.75	0.33
Il	3.55	3.63	4.06	4.08	2.22	2.20	2.18	2.18	1.37	1.37	1.94	1.20
Ap	1.75	1.70	2.82	2.64	1.16	1.18	1.18	1.22	0.66	0.74	1.14	0.55
volatile loss	nd	nd	0.59	0.60	0.68	0.60	nd	nd	0.64	nd	nd	0.57
total	99.66	99.41	100.06	99.90	100.10	99.46	98.90	99.01	99.43	98.83	100.40	100.26
Trace Elements (in ppm)												
Y	25	25	39	40	25	25	20	21	13	13	16	22
Sr	930	936	868	871	665	654	722	708	476	485	753	323
Rb	53	55	85	83	155	151	151	146	153	154	138	158
Ba					1071							
Th	8	8	4	5	34	39	20	35	39	36	25	32
Pb	25	26	22	22	43	41	44	46	61	61	48	50
Ga	22	22	20	21	23	23	23	22	19	20	22	19
Nb					21							
Zr					543							
Zn					107							
Ni					16							
Cr					37							
V					59							
La					112							
Ce					216							

Table 30, continued.

	porphyritic microcline granite		Fitzwilliam Granite						granite at Tom Swamp	granite at Sheep Rock			
Sample	P78-2	A3-6	M3	M4	M9	M11	A61-3A	A61-3B	Z93	A68-1-1	A68-1-2	A68-2-1	A68-2-2
SiO_2	70.35	67.96	73.51	72.64	73.70	71.73	69.30	69.37	71.68	70.48	70.96	70.89	70.83
TiO_2	0.62	0.91	0.18	0.27	0.29	0.28	0.82	0.82	0.55	0.52	0.55	0.54	0.54
Al_2O_3	14.86	15.03	15.01	14.67	14.76	14.58	15.10	15.13	15.29	14.13	13.89	14.08	14.05
Fe_2O_3	0.27	0.31	0.17	0.30	0.09	0.06	0.23	0.26	0.13	0.18	0.25	0.23	0.23
FeO	2.74	3.95	1.10	1.26	1.45	1.43	2.61	2.53	1.75	1.88	1.92	1.89	1.95
MnO	0.03	0.08	0.03	0.01	0.01	0.03	0.70	0.70	0.01	0.04	0.07	0.05	0.05
MgO	0.92	1.18	0.15	0.29	0.34	0.38	0.75	0.71	0.55	0.63	0.72	0.68	0.69
CaO	1.62	2.37	0.97	1.11	1.13	1.23	2.03	2.05	1.17	1.67	1.72	1.66	1.74
Na_2O	3.11	4.23	3.42	3.34	3.56	3.05	2.65	2.60	3.24	2.86	2.80	2.84	2.78
K_2O	5.50	3.84	4.85	5.45	5.17	5.18	5.48	5.59	5.14	5.11	4.86	5.01	4.90
P_2O_5	0.29	0.31	0.19	0.18	0.16	0.18	0.34	0.34	0.24	0.22	0.21	0.21	0.21
volatile loss	nd	0.61	0.41	nd	nd	0.89	nd	0.46	nd	0.71	0.74	0.79	nd
total	100.31	100.78	99.99	99.52	100.66	98.95	100.01	100.56	99.75	98.43	98.69	98.87	97.97
$Fe^{3+}/(Fe^{3+}+Fe^{2+})$	.17	.14	.24	.32	.11	.08	.15	.15	.13	.16	.21	.20	.19
Al/[K+Na+(Ca/2)]	1.07	.98	1.19	1.09	1.09	1.13	1.08	1.08	1.17	1.06	1.07	1.06	1.07
Q	25.35	20.04	32.49	29.25	29.71	30.66	26.23	26.27	29.44	29.18	30.91	30.18	30.64
Or	32.55	22.69	28.66	32.21	30.55	30.48	32.39	33.04	30.40	30.20	28.58	29.51	28.92
Ab	26.32	35.79	28.94	28.26	30.13	25.67	22.42	22.00	27.42	24.20	23.62	23.97	23.46
An	6.33	9.94	3.70	4.45	4.67	5.02	8.07	8.17	4.39	6.99	7.27	7.02	7.36
C	1.47	0.27	2.78	1.65	1.60	2.18	1.85	1.81	2.79	1.33	1.42	1.45	1.50
Di													
En													
Fs													
Wo													
Hy	6.13	8.58	2.01	2.36	2.97	3.13	6.42	6.15	3.57	4.10	4.31	4.16	4.29
En	2.29	2.94	0.37	0.72	0.85	0.95	1.87	1.77	1.37	1.57	1.75	1.68	1.70
Fs	3.84	5.64	1.64	1.64	2.13	2.18	4.55	4.38	2.20	2.54	2.56	2.48	2.59
Mt	0.39	0.45	0.25	0.43	0.13	0.08	0.33	0.38	0.19	0.26	0.35	0.33	0.32
Il	1.18	1.73	0.34	0.51	0.55	0.52	1.56	1.56	1.04	0.97	1.05	1.02	1.04
Ap	0.63	0.68	0.42	0.39	0.35	0.39	0.75	0.74	0.52	0.48	0.44	0.45	0.46
volatile loss	nd	0.61	0.41	nd	nd	0.89	nd	0.46	nd	0.71	0.74	0.79	nd
total	100.31	100.78	99.99	99.52	100.66	99.02	100.02	100.57	99.74	98.43	98.69	98.87	97.98
Trace Elements (ppm)													
Y	22	14	12	10		11	11	11	14	9	9	9	10
Sr	329	378	93	126		131	479	483	635	475	481	469	465
Rb	162	135	265	224		216	153	155	148	138	132	140	140
Ba						615			1079				
Th	32	34	13	23		23	32	32		35	35	37	39
Pb	51	37	35	43		41	48	47		53	54	58	58
Ga	20	20	20	21		21	19	18		15	15	16	16
Nb						7			12				
Zr						143			270				
Zn						67			46				
Ni						4			2				
Cr						15			19				
V						14			29				
La						34			89				
Ce						83			171				

LREE in the Bear Den sill are enriched compared to the surrounding schists with La 208 times chondritic abundance and Ce 164 times chondritic abundance. These values are below the LREE abundances for the Hardwick Tonalite. Contrasting with the behavior of the HFS major elements, P_2O_5 and TiO_2, Zr and Nb contents in the diorite are similar to the metamorphic rocks and lower than the Hardwick Tonalite. Ni and Cr contents of the diorite exceed those of the Hardwick Tonalite.

NICHEWAUG SILL OF QUARTZ DIORITE

Major Element Geochemistry

The augite-bearing quartz diorite of the Nichewaug sill has a SiO_2 content of between 52.76 and 55.62 weight percent. The quartz diorite is metaluminous with Al/[K+Na+(Ca/2)] between 0.82 and 0.86. The normative mineralogy of the sill contains corundum in samples from the contaminated chilled margin and sample 1153+50 from the Quabbin Tunnel and is diopside normative in the interior of the sill. The oxidation index appears to be somewhat correlated to the presence of diopside or corundum in the normative mineralogy. The diopside-normative quartz diorite is more oxidized than the corundum-normative quartz diorite. The $Na_2O/(Na_2O+K_2O)$ ratio ranges from 0.32 to 0.55.

In comparing the major element geochemistry of the interior of the sill with the perimeter of the sill, the chilled perimeter exhibits both a more primitive character and a contamination character. The reduced nature and the aluminous character of the chilled margin is indicative of contamination with the pelitic schist (Littleton Formation) it is in contact with, while its higher CaO content, higher $Na_2O/(K_2O+Na_2O)$ ratio and similar $Mg/(Mg+Fe^{2+})$ ratio is suggestive of a more primitive magma.

Trace Element Geochemistry

Only samples from the interior of the sill have been analyzed for trace elements. In the augite-bearing quartz diorite, the Rb/Sr ratio is approximately 0.04, the K/Rb ratio is approximately 400, the Ba/Rb ratio is 19 and the Sr/Ba ratio is 1.26. These ratios are similar to or more primitive than the Bear Den sill of diorite and the hornblende-biotite tonalite subdivision of the Hardwick Tonalite.

The LREE contents for the quartz diorite are similar to those of the hornblende-biotite tonalite of the Hardwick Tonalite. The La content is 295 times chondritic abundance and the Ce content is 231 times chondritic abundance. Unlike the diorite sill at Bear Den, Nb, Zr, and Cr are similar to the Hardwick Tonalite.

GOAT HILL DIORITE

Major Element Geochemistry

The SiO_2 content of the two-pyroxene diorite ranges from 54.55 to 54.79%, while the augite-bearing diorite contains approximately 56.40 weight percent SiO_2. The Al/[Na+K+(Ca/2] ratio for the two-pyroxene diorite ranges from 0.86 to 0.88 and is 0.94 for the augite-bearing diorite. With a larger P_2O_5 correction for the augite-bearing diorite, it has corundum in its normative mineralogy (1.67 to 1.82%) while the two-pyroxene diorite contains 0.80 to 1.63% normative diopside. The two-pyroxene diorite has an oxidation index of between .49 and .47 and the augite-bearing diorite has an oxidation index of between .21 and .19. Again a correlation exists between the normative mineralogy and the oxidation index. The K_2O content in the diorites is less than 3%, which is not typical of the Hardwick Tonalite or any other plutonic rock associated with the Hardwick Tonalite. The $Na_2O/(K_2O+Na_2O)$ ratio ranges from 0.46 to 0.50 with the augite-bearing diorite at the lower end of that range (0.46).

Trace Element Geochemistry

The two-pyroxene diorite has a Rb/Sr ratio of approximately 0.06, whereas the augite-bearing diorite has a higher Rb/Sr ratio of approximately 0.10. These Rb/Sr ratios are higher than the diorite of the Bear Den sill and the quartz diorite of the Nichewaug sill, but are similar to the ratios for the hornblende-biotite diorite of the Hardwick Tonalite. The two diorite types of the Goat Hill Diorite also have slightly different K/Rb ratios. The two-pyroxene diorite has a K/Rb ratio of between 261 and 270. These K/Rb ratios are lower than the diorite from the Bear Den sill and the quartz diorite of the Nichewaug sill, but similar to many of the tonalites from the Hardwick Tonalite.

PORPHYRITIC MICROCLINE GRANITE

Major Element Geochemistry

The porphyritic microcline granite has an SiO_2 content between 64.57 and 70.35 weight percent and is silica oversaturated with 18.90 to 28.45% normative quartz. These granites are weakly peraluminous with the Al/[Na+K+(Ca/2)] ratio ranging between 0.98 and 1.14 and the percent normative corundum between 0.27 and 2.58. The oxidation index for these granites ranges from 0.14 to 0.40, although this index is more commonly between 0.14 and 0.21. The weight percent K_2O exceeds 3.84% and the $Na_2O/(Na_2O+K_2O)$ ratio is between 0.28 and 0.52.

Trace Element Geochemistry

The Rb/Sr and K/Rb ratios of the porphyritic microcline granite range from 0.18 to 0.49 and 234 to 298, respectively. The Rb/Sr ratio in the granite is higher than the mafic plutonic rocks associated with the Hardwick

Tonalite and is similar to the biotite tonalite, biotite-muscovite tonalite and biotite-garnet tonalite of the Hardwick Tonalite. The K/Rb ratio of the granite is lower than the mafic plutonic rocks and similar to the previously mentioned members of the Hardwick Tonalite. In sample SA1-1 of the porphyritic microcline granite, the Ba/Rb ratio is 5.9 and the Sr/Ba ratio is .62.

The LREE of the granite is similar to that of the tonalites with the La content 356 times chondritic abundance and the Ce content 266 times chondritic abundance. The rest of the trace element geochemistry is similar to the Hardwick Tonalite.

EQUIGRANULAR BIOTITE-MUSCOVITE GRANITE

Major Element Geochemistry

The Fitzwilliam Granite contains between 69.30 and 73.70 weight percent SiO_2, the granite at Tom Swamp contains approximately 71.7 weight percent SiO_2, and the granite at Sheep Rock contains between 70.39 and 70.96 weight percent SiO_2. The Al/[K+Na+(Ca/2)] ratio varies from 1.08 to 1.19 for the Fitzwilliam Granite, 1.07 to 1.08 for the granite at Sheep Rock and is 1.18 for the granite at Tom Swamp. Corundum is in the norm of all the granites. The Fitzwilliam Granite contains between 1.50 and 2.78% corundum in its norm, the granite at Sheep Rock contains between 1.33 and 1.50% corundum in its norm and the granite at Tom Swamp contains 2.79% corundum in its norm. The percent normative corundum in these granites corresponds to the "S-type" granitoid characteristics of Chappell and White (1974), but is less than the normative corundum in minimum liquids derived from pelitic schists (Thompson and Tracy, 1977).

The oxidation index in the equigranular granites varies considerably. In the Fitzwilliam Granite the oxidation index is between 0.08 and 0.32, in the granite at Sheep Rock the oxidation index is between 0.15 and 0.21 and the granite at Tom Swamp has an oxidation index of 0.13. The (Na_2O/(Na_2O+K_2O) ratio in the equigranular granite varies from 0.32 to 0.41.

The equigranular granites contrast with the porphyritic microcline granite with their higher percent SiO_2, much higher FeO/(FeO+MgO) ratio, and lower TiO_2, P_2O_5 and CaO. The high FeO/(FeO+MgO) whole rock ratio is exemplified by biotite analyses.

Trace Element Geochemistry

The Rb/Sr ratio differentiates the main body of the Fitzwilliam Granite from its radiating sills intruding the Hardwick Tonalite (SA51-3) and the small granite bodies intruding the metamorphosed sedimentary country rock surround the Hardwick Tonalite. The main body of the Fitzwilliam Granite has a Rb/Sr ratio of between 1.65 and 2.85, where the radiating sills have an Rb/Sr ratio of 0.32 and the granites intruding the metamorphosed sedimentary rocks at Sheep Rock and Tom Swamp have Rb/Sr ratios of between 0.23 and 0.30.

The K/Rb ratio for the main body of the Fitzwilliam Granite is between 152 and 202, for the sills radiating from the Fitzwilliam Granite it is approximately 300, for the granite at Sheep Rock it is between 291 and 307 and for the granite at Tom Swamp the K/Rb ratio is 288. The Ba/Rb and Sr/Ba ratios for the Fitzwilliam Granite are 2.85 and 0.21, respectively, for sample SM11, and the Ba/Rb and Sr/Ba ratios for the granite at Tom Swamp are 7.29 and 0.59. The Rb/Sr, K/Rb, Ba/Rb, and Sr/Ba ratios of the Fitzwilliam Granite are very similar to the metamorphosed sedimentary rock, while the other equigranular granites have ratios similar to biotite tonalite and biotite-muscovite tonalite subdivisions of the Hardwick Tonalite.

The La content of the Fitzwilliam Granite (SM11) is 107 times chondritic abundance and the Ce content is 102 times chondritic abundance. In the granite at Tom Swamp, the La content is 281 times chondritic abundance and the Ce content is 211 times chondritic abundance. As suggested by the other lithophile elements, the LREE abundance of the Fitzwilliam Granite is similar to the pelitic country rock, whereas the LREE abundances of the granite at Tom Swamp is similar to some of the tonalites of the Hardwick Tonalite. The HFS elements are similar in behavior, although both granites have HFS element abundances much lower than the closely associated more mafic rocks.

DISCUSSION OF THE GEOCHEMISTRY OF THE PLUTONIC ROCKS ASSOCIATED WITH THE HARDWICK TONALITES

Major Element Geochemistry

One of the purposes of investigating the plutonic rocks associated with the Hardwick Tonalite was to explore the spatial versus genetic relationship between the rock types. Do the plutonic rocks define a coherent calc-alkaline suite in which the various mafic endmembers (diorites) are comagmatic parents to the tonalites and the granites are comagmatic progenies of the tonalites or is the coherent calc-alkaline trend a product of partial melting and mixing of a variety of source materials?

In a standard AFM plot (Figure 77), the diorite and quartz diorites associated with the Hardwick Tonalite plot at lower values of A (Na_2O+K_2O) and at overlapping and slightly higher values of M (MgO), whereas the granites associated with the Hardwick Tonalite plot closer to the A apex. The tonalite and associated plutonic rocks define a coherent calc-alkaline trend typical of many other calc-alkaline suites. In Figure 78, plutonic rocks from the Fitchburg Plutonic Complex form a similar trend (Maczuga, 1981; Robinson et al, 1981). Plutonic rocks from the Belchertown pluton do not plot on this calc-alkaline trend and define a totally different region in the AFM plot.

The plutonic rocks associated with the Hardwick Tonalite are compared with the tonalite in plots of SiO_2 against normative corundum/diopside (Figure 79), an oxidation index against normative corundum/diopside (Figure 80), and Na_2O against K_2O (Figure 81).

As shown by the Hardwick Tonalite, the plutonic rocks with low SiO_2 contents are commonly diopside normative and have a high oxidation index,

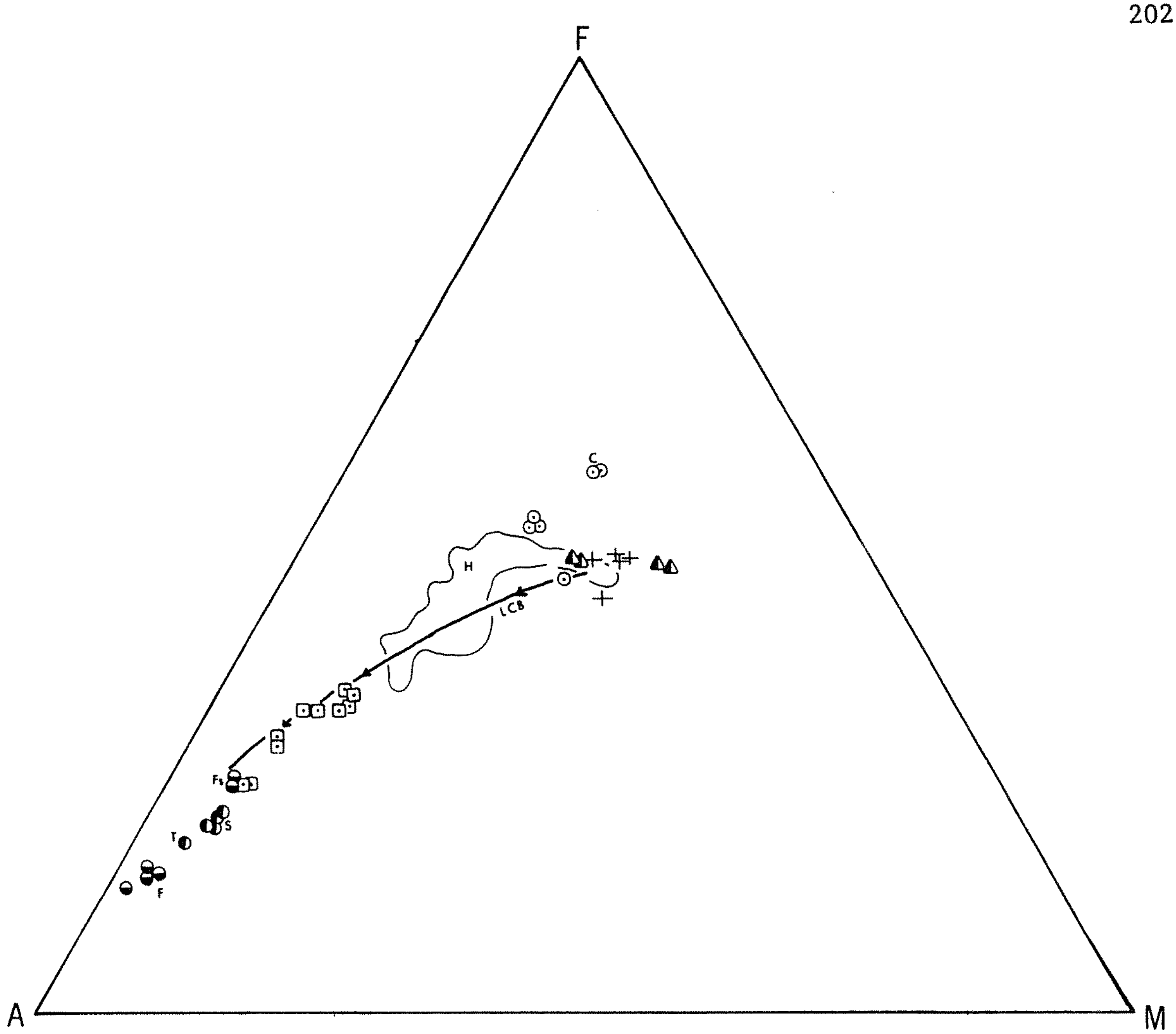

Figure 77. Whole rock analyses of the plutonic rocks associated with the Hardwick Tonalite plotted in a AFM diagram. Symbols are as follows- Augite-hornblende quartz diorite (⊙), Bear Den Sill of diorite (+), diorite at Goat Hill (◭), porphyritic microcline granite (⊡), Fitzwilliam Granite (◒), granites at Tom Swamp and Sheep Rock (◐). Letters designate variations within individual units: (C) chilled margin, (F) Fitzwilliam Granite, (Fs) sills associated with Fitzwilliam Granite, (T) granite at Tom Swamp, and (S) granite at Sheep Rock. Also plotted on figure are the AFM trends of the Lower California batholith (LCB) and Hardwick Tonalite.

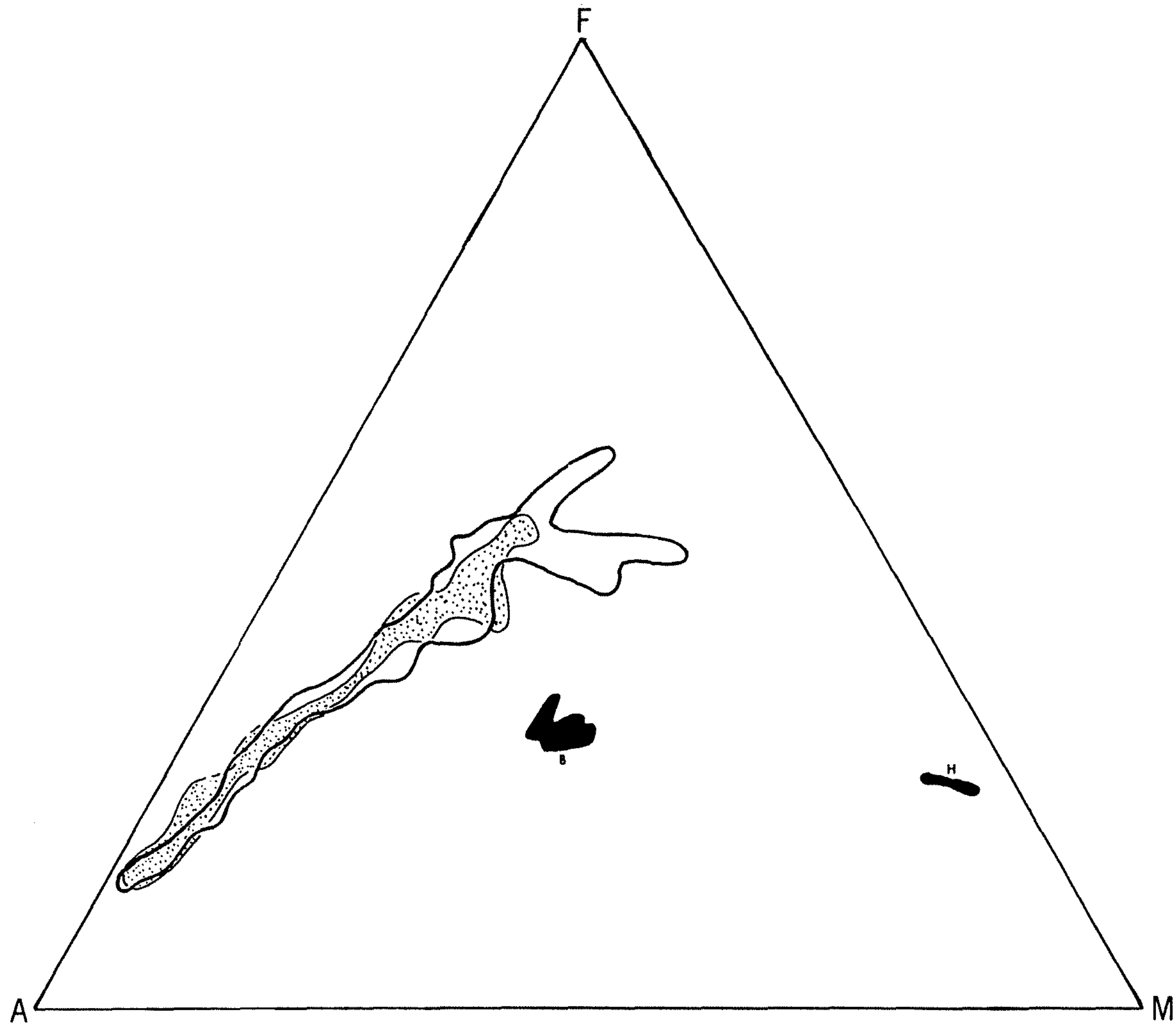

Figure 78. Comparison of AFM trends of the Hardwick Tonalite and associated plutonic rocks (open), Fitchburg plutonic complex (dotted) and the Belchertown complex (black) with B representing the monzodiorite of the Belchertown complex and H representing the hornblendite of the Belchertown Complex.

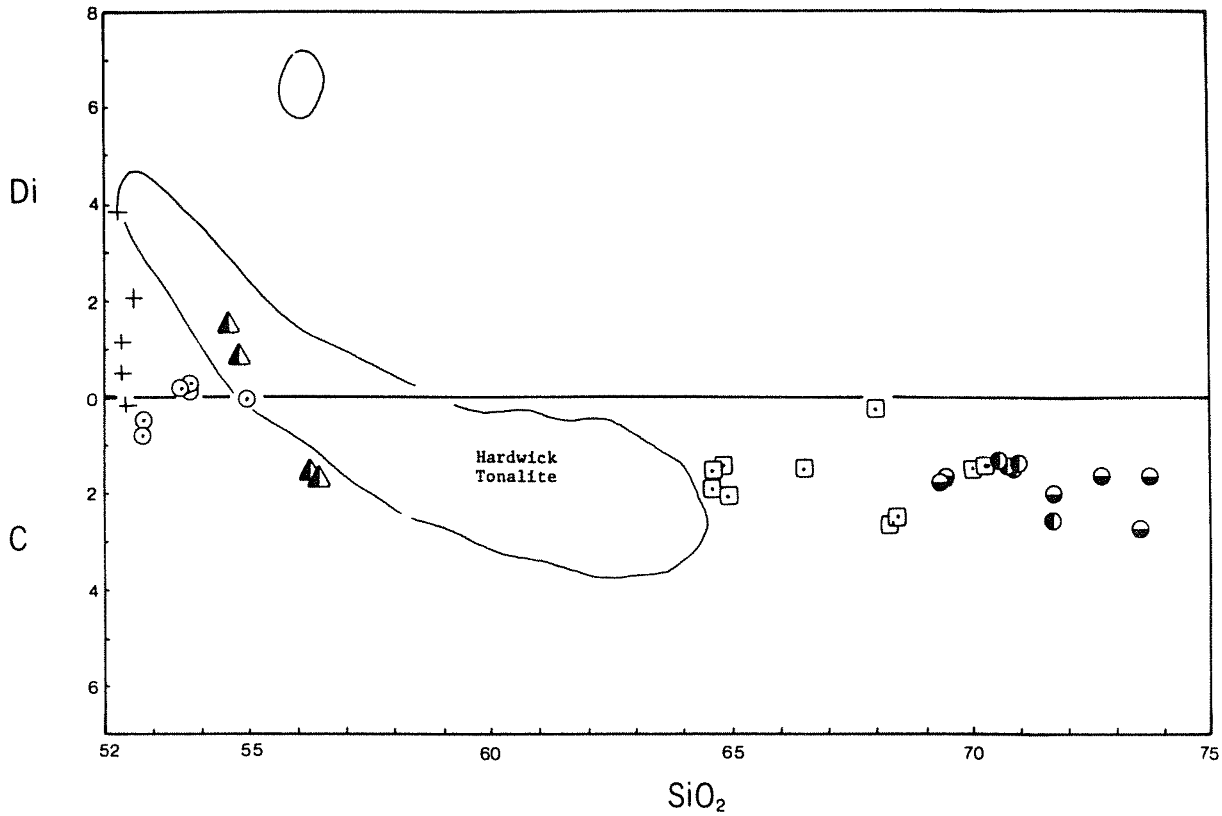

Figure 79. Plot of normative diopside and corundum versus weight percent SiO_2 for the plutonic rocks associated with the Hardwick Tonalite. Symbols: augite-hornblende quartz diorite (⊙), diorite at Goat Hill (◭) and Bear Den (+), porphyritic microcline granite (⊡), Fitzwilliam Granite (◒), granite at Sheep Rock and Tom Swamp (◐).

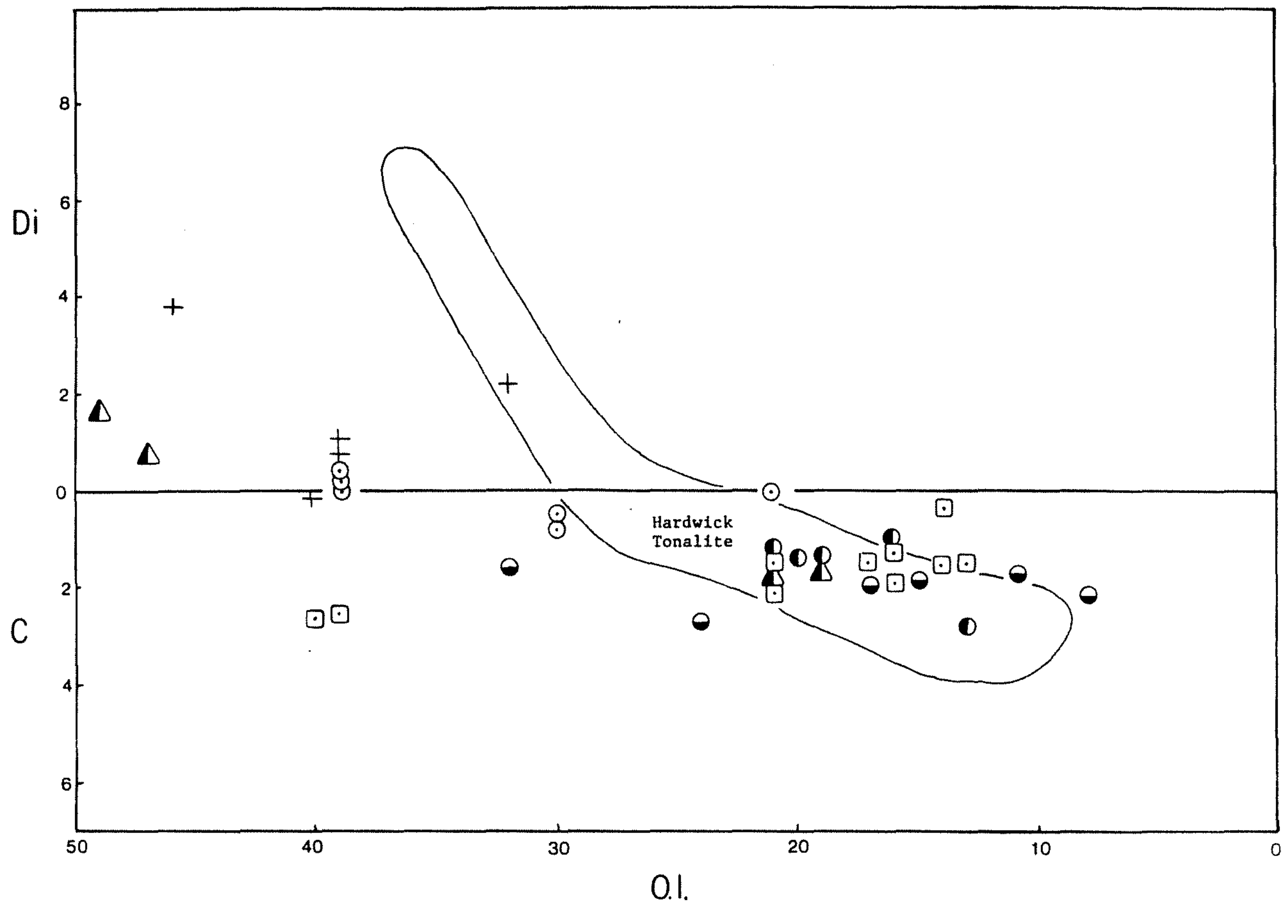

Figure 80. Plot of an oxidation index ($2Fe_2O_3/2Fe_2O_3$+FeO) versus normative diopside (Di) and corundum (C) for the plutonic rocks associated with the Hardwick Tonalite. Symbols same as in Figure 79.

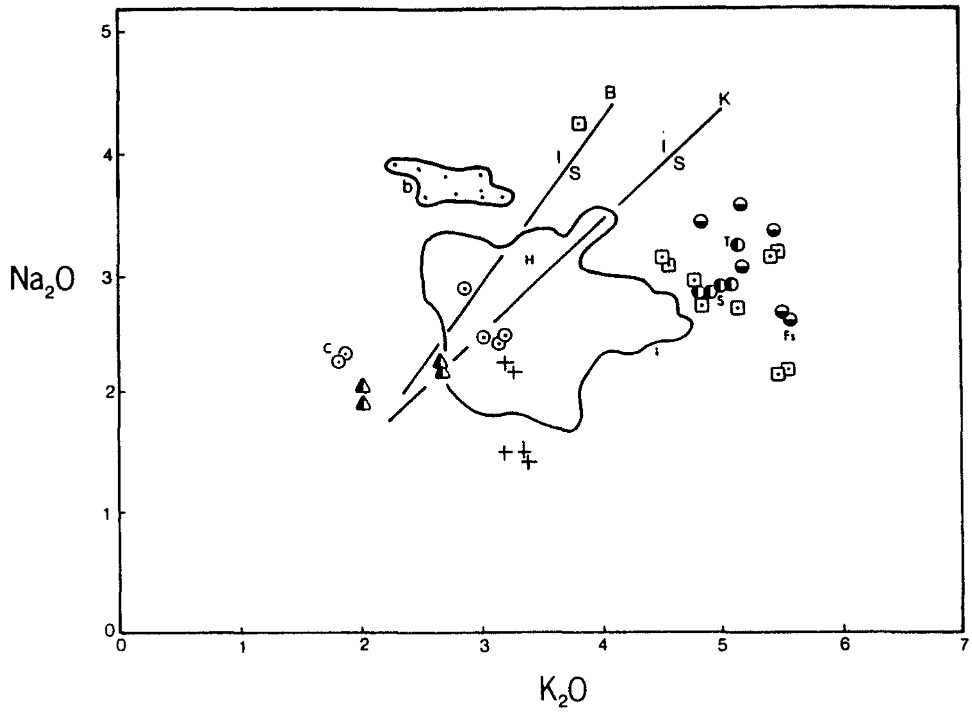

Figure 81. Plot of Na_2O versus K_2O for the plutonic rocks associated with the Hardwick Tonalite. Also shown for comparison are the Hardwick Tonalite (H) and the Belchertown Complex (b). Lines are discriminants between S-type and I-type granitoids of the Berridale and Kosciusko batholiths from the Lachlan fold belt of eastern Australia. Symbols are the same as Figure 79. Lettering: Fs (sills from the Fitzwilliam Granite), T (Tom Swamp) and S (Sheep Rock).

whereas the tonalites with a high SiO_2 content are corundum normative and have a low oxidation index. The diorite at Bear Den, the two-pyroxene diorite at Goat Hills and the interior of the Nichewaug sill of quartz diorite plot within the low SiO_2, oxidized, diopside normative region of Figures 79 and 80, although the percent normative diopside is not so high as some samples from the Hardwick Tonalite. The equigranular granites plot within the high SiO_2, reduced, corundum-normative region of Figures 79 and 80. The augite-bearing diorite of Goat Hill, the porphyritic microcline granite and the perimeter of the Nichewaug sill plot within intermediate and overlapping regions.

A plot of Na_2O against K_2O differentiates the plutonic rocks associated with the Hardwick Tonalite into three groups. One group, defined by the Goat Hills diorite and the Nichewaug sill of quartz diorite, plots on the K_2O poor side of the Hardwick Tonalite and is situated within an ambiguous area between "I- and S-type" granitoids of Chappell and White (1974). The second group, defined by the diorite sill at Bear Den, plots on the Na_2O poor side of group 1 and within the "S-type" region as defined by Chappell and White (1974). Group three, defined by the porphyritic microcline granite and the equigranular granites, plots to the K_2O rich side of the Hardwick Tonalite and near the composition of a minimum melt derived from an "S-type" source. Plutonic rocks of the Belchertown pluton plot within the "I-type" granitoid region and do not overlap with the other plutonic rocks.

Based upon major element data: (1) the Hardwick Tonalite and associated plutonic rocks differ considerably from the plutonic rocks of the Belchertown pluton, (2) the associated diorite and the quartz diorites do not represent pristine parent magma of the Hardwick Tonalite (hornblende-biotite tonalite), but may be progenies of the same parent magma, (3) the low normative corundum of the equigranular granite and the porphyritic microcline granite suggests they are not a product of partial melting of a purely pelitic source (Thompson and Tracy, 1979). A graywacke source may be an alternative (Barker, 1981).

Trace Element Geochemistry

In the diorites and quartz diorites the Rb/Sr, K/Rb, Ba/Rb, and Sr/Ba ratios are similar to Archean basalts, although the absolute amount of each of these lithophile elements are greatly enriched compared to the basalt. The enrichment of lithophile elements is typical of the Hardwick Tonalite.

In a plot of Rb aginst Sr, (Figure 82), the diorites (excluding the augite-bearing diorite of the Goat Hill diorite) and the quartz diorite define a coherent line characteristic of hornblende or pyroxene fractionation. The plot of K against Rb is less enlightening (Figure 83), but is also suggestive of the same mineral fractionation. In both plots, the fractionation lines are similar to the path of the hornblende-biotite tonalite which was attributed to hornblende fractionation.

The extension of the diorite-quartz diorite line to lower values of Rb and Sr intersects the region typical of basaltic magma. Rb, Sr, and K mineral/melt distribution coefficients for pyroxene and hornblende (Hanson, 1978)

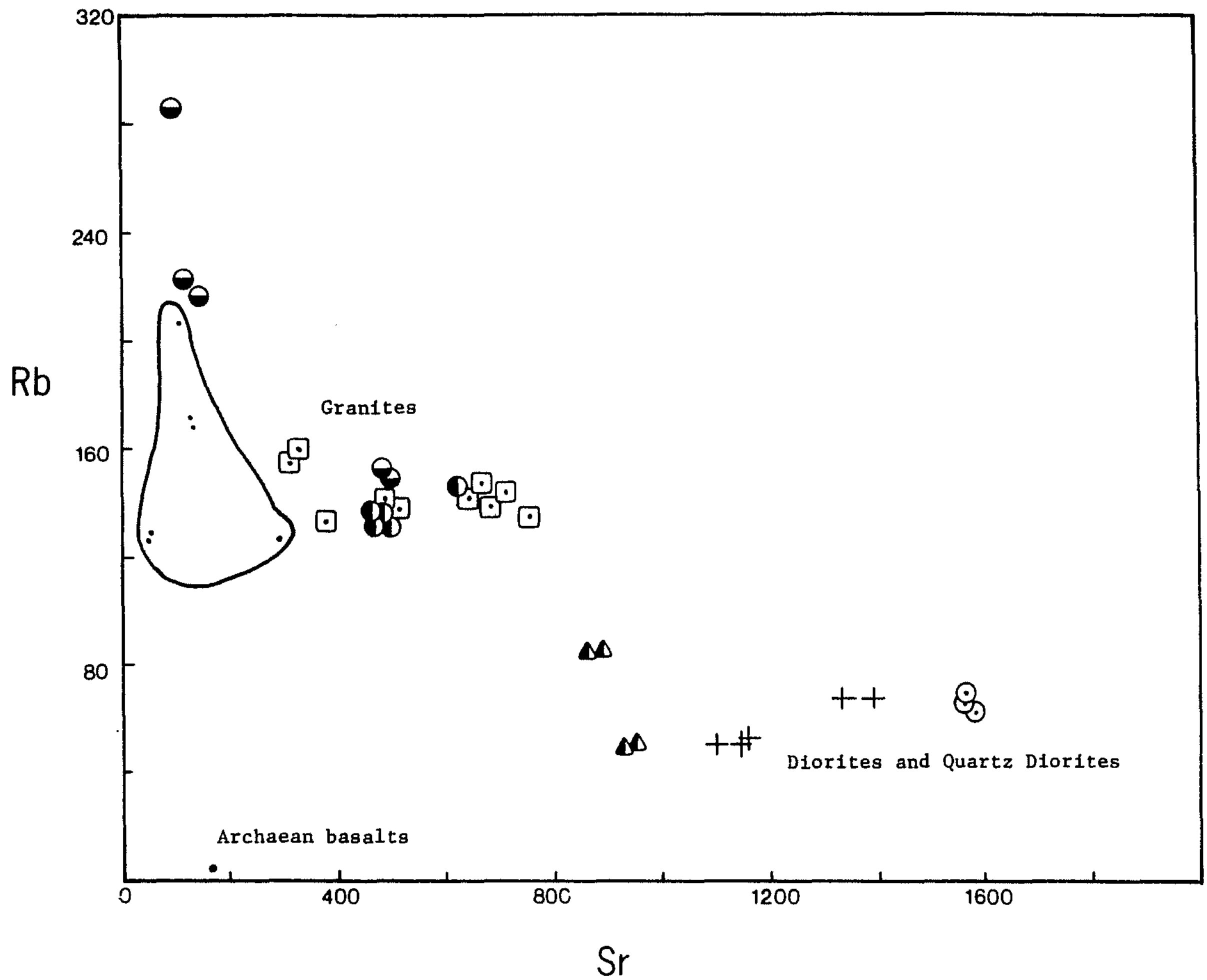

Figure 82. Plot of Rb versus Sr for the plutonic rocks associated with the Hardwick Tonalite. Also plotted is an average composition for Archaean basalts (Hart et al., 1970). Pelitic schist samples are also plotted (●). Symbols: augite-hornblende quartz diorite (⊙), diorite at Goat Hill (◭), diorite at Bear Den (+), porphyritic microcline granite (⊡), Fitzwilliam Granite (◒), and granites from Sheep Rock and Tom Swamp (◐).

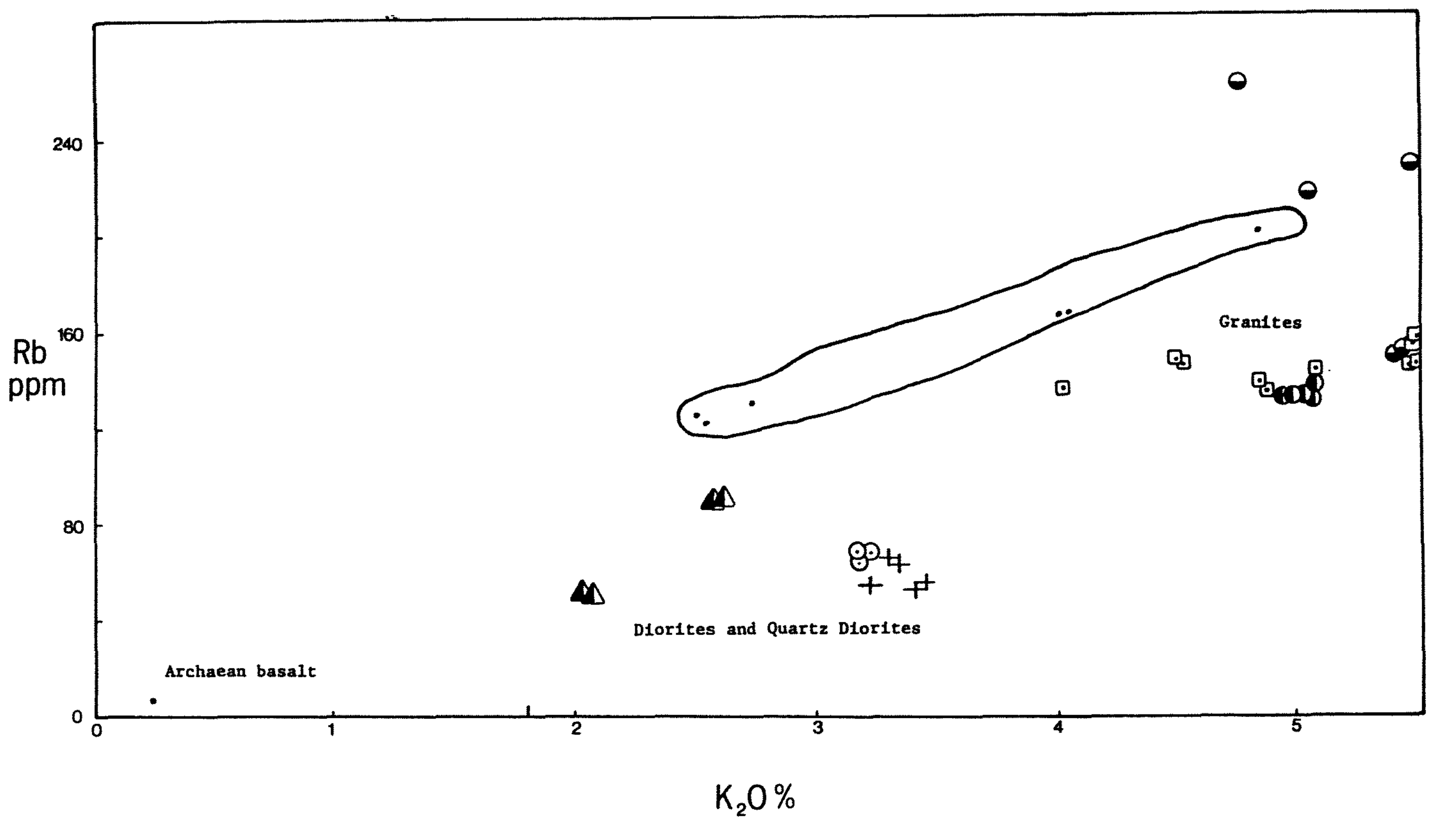

Figure 83. Plot of Rb versus K for the plutonic rocks associated with the Hardwick Tonalite. Also plotted is an average composition for Archaean basalts (Hart et al., 1970). Pelitic schist analyses are also plotted. Symbols: augite-hornblende quartz diorite (⊙), diorite at Goat Hill (▲△), diorite at the Bear Den Sill (+), porphritic microcline granite (⊡), Fitzwilliam Granite (◒), and granite at Sheep Rock and Tom Swamp (◐).

were used to calculate the percent crystal fractionation necessary to derive the diorites and quartz diorites from a typical Archean basalt (Hart et al., 1970). To derive the diorites and quartz diorites from a basalt with K=2100, Rb=5.9 and Sr-175, 90% hornblende fractionation or 90 to 98% clinopyroxene fractionation is needed. This fractionation model seems highly unlikely. Fractionation of a high percent of amphibole or clinopyroxene would be accompanied by co-precipitation of plagioclase.

In the Rb-Sr and K-Rb plots, the main body of the Fitzwilliam Granite is quite different from the other granites studied. The Fitzwilliam Granite trace element geochemistry is similar to the pelitic country rock, whereas the other granites, particularly the porphyritic microcline granite, has trace element characteristics similar to the Hardwick Tonalite.

The trace element data, Figures 82 and 83, suggests (1) the diorites and quartz diorites are not derived from a pristine basaltic source. Similar to the Hardwick Tonalite, the source must have been enriched in lithophile elements compared to typical unaltered basalts, (2) the contrast between the trace element geochemistry of the main body of the Fitzwilliam Granite and other granites studied suggests different sources. Perhaps the Fitzwilliam Granite is derived from a source containing more pelitic material. (3) The trace element data does not coherently distinguish between the other equigranular granites and the porphyritic microcline granite. The overlap of trace and major element characteristics between the porphyritic microcline granite and the peraluminous tonalites of the Hardwick Tonalite in addition to previously mentioned petrographic and mineral chemistry similarities suggests a genetic affinity. (4) Although a coherent calc-alkaline trend is defined by the Hardwick Tonalite and associated plutonic rocks, it appears evident that the magmas were derived from a variety of interacting source material in a heterogeneous source region.